HYDRODYNAMIC STUDIES IN TWO AND THREE-PHASE SLURRY BUBBLE COLUMN REACTORS

Volume I

A Dissertation

by

JAMES G. DALY

Submitted to the Office of Graduate Studies of
Texas A&M University
in partial fulfillment of the requirements for the degree of

DOCTOR OF PHILOSOPHY

August 1990

Major Subject: Chemical Engineering

HYDRODYNAMIC STUDIES IN TWO AND THREE-PHASE SLURRY BUBBLE COLUMN REACTORS

Volume I

A Dissertation

by

JAMES G. DALY

Approved as to style and content by:

Dragomir B. Bukur
(Chair of Committee)

Ahmed M. Gadalla
(Member)

Fred R. Best
(Member)

Albert T. Watson
(Member)

Raymond W. Flumerfelt
(Head of Department)

August 1990

ABSTRACT

Hydrodynamic Studies in Two and Three–Phase
Slurry Bubble Column Reactors.
(August 1990)
James G. Daly, B.S., Spring Hill College
Chair of Advisory Committee : Dr. Dragomir B. Bukur

Two and three–phase bubble columns have been used in various industrial processes. Bubble columns were initially used in the fermentation industry but more recently have been used as bioreactors and chemical reactors. One particular application of bubble column reactors is for Fischer–Tropsch synthesis. Some desirable characteristics of bubble columns are: (1) simplicity in operation, (2) low investment cost, and (3) flexibility in operation. The major drawback associated with bubble column reactors is the uncertainty associated with scale–up.

In order to properly design and scale–up multiphase reactors, both hydrodynamic and kinetic parameters are needed. The hydrodynamic parameters are often obtained in a non–reacting system; while, the kinetic parameters are obtained from a reactor designed to eliminate physical transport resistances. Experiments conducted in non–reacting systems are less expensive and provide information needed for scale–up.

The primary purpose of this research was to conduct a systematic study of the effects of solids concentration and upward slurry flow on average gas holdup, axial and radial gas holdup, and axial solids distribution using molten waxes as the liquid medium. Superficial slurry velocities up to 2 cm/s and solids loadings up to 30 wt% iron oxide and silica were used in this study. A dual energy nuclear density gauge was designed to measure axial and radial gas holdups in a large diameter bubble column (0.21 m ID). Bubble size distributions and specific gas–liquid interfacial areas were obtained using the dynamic gas disengagement technique. Flow regime transitions were determined in

both a small diameter (0.05 m ID) and large diameter bubble column using statistical analysis of both pressure fluctuations and nuclear density gauge fluctuations.

To my wife, Monica A. Daly

ACKNOWLEDGMENT

I would like to thank Dr. Bukur, my graduate advisor for his guidance and assistance throughout this project. I would also like to thank Dr. Gadalla, Dr. Watson, Dr. Best, and Dr. Seager for serving on my committee. Special appreciation goes to the United States Department of Energy for providing financial support for this project. Special thanks to Dr. Snehal A. Patel for assisting me throughout my work. Also, thanks to Mike Noak and Randy Marek for their ideas and help regarding the construction of my apparatus. Thanks to Hooshang Ghaeli for allowing me to use the comforts of his home while completing my work.

I am very grateful to my wife, Monica and to all my friends for not only their highly valued opinions but also for the good times we've had. I would also like to thank my parents for their understanding and patience while I completed my work.

TABLE OF CONTENTS

CHAPTER Page

Volume I

I. INTRODUCTION 1
Overview of Fischer–Tropsch Studies in Bubble Columns 3
Mass transfer coefficient 5
Heat transfer coefficient 6
Gas holdup and bubble size distribution 6
Flow regime characterization 10
Effect of solids 10
Effect of liquid velocity 11
Overview of Nuclear Density Gauge Studies 12
Objectives of This Study 16
II. MEASUREMENT OF GAS HOLDUPS BY CONVENTIONAL TECHNIQUES 17
Experimental Apparatus and Operating Procedure 17
Experimental Conditions 27
Data Acquisition and Reduction Procedures for Gas Holdups and Solids Concentration Profiles 29
Average gas holdup - glass columns 29
Phase fractions - stainless steel columns 32
Pressure measurements 32
Solid concentration measurements 36
Holdup calculations 42
Results and Discussion 47
Description of the flow field 47
Discussion of results 49
Effect of slurry velocity 51
Effect of solids concentration 62
Effect of solids type and size 77
Effect of liquid medium 82
Effect of temperature 85

CHAPTER Page

Effect of distributor type 87
Effect of column diameter 89
Reproducibility of results and effect of operating procedure 94
Physical Properties and Average Gas Holdup Correlations 104
Physical property measurements 104
Density measurements 104
Viscosity measurements 106
Surface tension measurements 107
Gas holdup correlations 109
III. MEASUREMENT OF PHASE FRACTIONS BY GAMMA-RAY DENSITOMETRY 123
Theoretical Discussion 123
Models used to describe three-phase systems 127
Case I. Perpendicular alignment 127
Case II. Parallel alignment 131
Comments on the alignment of the phases 134
Source Selection and Sensitivity Analysis 135
Experimental Apparatus and Operating Conditions 142
Movable assembly mechanism (MAM) 142
Sources and detectors 145
Nuclear electronics 147
Calibration procedures 153
Data Acquisition and Reduction Procedures 155
Gas holdups in two-phase systems 159
Gas holdups in three-phase systems 166
Discussion of Results 166
Independent treatment of all three phases 167
Two-phase and pseudo two-phase results 169

Volume II

IV. AXIAL SOLIDS DISTRIBUTION 196
Semi-Infinite Dispersion Model 196

CHAPTER Page

Summary of Solids Concentrations in the Column and Storage Tank 200

Results and Discussion 205

V. BUBBLE SIZE DISTRIBUTIONS 223

Experimental Techniques for Measurement of the Disengagement Profile 227

Theory 228

Case I. Constant rate disengagement process 229

Estimating bubble rise velocities and gas holdups during constant rate disengagement 235

Case II. Interactive disengagement process 235

Type 1. Interactive disengagement 237

Type 2. Interactive disengagement 243

Type 3. Interactive disengagement 243

Estimating bubble rise velocities during interactive disengagement 244

Estimating gas holdups during Type 1 interactive disengagement 244

Estimating gas holdups during Type 2 interactive disengagement 247

Estimating gas holdups during Type 3 interactive disengagement 248

Estimating bubble diameters and the specific gas-liquid interfacial area 248

Data Acquisition and Reduction Procedures for Experiments with Wax 253

Data Acquisition and Reduction Procedures for the Experiment with Water 256

Discussion of Results 258

Results from the experiments with wax 258

Effect of axial position 274

Effect of column diameter 276

Comparison of results obtained in the glass and stainless steel bubble columns 278

DGD results for the air-water system 283

CHAPTER Page

Comparison of results obtained in the glass and stainless steel bubble columns 285
Comparison of results with correlations from the literature 289
VI. FLOW REGIME CHARACTERIZATION 292
Theoretical Background 292
Discussion of Results 298
Flow regime transitions based on the MSE 304
Flow regime transitions based on the PSD 315
VII. CONCLUSIONS AND RECOMMENDATIONS 330
Gas Holdup 330
Axial Solids Concentration Distributions 331
Nuclear Density Gauge Measurements 332
Bubble Size Measurements 333
Flow Regime Transitions 334
Future Work 334
NOMENCLATURE 337
LITERATURE CITED 344
APPENDIX A 355
APPENDIX B 359
APPENDIX C 362
APPENDIX D 370
VITA 384

LIST OF TABLES

Table Page

Volume I

1.1. Summary of Bubble Column Hydrodynamic Studies. 4

1.2. Summary of Nuclear Density Gauge Studies. 14

2.1. Bubble Column Dimensions and Experimental Conditions 28

2.2a. Results from Archimedean Procedure (0-5 μm iron oxide in FT-300) . 40

2.2b. Results from Archimedean Procedure (20-44 μm iron oxide in FT-300) 40

2.2c. Results from Archimedean Procedure (0-5 μm silica in FT-300) . . . 40

2.3a. Results from Archimedean Procedure (0-5 μm iron oxide in SASOL) . 41

2.3b. Results from Archimedean Procedure (20-44 μm silica in SASOL) . . 41

2.4. Summary of Runs in the Small Stainless Steel Column 50

2.5. Summary of Runs in the Large Stainless Steel Column 52

2.6. Physical Properties of FT-300 Wax and SASOL Wax 105

2.7. Summary of Gas Holdup Correlations Presented in the Literature . . 110

2.8. Summary of Number of Points at a Given Set of Conditions 114

2.9. Mean Square Errors for Literature Correlations 116

2.10. Goodness of Fit and Parameters for Empirical Holdup Correlation . 119

3.1. Attenuation Coefficients (cm^{-1}) Used for Error Analysis Calculations 140

3.2a. Effect of Errors in the Count Rate of Co–60 on Volume Fractions Using the Am–241 and Co–60 System 140

3.2b. Effect of Errors in the Count Rate of Am–241 on Volume Fractions Using the Am–241 and Co–60 System 140

3.3a. Effect of Errors in the Count Rate of Co–60 on Volume Fractions Using the Cs–137 and Co–60 System 141

3.3b. Effect of Errors in the Count Rate of Cs–137 on Volume Fractions Using the Cs–137 and Co–60 System 141

3.4. Summary of Nuclear Density Gauge Electronics 151

3.5. Summary of Settings for the High Voltage Supply (HVS), Amplifier (AMP), and Single Channel Analyzer (SCA) 151

Table Page

3.6. Measured Attenuation Coeffcients (cm^{-1}) for FT–300 wax, SASOL wax, Iron Oxide, and Silica 156

3.7. Comparison of Measured and Theoretical Attenuation Coefficients (cm^{-1}) 156

3.8. Distance Through the Column for Both Sources at All Locations for the Experiments with FT-300 Wax 160

3.9a. Effect of Technique Used to Obtain Average Gas Holdups from Axial Gas Holdups (Data from Experiment 4 in Table 2.5, u_g=0.02 m/s) . 165

3.9b. Effect of Technique Used to Obtain Average Gas Holdups from Axial Gas Holdups (Data from Experiment 4 in Table 2.5, u_g=0.09 m/s) . 165

3.10a. Gas Holdups from Measuremets with the Nuclear Density Gauge at a Height of 1.5 m Above the Distributor (FT–300 Wax, 20 wt% 20-44 μm Iron Oxide) 168

3.10b. Gas and Solids Holdups from Measurements with the Nuclear Density Gauge at a Height of 1.5 m Above the Distributor After Modifying the Thickness (d) of the Absorbing Media (FT–300 Wax, 20 wt% 20–44 μm Iron Oxide) 168

3.11a. Gas Holdups from Measuremets with the Nuclear Density Gauge at a Height of 1.5 m Above the Distributor (SASOL Wax, 20 wt% 20-44 μm Silica) 170

3.11b. Gas and Solids Holdups from Measurements with the Nuclear Density Gauge at a Height of 1.5 m Above the Distributor After Modifying the Thickness (d) of the Absorbing Media (SASOL Wax, 20 wt% 20–44 μm Silica) 170

3.12a. Gas Holdups from Measuremets with the Nuclear Density Gauge at a Height of 2.1 m Above the Distributor (FT-300 Wax, 20 wt% 20-44 μm Iron Oxide) 171

3.12b. Gas and Solids Holdups from Measurements with the Nuclear Density Gauge at a Height of 2.1 m Above the Distributor After Modifying the Thickness (d) of the Absorbing Media (FT-300 Wax, 20 wt% 20–44 μm Iron Oxide) 171

3.13a. Gas Holdups from Measuremets with the Nuclear Density Gauge at a Height of 0.9 m Above the Distributor (SASOL Wax, 20 wt% 20-44 μm Silica) 172

Table Page

3.13b. Gas and Solids Holdups from Measurements with the Nuclear Density Gauge at a Height of 0.9 m Above the Distributor After Modifying the Thickness (d) of the Absorbing Media (SASOL Wax, 20 wt% 20–44 μm Silica) 172

3.14a. Gas Holdups from Measuremets with the Nuclear Density Gauge at a Height of 1.5 m Above the Distributor (SASOL Wax, 20 wt% 0-5 μm Iron Oxide) 173

3.14b. Gas and Solids Holdups from Measurements with the Nuclear Density Gauge at a Height of 1.5 m Above the Distributor After Modifying the Thickness (d) of the Absorbing Media (SASOL Wax, 20 wt% 0–5 μm Iron Oxide) 173

3.15a. Radial Gas Holdups Obtained Using the Co–60 Source (SASOL Wax, No Solids, u_ℓ=0 m/s) 179

3.15b. Radial Gas Holdups Obtained Using the Cs–137 Source (SASOL Wax, No Solids, u_ℓ=0 m/s) 179

3.16a. Radial Gas Holdups Obtained Using the Co–60 Source (SASOL Wax, 20 wt% 0-5 μm Iron Oxide, $u_{s\ell}$=0.005 m/s) 180

3.16b. Radial Gas Holdups Obtained Using the Cs–137 Source (SASOL Wax, 20 wt% 0-5 μm Iron Oxide, $u_{s\ell}$=0.005 m/s) 180

3.17a. Radial Gas Holdups Obtained Using the Co–60 Source (SASOL Wax, 20 wt% 20-44 μm Silica, $u_{s\ell}$=0 m/s) 181

3.17b. Radial Gas Holdups Obtained Using the Cs–137 Source (SASOL Wax, 20 wt% 20-44 μm Silica, $u_{s\ell}$=0 m/s) 181

3.18a. Radial Gas Holdups Obtained Using the Co–60 Source (FT-300 Wax, 20 wt% 20-44 μm Iron Oxide, $u_{s\ell}$=0 m/s) 182

3.18b. Radial Gas Holdups Obtained Using the Cs–137 Source (FT-300 Wax, 20 wt% 20-44 μm Iron Oxide, $u_{s\ell}$=0 m/s) 182

Volume II

4.1a. Summary of Solids Concentrations For Experiments in the 0.05 m ID Bubble Column 202

4.1b. Summary of Solids Concentrations For Experiments in the 0.21 m ID Bubble Column 203

5.1. Correlations for Estimating Bubble Size from Bubble Rise Velocity . 250

Table | Page

5.2a. DGD Results from the Experiment with FT-300 Wax at a Height of 1.3 m (0.21 m ID Stainless Steel Bubble Column, 265 °C) 262

5.2b. DGD Results from the Experiment with FT-300 Wax at a Height of 1.9 m (0.21 m ID Stainless Steel Bubble Column, 265 °C) 262

5.3a. DGD Results from the Experiment with SASOL Wax (Decreasing Gas Velocity) at a Height of 1.3 m (0.21 m ID Stainless Steel Bubble Column, 265 °C) 263

5.3b. DGD Results from the Experiment with SASOL Wax (Decreasing Gas Velocity) at a Height of 1.9 m (0.21 m ID Stainless Steel Bubble Column, 265 °C) 263

5.4a. DGD Results from the Experiment with SASOL Wax (Increasing Gas Velocity) at a Height of 1.3 m (0.21 m ID Stainless Steel Bubble Column, 265 °C) 264

5.4b. DGD Results from the Experiment with SASOL Wax (Increasing Gas Velocity) at a Height of 1.9 m (0.21 m ID Stainless Steel Bubble Column, 265 °C) 264

5.5a. DGD Results from the Experiment with FT-300 Wax (Increasing Gas Velocity) at a Height of 1.3 m (0.05 m ID Stainless Steel Bubble Column, 265 °C) 266

5.5b. DGD Results from the Experiment with SASOL Wax (Increasing Gas Velocity) at a Height of 1.9 m (0.05 m ID Stainless Steel Bubble Column, 265 °C) 266

5.6a. DGD Results from the Experiment with SASOL Wax (Increasing Gas Velocity) at a Height of 1.3 m (0.05 m ID Stainless Steel Bubble Column, 265 °C) 267

5.6b. DGD Results from the Experiment with SASOL Wax (Increasing Gas Velocity) at a Height of 1.9 m (0.05 m ID Stainless Steel Bubble Column, 265 °C) 267

5.7a. DGD Results from the Experiment with Tap Water at a Height of 1.3 m (0.05 m ID Stainless Steel Bubble Column) 287

5.7b. DGD Results from the Experiment with Tap Water at a Height of 1.9 m (0.05 m ID Stainless Steel Bubble Column) 287

D.1. Data Points for Type 1 Interactive Disengagement 372

D.2. Data Points for Type 2 Interactive Disengagement 379

LIST OF FIGURES

Figure Page

Volume I

2.1. Schematic of the slurry bubble column apparatus. 18

2.2. Schematic representation of the slurry inlet system for the large diameter stainless steel column. 20

2.3. Schematic representation of the slurry inlet system for the small diameter stainless steel column. 21

2.4. Schematic representation of the circulation loop for the large diameter stainless steel column. 24

2.5. Schematic representation of the circulation loop for the small diameter stainless steel column. 25

2.6. Schematic representation of the dipstick assembly. 26

2.7. Schematic representation of the perforated plate distributor. 30

2.8. Schematic representation of the bubble cap distributor plate. 31

2.9. Schematic diagram of the pressure ports and slurry sampling ports locations (all dimensions in m). 33

2.10. Schematic representation of the pressure transducer system. 34

2.11. Typical pressure transducer calibration curve. 37

2.12. Bubble column flow regime map (adopted from Deckwer et al., 1980). 48

2.13. Effect of superficial slurry velocity on average gas holdup in the (a) small and (b) large diameter columns with FT–300 wax. 53

2.14. Effect of superficial gas velocity on axial gas holdup in the (a) small and (b) large diameter columns with FT–300 wax. 55

2.15. Effect of superficial slurry velocity on axial gas holdup in the small diameter column with FT–300 wax. 57

2.16. Effect of superficial slurry velocity on average gas holdup in the small diameter column with FT–300 wax in the presence of solids; (a) 0–5 μm iron oxide; (b) 0–5 μm silica. 59

2.17. Effect of superficial slurry velocity on average gas holdup in the large diameter column with FT–300 wax (20–44 μm iron oxide). 60

Figure Page

2.18. Effect of superficial slurry velocity on average gas holdup in the (a) small and (b) large diameter columns with SASOL wax. 61

2.19. Effect of slurry velocity on average gas holdup in the large diameter column with SASOL wax ((a) 0–5 μm iron oxide, (b) 20–44 μm iron oxide, (c) 20–44 μm silica). 63

2.20. Effect of solids concentration on average gas holdup with FT–300 wax ((a) 0.05 m ID Column, 20 WT%, 0–5 μm iron oxide; (b) 0.21 m ID Column, 20 WT%, 20–44 μm iron oxide). 64

2.21. Effect of solids concentration and superficial gas velocity on axial gas holdup in the 0.05 m ID column with FT–300 wax (0–5 μm iron oxide particles; (a) $u_g = 0.02$ m/s; (b) $u_g = 0.04$ m/s; (c) $u_g = 0.12$ m/s). 66

2.22. Effect of solids concentration on average gas holdup in the 0.05 m ID column with FT–300 wax ((a) 20–44 μm iron oxide; (b) 0–5 μm silica). 67

2.23. Effect of solids concentration on average gas holdup neglecting foam (0–5 μm iron oxide). 70

2.24. Effect of solids concentration on average gas holdup in the continuous mode of operation with FT–300 wax (0–5 μm iron oxide; (a) $u_{s\ell} = 0.005$ m/s; (b) $u_{s\ell} = 0.02$ m/s). 72

2.25. Effect of solids concentration on average gas holdup with FT–300 wax ((a) 0.05 m ID column, 0–5 μm silica; (b) 0.21 m ID column, 20–44 μm iron oxide). 73

2.26. Effect of solids concentration on average gas holdup with SASOL wax ((a) 0.05 m ID column, 20–44 μm iron oxide, (b) 0.21 m ID column, 20–44 μm iron oxide, (c) 0.21 m ID column, 0–5 μm iron oxide). 74

2.27. Effect of solids concentration on average gas holdup with SASOL wax in the continuous mode of operation ((a) 0.05 m ID column, 20–44 μm iron oxide, (b) 0.21 m ID column, 20–44 iron oxide, (c) 0.21 m ID column, 0–5 μm iron oxide). 76

2.28. Effect of solids type and size on average gas holdup in the 0.05 m ID column with FT–300 wax. 78

Figure Page

2.29. Effect of solids type and size on average gas holdup in the 0.05 m ID column with FT–300 wax (volume fraction of solids at the distributor = 0.045). 80

2.30. Effect of solids type and size on average gas holdup in the 0.21 m ID column with SASOL wax ((a) $u_{s\ell} = 0.0$ m/s; (b) $u_{s\ell} = 0.005$ m/s). 81

2.31. Effect of liquid medium on average gas holdup in the 0.05 m ID column. 83

2.32. Effect of liquid medium on average gas holdup in the 0.21 m ID column. 84

2.33. Effect of temperature on average gas holdup in the 0.05 m ID column. 86

2.34. Effect of superficial gas velocity and distributor type on average gas holdup (20 – 44 μm iron oxide; (a) SASOL wax, $u_{s\ell} = 0.0$ m/s; (b) FT–300 wax, $u_{s\ell} = 0.005$ m/s). 88

2.35. Effect of superficial gas velocity and distributor type on average gas holdup with SASOL wax (0 – 5 μm iron oxide; (a) $u_{s\ell} = 0.0$ m/s; (b) $u_{s\ell} = 0.005$ m/s). 90

2.36. Effect of column diameter on average gas holdup with FT–300 wax. 91

2.37. Effect of column diameter on average gas holdup with SASOL wax. 93

2.38. Typical hysteresis loop observed in the 0.05 m ID glass column. . . . 96

2.39. Reproducibility of results with FT–300 wax in the 0.05 m ID column. 97

2.40. Reproducibility of results with FT–300 wax in the 0.05 m ID column (a) iron oxide; (b) silica. 99

2.41. Reproducibility of results with SASOL wax in the 0.05 m ID columns. 100

2.42. Reproducibility of gas holdup values and effect of operating procedure for batch experiments in the 0.21 m ID column ((a) SASOL wax; (b) FT–300 wax). 101

2.43. Effect of wax age on average gas holdup in the 0.21 m ID column with SASOL wax. 103

2.44. Effect of temperature on surface tension of fresh and used FT–300 and SASOL wax. 108

2.45. Parity plot of predicted versus measured gas holdup ((a and b) Badjugar et al., 1986; (c and d) Hughmark, 1967). . . . 117

Figure Page

2.46. Parity plot of predicted versus measured gas holdups for the correlations developed in this study. 120

2.47. Parity plot of predicted versus measured gas holdup (wax type: SASOL, FT-300, Mobil; u_g = 0.01 to 0.15 m/s; $u_{s\ell}$= 0, 0.005, and 0.02 m/s; d_c = 0.05 and 0.21 m ID; solids: 0, 10, 20, and 30 wt% iron oxide and silica). 122

3.1. Relative importance of the three major types of gamma–ray attenuation. 126

3.2. Schematic representation of multiple absorbers in series. 128

3.3. Schematic representation of Case I geometry (i.e. perpendicular alignment). 130

3.4. Schematic representation of Case II geometry (i.e. parallel alignment). 132

3.5. Schematic representations of (a) annular flow and (b) homogeneous flow in a square duct. 136

3.6. Schematic diagram of axial movement mechanism for the nuclear density gauge apparatus 143

3.7. Schematic diagram of the radial movement mechanism for the nuclear density gauge apparatus 144

3.8. Schematic representation of the Cobalt-60 source holder. 148

3.9. Schematic representation of the Cesium-137 source holder. 149

3.10. Schematic representation of the detector housing for the Cobalt-60 and Cesium-137 sources. 150

3.11. Schematic diagram of the nuclear density gauge electronic and data acquisition system. 152

3.12. Schematic diagram of the calibration chamber. 154

3.13. Schematic diagram of the nuclear density gauge measurement locations. 158

3.14. Schematic representation of the locations for radial measurements with the nuclear density gauge apparatus. 161

3.15. Schematic diagram of the regions used to obtain average gas holdups. 164

3.16. Effect of superficial gas velocity on radial gas holdup (SASOL wax, no solids, u_ℓ = 0.0 m/s). 174

3.17. Effect of superficial gas velocity on radial gas holdup (SASOL wax, 20 wt% 0 - 5 μm iron oxide, $u_{s\ell}$ = 0.005 m/s). . . . 175

Figure Page

3.18. Effect of superficial gas velocity on radial gas holdup (SASOL wax, 20 wt% 20 - 44 μm silica, $u_{s\ell} = 0.0$ m/s). 176

3.19. Effect of superficial gas velocity on radial gas holdup (FT-300 wax, 20 wt% 20 - 44 μm iron oxide, $u_{s\ell} = 0.0$ m/s). . . . 177

3.20. Schematic representation of bubble column wall. 183

3.21. Comparison of average gas holdups from the DP cells and nuclear density gauges (SASOL wax, no solids; (a) $u_\ell = 0.0$ m/s; (b) u_ℓ=0.005 m/s). 185

3.22. Comparison of average gas holdups from the DP cells and nuclear density gauges (SASOL wax, 20 wt% 0 - 5 μm iron oxide; (a) $u_{s\ell} = 0.0$ m/s; (b) $u_{s\ell} = 0.005$ m/s; (c) $u_{s\ell} = 0.02$ m/s). . . . 186

3.23. Comparison of axial gas holdups from the DP cells and nuclear density gauges (SASOL wax, no solids; (a) $u_g = 0.04$ m/s; (b) $u_g = 0.09$ m/s). 188

3.24. Comparison of average gas holdups from the DP cells and nuclear density gauges (SASOL wax, $u_{s\ell} = 0.0$ m/s; (a) 20 wt% 20-44 μm iron oxide; (b) 20 wt% 20-44 μm silica). 189

3.25. Comparison of axial gas holdups from the DP cells and nuclear density gauges (SASOL wax, 20 wt% 20-44 μm iron oxide - (a) $u_g = 0.02$ m/s; (b) $u_g = 0.08$ m/s; SASOL wax, 20 wt% 20-44 μm silica - (c) u_g=0.02 m/s; (d) u_g=0.08 m/s). 190

3.26. Comparison of average gas holdups from the DP cells and nuclear density gauges (FT-300 wax; (a) u_ℓ=0.0 m/s, no solids; (b) u_ℓ=0.005 m/s, no solids; (c) $u_{s\ell}$=0.0 m/s, 20 wt% 20-44 μm iron oxide). 192

3.27. Comparison of axial gas holdups from the DP cells and nuclear density gauges with FT-300 wax and no solids (u_ℓ=0.0 m/s - (a) u_g=0.04 m/s; (b) u_g=0.12 m/s; u_ℓ=0.005 m/s - (c) u_g=0.04 m/s; (d) u_g=0.12 m/s). 193

3.28. Comparison of axial gas holdups from the DP cells and nuclear density gauges (FT-300 wax, 20 wt% 20-44 μm iron oxide - (a) u_g=0.02 m/s; (b) u_g=0.04 m/s; (c) u_g=0.08 m/s). 195

Volume II

4.1. Schematic diagram of modified expansion unit. 204

Figure Page

4.2. Effect of axial position and superficial gas velocity on solids concentrations (0-5 μm particles, $u_{s\ell}$=0.0 m/s; (a) iron oxide, 0.05 m ID column; (b) silica, 0.05 m ID column; (c) iron oxide, 0.21 m ID column). 207

4.3. Effect of axial position and superficial gas velocity on solids concentrations (20-44 μm particles, 0.05 m ID bubble column; (a) iron oxide, $u_{s\ell}$=0 m/s; (b) silica, $u_s\ell$=0 m/s; (c) iron oxide,$u_{s\ell}$=0.02 m/s). 208

4.4. Effect of axial position and superficial gas velocity on solids concentrations (20 wt% 20-44 μm iron oxide particles, 0.21 m ID bubble column, $u_{s\ell}$=0 m/s; (a) 19 x 2 mm PP distributor; (b) bubble cap distributor). 209

4.5. Effect of axial position and superficial gas velocity on solids concentrations (20-44 μm iron oxide particles, 0.21 m ID bubble column, $u_{s\ell}$=0.005 m/s; (a) 30 wt%; (b) 20 wt%). 211

4.6. Effect of superficial gas velocity on u_p/E_s (20-44 μm particles, $u_{s\ell}$=0.0 m/s; (a) iron oxide, 0.05 m ID column; (b) silica 0.05 m ID column; (c)iron oxide, 0.21 m ID column). 213

4.7. Effect of superficial gas velocity on hindered particle settling velocity for 20-44 μm iron oxide particles in SASOL reactor wax. . . 214

4.8. Effect of superficial gas velocity on axial solids dispersion coefficients ((a) 0.05 m ID column, (b) 0.21 m ID column). 216

4.9. Parity plot of measured versus predicted solids concentrations; (20-44 μm iron oxide and silica particles; $u_{s\ell}$=0.0m/s and 0.005 m/s-0.21 m ID column only). 217

4.10. Effect of superficial gas velocity on axial solids concentrations (0-5 μm particles; 0.05 m ID bubble column; $u_{s\ell}$=0 m/s; (a) iron oxide; (b) silica). 219

4.11. Effect of particle size and superficial gas velocity on axial solids concentrations. 220

4.12. Effect of column diameter and superficial slurry velocity on axial solids concentrations. 222

5.1. Dispersion prior to disengagement (t = 0). 230

Figure Page

5.2. Dispersion during the constant rate disengagement process (Period 1). 231

5.3. Dispersion during the constant rate disengagement process (Period 2). 234

5.4. Plot of height vs. time for a multimodal distribution (constant rate process). 236

5.5. Schematic representation of slug flow in the small column with tap water as the liquid medium. 238

5.6. Schematic representation of the flow about a slug. 239

5.7a. Bubble rise velocity vs. bubble diameter correlation for FT-300 wax. . 251

5.7b. Bubble rise velocity vs. bubble diameter correlation for tap water. . . 252

5.8. Raw pressure transducer signal for DGD analysis from the experiment with FT-300 wax in the small diameter column at heights of (a) 0.6 m; (b) 1.3 m; and (c) 1.9 m above the distributor. 255

5.9. Effect of superficial gas velocity on disengagement (Tap water). . . . 257

5.10. Effect of axial position on disengagement (FT-300 wax, (a) u_g= 0.02 m/s; (b) u_g=0.12 m/s). 259

5.11. Effect of axial position on disengagement (SASOL wax, (a) u_g= 0.02 m/s; (b) u_g=0.09 m/s). 260

5.12. Effect of superficial gas velocity and wax type on (a) Sauter mean bubble diameter, (b) specific gas-liquid interfacial area, and (c) gas holdup in the 0.21 m ID column at a height of 1.3 m above the distributor. 268

5.13. Effect of superficial gas velocity and wax type on (a) Sauter mean bubble diameter, (b) specific gas-liquid interfacial area, and (c) gas holdup in the 0.21 m ID column at a height of 1.9 m above the distributor. 270

5.14. Effect of superficial gas velocity and wax type on (a) Sauter mean bubble diameter, (b) specific gas-liquid interfacial area, and (c) gas holdup in the 0.05 m ID column at a height of 1.3 m above the distributor. 271

5.15. Effect of superficial gas velocity and wax type on (a) Sauter mean bubble diameter, (b) specific gas-liquid interfacial area, and (c) gas holdup in the 0.05 m ID column at a height of 1.9 m above the distributor. 272

Figure Page

5.16. Effect of superficial gas velocity on axial gas holdup ((a) 0.05 m ID column, FT-300 wax; (b) 0.05 m ID column, SASOL wax; (c) 0.21 m ID column, FT-300 wax). 273

5.17. Effect of axial position on (a and c) Sauter mean bubble diameter and (b and d) gas holdup in 0.05 and 0.21 m ID bubble columns with wax (decreasing gas velocity - SASOL wax, 0.21 m ID column). 275

5.18. Effect of column diameter on Sauter mean bubble diameter for (a) FT-300 wax and (b) SASOL reactor wax - decreasing gas velocity in 0.21 m ID column. 277

5.19. Comparison of (a) Sauter mean bubble diameters and (b) gas holdup obtained in the 0.21 m ID stainless steel column (DP method, 1.9 m) and the 0.23 m ID glass column (visual method) with FT-300 wax. . 279

5.20. Comparison of (a) Sauter mean bubble diameters and (b) gas holdup obtained in the 0.05 m ID stainless steel column (DP method, 1.9 m) and the 0.05 m ID glass column (visual method) with FT-300 wax. . 280

5.21. Comparison of (a) Sauter mean bubble diameters and (b) gas holdup obtained in the 0.05 m ID stainless steel column (DP method, 1.9 m) and the 0.05 m ID glass column (visual method) with SASOL wax. . 282

5.22. Effect of superficial gas velocity on disengagement (Tap water). . . 284

5.23. Effect of axial position and disengagement model on (a) Sauter mean bubble diameter, (b) specific gas-liquid interfacial area, and (c) gas holdup in the 0.05 m ID column with tap water as the liquid medium. 286

5.24. Comparison of (a) Sauter mean bubble diameters, (b) specific gas-liquid interfacial areas, and (c) gas holdups obtained in the 0.05 m ID stainless steel and glass columns with tap water as the liquid medium. 288

5.25. Comparison of Sauter mean bubble diameters with correlations from the literature for tap water. 291

6.1. Typical raw signals from the nuclear density gauge apparatus during experiments in the 0.05 m ID bubble column. 300

6.2. Typical raw signals from the nuclear density gauge apparatus during experiments in the 0.21 m ID bubble column. 301

6.3. Effect of superficial gas velocity on the probability density function from the pressure transducer in the 0.05 m ID bubble column at a height of 1.8 m above the distributor. 302

6.4. Effect of superficial gas velocity on the probability density function from the pressure transducer in the 0.21 m ID bubble column at a height of 1.8 m above the distributor. 303

Figure Page

6.5. Effect of superficial gas velocity on the probability density function from the nuclear density gauge using the Cesium-137 source in the 0.05 m ID bubble column at a height of 1.5 m above the distributor. 305

6.6. Effect of superficial gas velocity on the probability density function from the nuclear density gauge using the Cesium-137 source in the 0.21 m ID bubble column at a height of 1.5 m above the distributor. 306

6.7. Effect of slurry flow rate on the mean square error of pressure fluctuations at the wall (FT-300 wax, 265 °C, 0-5 μm silica, 0.05 m ID column, 1.2 m above the distributor). 308

6.8. Effect of height above the distributor on the mean square error of pressure fluctuations at the wall (FT-300 wax, 265 °C,20 wt% 0-5 μm silica, 0.05 m ID column, $u_{s\ell}$=0.0 m/s). 310

6.9. Effect of superficial gas velocity on the mean square error of pressure fluctuations at the wall (FT-300 wax, 265 °C,20 wt% 0-5 μm silica, 0.05 m ID column, $u_{s\ell}$=0.0 m/s). 311

6.10. Effect of slurry flow rate and distributor on the mean square error of nuclear density gauge fluctuations (SASOL wax, 265 °C, 0.21 m ID column, Cesium-137 source, 1.5 m above the distributor). 313

6.11. Effect of height above the distributor on the mean square error of pressure fluctuations at the wall (SASOL wax, 265 °C, 0.21 m ID column, u_ℓ=0.0 m/s). 314

6.12. Effect of superficial gas velocity on the mean square error of pressure fluctuations at the wall (SASOL wax, 265 °C, 0.21 m ID column, u_ℓ=0.0 m/s). 316

6.13. Effect of superficial gas velocity on the power spectral density function for pressure fluctuations at the wall (FT-300 wax, 265 °C, 0.05 m ID column, 10 wt% 20-44 μm iron oxide, $u_{s\ell}$=0.02 m/s, height=1.8 m). 318

6.14. Effect of height above the distributor on the power spectral density function for pressure fluctuations at the wall (FT-300 wax, 265 °C, 0.05 m ID column, 10 wt% 20-44 μm iron oxide, $u_{s\ell}$=0.02 m/s, u_g=0.12 m/s). 319

6.15. Effect of height above the distributor on the power spectral density function for pressure fluctuations at the wall (FT-300 wax, 265 °C, 0.05 m ID column, 20 wt% 0-5 μm silica, $u_{s\ell}$=0.0 m/s, u_g=0.09 m/s). 320

6.16. Effect of superficial gas velocity on the power spectral density function from the nuclear density gauge (FT-300 wax, 265 °C, 0.05 m ID column, u_ℓ=0.0 m/s, Cesium-137, height=1.5 m). . . . 322

Figure Page

6.17. Effect of superficial gas velocity on the power spectral density function for pressure fluctuations at the wall (SASOL wax, 265 °C, 0.21 m ID column, u_ℓ=0.0 m/s, height=0.08 m). 324

6.18. Effect of superficial gas velocity on the power spectral density function for pressure fluctuations at the wall (SASOL wax, 265 °C, 0.21 m ID column, u_ℓ=0.0 m/s, height=1.8 m). 325

6.19. Effect of height above the distributor on the power spectral density function for pressure fluctuations at the wall (SASOL wax, 265 °C, 0.21 m ID column, u_ℓ=0.0 m/s, u_g=0.02 m/s). 326

6.20. Effect of height above the distributor on the power spectral density function for pressure fluctuations at the wall (SASOL wax, 265 °C, 0.21 m ID column, u_ℓ=0.0 m/s, u_g=0.06 m/s). 327

6.21. Effect of height above the distributor on the power spectral density function for nuclear density gauge fluctuations (FT-300 wax, 265 °C, 0.21 m ID column, Cobalt 60, height=1.5 m). 329

A.1. Schematic diagram of solvent cleaning system for the small diameter column. 356

C.1. Schematic diagram of the radial and axial measurement locations. 363

D.1. Dynamic gas disengagement curve for Type 1 interactive disengagement. 371

CHAPTER I

INTRODUCTION

Fischer–Tropsch (F–T) synthesis represents an important route for indirect coal liquefaction. During World War II, Germany utilized F–T synthesis to produce motor fuels. Currently, commercial size units are in operation at SASOL in South Africa. Fixed bed (Germany and SASOL) and entrained bed (SASOL) type of reactors have been used for conversion of synthesis gas into hydrocarbon products.

Interest in F–T synthesis has been renewed following the oil embargo in 1973. In particular, slurry phase F–T synthesis has received a great deal of attention. Slurry phase bubble column reactors offer several advantages over conventional reactors. These include better mixing, heat transfer, and temperature control. Also, fine catalyst particles, which minimize intraparticle diffusion effects, may be used in a slurry bubble column reactor. One of the major disadvantages of bubble column reactors is the uncertainty associated with scale–up from a laboratory size reactor to a commercial size reactor.

Recent studies by Gray et al. (1980) and Thompson et al. (1981) have shown that F–T synthesis in slurry phase bubble column reactors has significant advantages over other types of reactors that are currently employed. A number of slurry phase F–T pilot plant reactors have been constructed and operated by several U.S.A. and German companies (e.g., Air Products and Chemical Inc., Mobil, Schering, and Rurhchemie). Also, a number of studies have been conducted by several academic institutions (e.g., MIT; University of California, Berkley; University of Oldenberg; and Texas A&M University).

The *AIChE Journal* is used as a pattern for style and format.

The majority of these studies, with the exception of those at Texas A&M, were conducted in relatively small diameter columns (less than 0.05 m ID) and superficial gas velocities less than 0.05 m/s. Under these conditions, either the homogeneous bubbly regime or slug flow regime will exist (Deckwer et al., 1980; Shah et al., 1982). However, commercial size reactors are expected to operate in the churn–turbulent flow regime, and extrapolation of results obtained in smaller diameter columns may not be warranted. The specific gas–liquid interfacial area, as well as gas and liquid phase mixing differ in different flow regimes. Since construction and operating costs are expected to be high for large diameter bubble column reactors, hydrodynamic data obtained in large diameter columns operating in the churn–turbulent flow regime are needed to properly scale–up slurry phase F–T bubble column reactors.

The common procedure in the design and scale–up of multiphase reactors is to obtain hydrodynamic parameters in a non–reacting system, and kinetic parameters from a reactor system designed to eliminate physical transport resistances. Experiments in non–reacting systems are less expensive and provide information on scale–up effects. Results obtained in these two types of experiments are used as inputs into a mathematical model for the multiphase reactor. Computer simulated results then provide basis for economic evaluations, process optimization, and the reactor design and scale–up. This approach has been successfully used in the design of large scale fluidized bed reactors (e.g., Shell Chlorine process, de Vries et al., 1972; and Mobil's methanol to gasoline (MTG) process, Krambeck et al., 1985).

Many of the techniques commonly used to measure hydrodynamic parameters in laboratory scale bubble column reactors may not be used to monitor the hydrodynamics of large scale reactors. For example, gas holdups in laboratory reactors are usually measured by visual observations which involve terminating the gas flow to the column, or through differential pressure measurements. In an industrial application, the gas flow

to the system cannot be shut–off during operation of the reactor. For applications which involve the use of small catalyst particles, pressure transducers are likely to plug, particularly in high pressure applications, giving rise to errors in volume fraction measurements. One technique which has found some success in industrial applications for monitoring gas holdups is the nuclear density gauge technique. This technique is a non–intrusive technique and may be used with systems that operate at high temperatures and pressures.

Overview of Fischer-Tropsch Studies in Bubble Columns

Hydrodynamic studies of direct relevance to Fischer–Tropsch synthesis in slurry bubble column reactors are summarized in Table 1.1. These studies have provided useful information on the effects of superficial gas velocity, distributor design, liquid static height, solid concentration, pressure, gas and wax type, temperature, and column diameter on average gas holdup and to a limited extent on bubble size distribution. However, with the exception of the study conducted by Bukur et al. (1987a), these studies were limited to bubble columns with diameters less than 0.12 m, where the churn–turbulent flow regime could not be achieved. A systematic study of the hydrodynamics of two–phase F–T slurry bubble columns operating in the batch mode (i.e. no liquid circulation) was conducted at Texas A&M University (Bukur et al., 1987a,b,c; Bukur and Daly, 1987; Patel et al., 1990) in 0.05 m ID and 0.23 m ID bubble columns using various types of distributors and waxes. In particular, average and axial gas holdups were obtained together with bubble size distributions. The churn–turbulent flow regime was observed in the large diameter bubble column.

In order to model slurry bubble column reactors, the following hydrodynamic parameters are needed: specific gas–liquid interfacial area; axial solids dispersion coefficients; Sauter mean bubble diameters; axial dispersion coefficients for the gas and liquid; overall heat transfer coefficient between the slurry and immersed heat transfer internals;

Table 1.1. Summary of Bubble Column Hydrodynamic Studies

Investigator	Column ID (m)	u_g (m/s)	ω_s (%)	T (°C)	P (MPa)	Liquid[a]	Quantity Measured
Calderbank et al. (1963)	0.051	0 - 0.055	0	265	0.1	KW	ϵ_g, a_g
Farley and Ray (1964)	0.25	0.03-0.073	13	265	0.15-1.1	KW	ϵ_g
Zaidi et al. (1979)	0.04-0.10	0-0.038	2-14	250-290	1.0	MP	ϵ_g, d_s
Deckwer et al. (1980)	0.04-0.10	0-0.04	0-16	143-270	0.4-1.1	MP	ϵ_g, d_s
Quicker and Deckwer (1981)	0.0.95	0.04	0	130-170	0.1	FT-300	ϵ_g, d_s
Kuo (1985)	0.032,0.053	0-0.05	0	200-230	0.1	FT-200,PW	ϵ_g
"	0.051	0-0.12	"	138-260	0.1-0.2	FT-200,PW	ϵ_g
"	0.102	0-0.065	"	260	0.1-0.2	FT-200,PW	ϵ_g
"	0.026	0-0.035	15	177	0.1-1.15	PW	ϵ_g
Sanders et al. (1986)	0.05	0-0.06	0-30	240	1.0	FT-300,PW	ϵ_g
O'Dowd et al. (1987)	0.022	0-0.02	0	250,280	1.5-2.2	PW,MP	ϵ_g, d_s
Bukur et al. (1987a,b,c)	0.05, 0.23	0-0.15	0	160-280	0.1	FT300,FT200 SASOL,PW	ϵ_g, a_g, d_s

[a] KW-Krupp wax; MP-Molten paraffin wax; PW-Product wax

mass transfer coefficients for all species; gas holdups; and physico–chemical properties of the liquid medium. Axial solids dispersion coefficients have not been measured experimentally in systems with paraffin wax as the liquid medium. A limited amount of experimental data can be found in the literature on some of the other parameters mentioned above.

Mass Transfer Coefficient

Zaidi et al. (1979) measured values of the the volumetric mass transfer coefficient, $k_\ell a_g$, for carbon monoxide in a small bubble column reactor. The mass transfer coefficient, k_ℓ, for carbon monoxide was calculated using the experimentally determined value of the specific gas–liquid interfacial area, a_g. The gas–liquid interfacial area was determined from measurements of the gas holdup and Sauter mean bubble diameter in a non–reacting system. The experimental value for the mass transfer coefficient of carbon monoxide agreed fairly well with the value predicted using the empirical correlations proposed by Hughmark (1967) and Calderbank and Moo–Young (1961).

More recent measurements of volumetric mass transfer coefficients were made using stirred tank reactors (Albal et al., 1984; Ledakowicz et al., 1984; Deimling et al., 1984). Only Deimling et al. determined mass transfer coefficients separately for hydrogen and carbon monoxide. These values agreed with those predicted using the correlation presented by Calderbank and Moo–Young. Thus, it appears that this correlation may be used to estimate mass transfer coefficients in F–T slurry bubble column reactors. Calderbank and Moo–Young's correlation requires an estimate for the Sauter mean bubble diameter, as well as, the physico–chemical properties of the liquid medium (i.e. density, viscosity, and diffusivity).

The physico–chemical properties of F–T derived waxes are available. Solubilities of hydrogen, carbon monoxide, water and carbon dioxide were measured by Peter and Weinert (1955), and subsequently by other investigators (e.g. Calderbank et al., 1963

– hydrogen only; Albal et al., 1984 – hydrogen and carbon monoxide; Ledakowicz et al., 1984 – carbon monoxide; Deimling et al., 1984 – hydrogen and carbon monoxide). Good agreement exists between the data obtained in different studies. Values of the liquid density and viscosity were reported by Calderbank et al., Deckwer et al. (1980), researchers at Mobil (e.g. Gupte et al., 1984), and Bukur et al. (1987a). The values of density are in good agreement, while there is some variation in reported values of the liquid viscosity. The latter is caused by the fact that different waxes were used in the different studies. Apparently, the density does not vary appreciably with wax type. Liquid phase diffusivities of hydrogen, carbon monoxide, water and carbon dioxide were determined by Peter and Weinert (1955). Rodden (1988) and Rodden et al. (1988) measured the diffusion coefficients for several dilute solutes in Fischer–Tropsch wax.

Heat Transfer Coefficient

In F–T slurry bubble column reactors, internal heat transfer rods are used to maintain a constant temperature inside the reactor. The heat transfer coefficient between internal heat transfer rods and the slurry was determined by Deckwer et al. (1980). Deckwer et al. conducted experiments in a 0.10 m ID bubble column using paraffin wax as the liquid medium and up to 16 wt% alumina particles (less than 5 μm) as the solid phase.

Additional experimental studies in a larger diameter column with heat transfer internals are needed to minimize the risks in bubble column reactor scale–up. The effect of heat transfer internals on average gas holdup, bubble size distribution, and solids mixing needs to be determined for bubble columns which operate in the churn–turbulent flow regime.

Gas Holdup and Bubble Size Distribution

Average gas holdup in paraffin wax systems have been studied by several investigators. Calderbank et al. (1963) measured gas holdup and specific gas–liquid interfacial

area in a 0.05 m ID column using a ball and cone distributor with Krupp wax as the liquid medium. The experiments were conducted at a temperature of 265 °C for gas velocities up to 0.055 m/s. Gas holdups from this study varied linearly with gas velocity, with gas holdups reaching approximately 0.2 at a gas velocity of 0.055 m/s. The specific gas–liquid interfacial area increased significantly with increasing gas velocity for gas velocities less than 0.03 m/s. For gas velocities greater than 0.03 m/s, the specific gas–liquid interfacial area remained fairly constant ($\approx$ 400 m^2/m^3).

Deckwer et al. (1980) examined the effects of column diameter (0.041 m and 0.10 m), superficial gas velocity (up to 0.04 m/s), temperature (143 – 285 °C), pressure (400–1100 kPa) and solids concentration (up to 16 wt%) on gas holdup using a hard paraffin wax as the liquid medium. Both columns were equipped with a 75 μm sintered metal plate distributor. In their experiments, gas holdup was independent of temperature for temperatures greater than 240 °C, column diameter and pressure, and it decreased slightly with the addition of solids. The gas holdups obtained in this study were higher than those predicted using existing literature correlations, as well as those obtained in the Calderbank et al. study. Deckwer et al. also determined the Sauter mean bubble diameter using photography in a 0.05 m ID glass column. The Sauter mean bubble diameter was found to be independent of gas velocity and was approximately 0.7 mm. The Sauter mean bubble diameter and gas holdup were used to estimate the specific gas–liquid interfacial area. The interfacial area was approximately three times greater than that obtained in the study by Calderbank et al.

Quicker and Deckwer (1981) studied the effect of distributor design on gas holdup and Sauter mean bubble diameter in a 0.095 m ID column at temperatures of 130 °C and 170 °C. In their study, there was no effect of distributor type on bubble size; however, higher holdups were obtained with a single nozzle distributor (0.9 mm in diameter) than with a perforated plate distributor (19 holes x 1.1 mm in diameter). The holdups from

this study with the single nozzle distributor were also higher than the holdups obtained in the study by Deckwer et al. (1980) with the 75 μm distributor.

Researchers at Mobil (Smith et al., 1984; Kuo, 1985) have conducted a comprehensive study of this system. They reported results illustrating the effects of distributor type, liquid static height, wax type, operating conditions, gas type, and column diameter on average gas holdup. Wax type, distributor design, and temperature had a significant effect on gas holdup in their study. For experiments with sintered metal plate distributors, the effect of liquid static height was very pronounced, with higher holdups (up to 0.70) being observed as the liquid static height was decreased. The column diameter (0.032 – 0.12 m) had some effect on gas holdup, while the effects of pressure (0.1 to 1.48 mPa) and gas type (nitrogen, hydrogen, or hydrogen/carbon monoxide mixtures) on gas holdup were negligible. The bubbles produced by the orifice plate distributors were non–uniform in size and larger than the ones produced by the sintered metal plate distributors; however, bubble sizes were only reported for experiments conducted at low superficial gas velocities. The gas holdups from Mobil's studies with the sintered metal plate distributors were higher than those reported by Deckwer et al. (1980); whereas, the holdups obtained from the orifice plate distributors were lower than those reported by Deckwer et al.

Also, a systematic study of this system (two–phase) has been conducted in our laboratory (Bukur et al., 1987a,b; Bukur and Daly, 1987). Experiments were conducted in 0.05 and 0.23 m ID columns approximately 3 m in height using nitrogen as the gas phase and both FT–300 wax and various reactor waxes (primarily in the 0.05 m ID column) as the liquid medium. In experiments in the small diameter column (FT–300 wax) with the 40 μm sintered metal plate distributor and with 2 and 4 mm orifice plate distributors it was found that for a given temperature in the range 230 – 280 °C, there is a range of superficial gas velocities where one can have two values of gas holdup (Bukur

et al., 1987a,b, Bukur and Daly 1987). The higher holdups are caused by the existence of a stable foam layer which exists at the top of the dispersion, and this is referred to as the "foamy" regime. In the slug flow regime, gas holdups are significantly lower than those observed in the foamy regime (i.e. approximately one half). In experiments conducted with reactor waxes (SASOL and Mobil) the foamy regime was not observed.

These findings may be used to explain the discrepancies reported in the previously reported values of gas holdup. If the data from different experiments are grouped together according to flow regime type, then they are well represented by two curves (one for the "foamy" flow regime and one for the slug flow regime (Bukur et al., 1987b).

The existence of the foamy flow regime has also been observed in the large diameter column with FT–300 wax at 265 °C (Bukur and Daly, 1987). However, the difference in gas holdups between the "foamy" and churn–turbulent regime is significantly less, and foam breakup usually occurs between gas velocities of 0.03 and 0.05 m/s. Foam was not observed during experiments at 200 °C. This was attributed to the fact that at lower temperatures, the viscosity of the liquid is greater which enhances bubble coalescence. Similar results (i.e. the effect of increasing viscosity on gas holdup) has been reported by others.

Bubble sizes were also measured in our laboratory (Patel et al., 1990; Bukur et al., 1987a,b) using various wax types in the 0.05 m ID column and with FT–300 wax in the 0.23 m ID column using both photography and the dynamic gas disengagement technique. Results obtained from the two techniques were comparable. Sauter mean bubble diameters in both the small diameter column and large diameter column with FT–300 wax were approximately 0.8 mm at gas velocities greater than 0.04 m/s. This value is in good agreement with the value of 0.7 mm reported by Deckwer et al. (1980). However, Sauter mean bubble diameters for reactor waxes were significantly higher (Bukur et al., 1987a,b). The Sauter mean bubble diameter for SASOL wax in the 0.05

m ID column approached a value of 2 mm at gas velocities greater than 0.05 m/s and for Mobil reactor wax in the 0.05 m ID column, the Sauter mean bubble diameter approached a value of 4 to 5 mm. Sauter mean bubble diameters estimated from the gas holdups and interfacial areas reported by Calderbank et al. (1963) range from approximately 3 to 5 mm. The important conclusion from our studies is that similar gas holdups do not imply similar Sauter mean bubble diameters.

Flow Regime Characterization

As mentioned previously, the majority of Fischer–Tropsch hydrodynamic studies have been conducted in small diameter columns where only the homogeneous bubbly and slug flow regimes occur. In the studies by Deckwer et al. (1980) and Quicker and Deckwer (1981), the bubble size distribution was found to be fairly uniform for the gas velocities (< 0.04 m/s) employed in their studies. A uniform bubble size distribution is characteristic of the homogeneous bubbly flow regime. In experiments conducted at Texas A&M (Bukur et al., 1987a) and by researchers at Mobil (Kuo, 1985) in 0.05 m ID columns, it was observed that slugs start developing between gas velocities of 0.02 and 0.03 m/s.

Experiments conducted at Texas A&M by Bukur et al. (1987a) in a 0.23 m ID glass column revealed that the homogeneous bubbly regime exists at gas velocities up to 0.02 m/s, and the churn–turbulent flow regime was observed at higher gas velocities (up to 0.15 m/s). The churn–turbulent flow regime was characterized by a wide bubble size distribution, with bubbles ranging in size from less than 1 mm to greater than 100 mm in diameter.

Effect of Solids

There have been very few studies on the effect of solids on hydrodynamic parameters in bubble columns with wax as the liquid medium. Deckwer et al. (1980) examined the effect of solids (up to 16 wt%) on gas holdup in a 0.10 m ID bubble column. Their

work showed than the presence of solids causes a slight decrease in the gas holdup; however, they did not observe any difference in the gas holdup between solids loadings of 5 and 16 wt %. Researchers at Mobil (Kuo, 1985) monitored solids concentrations in a 0.05 m ID by 9 m tall Fischer–Tropsch slurry bubble column reactor. In some of their studies, they observed catalyst settling near the distributor which resulted in a non–uniform temperature distribution. Non–uniform catalyst distribution may have a detrimental effect on bubble column reactor performance as shown by Bukur and Kumar (1986). Since Fischer–Tropsch slurry bubble column reactors are characterized by low space–time yields due to low catalyst concentrations, it is necessary to determine the upper limit of catalyst concentration. This has not been investigated in a systematic way.

Smith et al. (1984) determined the axial solids dispersion coefficient for ethanol–water mixtures. They found that under foamy conditions (1.8 wt% ethanol) the axial dispersion coefficient was significantly lower than that under nonfoamy conditions (pure water). Since Fischer–Tropsch derived paraffinic waxes have a tendency to foam, it is possible that under foamy conditions, catalyst distribution profiles may be significantly greater than those under nonfoamy conditions.

Effect of Liquid Velocity

During Fischer–Tropsch synthesis, high molecular weight compounds (reactor wax) are formed. As these compounds are formed, they remain in the reactor and as a result, there is a continuous increase in the slurry volume with time on stream. Thus, during actual operations, some of the slurry must be removed without loosing much of the dispersed catalyst. Researchers at Mobil (Kuo, 1985) accomplished this by withdrawing slurry from the reactor and transferring it to a catalyst/wax separation unit where the slurry was separated into two streams. The stream with high catalyst concentration was returned to the reactor and the stream with low catalyst concentration (less than 1 wt%

solids) was sent to a filtration system for separation. The effect of slurry removal and return of concentrated slurry to the reactor may be simulated in a non–reacting system by using a continuous slurry flow. No studies of this nature have been conducted in bubble columns with paraffin derived waxes as the liquid medium.

This may have a pronounced effect on gas holdup in bubble columns with foaming systems as shown by Shah et al. (1985). Shah et al. studied the aqueous ethanol mixture and observed that a small upward liquid flow (0.0077 m/s) was sufficient to significantly reduce the gas holdup (e.g. at u_g =0.15 m/s ϵ_g= 0.80 in the absence of liquid flow and ϵ_g=0.2 with $u_{s\ell}$ = 0.0077 m/s).

Overview of Nuclear Density Gauge Studies

With an increase in the utilization of multiphase reactor systems, there is a need to develop techniques or methods to measure various component properties. In order to properly design and scale–up multiphase reactors such as fluidized beds and bubble columns, hydrodynamic parameters (e.g. gas hold–up, bubble size distribution, solids concentration profiles, and flow regime transitions) are needed. Many fluidized beds and bubble columns operate at high pressures and high temperatures and extrapolation of results obtained at lower pressures and lower temperatures may not be warranted. Therefore, there is a need to develop techniques which may be used to measure hydrodynamic parameters at operating conditions. Another problem that exists with conventional techniques that are currently used to measure some of these properties is the fact that the system is disturbed either by altering the gas and/or liquid flow rates or removing samples of the slurry. Therefore, it would be advantageous to design a system which is capable of obtaining hydrodynamic parameters without interfering with the reaction environment. An attractive technique for measuring holdups and flow regime transitions is radiation absorption.

Radiation absorption has been used since the early 1950's. It was first used to measure liquid levels in opaque tanks. Two different types of methods were used: (1) A radioactive source was allowed to float on the liquid surface, and a detector was placed on the outside of the vessel. (2) A beam of radiation located from a source on the outside of the vessel was passed through the vessel to a detector on the opposite side. A change in the amount of radiation absorbed by the detector indicated the top of the liquid level (Gibson et al., 1957). The second method is capable of providing more information than just the liquid level. The amount of radiation that is absorbed as it passes through a medium is a function of several things including the mass of the medium. Through proper calibrations, one can obtain mean densities or void fractions of the various components which comprise the medium. A device such as the second one is called a nuclear density gauge. Nuclear density gauges have been used in numerous two–phase studies; however, each of these studies, with the exception of one, were directed towards studying a particular property.

The majority of previous investigations which utilized gamma–ray absorption were conducted in two–phase fluidized beds and are summarized in Table 1.2. Bartholemew and Casagrande (1957) used Cobalt–60 to measure radial solids concentration profiles in a two–phase fluidized system. Fan et al. (1962) measured axial density profiles in a fluidized bed using gamma–ray absorption. El Halwagi and Gomezplata (1967) also used a nuclear density gauge to measure the solids concentration in a fluidized bed. Baumgarten and Pigford (1960) used Thalium–170 to study density fluctuations in a fluidized bed. Their measurements allowed bubble size, frequency and velocity to be determined. Orcutt and Carpenter (1971) used a dual energy nuclear density gauge (Cesium–137 and Cobalt–60) to measure steady state bubble coalescence. From their measurements, they were able to determine bubble diameters. Gidaspow et al. (1983) utilized a movable nuclear density gauge to obtain density profiles in a fluidized

Table 1.2. Summary of Nuclear Density Gauge Studies

Investigator	Source	System
Bernatowicz et al. (1987)	Cesium–137 Americium–241	3–phase, 1 inch pipe phase fractions and bubble length
Weimer et al. (1985)	Cesium–137	2–phase fluidized bed, 0.292 m cast acrylic and 0.128 m steel hold–up, bubble size, bubble velocity, bubble frequency
Gidaspow et al. (1983)	Cesium–137	2–phase fluidized bed, .40 by 0.0381 m bed porosity distributions above gas jets
Abouelwafa and Kendall (1980)	Barium–133 Cobalt–57 Radium–226	3–phase, no flow, 10 cm thick volume fractions
Lassahn (1975)	Cesium–137	2–phase vertical pipe 16 mm, bubble flow rate
Orcutt and Carpenter (1971)	Cesium–137 Cobalt–60	2–phase fluid bed, bubble coalescence
Basov et al. (1969)	Cesium–137	2–phase, height of gas jets
Farley and Ray (1964)	Cesium–137	3–phase bubble column (0.247 m ID), gas hold–up
Baumgarten and Pigford (1960)	Thulium–170	2–phase fluid bed 3 x 6 inch, density fluct
Bartholemew and Casagrande (1957)	Cobalt–60	2–phase 20.4 in catalyst riser, catalyst density
Gibson et al. (1957)	Cesium–137	3–phase 10 in BC, gas hold–up

bed. As is evident, the majority of the previous studies were directed toward studying a certain aspect or property of two–phase fluidized beds. However, Weimer et al. (1981) measured expanded bed height , dense phase voidage, dense phase superficial gas velocity, bubble volume fraction, bubble size, and bubble frequency using a single source (Cesium–137) nuclear density gauge. Their study dealt primarily with the performance of the density gauge system and the techniques used to analyze data obtained from the nuclear density gauge.

Nuclear density gauges have also been used for studies involving bubble column reactors. Gibson et al. (1957) used gamma–ray absorption to determine the liquid level in a batch operated two–phase bubble column operating between 160 and 250 °C and pressures between 3 and 20 atm. Farley and Ray (1964) used a single source nuclear density gauge to measure axial gas hold–up and density profiles in a three–phase bubble column reactor. They treated a three–phase system as a two–phase system by assuming that the liquid and solid phases remained in the same proportions throughout the entire column.

Abouelwafa and Kendall (1980) proposed the concept of using a dual source nuclear density gauge to measure component fractions in three–phase systems. They reported results for component fractions in a three–phase liquid–liquid–gas pipeline. The difference between measured component fractions and known component fractions was small. Bernatowicz et al. (1987) used a dual source nuclear density gauge to monitor in real–time the ratio of solids to liquid to gas in a process stream at the Solvent Refined Coal facility in Wilsonville, Alabama. They were not only able to monitor changes in the process stream, but they were also able to determine bubble lengths in the stream. A nuclear density gauge has also been used to measure the slurry density in LaPorte's liquid phase methanol reactor (0.572 m in diameter) operated by Air Products (Tsao, 1984).

Seo and Gidaspow (1987) have used a dual energy nuclear density gauge to measure volume fractions in a three–phase two–dimensional fluidized bed (2.54 cm wide). They used a Cs–137 source and an X-ray source to measure the volume fraction of solids (two types) and gas.

The results obtained by Abouelwafa and Kendall (1980), Bernatowicz et al. (1987), and Seo and Gidaspow (1987) indicate that dual source nuclear density gauges can provide information regarding component fractions and bubble lengths in three–phase systems. However, a systematic study of the use of dual energy nuclear density gauges in large diameter three–phase systems, including further applications and means of analysis is needed.

Objectives of This Study

As shown above, very few hydrodynamic studies of direct relevance to the Fischer–Tropsch synthesis have been conducted in large diameter columns which are of practical industrial importance. One of the goals of this research is to conduct a systematic study of the effect of solids type, size and concentration and superficial liquid flow rate on gas holdup and solids concentration profiles in a relatively large diameter column (0.21 m ID) in the churn–turbulent flow regime. Another goal of this project is to assess the possibility of using a dual energy nuclear density gauge to measure volume fractions in a large diameter bubble column. Also, an attempt will be made to obtain information regarding bubble size distribution and flow regime transitions. The results from this study should provide useful information necessary to properly design and scale–up large diameter bubble column reactors for Fischer–Tropsch synthesis, as well as, information on the applicability of dual energy nuclear density gauges for determination of hydrodynamic parameters in large diameter multiphase systems.

CHAPTER II

MEASUREMENT OF GAS HOLDUPS BY CONVENTIONAL TECHNIQUES

Gas holdups and solids concentration profiles were measured using conventional techniques. In particular, gas holdup was calculated from visual observations of the expanded and static liquid height in the glass columns, and from measurements of differential pressures and solids concentrations in the stainless steel columns. The experimental apparatus, operating conditions, data reduction procedures, and results from both two–phase and three–phase experiments are described below. Also, empirical correlations which may be used to predict overall (or average) gas holdup in a Fischer–Tropsch slurry bubble column reactor will be presented.

Experimental Apparatus and Operating Procedure

Figure 2.1 is a schematic representation of the slurry bubble column apparatus which was constructed for these studies. The majority of experiments were conducted in 0.05 and 0.21 m ID by 3 m tall stainless steel columns. Experiments in both the batch mode (i.e. without slurry circulation) and continuous mode (i.e. with slurry circulation) of operation were conducted in the stainless steel columns. Five pressure transducers (Valydine Model DP 15) and five slurry sampling valves (1/4" Whitey ball valves) with pneumatic actuators were located along the column (see the Figure on page 33 for their locations).

The flow rate of prepurified nitrogen from gas cylinders was measured and controlled by a Brooks Model 5816 mass flow meter for experiments conducted in the 0.05 m ID column. A Sierra Series 840 mass flow meter was used to measure the gas flow rate during experiments conducted in the 0.21 m ID column. For the 0.21 m ID column, the flow rate was controlled manually by adjusting the outlet pressure from the nitrogen cylinder (cryogenic). Prior to each series of experiments, the mass flow

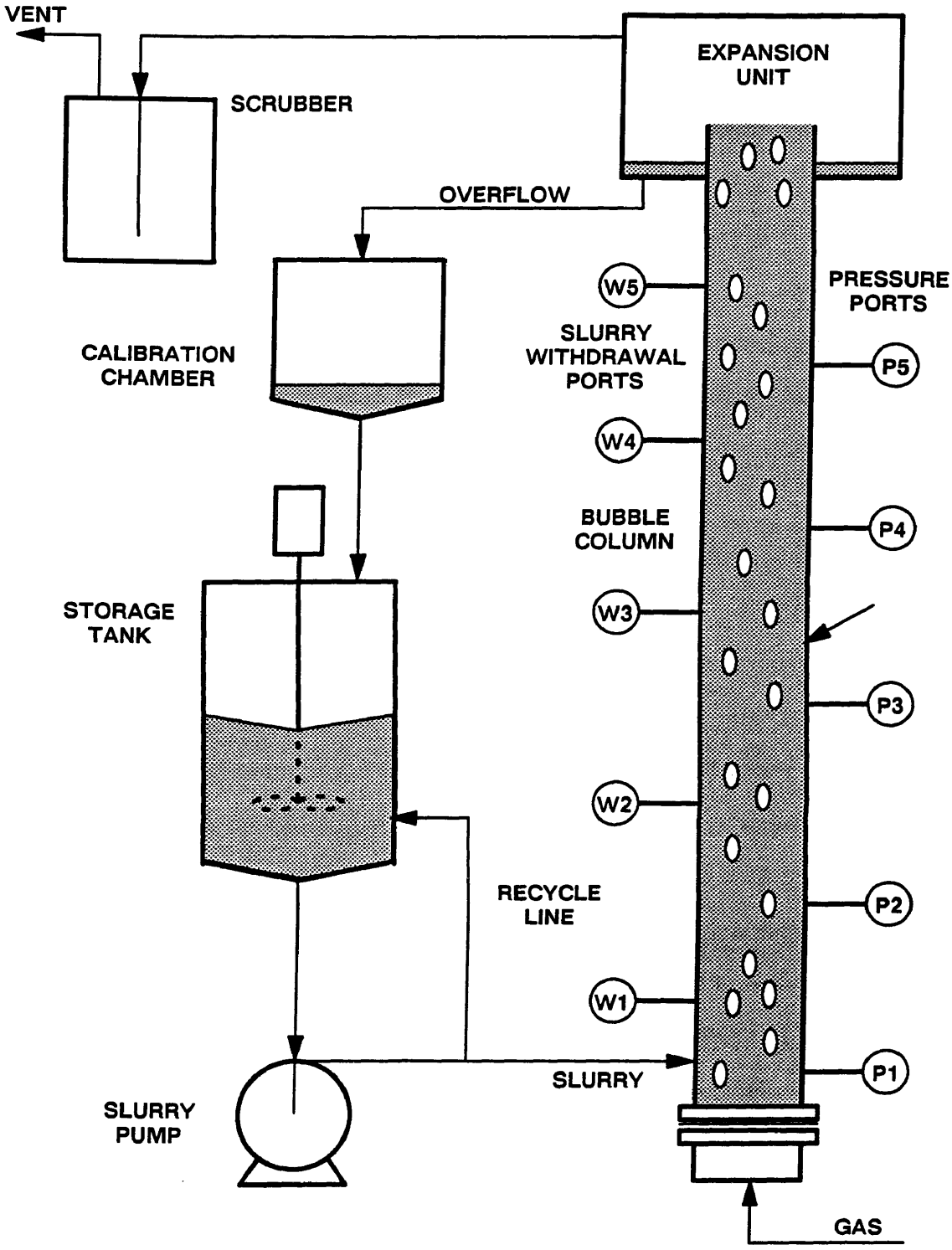

Figure 2.1. Schematic of the slurry bubble column apparatus.

meters were calibrated. The Brooks mass flow meter was calibrated using a wet test meter, and the Sierra mass flow meter was calibrated using a flow prover (i.e. an orifice meter). The metered gas entered the bubble column through the distributor which was located between two flanges at the bottom of the column. For experiments in the 0.21 m ID column, the gas was passed through an electrically heated U–shaped preheater before entering the column at the distributor. The gas inlet temperature was manually controlled using two variable voltage transformers. The temperature of the gas was monitored by three thermocouples (one located in the middle of the preheater – 0.21 m ID column only; one located after the preheater; and one located just below the distributor). The thermocouples were connected to an Omega (Model 199) ten channel temperature indicator.

The wax was charged in the storage tank and the tank was electrically heated to bring the wax to the desired temperature. The wax storage tank for the large diameter column was 0.61 m in diameter and 0.91 m long; and the wax storage tank for the small diameter column was 0.3 m in diameter and 0.46 m long. The slurry inlet systems for the large and small diameter columns are shown in Figures 2.2 and 2.3, respectively. Once the solid wax was melted ($\approx$ 150 °C), the stirrer was switched on to improve the heating process. For experiments conducted with solids, the solids were added to the storage tank once the wax was at the desired temperature (220 °C for batch experiments and 265 °C for continuous experiments). The column was heated to the desired operating temperature (265 °C) before the slurry was introduced. The column temperature was controlled using two temperature controllers, one for the bottom half of the column and one for the top half of the column. For all experiments, batch and continuous, the wax was transported to the column using a slight nitrogen overpressure in the storage tank. For the continuous mode experiments, the pump (Pulsafeeder, Model G12 – 0.05 m ID column; Tuthill Corporation, Model 3A – 0.21 m ID column) was not switched on

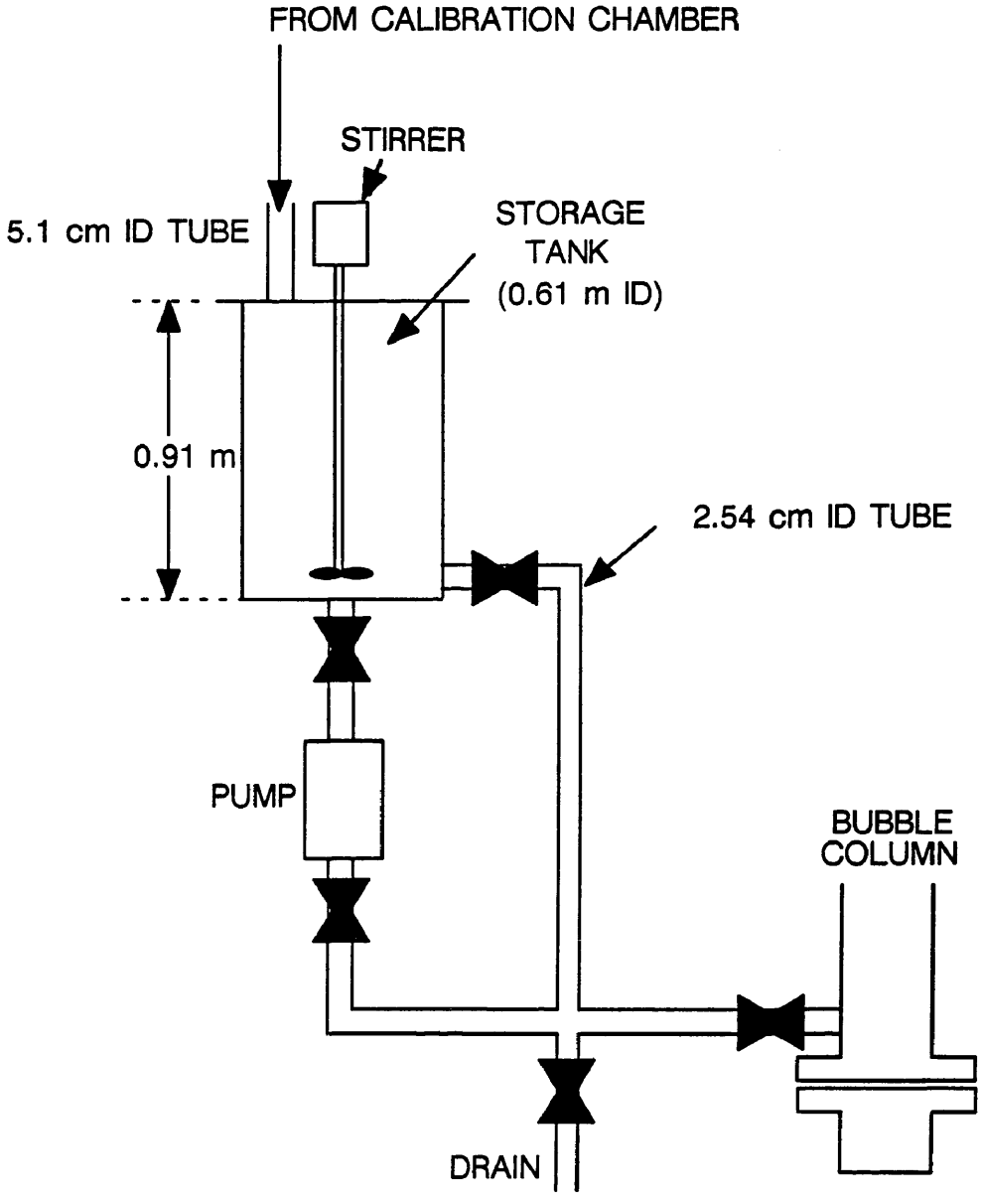

Figure 2.2. Schematic representation of the slurry inlet system for the large diameter stainless steel column.

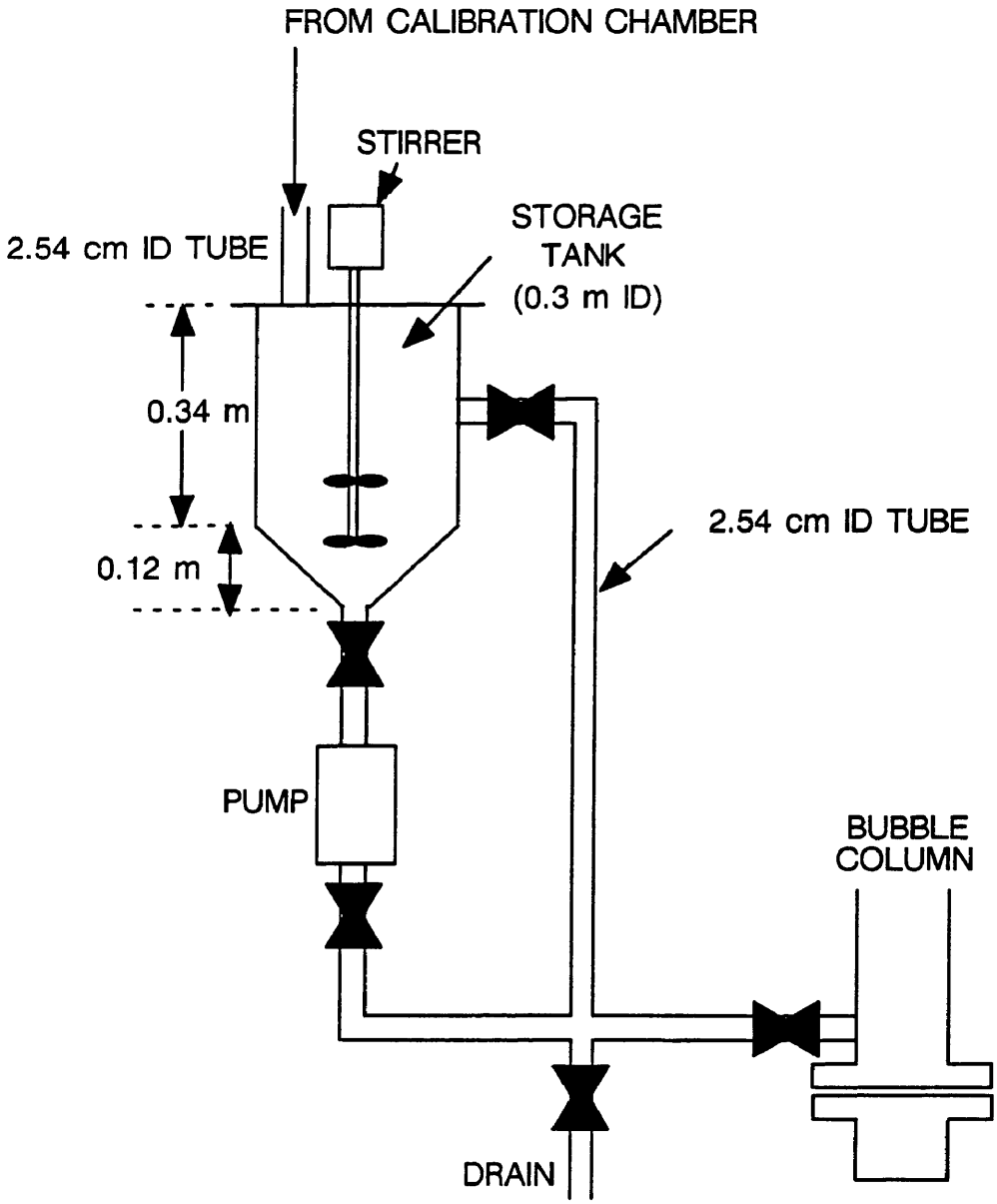

Figure 2.3. Schematic representation of the slurry inlet system for the small diameter stainless steel column.

until the column was at least half filled with wax. This was done to prevent clogging of the pump by solids which might have settled in the storage tank. Throughout the preheating period and during the transportation of wax to the column, nitrogen flowed through the column. Once the wax was in the column, the temperatures of the various units were allowed to stabilize before the actual run was started. For experiments in the batch mode of operation, only the column was maintained at the desired operating temperature. The exit lines and expansion unit were maintained at a temperature of approximately 200 °C. The hot gas leaves the separator and passes through the scrubber which is filled with Varsol (mineral spirits), before it is vented to the atmosphere. The scrubber is used to recover components of the wax that evaporate from the column and is maintained at approximately 70 °C. The lines connected to the pressure transducers and slurry sampling valves were maintained at 200 °C. For experiments in the continuous mode of operation, all lines and vessels carrying the slurry were maintained at the operating temperature. The remaining temperatures were the same as those used for batch experiments. All temperatures were monitored regularly, every half hour during the preheat period and every hour during the experiment.

Once the column reached the desired temperature, the experiment was initiated. Superficial gas velocities in the range 0.02 – 0.12 m/s were employed in all runs. A duration of at least one and a half hours was used for each velocity. Pressure measurements were made three times for every gas velocity (i.e. approximately every half hour), with the first measurement made one half hour after the gas velocity was changed. Slurry samples were withdrawn at the five different locations after the final pressure measurement. The gas flow rate was then changed to the next setting. For experiments conducted in the continuous mode of operation, the superficial slurry velocity was monitored using the calibration chamber. The calibration chamber for the large diameter column was a 0.46 m ID cylindrical tank with an internal volume of approximately

50000 cm^3, and for the small diameter column, the calibration chamber was a 0.23 m ID cylindrical tank with an internal volume of approximately 4000 cm^3. Figures 2.4 and 2.5 are schematic representations of the circulation loops associated with the large and small diameter columns, respectively. The desired slurry flow rate was set by varying the pump speed, and slurry flow rate checks were made prior to each pressure reading (i.e. three times per gas velocity).

For three–phase experiments, slurry samples were withdrawn from the storage tank at the beginning and end of each experiment; as well as, at the end of each gas velocity for experiments conducted in the continuous mode of operation. In order to determine the volume of slurry in the storage tank, a dipstick, similar to that used to determine the oil level in an automobile, was designed (see Figure 2.6). The dipstick assembly consisted of a casing (2.54 cm diameter tube), which was welded to the lid of the storage tank, and the dipstick (0.635 cm diameter shaft). The casing extended half way into the storage tank and had vent holes at the top to allow any gas which might be trapped in the casing to disengage.

Following the completion of a run, the slurry was withdrawn into the storage tank using a slight vacuum (the pump was switched off for runs conducted in the continuous mode of operation). After each run, solids and wax inventories were made to check for any losses, particularly losses in solids due to settling in the various lines and process vessels. Solids and wax inventories are discussed in Chapter IV.

Following the completion of a series of experiments, the bubble column apparatus was cleaned (see Appendix A for a description of the cleaning procedure). Any slurry which may have remained in the system was collected and weighed, so that an overall mass balance (solids + wax) could be obtained (see Chapter IV).

Two–phase experiments were also conducted in two columns (0.05 m ID and 0.23 m ID by 3 m tall) made of borosilicate glass. A detailed description of these columns has

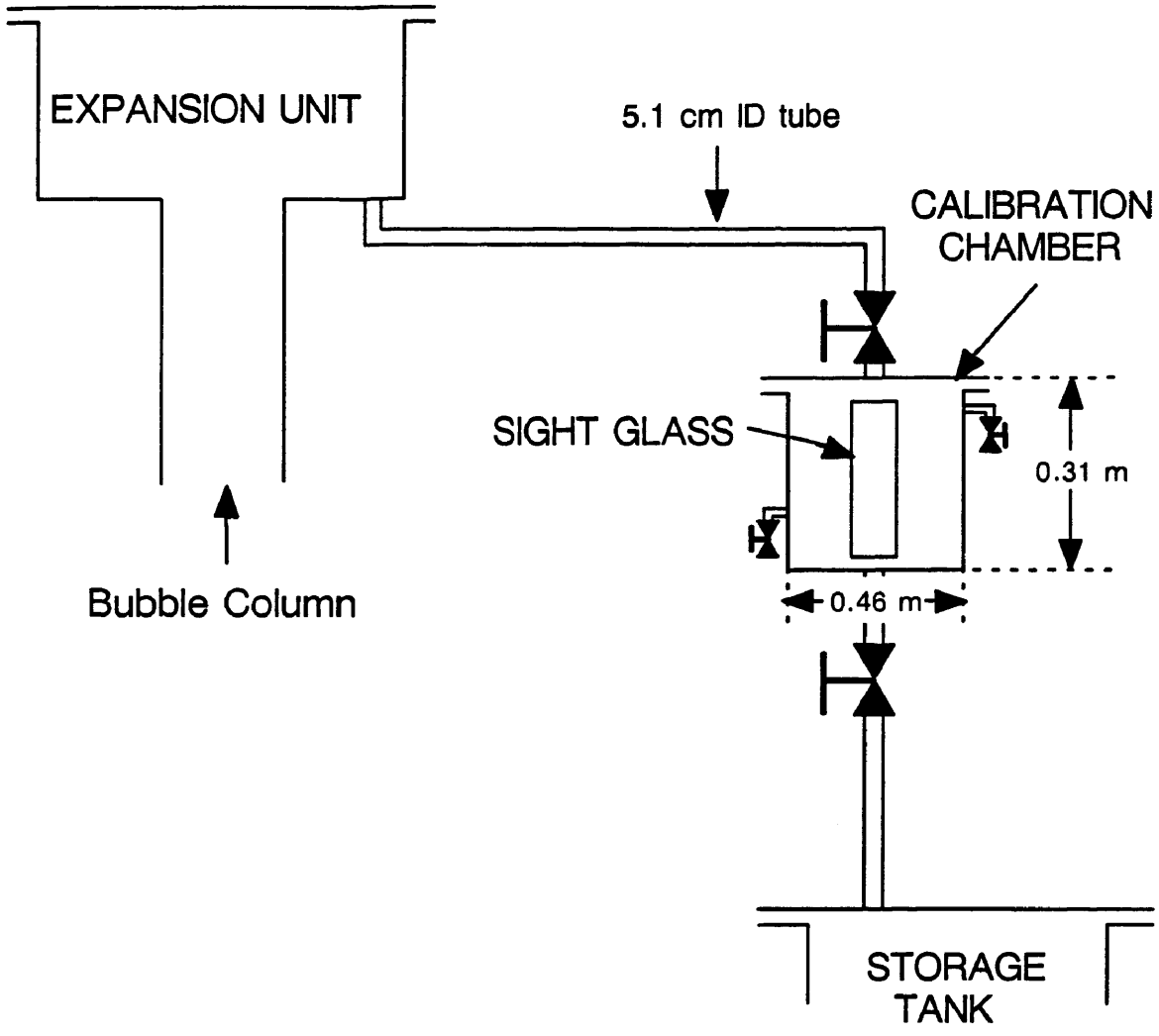

Figure 2.4. Schematic representation of the circulation loop for the large diameter stainless steel column.

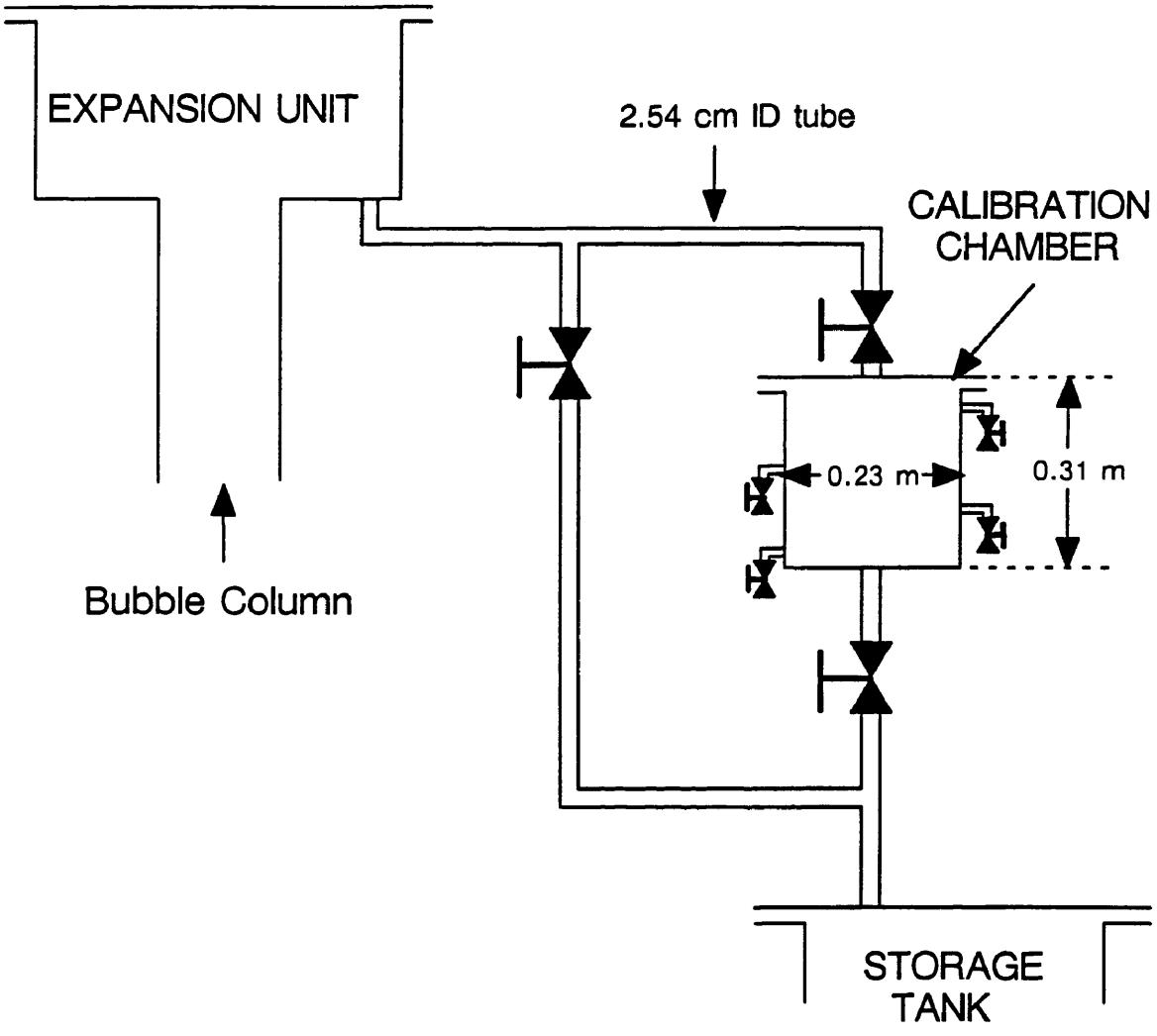

Figure 2.5. Schematic representation of the circulation loop for the small diameter stainless steel column.

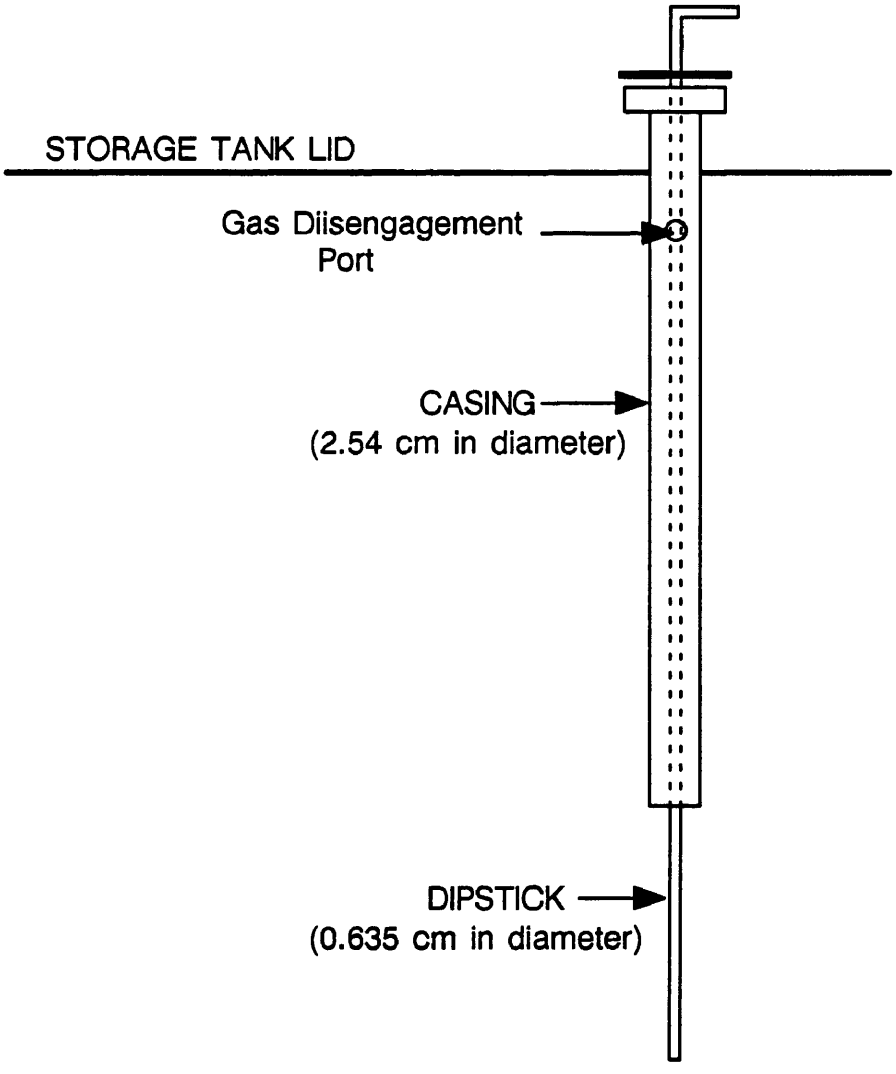

Figure 2.6. Schematic representation of the dipstick assembly.

been given elsewhere (Bukur et al., 1987a,b,c). All experiments in the glass columns were conducted in the batch mode of operation. The glass columns were used to obtain average gas holdups and bubble size distributions. Average gas holdups obtained from two–phase studies in the glass columns will be compared to average gas holdups measured in the stainless steel column.

Experimental Conditions

The effects of operating conditions (slurry and gas superficial velocity and temperature), gas distributor design, column diameter, and solids concentration, type, and size were studied. Table 2.1 summarizes the experimental conditions employed in the stainless steel bubble columns. Experiments were conducted with SASOL's Arge reactor wax and FT–300 wax. SASOL reactor wax consists of high molecular weight products of the Fischer–Tropsch synthesis. FT–300 wax (also known as SH–105) is a hard paraffin wax obtained by hydrotreating and fractionation of reactor wax and it has an average molecular weight of 730 (Dura Commodities, New York).

Nitrogen was used as the gas for all experiments because it is inert, non–toxic, and inexpensive. Also, in earlier studies, it was found that the effect of gas type on the average gas holdup is small (Deckwer et al., 1980; Kuo, 1985). Superficial gas velocities in the range 0.02 – 0.12 m/s were employed in all experiments. With this range of gas velocities in the two columns, all important flow regimes were observed. A superficial gas velocity of 0.095 m/s was employed in the Rheinpreussen demonstration plant unit (Kolbel and Ralek, 1980), and thus, the higher velocities (0.08 – 0.12 m/s) chosen in this study are representative of gas velocities employed in large diameter reactors.

All of the experiments in the stainless steel bubble columns were conducted at a temperature of 265 °C, which is a typical temperature for the Fischer–Tropsch synthesis with precipitated iron catalysts. Also, some experiments were conducted in the small

Table 2.1. Bubble Column Dimensions and Experimental Conditions

COLUMN DIMENSIONS		
DIAMETER (m)	0.05	0.21
HEIGHT (m)	3.0	3.0
GAS DISTRIBUTOR	2 mm ORIFICE	PERFORATED PLATE BUBBLE CAPS
GAS	NITROGEN	NITROGEN
LIQUID	FT-300 and SASOL	FT-300 and SASOL
SOLIDS	IRON OXIDE (< 44 μm)	IRON OXIDE (< 44 μm)
	SILICA (< 44 μm)	SILICA (< 44 μm)
VARIABLES		
PRESSURE (atm)	1	1
TEMPERATURE (^{o}C)	265	265
SUPERFICIAL GAS VELOCITY (m/s)	0.02 - 0.12	0.02 - 0.12
LIQUID UPFLOW VELOCITY (m/s)	0.0 - 0.02	0.0 - 0.02
SOLIDS CONCENTRATION (wt%)	0 - 30	0 - 30

diameter glass column at other temperatures (160 – 280 °C). The temperature was varied in order to study the effect of liquid viscosity on overall holdups.

A 2 mm single hole orifice plate distributor was used for experiments conducted in the 0.05 m ID column. Whereas, for experiments in the 0.21 m ID column, both a 19 x 2 mm perforated plate and bubble cap distributor were used (see Figures 2.7 and 2.8, respectively). Perforated plates and bubble caps are commonly used in slurry bubble columns.

Solids concentrations in the range 0 – 30 wt% were employed throughout this work. This range of concentrations encompasses the range of catalyst concentrations used in slurry bubble column reactors for Fischer–Tropsch synthesis. Iron oxide particles (0 – 5 μm and 20 – 44 μm) were used as the primary solid. Some experiments were also conducted with silica particles (0 – 5 μm and 20 – 44 μm) to study the effect of solid density on the hydrodynamics of the system. The two types of solids used, iron oxide and silica, simulate typical catalysts and supports, respectively, employed in Fischer–Tropsch synthesis.

Data Acquisition and Reduction Procedures for Gas Holdups and Solids Concentration Profiles

Average gas holdups, axial gas holdups, and axial solid concentration profiles were measured experimentally. Experiments in the glass column were limited to two–phase (i.e. liquid/gas systems) batch studies; whereas, experiments in the stainless steel columns were conducted using both two–phase and three–phase systems with and without slurry circulation.

Average Gas Holdup – Glass Columns

For experiments conducted in the glass columns, only average (or overall) gas holdups were measured. The average gas holdup, which is the volume fraction of

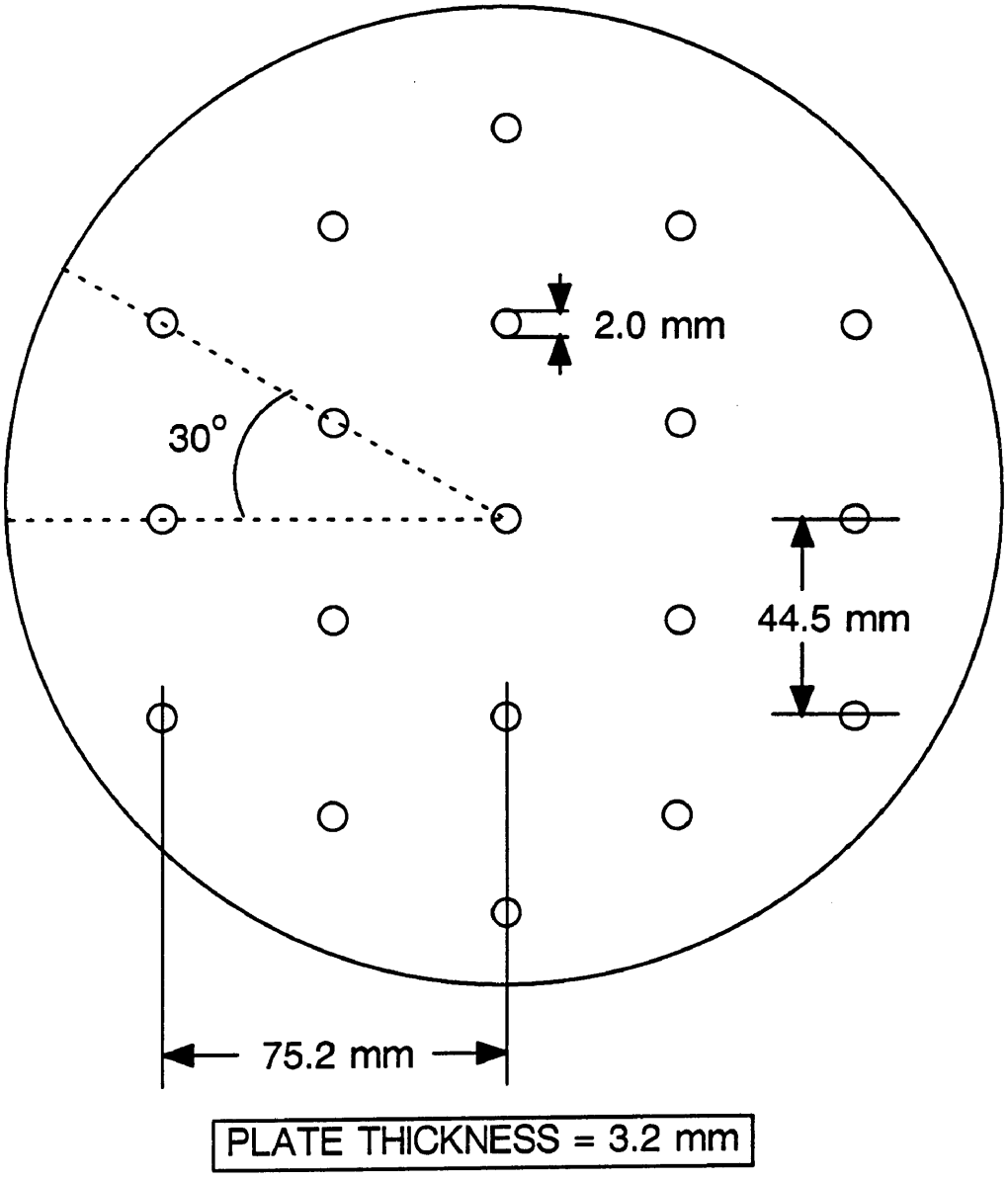

Figure 2.7. Schematic representation of the perforated plate distributor.

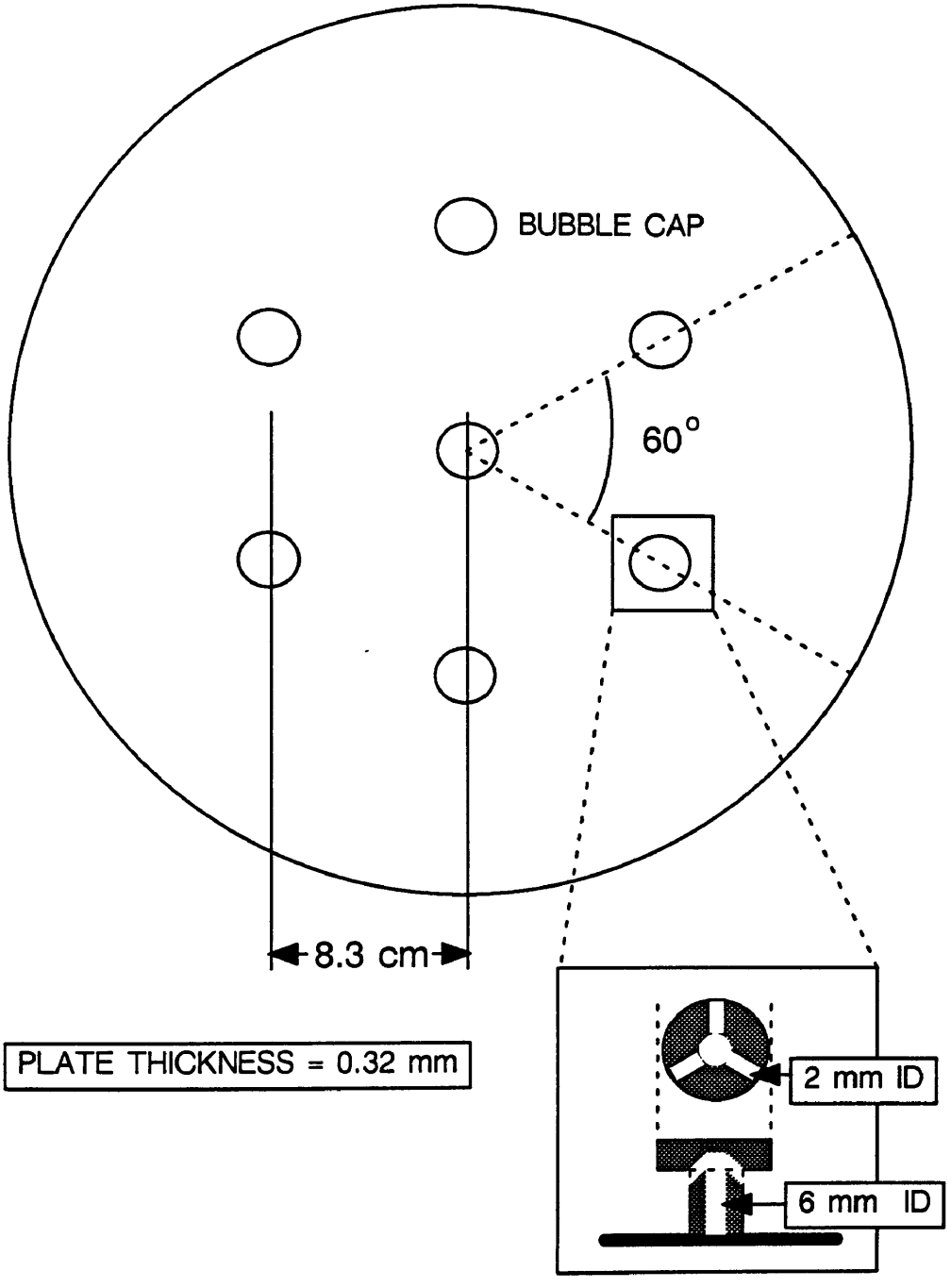

Figure 2.8. Schematic representation of the bubble cap distributor plate.

gas in the suspended slurry, is calculated from visual observations of the expanded and static liquid heights, i.e.

$$\epsilon_g = 1 - \frac{h_s}{h_{exp}} \tag{2.1}$$

where h_s is the static liquid height and h_{exp} is the expanded height of the slurry, and the quantity h_s/h_{exp} is the volume fraction of liquid in the gas/liquid dispersion. The expanded height was recorded three times per gas velocity at intervals of approximately 30 minutes. Once the expanded height was recorded three times, the gas flow was shut off and the static liquid height was recorded.

Phase Fractions – Stainless Steel Columns

In the stainless steel columns, axial gas holdups, axial solids concentrations, and average gas holdups were obtained. Axial pressure measurements and axial solids concentrations were used to calculate gas holdups (average and axial). Figure 2.9 is a schematic representation of the locations of the five pressure transducers and five slurry sampling ports.

Pressure Measurements

During experiments in the stainless steel columns, the pressure drop across the column and the weight fractions of solids were measured at various axial locations. A purgeless pressure transducer system was designed which prevents hot slurry from coming in contact with the DP cell (see Figure 2.10). The system consisted of a 0.635 cm diameter tube attached to the column wall and a 20 cm^3 chamber. When the column is filled with slurry, the nitrogen trapped in the chamber serves as a buffer between the hot slurry in the column and the low temperature DP cell. The chamber also serves as a trap for any slurry that flows into the 0.635 cm tube. A drain located at the bottom of the chamber is used to clean the trap between runs. A ball valve located in the 0.635 cm line serves to isolate the system from the column, in case the

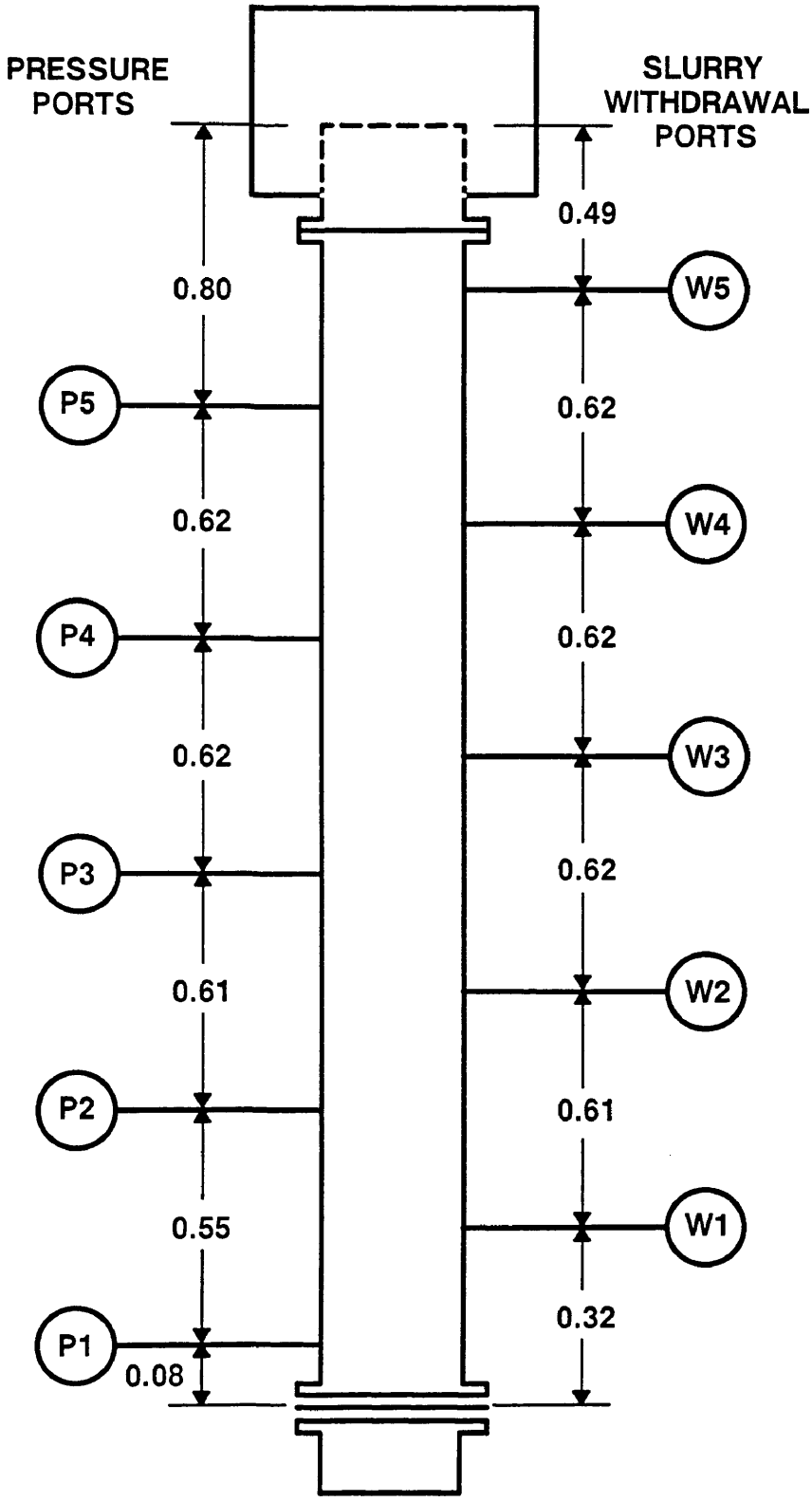

Figure 2.9. Schematic diagram of the pressure ports and slurry sampling ports locations (all dimensions in m).

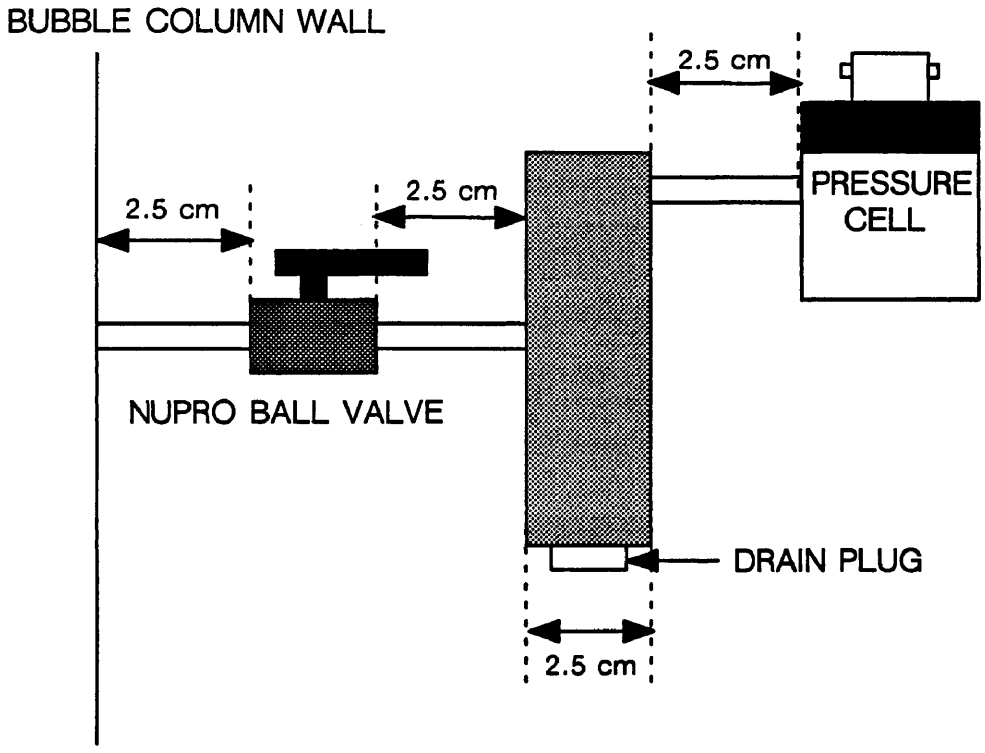

Figure 2.10. Schematic representation of the pressure transducer system.

trap has to be emptied during a run. The 0.635 cm line and chamber are heat traced and insulated to prevent solidification of slurry in this section.

The pressure transducers (Valydine Model DP–15) were connected to dual channel indicators (Valydine Model CD–223). The indicators have a digital display, as well as a 0 – 15 volt DC output. A data acquisition system which consisted of an A/D converter (Metrabyte Model DAS–16G), associated software, and a Zenith 286 personal computer was used to record the output voltage from the pressure transducer indicators. The pressure transducer indicators were adjusted so that the output voltage (proportional to pressure in inches of water) was scaled down by a factor of 10 before being sent to the data acquisition system. Thus, an output voltage of 1 corresponded to a height of approximately 10 inches of water. The calibration procedure for a single pressure transducer is outlined below. All pressure transducers were calibrated using the same procedure.

Before beginning each series of experiments, the pressure transducers were calibrated using tap water. The density of water was assumed to be 1000 kg/m^3. Initially, the output voltage from the pressure transducer indicator was set to zero. In order to calibrate a pressure transducer, the column was filled with water. The height of water above the transducer is the height of water in the column minus the height of the pressure transducer (both measured from the bottom of the column). The output voltage from the transducer indicator was forced to be 1/10th of the height of water (in inches) above the transducer by adjusting the span. The column was then drained and the zero was readjusted if necessary. Next, the column was filled with water again, and the output voltage was recorded. By making several measurements with different amounts of water in the column once the zero and span were set, a calibration curve of height of water (in inches) above the pressure transducer versus output voltage from the

pressure transducer indicator was obtained. Figure 2.11 is a sample calibration curve. The form of the calibration equation for a given pressure transducer is:

$$\text{Pressure (inches of water)} = \text{slope} * (\text{output voltage}) + \text{intercept} \qquad (2.2)$$

For all pressure transducers, the slope of the calibration curve was in the range 9.9 to 10.1 and the intercept was in the range -0.6 to 0.6.

Data acquisition software was written which would display a "running" average of the pressure indicator output voltage. During the experiments, data was collected at a rate of 50 Hz for a period of 2 to 3 minutes. As previously described, measurements were made three times per gas velocity (i.e. approximately every 30 minutes), and the average of the three values (output voltage) was used to calculate the pressure, in inches of water, above a given pressure transducer using Eq. 2.2.

Solid Concentration Measurements

For three–phase systems, both pressure measurements and weight fractions of solids are needed to determine the phase holdups (i.e. gas, liquid, and solids holdup). The weight fraction of solids in the slurry samples withdrawn at the various axial locations (see Figure 2.9) was measured using the Archimedean principle (the apparent loss in weight of a solid body, when completely immersed in a liquid, equals the weight of the displaced fluid). The procedure used is outlined below.

The slurry withdrawn into the sampling cylinder is allowed to cool and solidify. The solid slurry plug is then removed for solids fraction determination. The sample is first weighed on a precision balance ($m_{s\ell}$). It is then suspended with a thin wire from a support structure placed on the balance and the combined weight of the support structure and sample recorded (m_1). The sample, while still suspended from the support structure, is then completely immersed in a beaker of acetone and the balance reading recorded (m_2). The three measured quantities, along with the known densities of

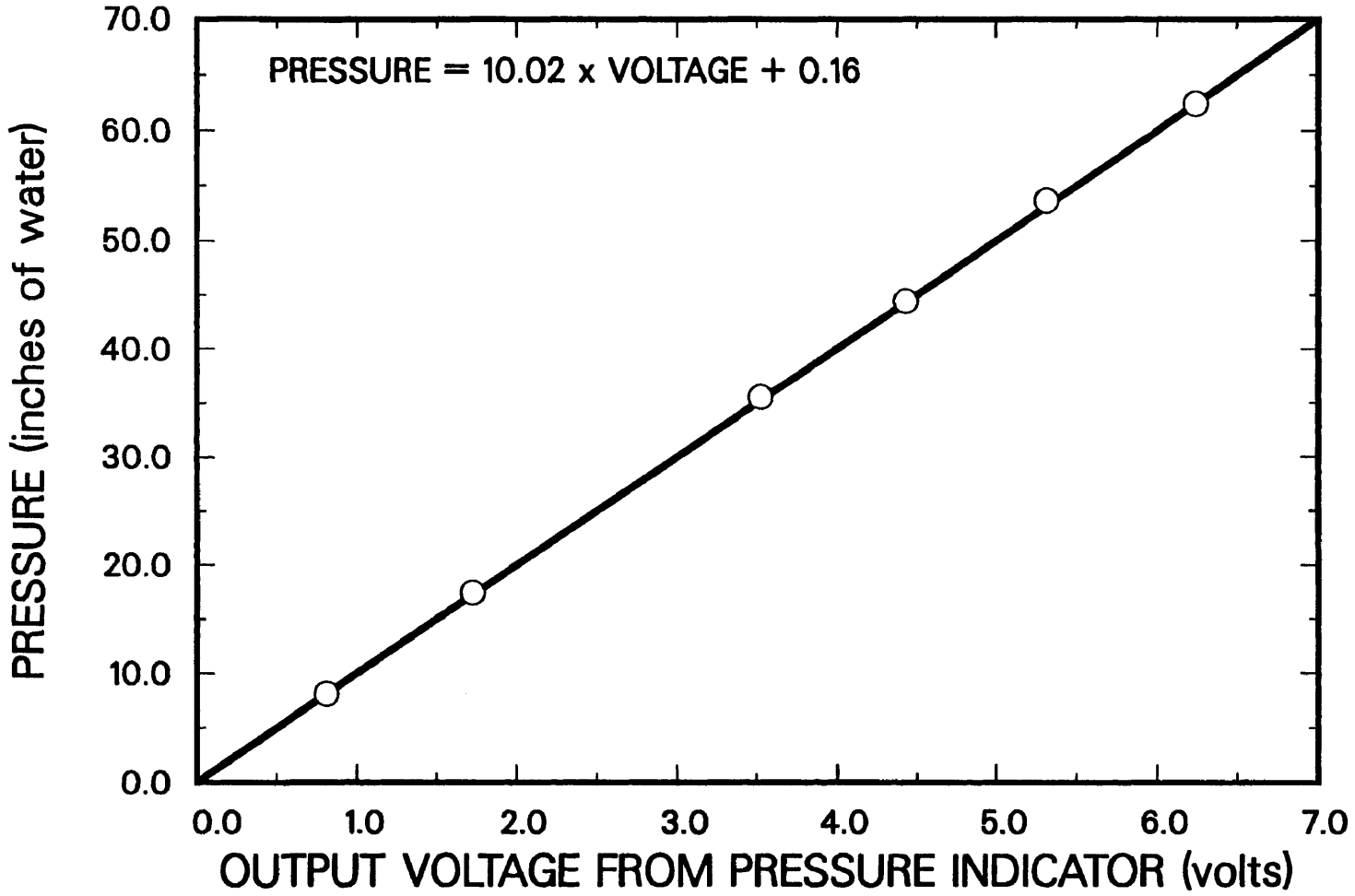

Figure 2.11. Typical pressure transducer calibration curve.

solidified wax (ρ_w), solids (ρ_s), and acetone (ρ_{acet}), were used to determine the weight fraction of solids (ω_s) in the slurry sample. By the definition of the Archimedean principle,

$$W_{acet} = m_1 - m_2 \tag{2.3}$$

where W_{acet} is the weight of acetone displaced. The volume of acetone displaced, which is the same as the volume of the slurry sample, is given by

$$V_{s\ell} = \frac{W_{acet}}{\rho_{acet}} \tag{2.4}$$

By substituting Eq. 2.3 into Eq. 2.4 and dividing the weight of the slurry sample ($m_{s\ell}$) by the volume of the sample ($V_{s\ell}$), the following expression is obtained for the density of the slurry sample

$$\rho_{s\ell} = \frac{m_{s\ell}\rho_{acet}}{m_1 - m_2} \tag{2.5}$$

The density of the sample may be expressed in terms of ω_s as follows

$$\rho_{s\ell} = \frac{1}{\frac{\omega_s}{\rho_s} + \frac{(1-\omega_s)}{\rho_w}} \tag{2.6}$$

Equating Eqs. 2.5 and 2.6 to eliminate $\rho_{s\ell}$, and rarranging the terms, yields the following expression for ω_s

$$\omega_s = \frac{\rho_s - (\frac{\rho_w \rho_s}{\rho_{acet}})(\frac{m_1 - m_2}{m_{s\ell}})}{\rho_s - \rho_w} \tag{2.7}$$

The density of solidified wax was determined experimentally. The density of fresh FT–300 wax is 950 kg/m^3, and the density of fresh SASOL wax is 930.5 kg/m^3. Acetone was selected as the liquid medium for this procedure because it has a lower density than wax (ρ_{acet} = 792 kg/m^3), it evaporates quickly from the sample surface, and the solubility of wax in acetone at room temperature is negligible. The procedure was tested using both FT–300 and SASOL wax containing known quantities of solids. Samples containing 3, 7, 10, 15, 20, 25, 30, and 35 wt.% solids in wax were prepared. Samples

with 0–5 μm iron oxide, 20–44 μm iron oxide and 0–5 μm silica were used with FT–300, and samples with 0–5 μm iron oxide and 20–44 μm silica were used with SASOL wax. Solid densities of 5100 kg/m^3 for iron oxide and 2650 kg/m^3 for silica were employed. Tables 2.2a, 2.2b, and 2.2c show results obtained with slurries of 0 – 5 μm iron oxide particles, 20 – 44 μm iron oxide particles, and 0 – 5 μm silica particles in FT–300 wax, respectively. For these samples, the relative error between the calculated (Eq. 2.7) and the actual weight fraction of solids was highest for the sample containing 3 wt% 0 – 5μm silica particles (6.5 %). For all other solids concentrations, the relative error between the actual and calculated weight fractions was less than 2.2 %. Tables 2.3a and 2.3b show results from measurements with 0 – 5 μm iron oxide and 20 – 44μm silica particles in SASOL wax, respectively. For all samples analyzed, the calculated weight fractions of solids were within 1.02 % (relative) of the actual weight fraction of solids.

Sensitivity analysis of Eq. 2.7 revealed that the results were very sensitive to small variations in the density of solidified wax. A variation of only 1 % in the density of wax caused a 12 % change in ω_s; whereas, a 5 % change in the density of solids caused only a 2 % change in ω_s for slurries containing iron oxide, and a 4 % change in ω_s for slurries containing silica. Because of the high sensitivity to wax density, we determined the density of fresh wax and used wax. For FT–300, the density of fresh wax and used wax (100 hours on stream) was the same. However, the density of SASOL wax varied with time on stream. The density of fresh SASOL wax was 930.5 kg/m^3 and the density of used SASOL wax (72 hours on stream) was 941.2 kg/m^3. There was less than 0.07 % difference in the density of SASOL wax between 72 hours on stream and 144 hours on stream. The change in density between fresh and used SASOL wax was probably caused by changes in the composition of SASOL wax with time on stream. SASOL wax contains a significantly higher concentration of lower molecular weight components

Table 2.2a. Results from Archimedean Procedure (0 – 5 μm iron oxide in FT–300)[a]

Nominal	Actual wt.%	Measured wt.%	% Error
3	2.94	2.96	0.74
7	6.61	6.60	-0.13
10	9.15	9.09	-0.61
15	13.13	12.92	-1.59
20	20.20	20.26	0.31
25	25.15	24.95	-0.78
30	30.25	30.04	-0.68
35	35.22	34.90	-0.91

[a] densities used: $\rho_W = 0.9495$ g/cc, $\rho_S = 5.1$ g/cc, $\rho_{acet} = 0.792$ g/cc

Table 2.2b. Results from Archimedean Procedure (20 – 44 μm iron oxide in FT–300)[b]

Nominal	Actual wt.%	Measured wt.%	% Error
3	3.09	2.89	-6.54
7	7.11	7.25	2.02
10	10.24	10.01	-2.21
15	15.13	15.17	0.26
20	20.00	20.02	0.10
25	25.13	25.25	0.49
30	30.33	30.43	0.32
35	35.03	35.07	0.11

[a] densities used: $\rho_W = 0.9495$ g/cc, $\rho_S = 5.1$ g/cc, $\rho_{acet} = 0.792$ g/cc

Table 2.2c. Results from Archimedean Procedure (0 – 5 μm silica in FT–300)[c]

Nominal	Actual wt.%	Measured wt.%	% Error
3	3.04	3.09	1.54
7	7.06	7.04	-0.39
10	10.04	10.07	0.27
15	15.10	15.07	-0.23
20	20.09	20.00	-0.44
25	25.09	24.93	-0.67
30	30.15	30.05	-0.32
35	35.05	34.87	-0.51

[a] densities used: $\rho_W = 0.9495$ g/cc, $\rho_S = 2.65$ g/cc, $\rho_{acet} = 0.792$ g/cc

Table 2.3a. Results from Archimedean Procedure (0 – 5 μm iron oxide in SASOL)[a]

Nominal	Actual wt.%	Measured wt.%	% Error
3	3.03	3.02	-0.34
7	6.78	6.74	-0.65
10	9.81	9.89	0.77
15	14.94	14.99	0.31
20	20.26	20.05	-1.02
25	24.63	24.45	-0.72
30	28.95	29.04	0.32
35	35.21	34.90	-0.89

[a] densities used: $\rho_W = 0.9305$ g/cc, $\rho_S = 5.1$ g/cc, $\rho_{acet} = 0.792$ g/cc

Table 2.3b. Results from Archimedean Procedure (20 – 44 μm silica in SASOL)[b]

Nominal	Actual wt.%	Measured wt.%	% Error
3	2.97	2.97	0.0
7	7.02	6.97	-0.71
10	9.94	10.00	0.06
15	15.03	14.91	-0.83
20	19.94	19.86	-0.41
25	24.81	24.91	0.39
30	29.88	29.93	0.18
35	35.12	35.08	-0.10

[a] densities used: $\rho_W = 0.9305$ g/cc, $\rho_S = 2.65$ g/cc, $\rho_{acet} = 0.792$ g/cc

than FT–300 wax. These low molecular weight components evaporate when the slurry is held at 265 °C for extended periods of time. As mentioned previously, slight errors (or changes) in wax density result in large errors of the estimated solids concentration. In order to compensate for changes in wax density (SASOL wax) with time on stream, the density of used wax (i.e. 941.2 kg/m^3) was used to calculate the solids concentration once the wax had been on stream for over 72 hours, and the density of fresh wax (930.5 kg/m^3) was used prior to that.

Holdup Calculations

The system constants used to determine the gas holdup, liquid holdup, and solid holdup include the densities of solids (ρ_s), liquid (ρ_ℓ), solidified wax (ρ_w) and acetone (ρ_{acet}), heights of the five pressure ports above the distributor (h_1 to h_5), and the distance between the distributor (bottom of the column) and the top of the column (h_t). The measured quantities include the meter readings (i.e. average output voltages, OV_1 to OV_5), the weights of solidified slurry samples ($m_{s\ell_{ij}}$), the weight of the slurry sample suspended in air ($m_{1_{ij}}$), and its weight when immersed in acetone (m_{2ij}). For simplicity, the measured quantities have been replaced with the primary derived quantities, i.e. the differential pressure across section i–j (ΔP_{ij}), and the average weight fraction of solids for the section i–j ($< \omega_s >_{ij}$).

The differential pressure is defined by

$$\Delta P_{ij} = P_i - P_j = (a_i OV_i + b_i) - (a_j OV_j + b_j) \qquad i = 1 \text{ to } 5 \text{ and } j = i + 1 \qquad (2.8)$$

where a_i and a_j are the slopes of the calibration curves relating the meter readings to pressure (in inches of water) for transducers at ports i and j, respectively, and b_i and b_j are the intercepts of the two curves (see Eq. 2.2). Note, j = 6 corresponds to the top

of the column, and the pressure at the top of the column is assumed to be atmospheric pressure. The distance between pressure ports i and j is defined as

$$\Delta h_{ij} = h_j - h_i \qquad i = 1 \text{ to } 5 \text{ and } j = i + 1 \tag{2.9}$$

The average weight fraction of solids (see Eq. 2.7) between pressure ports i and j is given by

$$< \omega_s >_{ij} = \frac{\rho_s - \left(\frac{\rho_w \rho_s}{\rho_{acet}}\right)\left(\frac{m_{1_{ij}} - m_{2_{ij}}}{m_{s\ell_{ij}}}\right)}{\rho_s - \rho_w} \qquad i = 1 \text{ to } 5 \text{ and } j = i + 1 \tag{2.10}$$

The gas holdup in a three–phase (gas/liquid/solid) system may be expressed in terms of the slurry (liquid/solid) density, $\rho_{s\ell}$ and the density of the gas–liquid–solid dispersion, ρ_d (i.e. density of the expanded slurry) as,

$$\epsilon_g = \frac{\rho_{s\ell} - \rho_d}{\rho_{s\ell} - \rho_g} \approx 1 - \frac{\rho_d}{\rho_{s\ell}} \tag{2.11}$$

since the density of the gas, ρ_g is small in comparison to the density of the slurry at low pressures.

The density of the expanded slurry between any two pressure ports, i and j may be calculated from the measured pressure drop ΔP_{ij} and the known distance between the pressure taps, Δh_{ij},

$$s_{d_{ij}} = \frac{\Delta P_{ij}}{\Delta h_{ij}} \text{ and } \rho_{d_{ij}} = s_{d_{ij}} \rho_{water} \qquad i = 1 \text{ to } 5 \text{ and } j = i + 1 \tag{2.12}$$

where $s_{d_{ij}}$ is the specific gravity of the dispersion between pressure ports i and j. Substituting this expression into Eq. 2.11, yields:

$$< \epsilon_{g_{ij}} > = 1 - \frac{\Delta P_{ij}}{s_{s\ell_{ij}} \Delta h_{ij}} \tag{2.13}$$

where $s_{s\ell_{ij}}$ is the specific gravity of the slurry (liquid/solid) in the i–j section. The specific gravity of the slurry between pressure ports i and j can be calculated from the

weight fraction of solids between pressure ports i and j, the density of the solid, and the density of the liquid using the following expression

$$s_{s\ell_{ij}} = \frac{1}{\rho_{water}} \frac{1}{\left[\frac{<\omega_s>_{ij}}{\rho_s} + \frac{1-<\omega_s>_{ij}}{\rho_\ell}\right]} \qquad i = 1 \text{ to } 5 \text{ and } j = i+1 \tag{2.14}$$

Substituting Eq. 2.14 into Eq. 2.13 yields

$$< \epsilon_g >_{ij} = 1 - \left(\frac{\Delta P_{ij}\rho_{water}}{\Delta h_{ij}}\right)\left[\frac{< \omega_s >_{ij}}{\rho_s} + \frac{1- < \omega_s >_{ij}}{\rho_\ell}\right] \qquad i = 1 \text{ to } 5,\ j = i+1 \tag{2.15}$$

The latter expression was used to calculate the gas holdup between pressure ports i and j.

The liquid holdup may be expressed in terms of ρ_ℓ, ρ_d, ρ_s, ϵ_g, and ϵ_s as follows:

$$\epsilon_\ell = \frac{\rho_d - \epsilon_g\rho_g - \epsilon_s\rho_s}{\rho_\ell} \tag{2.16}$$

where ϵ_s is the volume fraction of solids (i.e. solids holdup) in the dispersion. Assuming $\epsilon_g\rho_g$ is negligible, Eq. 2.16 may be rewritten as:

$$\epsilon_\ell = \frac{\rho_d - \epsilon_s\rho_s}{\rho_\ell} \tag{2.17}$$

The volume fraction of solids in the dispersion may be expressed in terms of the weight fraction of solid in the dispersion using

$$\epsilon_s = \frac{\omega_s\rho_d}{\rho_s} \tag{2.18}$$

Substituting Eq. 2.18 into Eq. 2.17 upon rearrangement yields the following expression for ϵ_ℓ

$$\epsilon_\ell = \frac{\rho_d(1-\omega_s)}{\rho_\ell} \tag{2.19}$$

Thus the liquid holdup in the section i–j is given by

$$< \epsilon_{\ell_{ij}} > = \frac{\rho_{d_{ij}}(1- < \omega_{s_{ij}} >)}{\rho_\ell} \qquad i = 1 \text{ to } 5 \text{ and } j = i+1 \tag{2.20}$$

Substituting the expression for $\rho_{d_{ij}}$ (Eq. 2.12) into Eq. 2.20 the following expression is obtained for the average liquid holdup between pressure ports i and j

$$< \epsilon_\ell >_{ij} = \left(\frac{\Delta P_{ij}\rho_{water}}{\Delta h_{ij}}\right)\left(\frac{1 - < \omega_s >_{ij}}{\rho_\ell}\right) \qquad i = 1 \text{ to } 5, \;\; j = i + 1 \qquad (2.21)$$

Since the sum of the volume fractions of gas, liquid and solids equals one, the volume fraction of solids in the dispersion between pressure ports i and j may be expressed as:

$$< \epsilon_{s_{ij}} > = 1 - < \epsilon_{\ell_{ij}} > - < \epsilon_{g_{ij}} > \qquad i = 1 \text{ to } 5 \text{ and } j = i + 1 \qquad (2.22)$$

Substituting Eqs. 2.15 and 2.21 into Eq. 2.22 yields the following expression for the average volume fraction of solids in the i–j section

$$< \epsilon_s >_{ij} = \left(\frac{\Delta P_{ij}\rho_{water}}{\Delta h_{ij}}\right)\left(\frac{< \omega_s >_{ij}}{\rho_s}\right) \qquad i = 1 \text{ to } 5, \;\; j = i + 1 \qquad (2.23)$$

Equations 2.15, 2.21, and 2.23 were used to estimate holdups of the three phases in the section between any two adjacent pressure ports; however, for the equations to be valid the entire section must be filled with the dispersion. For runs conducted in the continuous mode of operation, all five sections are always full, since the dispersion fills the entire column. For runs conducted in the batch mode of operation, Eqs. 2.15, 2.21, and 2.23 may be used for those sections that are full, i.e. all sections below the top most non-zero pressure port. The section just above this pressure port (say section n) is only partially full, therefore the height of the dispersion in this section (Δh_n) is not known. However, the differential pressure for this section (ΔP_n) is known. If a slurry sample was not withdrawn from this section, $< \omega_s >_n$ would also be an unknown quantity. For such cases, the gas holdup and if necessary, the weight fraction of solids in this section are either estimated by extrapolation of the $< \epsilon_g >$ and $< \omega_s >$ profiles or they are assumed to have the same values as in the section below (i.e. $< \epsilon_{g_{n,n+1}} > = < \epsilon_{g_{n-1,n}} >$

and $< \omega_{s_{n,n+1}} >=< \omega_{s_{n-1,n}} >$). The height of the dispersion in this section is then calculated using (see Eq. 2.15)

$$\Delta h_n = \left(\frac{\Delta P_n \rho_{water}}{1- < \epsilon_g >_n}\right)\left[\frac{< \omega_s >_n}{\rho_s} + \frac{1- < \omega_s >_n}{\rho_\ell}\right] \tag{2.24}$$

Equations 2.21 and 2.23 can then be used to estimate the liquid and solids holdups for this section. For all runs, no measurements are made between the distributor and pressure port 1 (see Figure 2.9). It is assumed that the volume fractions of the three phases in this section are the same as those in the section above (i.e. section 1-2).

The average gas holdup for the entire dispersion can be obtained using a weighted (volume) average of the gas holdups in the individual sections and is expressed as

$$< \epsilon_g >= \sum_{i=1}^{n} f_{d_{ij}} < \epsilon_{g_{ij}} > \qquad j = i + 1 \tag{2.25}$$

where $f_{d_{ij}}$ is the volume fraction of the dispersion between pressure ports i and j and is given by

$$f_{d_{ij}} = \frac{\Delta h_{ij}}{\sum_i \Delta h_{ij}} \qquad i = 1 \text{ to } 5 \text{ and } j = i + 1 \tag{2.26}$$

Substituting Eqs. 2.15 and 2.26 into Eq. 2.25 yields

$$< \epsilon_g >= 1 - \frac{\sum_{i=0}^{n} \left(\Delta P_{ij} \rho_{water}\right)\left[\frac{< \omega_s >_{ij}}{\rho_s} + \frac{1- < \omega_s >_{ij}}{\rho_\ell}\right]}{\sum_{i=0}^{n} \Delta h_{ij}} \qquad j = i + 1 \tag{2.27}$$

where $\Delta P_{01} = \Delta P_{12} \Delta h_{01} / \Delta h_{12}$, and $< \omega_s >_{01} =< \omega_s >_{12}$. For the continuous mode of operation n = 5; whereas, for the batch mode of operation, n is dependent on the location of the top of the dispersion.

For two–phase experiments in the stainless steel column, the same procedure was used to calculate gas holdups and liquid holdups. However, the weight fraction of solids, ω_s, was set equal to 0.

Results and Discussion

Average and axial gas holdups obtained from experiments in the stainless steel columns are presented here. Axial solids concentration profiles will be discussed in Chapter 4. The discussion is divided into three main sections. In the first part, definitions and descriptions of the various flow regimes which were observed are presented. Following this, the effect of various operating conditions and column diameter on gas holdups are discussed. Finally, various correlations which may be used to predict average gas holdup in a three–phase Fischer–Tropsch bubble column reactors are presented.

Description of the Flow Field

The hydrodynamics (e.g. mixing characteristics, bubble size distribution, etc.) of a bubble column is significantly affected by the flow regime prevailing in the column. Ample evidence of this dependency is available in the literature (e.g. Shah et al., 1982) and various criteria have been proposed by different researchers to delineate the flow regimes (e.g. Taitel et al., 1981; Deckwer et al., 1980). Deckwer et al. presented a flow regime map (see Figure 2.12) which qualitatively characterizes the dependence of flow regimes on column diameter and superficial gas velocity. At low gas velocities, regardless of column diameter, the homogeneous (or homogeneous bubbling) regime exists. This regime is characterized by a uniform bubble size distribution in which there is very little interaction between neighboring bubbles. As the gas velocity increases, bubble coalescence and breakup occur. In columns less than 0.10 m in diameter, the large bubbles may fill the entire column diameter forming slugs; this is known as the slug flow regime. In larger diameter columns, large bubbles are formed without producing slugs. As these large bubbles rise through the column, there is an increase in turbulence; hence, this is called the churn–turbulent flow regime. The shaded regions in Figure 2.12

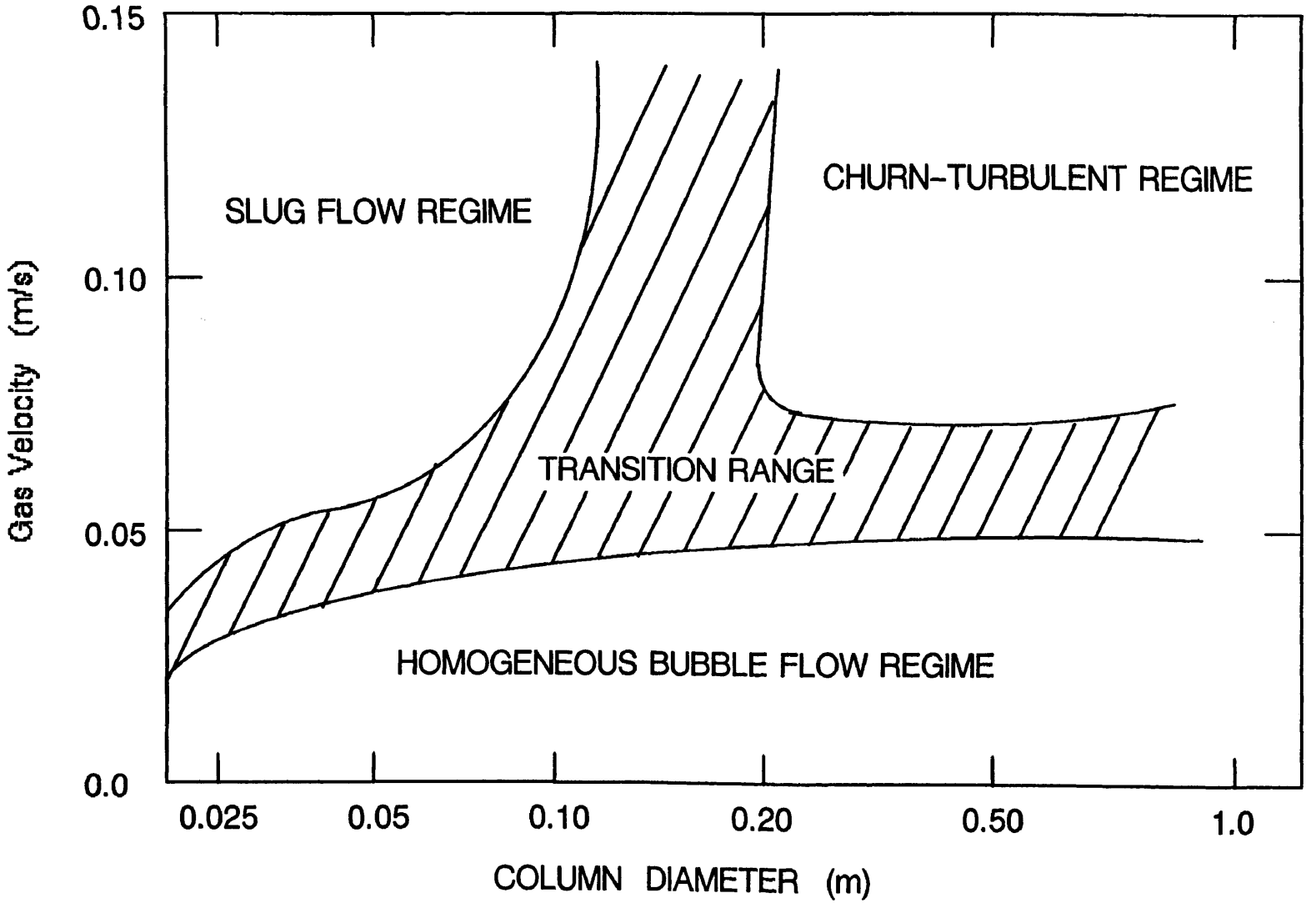

Figure 2.12. Bubble column flow regime map (adopted from Deckwer et al., 1980).

indicate the transition regions between the various flow regimes. The exact boundaries associated with the transition regions will probably vary with the system studied.

The flow regimes described above are typically associated with nonfoaming systems. For foaming systems, Shah et al. (1985) include an additional flow regime called the foaming (or foamy) regime. The foamy regime overlaps the previously described regimes and is characterized by high gas holdups and substantial recirculation of bubbles.

In our experiments, all of the flow regimes described above were observed. In the 0.05 m ID column, the homogeneous bubbly regime prevailed at superficial gas velocities less than 0.04 m/s and the slug flow regime at higher gas velocities. For experiments conducted with FT–300 wax, the foamy regime was also observed; however, with SASOL reactor wax, very little foam, if any, was present. In the 0.21 m ID column, the homogeneous bubbling regime was observed at low gas velocities (u_g <0.04 m/s) and the churn–turbulent regime at higher gas velocities. The amount of foam observed in experiments with FT–300 wax in the large diameter column was significantly less than that observed under similar operating conditions in the small diameter column. As in the 0.05 m ID column, little or no foam was observed during experiments conducted with SASOL wax in the 0.21 m ID column.

Discussion of Results

FT–300 and SASOL wax were used for experiments in both the small (0.05 m ID) and large (0.21 m ID) diameter columns. The majority of experiments in the small diameter column were conducted with FT–300 wax, since SASOL wax was not available during the initial stages of this study. Once SASOL wax became available, some experiments were preformed in order to study the effect of wax type on gas holdup and solid concentration profiles. Table 2.4 is a summary of the experiments conducted in the small diameter column. An increasing order of gas velocities was employed for all

Table 2.4. Summary of Runs in the Small Stainless Steel Column

EXP. No.	WAX TYPE	T (°C)	d_p (μm)	ω_s (%)	SOLIDS TYPE	u_ℓ (m/s)	TOS (hr)	TIME HOT (hr)
1	FT-300	265	–	–	—	0.0	0	12
2	FT-300	265	–	–	—	0.005	8	36
3	FT-300	265	–	–	—	0.02	16	60
4	FT-300	265	0 – 5	10	IRON OX	0.005	24	84
5	FT-300	265	0 – 5	10	IRON OX	0.02	32	108
6	FT-300	265	0 – 5	10	IRON OX	0.0	40	132
7	FT-300	265	0 – 5	20	IRON OX	0.005	0	12
8	FT-300	265	0 – 5	20	IRON OX	0.02	8	36
9	FT-300	265	0 – 5	20	IRON OX	0.0	16	60
10	FT-300	265	0 – 5	30	IRON OX	0.005	24	84
11	FT-300	265	0 – 5	30	IRON OX	0.02	32	108
12	FT-300	265	0 – 5	30	IRON OX	0.0	40	132
13	FT-300	265	20 – 44	10	IRON OX	0.005	0	12
14	FT-300	265	0 – 5	10	SILICA	0.005	0	12
15	FT-300	265	0 – 5	20	SILICA	0.005	8	36
16	FT-300	265	0 – 5	20	SILICA	0.02	16	60
17	FT-300	265	0 – 5	20	SILICA	0.0	24	84
18	FT-300	265	0 – 5	30	SILICA	0.005	32	108
19	FT-300	265	20 – 44	10	IRON OX	0.005	0	12
20	FT-300	265	20 – 44	10	IRON OX	0.02	8	36
21	FT-300	265	20 – 44	20	IRON OX	0.0	16	84
22	FT-300	265	20 – 44	20	SILICA	0.0	0	36
23	FT-300	265	–	–	—	0.0	0	12
24	FT-300	265	–	–	—	0.005	8	36
25	FT-300	265	20 – 44	20	IRON OX	0.0	16	60
26	FT-300	265	20 – 44	20	IRON OX	0.02	24	84
27	FT-300	265	20 – 44	20	IRON OX	0.005	32	108
28	FT-300	265	20 – 44	20	SILICA	0.0	0	12
29	SASOL	265	–	–	—	0.0	0	12
30	SASOL	265	–	–	—	0.005	8	36
31	SASOL	265	0 – 5	20	IRON OX	0.005	16	60
32	SASOL	265	20 – 44	20	IRON OX	0.0	0	12
33	SASOL	265	20 – 44	20	IRON OX	0.005	8	36
34	SASOL	265	20 – 44	20	IRON OX	0.005	12	60

Note: Horizontal lines separate batches
TOS – Time on stream
TIME HOT – Total time heated

experiments in the small diameter column, with the exception of the two batch experiments conducted with 20–44 μm silica particles (experiments 22 and 28 in Table 2.4) and the last two continuous experiments with large iron oxide particles suspended in FT–300 wax (experiments 26 and 27 in Table 2.4). For these experiments, a decreasing order of gas velocities was used. Experiments in the large diameter column were conducted once all experiments in the small diameter column were completed. SASOL wax was chosen as the primary fluid for experiments in the 0.21 m ID column since it is more representative of the reactor wax present in a slurry bubble column reactor during Fischer–Tropsch synthesis. Also, a limited number of experiments was conducted with FT–300 wax in the 0.21 m ID column. A summary of the experiments conducted in the large diameter column is presented in Table 2.5. The 19 x 2 mm perforated plate (PP) was used for majority of these experiments. With the exception of a few experiments without solids (i.e. experiments 1 – 4 in Table 2.5), all experiments in the large diameter column were performed using a decreasing order of gas velocities. The effect of slurry flow rate, solids concentration, type and size, liquid medium, temperature, distributor type, and column diameter on gas holdup is discussed below.

Effect of Slurry Velocity

Figures 2.13a and 2.13b show the effect of slurry velocity on average gas holdup for experiments conducted with FT–300 wax in the small and large diameter columns, respectively. A substantial amount of foam was produced during the batch (i.e. $u_{s\ell} = 0$) experiment in the 0.05 m ID column, with gas holdup values as high as 0.29 at a gas velocity of 0.04 m/s (see Figure 2.13a). Gas holdups decreased significantly for gas velocities in the range 0.04 – 0.09 m/s when the superficial slurry velocity was increased to 0.005 m/s. A further decrease in gas holdup was observed when the slurry velocity was increased to 0.02 m/s. It should be noted that at higher gas velocities,

Table 2.5. Summary of Runs in the Large Stainless Steel Column

EXP. No.	WAX TYPE	T (°C)	d_p (μm)	ω_s (%)	SOLIDS TYPE	u_ℓ (m/s)	DIST —	TOS (hr)	TIME HOT (hr)
1	SASOL	265	—	—	—	0.0	PP	0	12
2	SASOL	265	—	—	—	0.005	PP	6	36
3	SASOL	265	—	—	—	0.02	PP	12	42
4	SASOL	265	—	—	—	0.005	BC	18	78
5	SASOL	265	—	—	—	0.0	PP	0	72
6	SASOL	265	0 – 5	IRON OX	10	0.0	PP	8	96
7	SASOL	265	0 – 5	IRON OX	20	0.0	PP	16	120
8	SASOL	265	0 – 5	IRON OX	20	0.005	PP	24	124
9	SASOL	265	0 – 5	IRON OX	20	0.02	PP	32	130
10	SASOL	265	0 – 5	IRON OX	20	0.0	BC	40	154
11	SASOL	265	0 – 5	IRON OX	20	0.005	BC	48	162
12	SASOL	265	0 – 5	IRON OX	20	0.0	PP	56	186
13	SASOL	265	0 – 5	IRON OX	30	0.0	PP	64	210
14	SASOL	265	0 – 5	IRON OX	30	0.005	PP	72	234
15	SASOL	265	20 – 44	IRON OX	10	0.005	PP	0	12
16	SASOL	265	20 – 44	IRON OX	10	0.02	PP	6	18
17	SASOL	265	20 – 44	IRON OX	20	0.0	PP	12	42
18	SASOL	265	20 – 44	IRON OX	20	0.005	PP	18	48
19	SASOL	265	20 – 44	IRON OX	20	0.02	PP	24	72
20	SASOL	265	20 – 44	IRON OX	20	0.0	BC	30	120
21	SASOL	265	20 – 44	IRON OX	20	0.0	PP	36	144
22	SASOL	265	20 – 44	IRON OX	30	0.0	PP	42	150
23	SASOL	265	20 – 44	IRON OX	30	0.005	PP	48	174
24	SASOL	265	20 – 44	IRON OX	30	0.02	PP	54	180
25	SASOL	265	—	—	—	0.005	BC	0	12
26	SASOL	265	20 – 44	SILICA	20	0.0	PP	6	36
27	SASOL	265	20 – 44	SILICA	20	0.005	PP	12	42
28	SASOL	265	20 – 44	SILICA	20	0.02	PP	18	48
29	SASOL	265	20 – 44	SILICA	30	0.005	PP	24	72
30	FT–300	265	—	—	—	0.0	PP	0	12
31	FT–300	265	—	—	—	0.005	PP	6	18
32	FT–300	265	—	—	—	0.02	PP	12	24
33	FT–300	265	20 – 44	IRON OX	20	0.0	PP	18	48
34	FT–300	265	20 – 44	IRON OX	20	0.005	PP	24	54
35	FT–300	265	20 – 44	IRON OX	20	0.005	BC	30	78

Note: Horizontal lines separate batches
TOS – Time on stream
TIME HOT – Total time heated
PP – Perforated plate distributor
BC – Bubble cap distributor

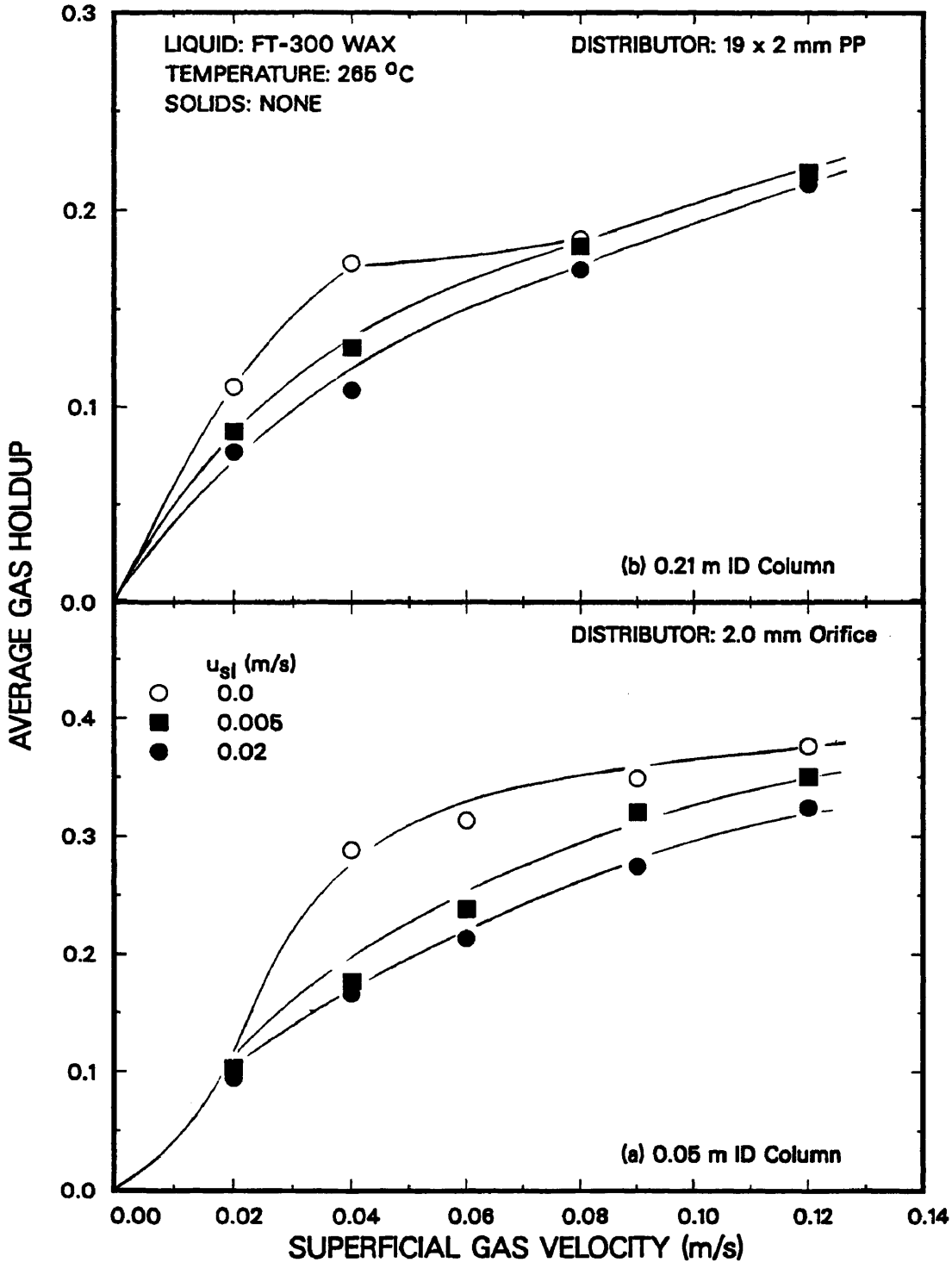

Figure 2.13. Effect of superficial slurry velocity on average gas holdup in the (a) small and (b) large diameter columns with FT-300 wax.

the difference in gas holdup between the batch experiment (i.e. $u_{s\ell}$=0.0 m/s) and the continuous experiments decreases. At a gas velocity of 0.02 m/s, the holdups from all three runs were similar (see Figure 2.13a). At this gas flow rate, the homogeneous bubbling regime exists, and one would expect holdups to be similar for all three slurry velocities.

Foam was also observed during the batch experiment in the large diameter column at a gas velocity of 0.04 m/s (see Figure 2.13b). At this gas velocity (i.e. 0.04 m/s), the amount of foam produced in the large diameter column was less than the amount of foam produced in the small diameter column (i.e. the gas holdup was 0.18 in the large diameter column as opposed to 0.29 in the small diameter column). Gas holdups during the continuous experiments at u_g = 0.04 m/s were lower than the gas holdups at this velocity during the batch experiment. Only a marginal decrease in gas holdup was observed when the slurry flow rate was increased from 0.005 to 0.02 m/s. At gas velocities of 0.08 and 0.12 m/s gas holdups from all three experiments were similar. At a gas velocity of 0.02 m/s, the gas holdup associated with the batch experiment was slightly higher than those from the continuous experiment. This was due to a slight increase in the gas holdup during the batch experiment in uppermost section of the column at this velocity (see Figure 2.14b).

Axial gas holdup profiles at gas velocities of 0.02, 0.04, and 0.12 m/s, from the batch experiments in the 0.05 and 0.21 m diameter columns are shown in Figures 2.14a and 2.14b, respectively. At a gas velocity of 0.02 m/s, axial gas holdup profiles in both columns are nearly uniform; however, at a gas velocity of 0.04 m/s, there is a significant increase in the gas holdup between heights of 1.5 and 2.2 m above the distributor (i.e. in the small diameter column the gas holdup increases from 0.17 to 0.64 and in the large diameter column, the gas holdup increases from 0.16 to 0.28). This increase in gas holdup indicates the presence of a foam layer at the top of the dispersion. The

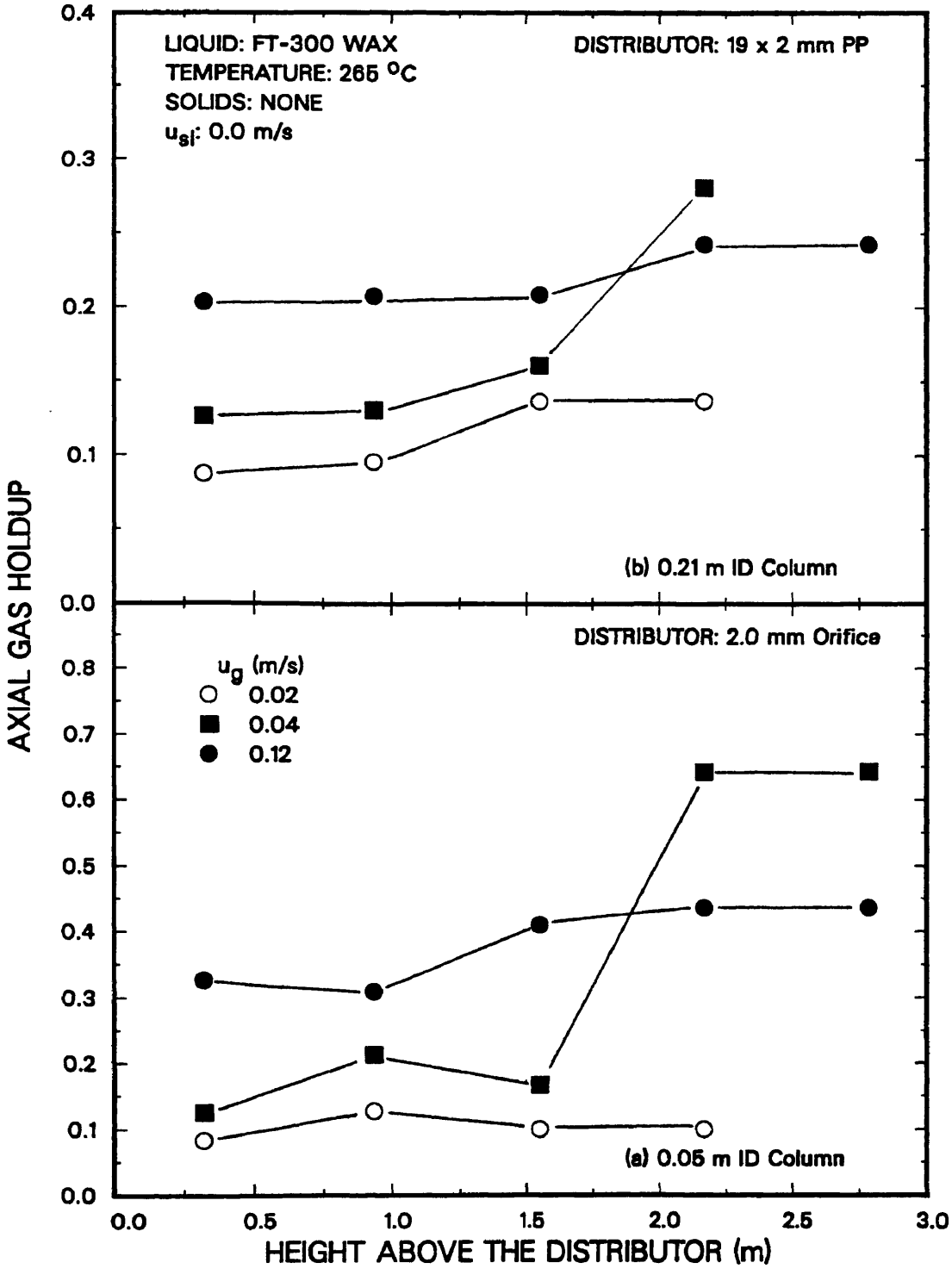

Figure 2.14. Effect of superficial gas velocity on axial gas holdup in the (a) small and (b) large diameter columns with FT-300 wax.

amount of foam present in the large diameter column at a gas velocity of 0.04 m/s was substantially less than the amount of foam present in the small diameter column at this gas velocity. The difference in the amount of foam produced in the two columns is due to differences in the flow patterns present in the two columns at this gas velocity. Liquid circulation patterns develop in the large diameter column at a gas velocity of 0.04 m/s which help break up the foam. At a gas velocity of 0.12 m/s, the gas holdup in the uppermost region of both columns was lower than that observed at a gas velocity of 0.04 m/s (see Figures 2.14a and 2.14b). Also, the gas holdup profile along the column height was fairly uniform in both columns. This indicates that the foam layer which was present in both columns at a gas velocity of 0.04 m/s had dissipated. Figure 2.15 compares axial gas holdup profiles at slurry velocities of 0.0, 0.005, and 0.02 m/s in the small diameter column. At a gas velocity of 0.02 m/s (Figure 2.15a) axial gas holdup profiles are similar for all slurry flow rates. At a gas velocity of 0.04 m/s there is a significant difference in the gas holdup profiles in the uppermost section of the column (i.e. at a height greater than 1.5 m above the distributor; see Figure 2.15b) between experiments conducted in the continuous mode of operation and the experiment conducted in the batch mode of operation. In the lower section of the column (i.e. <2.2 m above the distributor), the holdups from all three experiments are similar. This, shows that in the absence of foam, there is very little effect of liquid flow rate on gas holdup. Also, this substantiates the claim that a slight upward liquid flow rate is sufficient to dissipate the foam layer. At a gas velocity of 0.12 m/s (Figure 2.15c), we once again observe similar axial gas holdup profiles at all slurry flow rates. However, axial gas holdups are consistently lower at a slurry velocity of 0.02 m/s.

Experiments were conducted in both columns with FT–300 wax to study the effect of slurry flow rate on average gas holdup in three–phase systems. Results similar to those with FT–300 wax (no solids) were obtained (i.e. an increase in slurry flow rate

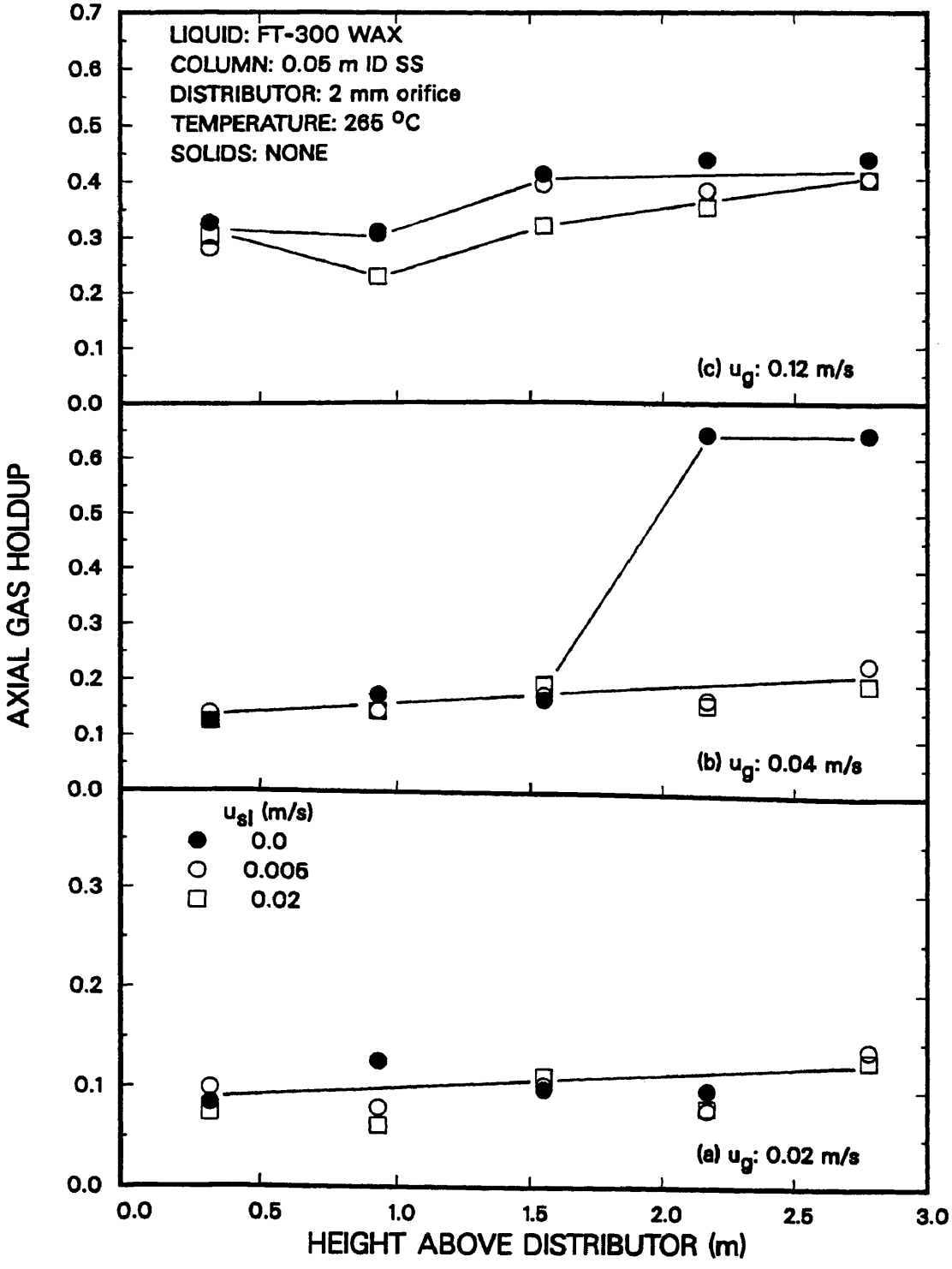

Figure 2.15. Effect of superficial slurry velocity on axial gas holdup in the small diameter column with FT-300 wax.

causes a decrease in gas holdup when foam is present). Figure 2.16 shows results for experiments in the 0.05 m ID column with 20 wt% slurries of 0 – 5 μm iron oxide (Figure 2.16a) and 0 – 5 μm silica particles (Figure 2.16b). For these systems, gas holdups from experiments conducted in the batch mode of operation were consistently higher than those obtained from experiments conducted in the continuous mode of operation. A substantial decrease in holdup was observed when the slurry velocity was increased from 0.0 to 0.005 m/s. This decrease in gas holdup with increasing slurry velocity is due to the dissipation of the foam present in batch experiments. Similar trends were observed for 10 and 30 wt% slurries of 0 – 5 μm iron oxide particles.

Results from experiments in the large diameter column, with 20 – 44 μm iron oxide particles are shown in Figure 2.17. During the batch experiment, foam was produced at a gas velocity of 0.04 m/s. Increasing the slurry velocity to 0.005 m/s decreased the gas holdup (i.e. $\epsilon_g = 0.28$ for $u_\ell = 0$ and 0.11 for u_ℓ=0.005) at a gas velocity of 0.04 m/s. In the absence of foam (i.e. $u_g = 0.08$ and 0.12 m/s), there is not a significant effect of slurry flow rate on gas holdup.

Thus, gas holdup decreases with increasing slurry velocity for experiments conducted with FT–300 wax (with and without solids) in the 0.05 and 0.21 m ID columns. The decrease in holdup with increasing slurry flow rate is most pronounced at gas velocities which favor the formation of foam. In the absence of foam, the effect of slurry flow rate on gas holdup is negligible.

Results from experiments with SASOL wax (no solids) in the 0.05 and 0.21 m ID columns are shown in Figures 2.18a and 2.18b, respectively. SASOL wax behaves quite differently from FT–300, i.e. it does not have a tendency to foam. An increase in slurry flow rate from 0.0 to 0.005 m/s caused a slight decrease in gas holdup in both columns (see Figures 2.18a and 2.18b). This behavior (i.e. negligible effect of $u_{s\ell}$ on ϵ_g) is consistent with that observed in experiments with FT–300 wax in the absence of foam.

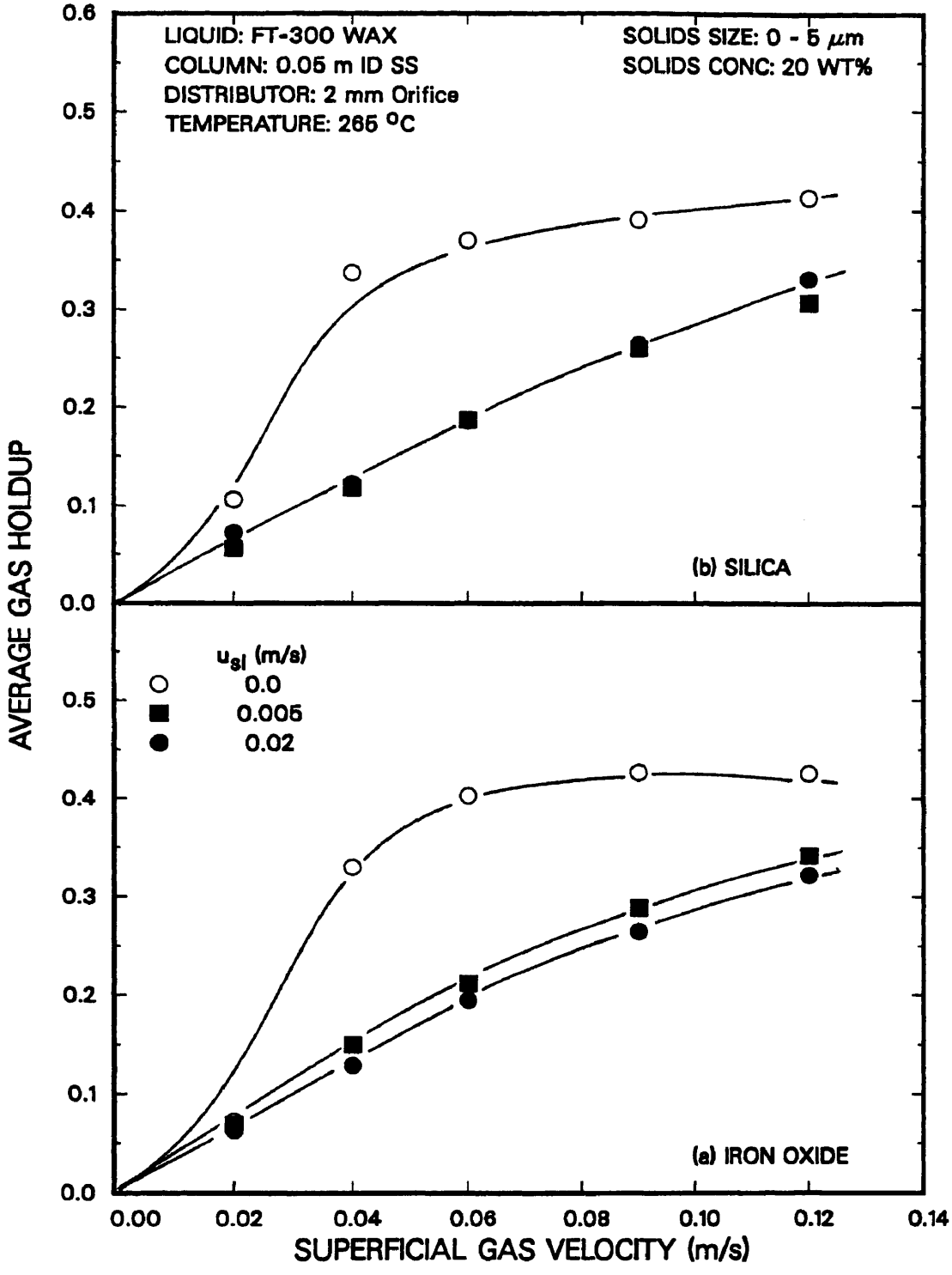

Figure 2.16. Effect of superficial slurry velocity on average gas holdup in the small diameter column with FT-300 wax in the presence of solids; (a) 0 - 5 μm iron oxide; (b) 0 - 5 μm silica.

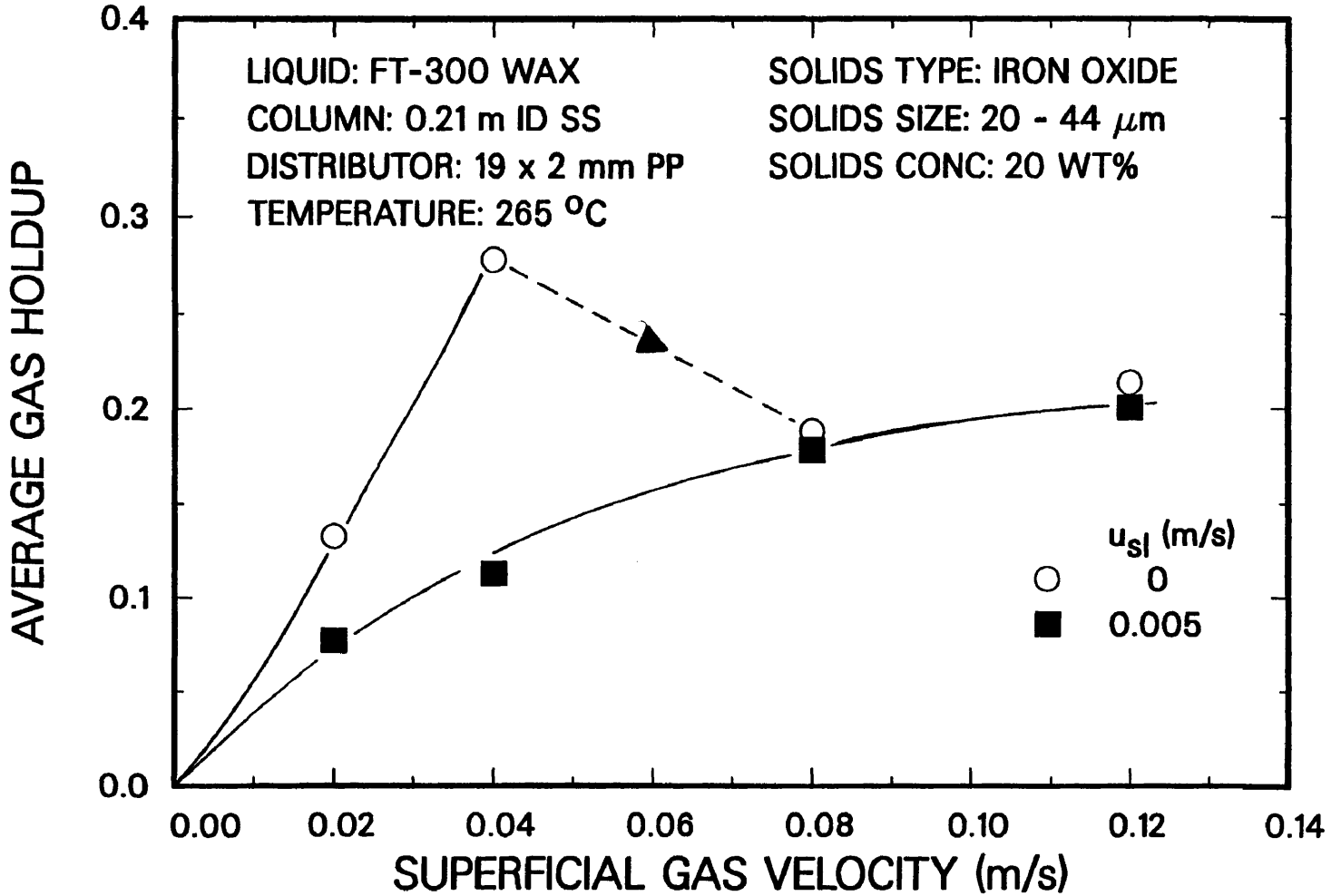

Figure 2.17. Effect of superficial slurry velocity on average gas holdup in the large diameter column with FT-300 wax (20 - 44 μm iron oxide).

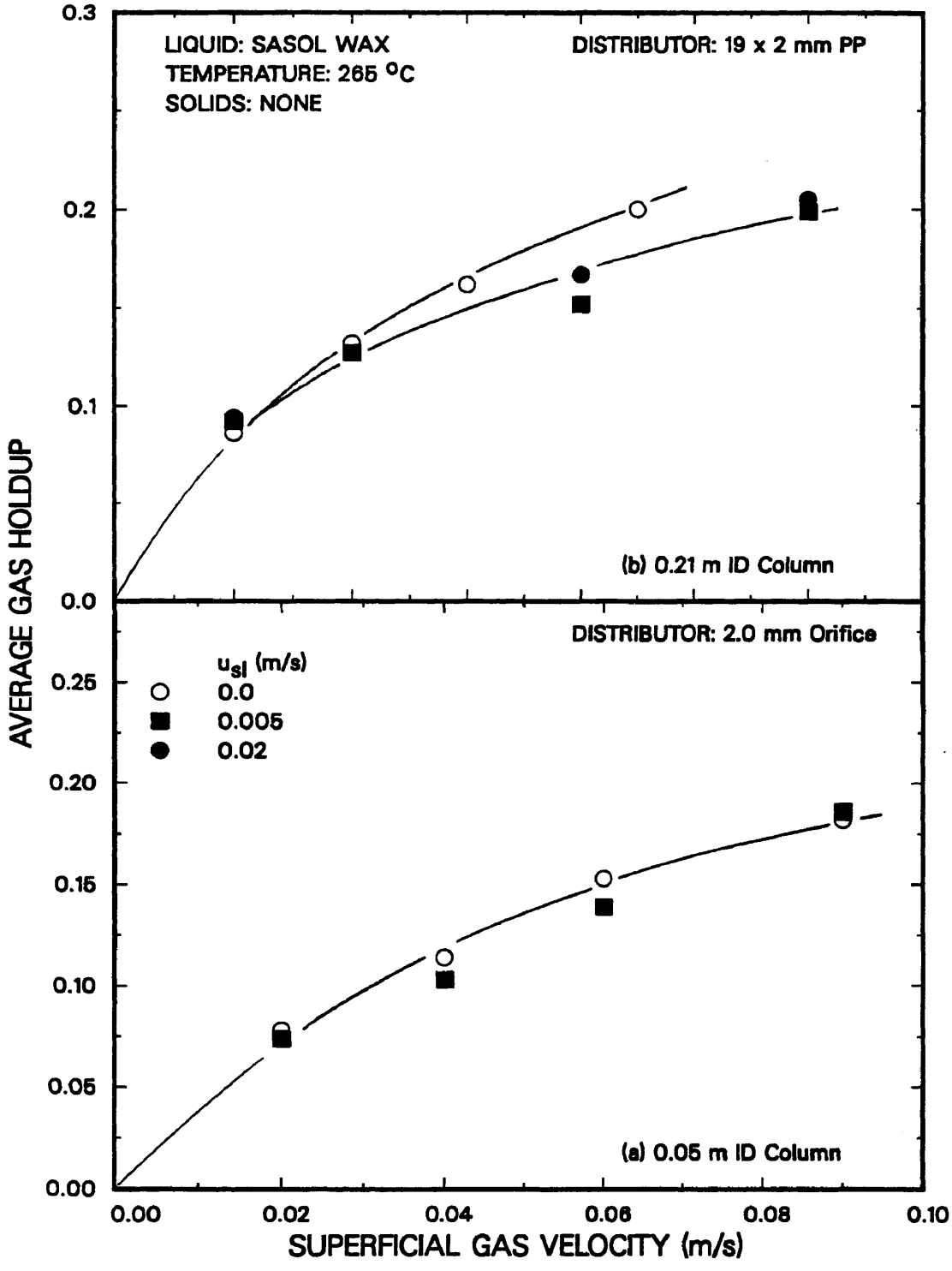

Figure 2.18. Effect of superficial slurry velocity on average gas holdup in the (a) small and (b) large diameter columns with SASOL wax.

Gas holdup results from three–phase experiments with SASOL reactor wax in the large diameter column are shown in Figure 2.19. There was no significant effect of slurry flow rate on average gas holdups for experiments with 0 – 5 μm and 20 – 44 μm iron particles (see Figures 2.19a and 2.19b, respectively). Results from the experiments conducted with 20 – 44 μm silica particles are shown in Figure 2.19c. During these experiments, the gas holdup decreased slightly with increasing slurry flow rate.

The trends observed in this study in the continuous mode of operation are in qualitative agreement with results from other studies. Studies with systems which do not foam (e.g., water – air) indicate that slurry (or liquid) velocity either has no effect on gas holdup (e.g., Akita and Yoshida, 1974; Shah et al., 1982), or decreases holdup only slightly (e.g., Kara et al., 1982; Buchholz et al., 1983; Kelkar et al., 1984; Ouyang and Tatterson, 1987). However, for systems which foam, gas holdup decreases markedly with increasing slurry velocity (e.g. Shah et al., 1985; Kelkar et al., 1983). For example, Shah et al. reported holdup values as high as 80 % with an aqueous ethanol solution at a superficial gas velocity of 0.20 m/s in the batch mode of operation; however, upon increasing the slurry flow rate to 0.0077 m/s, the gas holdup dropped to approximately 20 %.

Effect of Solids Concentration

The effect of solids concentration (iron oxide) on gas holdup in the 0.05 m (d_p = 0 – 5 μm) and 0.21 m ID (d_p = 20 – 44 μm) bubble columns with FT–300 wax as the liquid medium is shown in Figures 2.20a and 2.20b, respectively. Gas holdups in the small diameter column are highest for a solids concentration of 20 wt% at gas velocities greater than 0.02 m/s. At a solids concentration of 30 wt% the gas holdup values are lower than those for a 20 wt% slurry; however, the holdups are still higher than those with no solids present. In the large diameter column, gas holdups increased

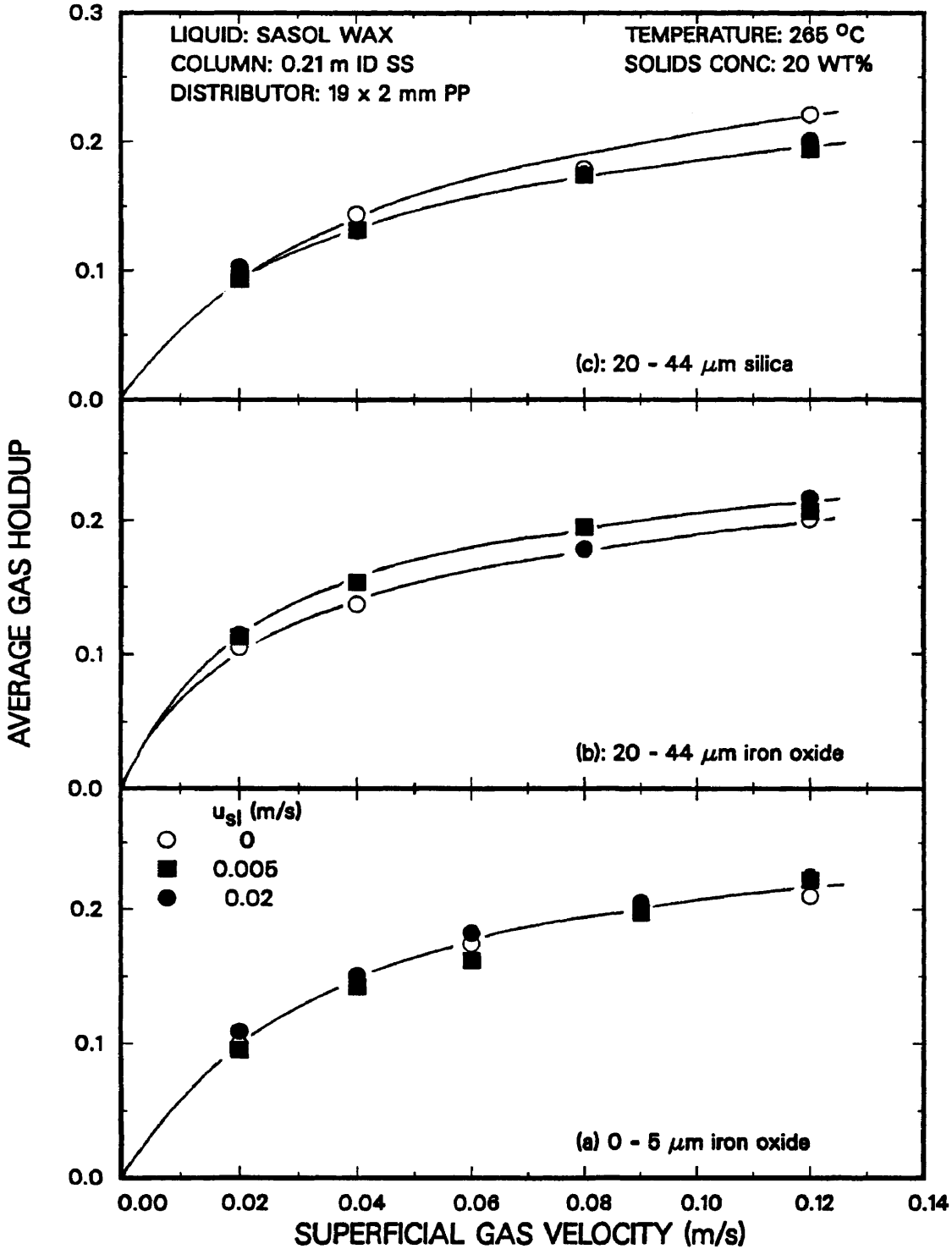

Figure 2.19. Effect of slurry velocity on average gas holdup in the large diameter column with SASOL wax ((a) 0 - 5 μm iron oxide, (b) 20 - 44 μm iron oxide, (c) 20 - 44 μm silica).

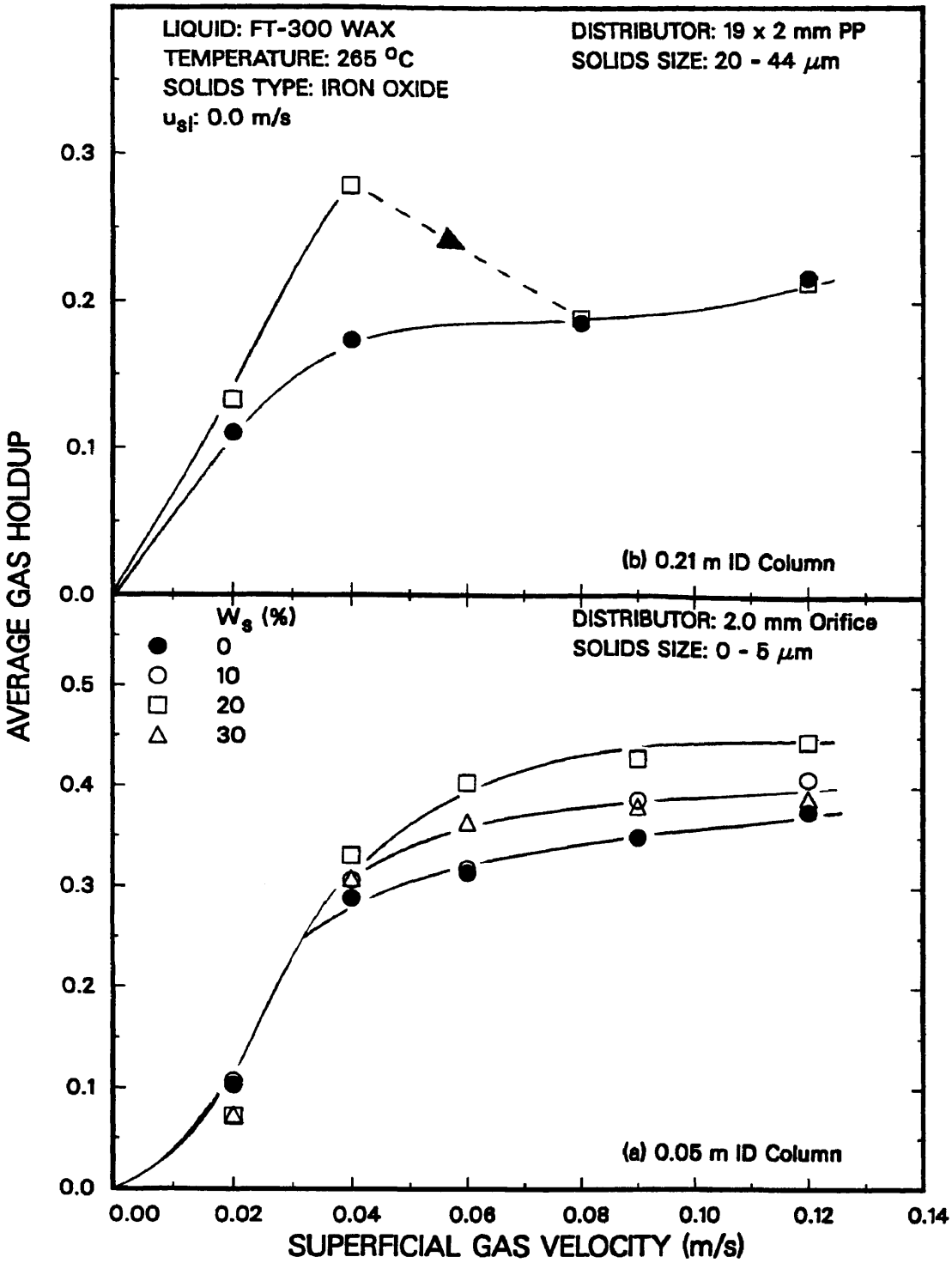

Figure 2.20. Effect of solids concentration on average gas holdup with FT-300 wax ((a) 0.05 m ID Column, 20 WT%, 0 - 5 μm iron oxide; (b) 0.21 m ID Column, 20 WT%, 20-44 μm iron oxide).

at gas velocities of 0.02 and 0.04 m/s with the addition of solids, but at gas velocities of 0.08 and 0.12 m/s, there was no effect of solids concentration on gas holdup.

Figure 2.21 shows axial gas holdup profiles at gas velocities of 0.02, 0.04, and 0.12 m/s for the four experiments conducted in the batch mode of operation with 0 – 5 μm iron oxide particles in the small diameter column. At a gas velocity of 0.02 m/s (Figure 2.21a), there was no consistent effect of solids concentration. However, at gas velocities of 0.04 and 0.12 m/s (Figures 2.21b and 2.21c, respectively), a definite trend exists in the uppermost sections of the column (i.e. above a height of 1.5 m above the distributor). The holdup in the presence of solids is consistently higher than that in the absence of solids. Also, the holdup increases with increasing concentration of solids up to a concentration of 20 wt %. Upon increasing the concentration of solids further (i.e. to 30 wt%), the holdup in the uppermost section of the column decreases.

Experiments were also conducted in the batch mode of operation with 20 wt% slurries of 20 – 44 μm iron oxide particles and 0 – 5 μm silica particles in the small diameter column. Average gas holdups from these experiments together with the experiment conducted without solids is shown in Figure 2.22. Once again, the gas holdup increased with the addition of both large iron oxide particles (Figure 2.22a) and small silica particles (Figure 2.22b).

As described below, the opposite trends were reported in the literature for the effect of solids concentration on gas holdup. In some studies, it was observed that gas holdup decreases with the addition of solids. This decrease in gas holdup was usually attributed to an increase in the slurry viscosity. Other investigators have found that when relatively small particles or low density particles are used, the addition of solids may cause the gas holdup to increase. In general, it was claimed that the increase in gas holdup is due to poor wettability of the solids.

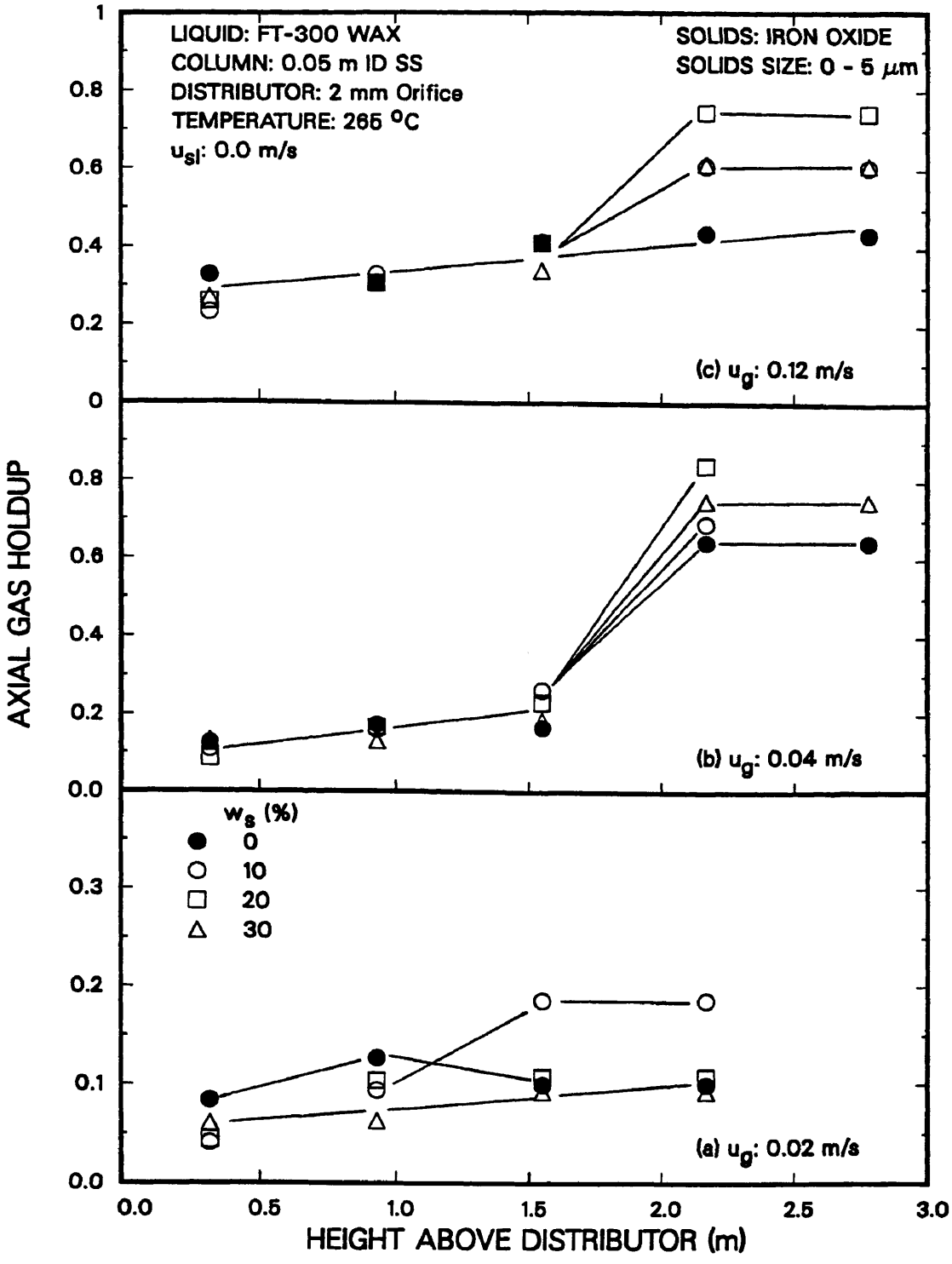

Figure 2.21. Effect of solids concentration and superficial gas velocity on axial gas holdup in the 0.05 m ID column with FT-300 wax (0 - 5 μm iron oxide particles; (a) u_g=0.02 m/s; (b) u_g=0.04 m/s; (c) u_g=0.12 m/s).

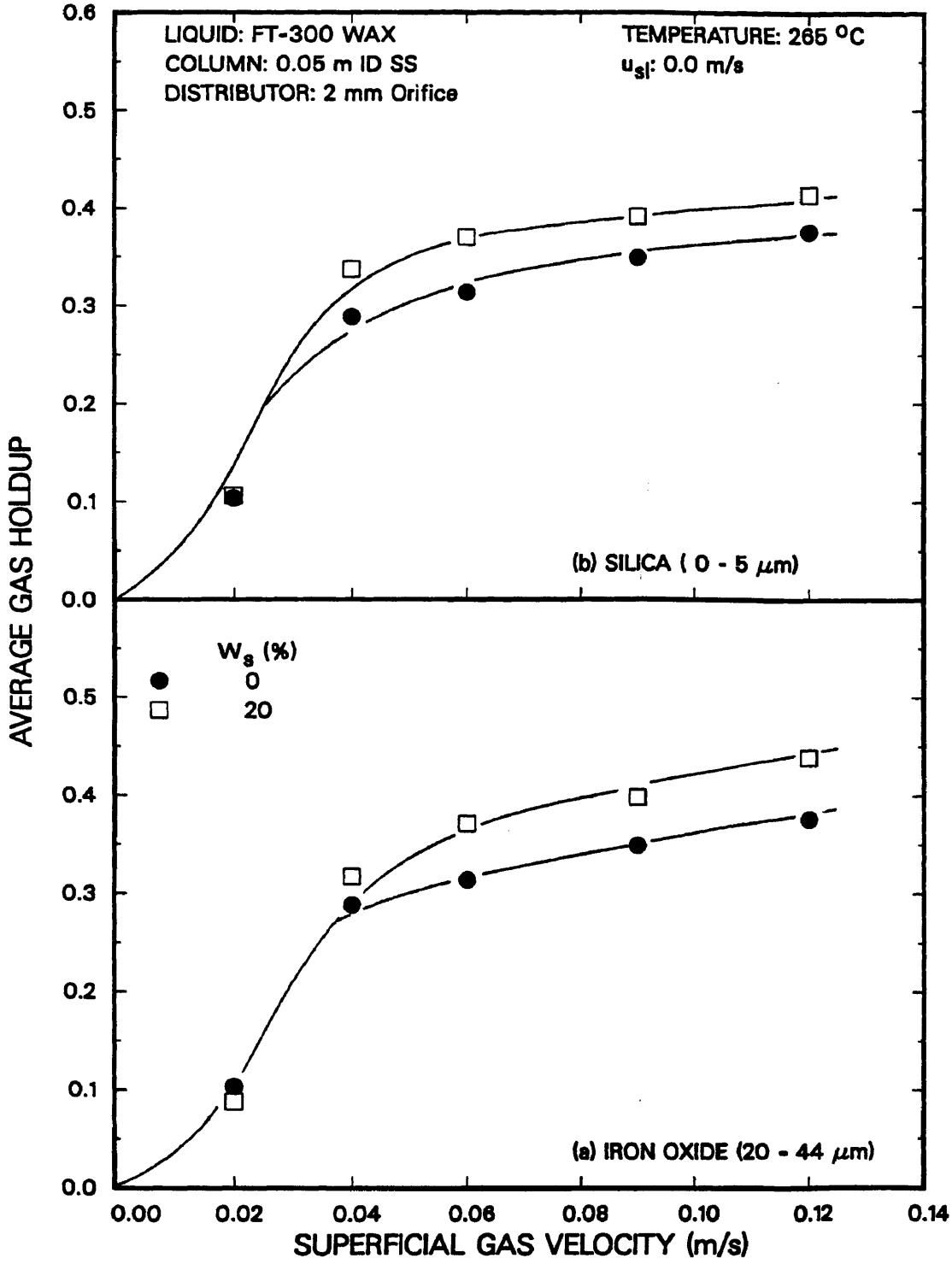

Figure 2.22. Effect of solids concentration on average gas holdup in the 0.05 m ID column with FT-300 wax ((a) 20 - 44 μm iron oxide; (b) 0 - 5 μm silica)

Deckwer et al. (1980) studied the effect of solids concentration (up to 16 wt%) in a paraffin wax/Al_2O_3/ nitrogen system. The solids were 0 – 5 μm in diameter. Their results, limited to low gas flow rates (u_g <0.04 m/s), showed that the addition of solids reduces gas holdup slightly ($\Delta\epsilon_g = 0.01$ to 0.02). However, they did not observe any specific trend in terms of the effect of solids concentration in the range 5.5 to 16 wt% on gas holdup. Ying et al. (1980) and Kato et al. (1972) also reported a decrease in gas holdup with increasing solids concentration. Kara et al. (1982) used various coal/water slurries with coal particles ranging from 10 to 70 μm in diameter, and solids loadings up to 44 wt%. In general, they observed a decrease in gas holdup with increasing solids concentration. However, with 10 μm particles, they observed a slight increase in gas holdup values relative to experiments conducted without solids. They postulated that the observed increase in gas holdup might be due to poor wettability. Results obtained from several other investigators show that the addition of solids increases gas holdup. Sada et al. (1986) examined the effect of fine particles (Al_2O_3 and $CaCO_3$) in both an electrolyte solution and in distilled water. Solids concentrations up to 1 wt% were used. Results from their study indicate that gas holdup decreases with the addition of solid particles ($d_p > 50$ μm). However, for particles less than 10 μm in diameter, in low concentrations, the gas holdup increases. They attributed this increase in gas holdup to the bubble coalescence hindering action of fine solids dispersed in the liquid film around the bubbles. They also observed, that the increase in gas holdup was more pronounced for systems which produce very fine bubbles. The effect of solids concentration and type was also studied by Sauer and Hempel (1987). They observed an increase in gas holdup with increasing solids concentrations (up to 13 wt%) for particles with densities less than 1300 kg/m^3 and superficial gas velocities in the range 0.01 to 0.04 m/s. They explained their results by using the qualitative model of Rabiger (1985). According to Rabiger, there exists an optimum ratio between the particle diameter

and microscale of turbulence which depends on density, particle shape and structure of liquid turbulence. Upon reaching the optimum ratio, the turbulence associated with the three–phase system is greater than that with the two–phase system, and as a result, smaller bubbles are produced and this gives rise to higher gas holdups. This increase in turbulence is only possible up to certain values of gas holdups and solids concentrations because the distances between bubbles and particles become very small in the swarm. Thus, on exceeding certain values, the turbulence subsides, resulting in larger bubbles and consequently lower holdups.

The increase in gas holdup with the addition of solids which we observed during experiments conducted in the batch mode of operation with FT–300 wax may be attributed to poor solids wettability in the region of high gas holdup (i.e. at heights greater than 1.5 m above the distributor). Bhatia et al. (1972) have shown that non-wettable particles cause an increase in bed expansion in a three–phase fluidized bed. They attributed the increase in bed expansion to solid particles adhering to the surface of the large fast rising gas bubbles and being carried upward through the column. In our case, we have relatively high density particles (ρ_s = 2650 and 5100 kg/m^3) and very small, slow rising gas bubbles (see Chapter V). Thus, when particles adhere to the surface of these small bubbles, they not only reduce coalescence, but they also reduce the effective rise velocity of the gas bubble, which results in a longer residence time. This in turn causes an increase in the gas holdup. In the lower portion of the column (i.e. below the foam layer), gas holdups are substantially lower than they are in upper portion of the column (see Figure 2.21). Figure 2.23 shows average gas holdups, excluding foam (i.e. neglecting axial gas holdups at heights of 2.2 and 2.8 m above the distributor when calculating the average gas holdup), for experiments conducted with small iron oxide particles in the 0.05 m ID column. As can be seen, there is a slight decrease in gas holdup with increasing solids concentration when the foam is neglected.

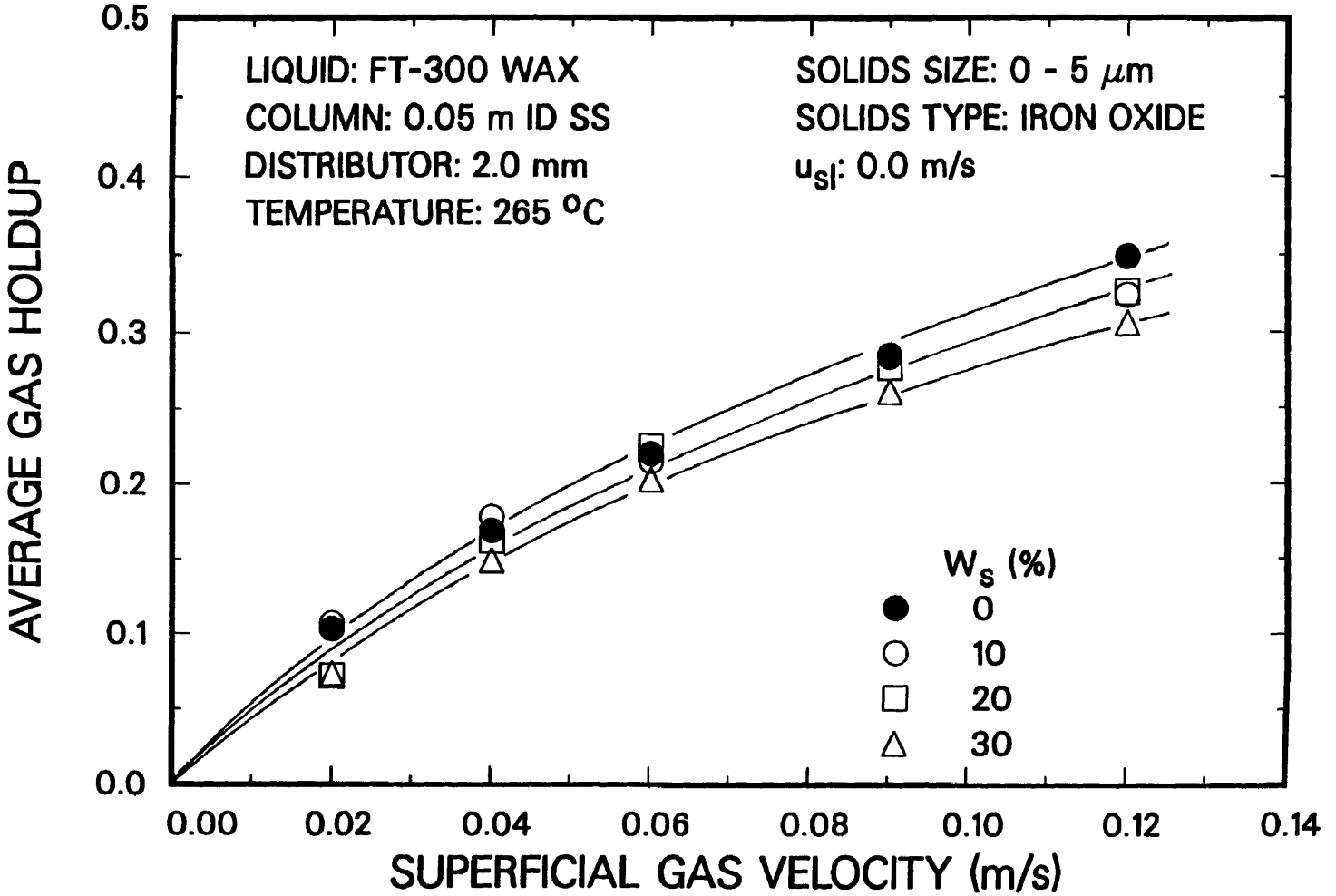

Figure 2.23. Effect of solids concentration on average gas holdup neglecting foam (0 - 5 μm iron oxide).

This decrease in gas holdup with increasing solids concentration may be attributed to an increase in the apparent viscosity of the slurry. It has been shown that an increase in slurry viscosity produces larger bubbles which in turn reduces the gas holdup (Bukur et al., 1987a). Thus, the variation in the effect of solids concentration on gas holdup may be due to: (1) poor wettability of solids, and (2) an increase in the slurry viscosity with the addition of solids. The former causes the gas holdup to increase, while the latter causes the gas holdup to decrease. These competing phenomena might be responsible for the maximum in gas holdup observed with the 20 wt% slurry of small iron oxide particles.

Some experiments were also conducted with FT–300 wax in the continuous mode of operation to determine the effect of solids concentration on average gas holdup. Figures 2.24a and 2.24b show results from experiments conducted with iron oxide particles (0 – 5 μm) in the small diameter column using slurry velocities of 0.005 and 0.02 m/s, respectively. The average gas holdup decreased with increasing solids concentration for experiments conducted in the continuous mode of operation. Thus, it appears that a small upward liquid flow is sufficient to disperse the fine bubbles at the top of the dispersion, and as a result, the adhesion of the solid particles to the liquid film of the bubbles comprising the foam no longer has a significant effect on the gas holdup. The decrease in gas holdup is due solely to the increase in slurry viscosity associated with the addition of solids. Similar results were observed for experiments with small silica silica particles in the 0.05 m ID column and with large iron oxide particles in the 0.21 m ID column at a slurry velocity of 0.005 m/s (see Figures 2.25a and 2.25b, respectively).

Gas holdups from batch experiments with SASOL reactor wax in the 0.05 m ID column with 20 – 44 μm iron oxide particles and in the 0.21 m ID column with both 20 – 44 and 0 – 5 μm iron oxide particles are shown in Figure 2.26. The trends were qualitatively similar to those observed in experiments with FT–300 wax in the presence

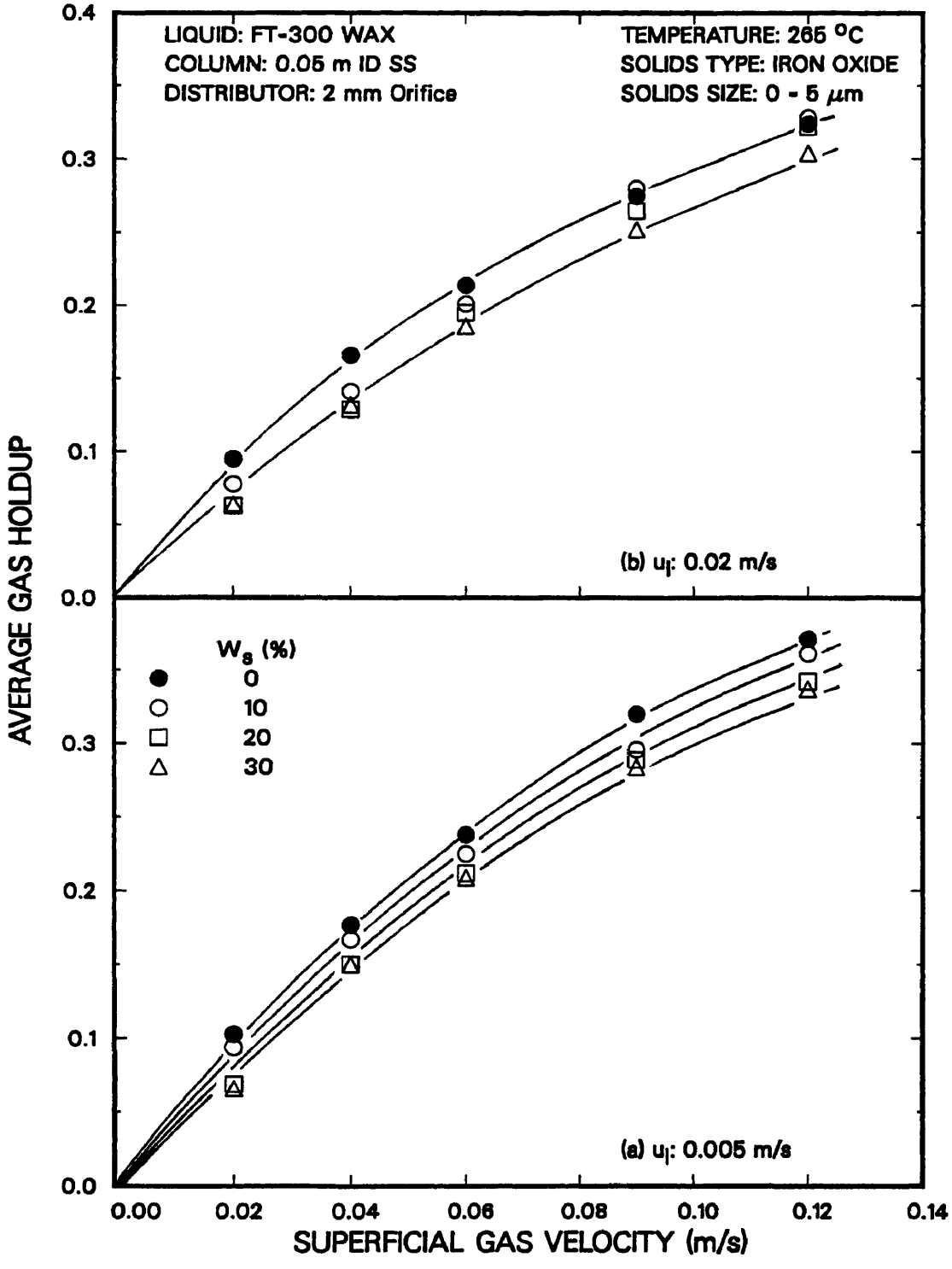

Figure 2.24. Effect of solids concentration on average gas holdup in the continuous mode of operation with FT-300 wax (0 - 5 μm iron oxide; (a) u_{sl} = 0.005 m/s; (b) u_{sl} = 0.02 m/s).

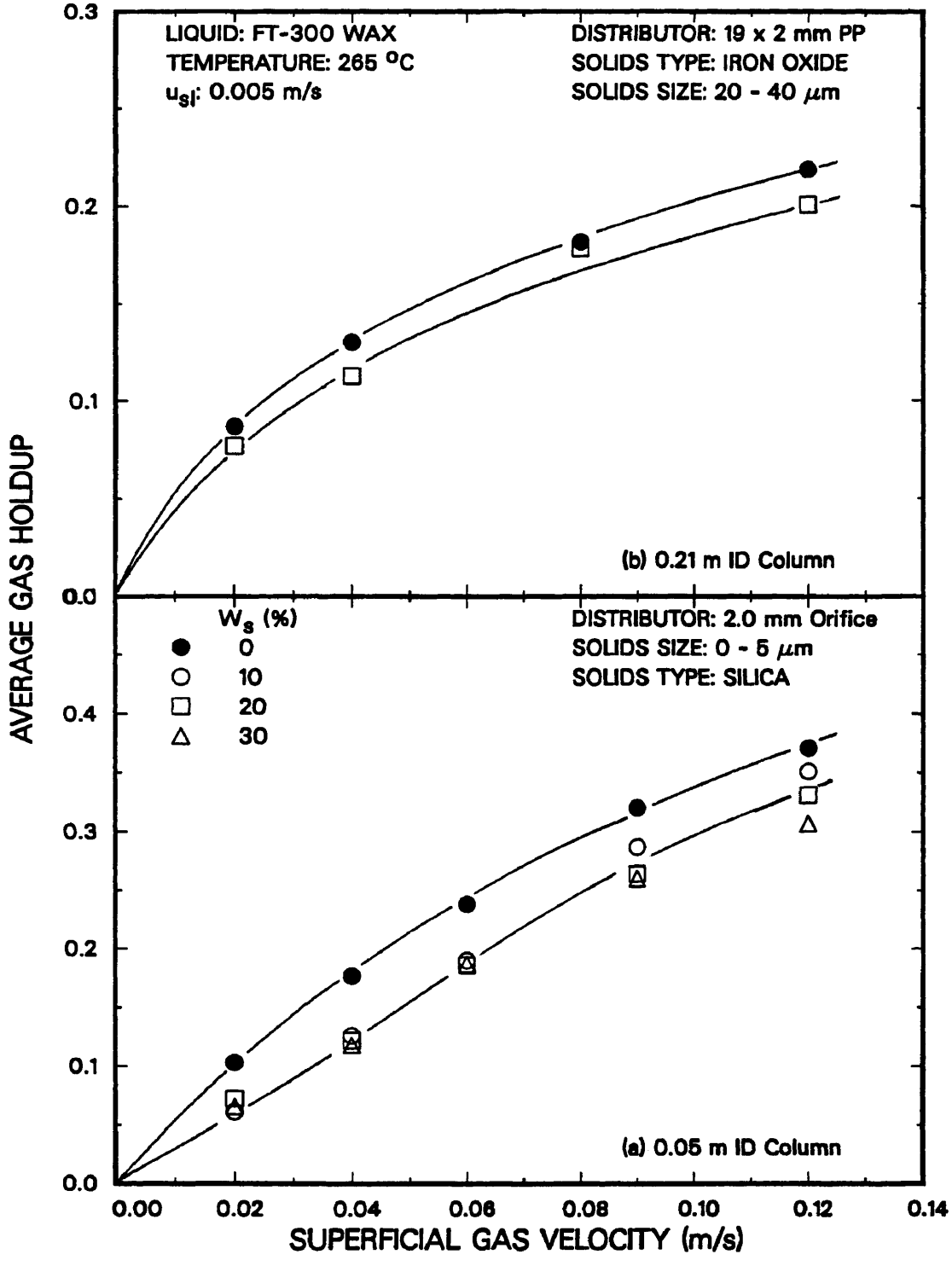

Figure 2.25. Effect of solids concentration on average gas holdup with FT-300 wax ((a) 0.05 m ID column, 0 - 5 μm silica; (b) 0.21 m ID column, 20 - 44 μm iron oxide).

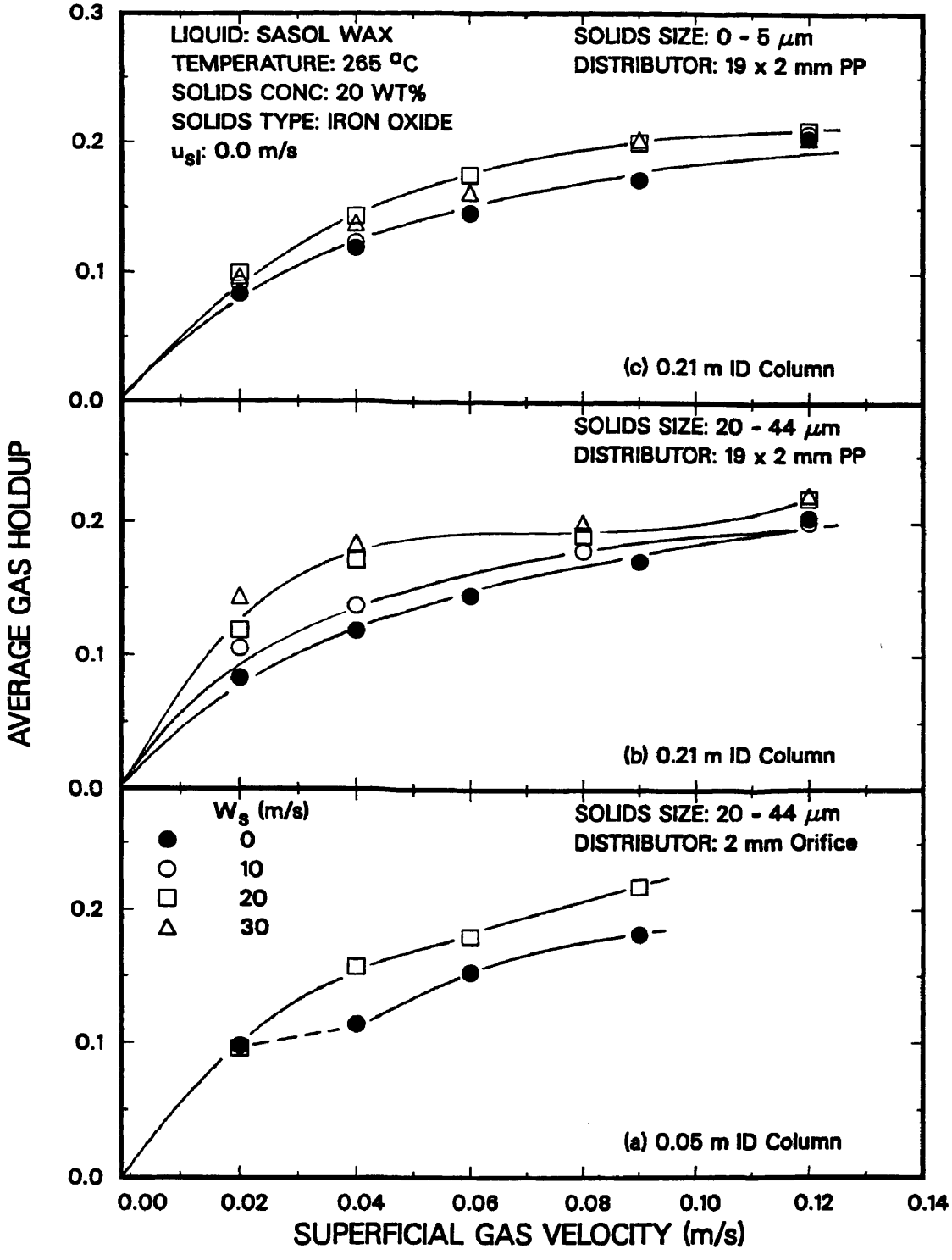

Figure 2.26. Effect of solids concentration on average gas holdup with SASOL wax ((a) 0.05 m ID column, 20 - 44 μm iron oxide, (b) 0.21 m ID column, 20 - 44 μm iron oxide, (c) 0.21 m ID column, 0 - 5 μm iron oxide).

of solids (i.e. the addition of solids caused an increase in gas holdup). These results were somewhat surprising since SASOL wax does not produce foam. Since we observed a decrease in gas holdup with the addition of solids in the absence of foam with FT–300 wax (see Figures 2.23 and 2.24), we expected gas holdups with SASOL reactor wax to decrease with increasing solids concentration. However, the solids used in this study may be less wettable in SASOL wax as compared to FT–300 wax, and as a result the holdups increased. One indication of this is the fact that the holdup in the uppermost section of the small diameter column increased by 50 to 70 % (relative) with the addition of large iron oxide particles for the experiment with SASOL wax, but increased only by 30 to 50 % (relative) for the experiment conducted with FT–300 wax.

Experiments were also conducted with SASOL wax in the continuous mode of operation. The addition of solids increased the gas holdup for experiments in both the small and large diameter columns. Figure 2.27a shows results from experiments conducted with small iron oxide particles in the 0.05 m ID column. Results from experiments conducted with various concentrations of large iron oxide particles and various concentrations of small iron oxide particles are shown in Figures 2.27b and 2.27c respectively. Gas holdups increased with increasing solids concentration. Holdup values from experiments in the large diameter column approached the same value at superficial gas velocities greater than 0.08 m/s. A similar trend was observed during batch experiments in the large diameter column (see Figures 2.26b and 2.26c).

Similar results were observed for experiments conducted with silica particles in the large diameter column; however, the increase in gas holdup with increasing solids concentration was less pronounced. The convergence of gas holdup values at high gas velocities for various slurry concentrations in the large diameter column is due to an increase in turbulence. Turbulence is greater in the large diameter column than the small diameter column (i.e. the flow patterns present in the large diameter column are

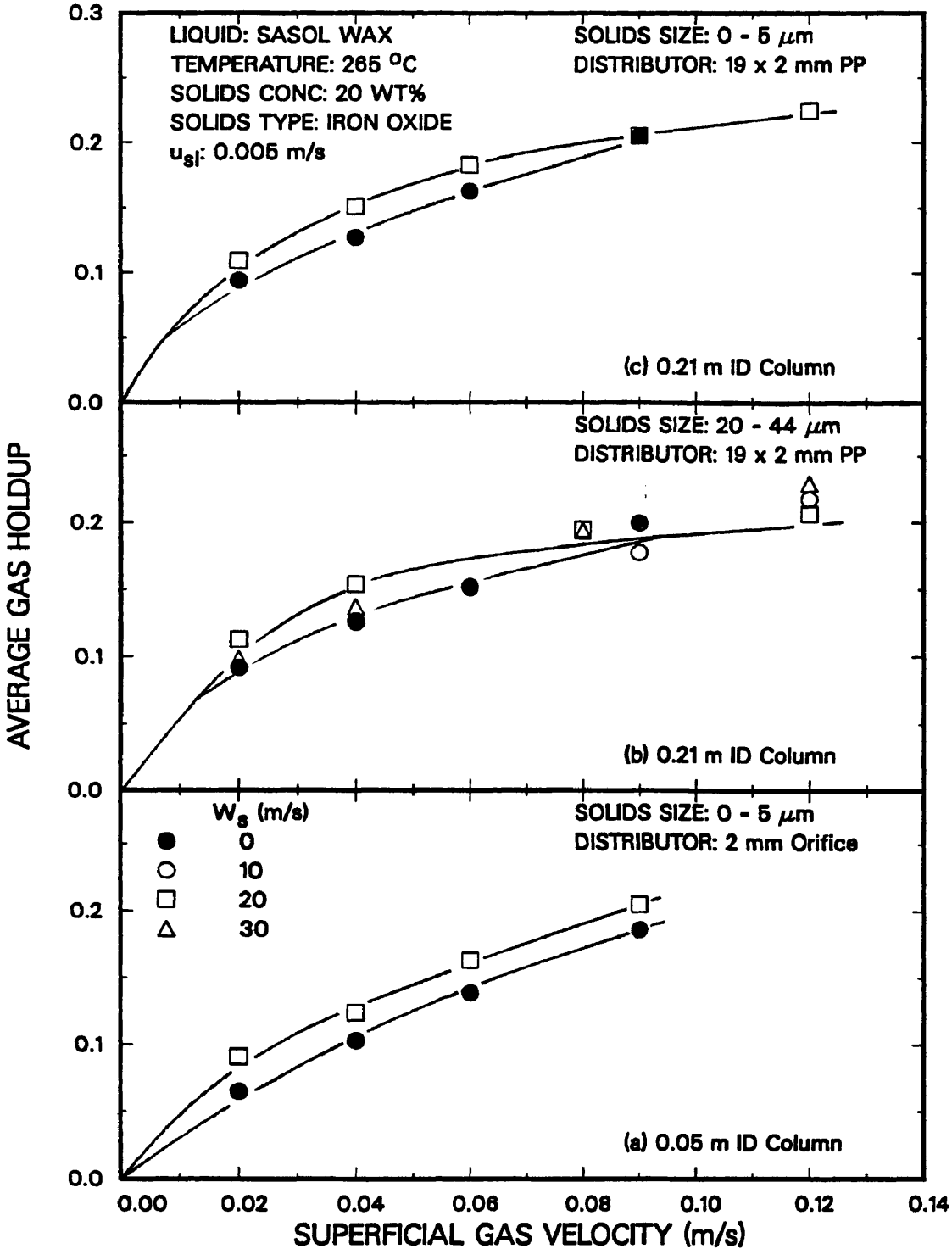

Figure 2.27. Effect of solids concentration on average gas holdup with SASOL wax in the continuous mode of operation ((a) 0.05 m ID column, 20 - 44 μm iron oxide, (b) 0.21 m ID column, 20 - 44 μm iron oxide, (c) 0.21 m ID column, 0 - 5 μm iron oxide).

much more chaotic). Therefore, at high superficial gas velocities, any particles which may adhere to the surface of gas bubbles are likely to be stripped away, and as a result, gas holdups in the presence of solids become similar to those in the absence of solids.

Thus, the addition of solids increases gas holdup for experiments conducted in the batch mode of operation with both FT–300 and SASOL reactor wax. However, in the continuous mode of operation, addition of solids to FT–300 wax causes a slight decrease in the gas holdup; whereas, addition of solids to SASOL wax causes a slight increase in the gas holdup. The differences in the behavior of the two waxes might be due to differences in the wettability of the particles with respect to each wax type.

Effect of Solids Type and Size

The effect of solids type and size for batch experiments with FT–300 wax in the small diameter column are shown in Figure 2.28. The highest holdups were obtained in experiments with small iron oxide particles. Gas holdups from experiments with large iron oxide particles and small silica particles were similar. An increase in gas holdup with increasing particle size has been observed in some earlier studies (Kim et al., 1977, Shah et al., 1982). A possible explanation for this is that the particles are breaking up the bubbles as they rise through the column, thus producing smaller bubbles and consequently higher gas holdups. Kim et al. showed that when solids have sufficient kinetic energy, they can cause bubble breakage which results in an increase in gas holdup. Using a balance between the surface tension forces of the bubble, and the force exerted by the particle, their proposed criterion for bubble breakage is:

$$\mathrm{We} = \frac{\rho_p u_r^2 d_p}{\sigma_\ell} > 3 \qquad (2.28)$$

For the system in our study, the Weber number, We, has a maximum value of 1.5 and is obtained for large iron oxide particles suspended in FT–300 wax at u_g=0.12 m/s.

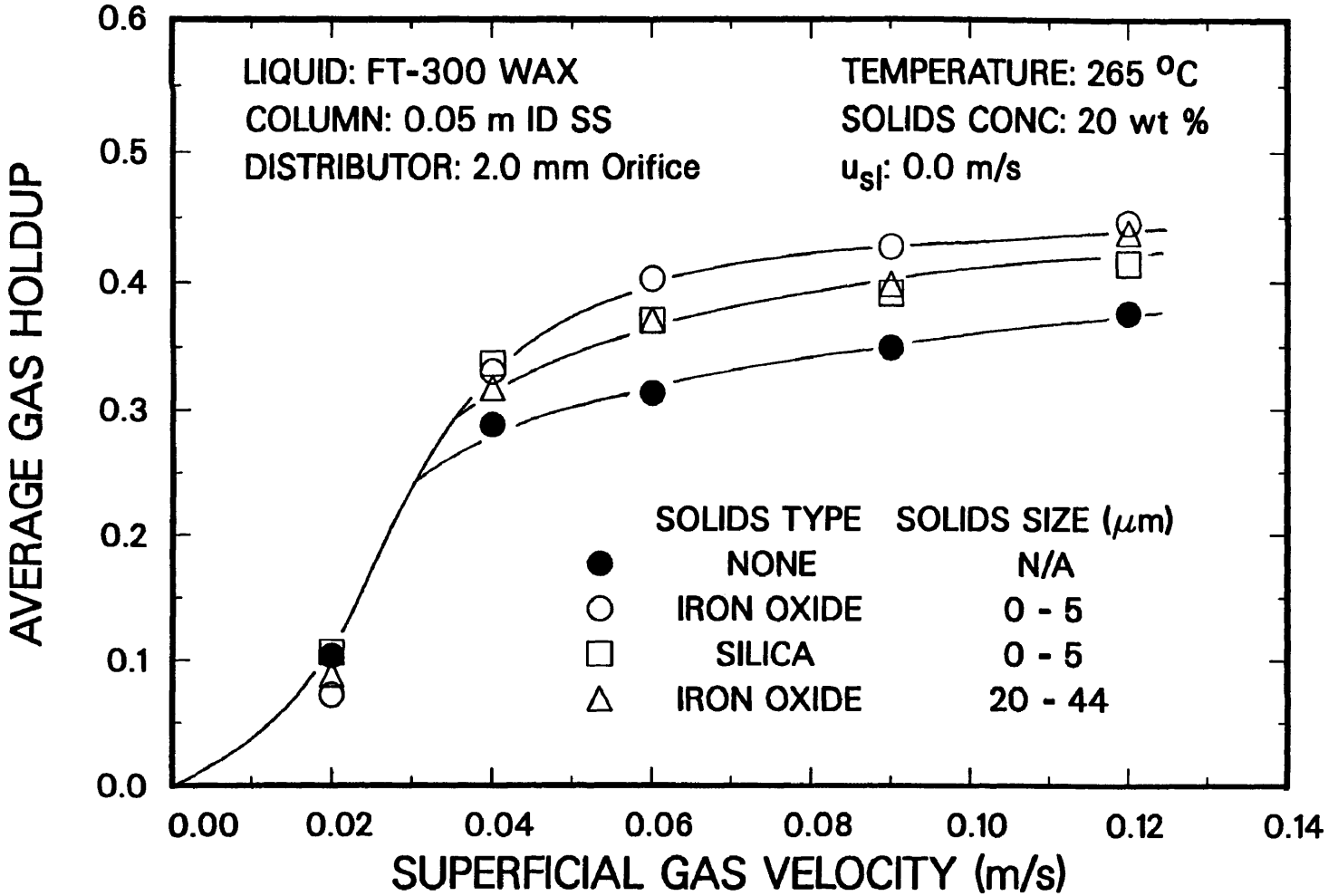

Figure 2.28. Effect of solids type and size on average gas holdup in the 0.05 m ID column with FT-300 wax.

Thus, we can assume that with our particles, no bubble breakage is occurring due to the presence of solids.

One possible explanation for the decrease in gas holdup with increasing particle size that was observed, might be due to the non–uniformity in the axial solids distribution of large particles. For the experiment conducted with small iron oxide particles, the solids concentration remains axially uniform ($\approx$ 20 wt%); however, in experiments with large iron oxide particles, the solids concentration at the bottom of the column ranged from 30 to 35 wt% (see the Figure on page 208). This increase in solids concentration at the bottom of the column results in a higher apparent slurry viscosity near the orifice plate. As a result, larger bubbles may be formed in the region near the distributor which results in lower gas holdups.

Figure 2.29 shows results for experiments conducted in the batch mode of operation with 30 wt % small iron oxide, 20 wt% small silica, and 20 wt% large iron oxide slurries. The gas holdups from all three runs are similar. All three experiments had similar volume concentrations of solids near the distributor (i.e. $\approx$ 0.045). These results indicate that the volume concentration of solids near the distributor may be important in determining the gas holdup. Similar results were observed for experiments conducted in the continuous mode of operation with small iron oxide and silica particles.

The effect of solids type and size for experiments with 20 wt% slurries (SASOL wax) in the large diameter column is shown in Figures 2.30a and 2.30b for experiments conducted in the batch and continuous modes of operation, respectively. Gas holdups were similar for batch experiments with small iron oxide particles and large iron oxide and silica particles. In the continuous mode of operation, there is no discernible effect of either solids type or size on gas holdup.

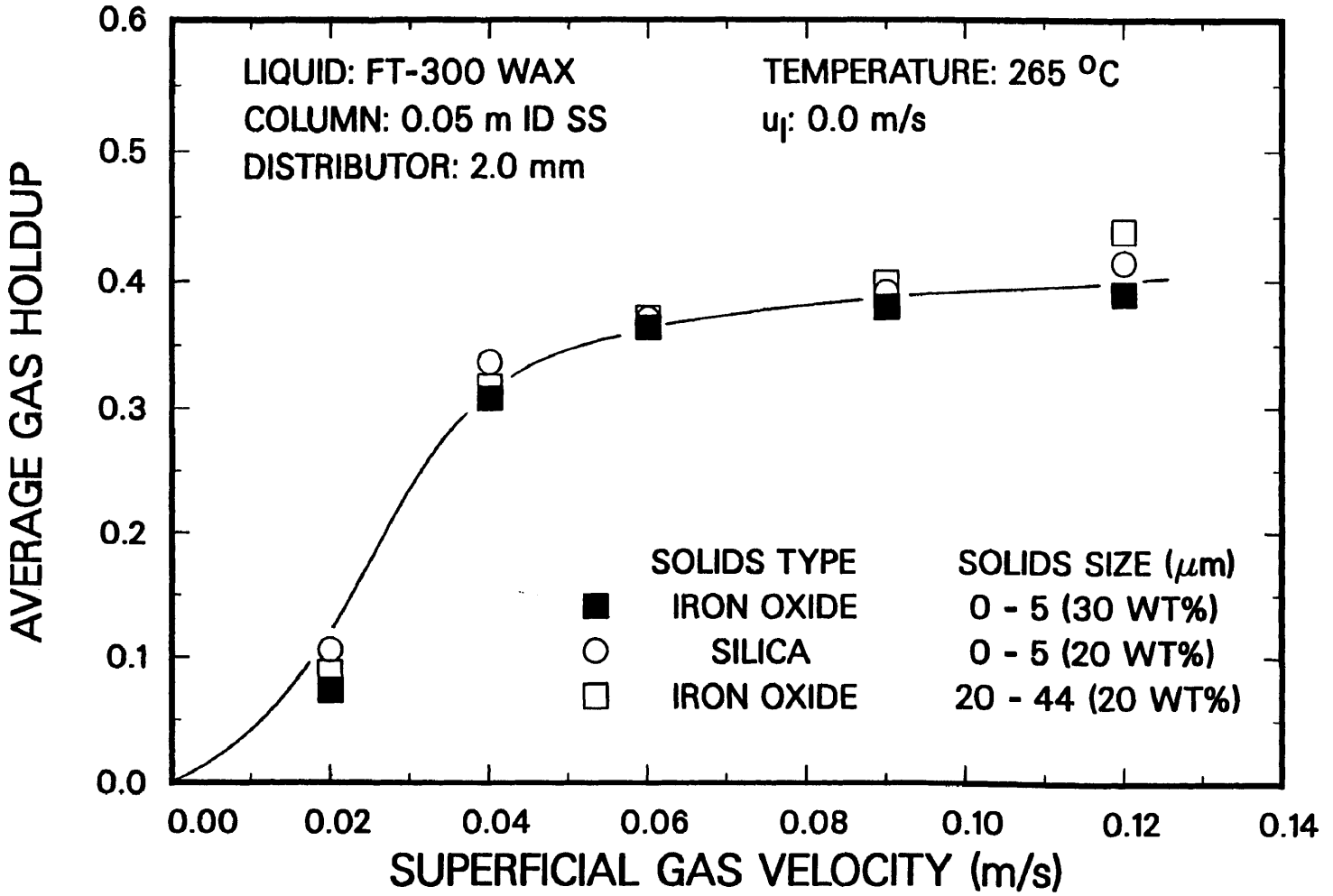

Figure 2.29. Effect of solids type and size on average gas holdup in the 0.05 m ID column with FT-300 wax (volume fraction of solids at the distributor = 0.045).

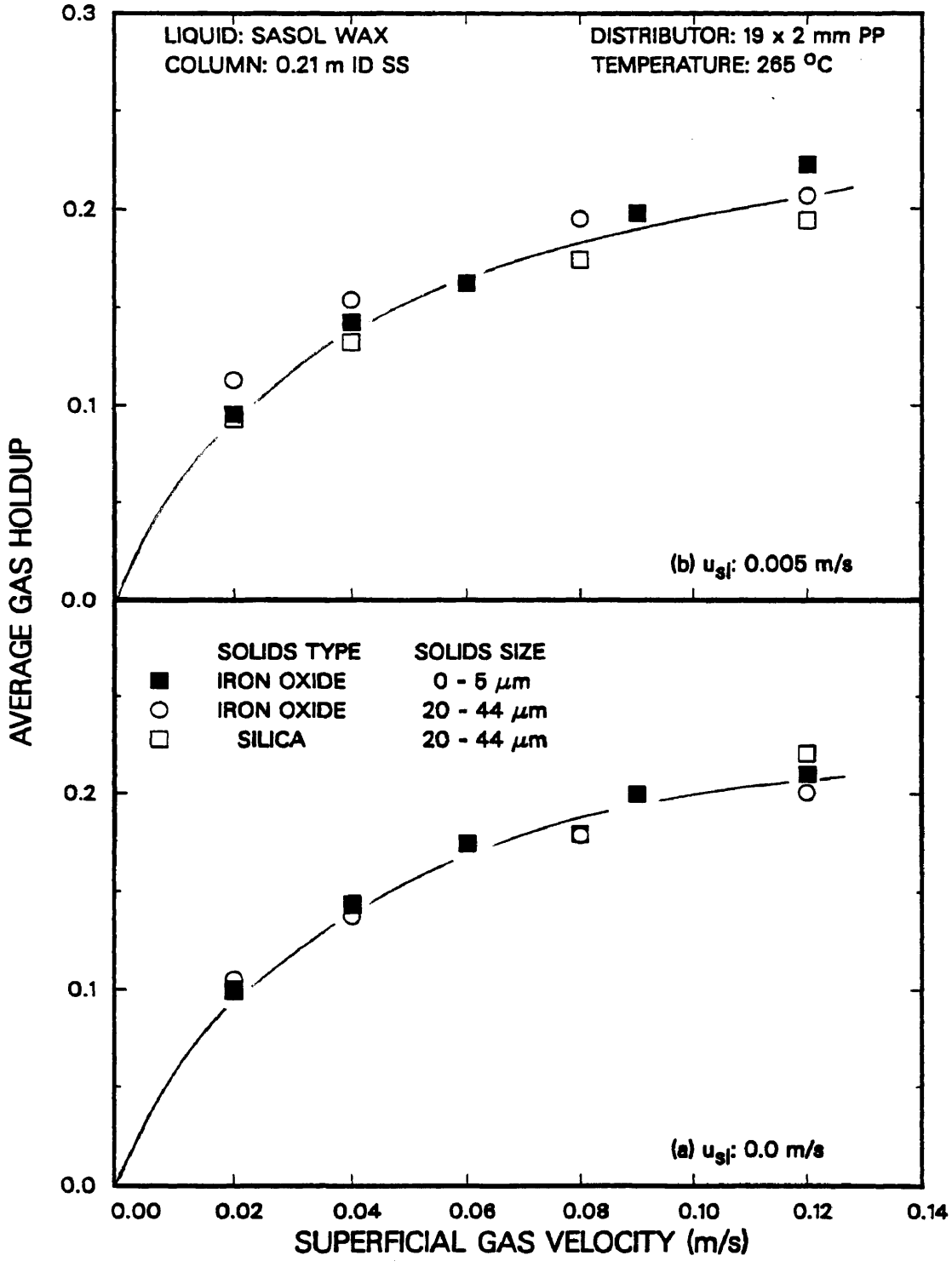

Figure 2.30. Effect of solids type and size on average gas holdup in the 0.21 m ID column with SASOL wax ((a) u_{sl} = 0.0 m/s; (b) u_{sl} = 0.005 m/s).

Effect of Liquid Medium

As mentioned previously, SASOL reactor wax and FT–300 wax behaved differently in the 0.05 m ID column. FT–300 wax has a tendency to foam, and as a result, gas holdups obtained with FT–300 wax were substantially higher than those obtained with SASOL reactor wax. Results from experiments with SASOL wax and FT–300 wax are shown in Figure 2.31. In particular, Figure 2.31a shows results from batch experiments conducted without solids and Figure 2.31b shows results for experiments conducted with 20 wt% 0 – 5 μm iron oxide particles at a superficial slurry velocity of 0.005 m/s. The results indicate that regardless of the presence of solids or liquid circulation, gas holdups are substantially higher with FT–300 wax. This increase in gas holdup is due to a higher concentration of fine bubbles present throughout the dispersion in FT–300 wax. Bubble sizes associated with FT–300 wax and SASOL reactor wax will be discussed in detail in Chapter V.

In the large diameter column, the foaming capacity of FT–300 wax is greatly reduced. This is primarily due to the increase in liquid mixing (or turbulence) with increasing column diameter (Kato et al., 1972; Heijnen and Van't Riet, 1984). This increase in liquid mixing hinders the production of a stable foam layer at the top of the dispersion and as a result, the nonfoamy or churn–turbulent regime dominates.

For experiments conducted in the batch mode of operation, gas holdups with FT–300 wax are significantly greater than those with SASOL wax at low gas velocities (see Figure 2.32a). In the fully developed churn–turbulent regime (i.e. at $u_g \geq 0.08$ m/s) gas holdups with FT–300 wax and SASOL wax are similar. The same trend was observed in experiments conducted in the batch mode of operation with 20 – 44 μm iron oxide particles (see Figure 2.32b). At a superficial gas velocity of 0.04 m/s the gas holdup with FT–300 was significantly greater than that of SASOL wax (28% for FT–300 and

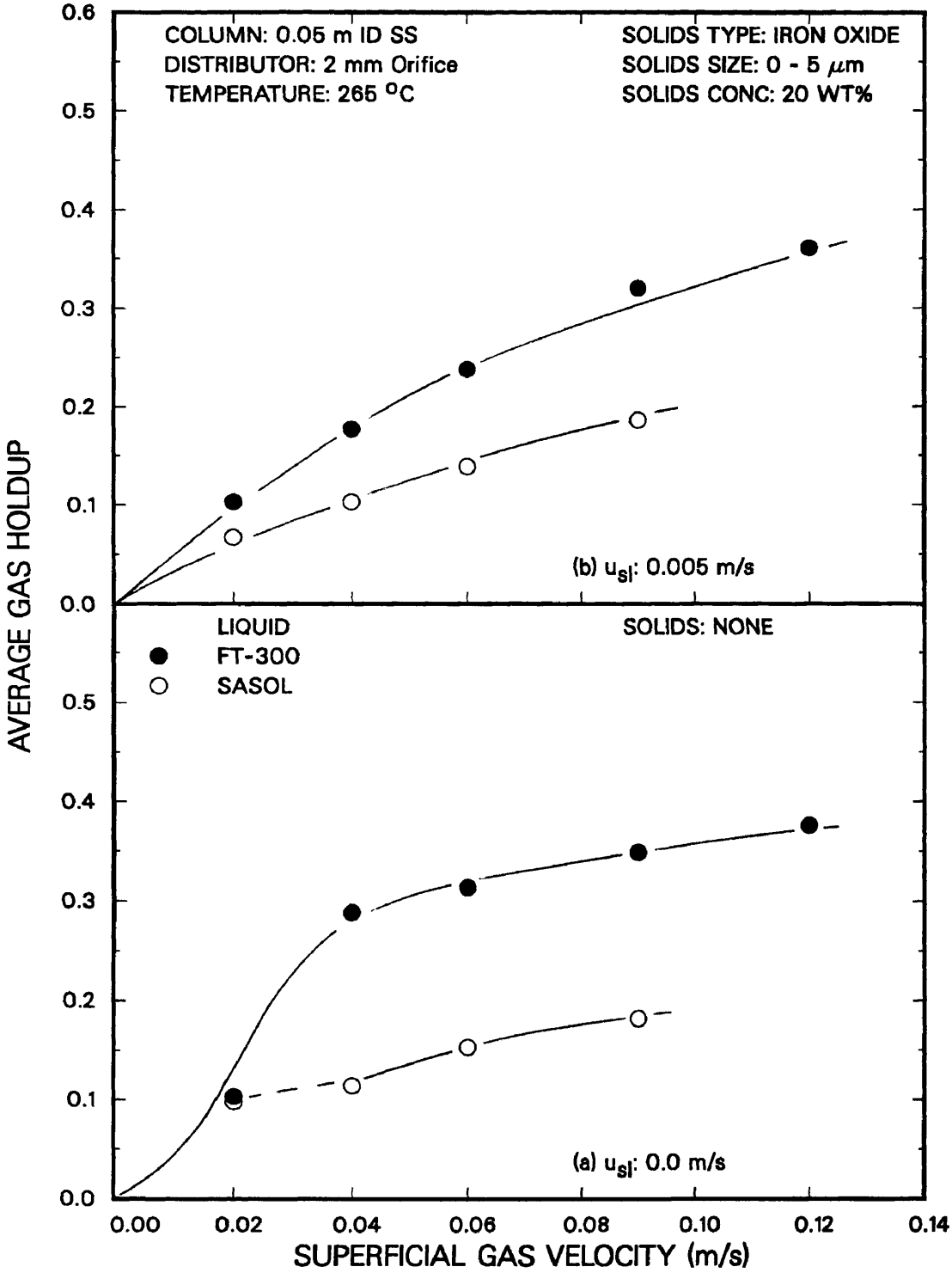

Figure 2.31. Effect of liquid medium on average gas holdup in the 0.05 m ID column.

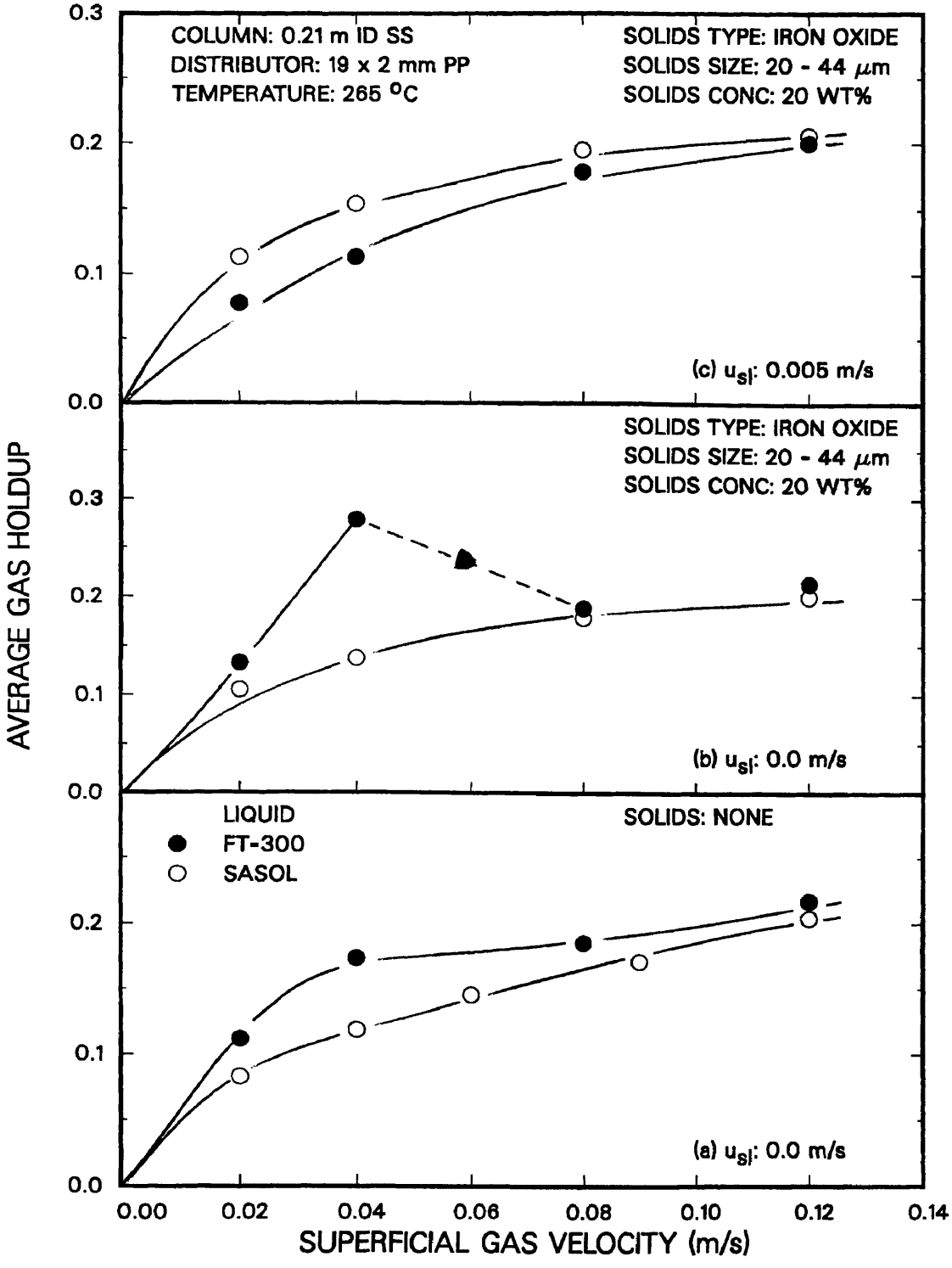

Figure 2.32. Effect of liquid medium on average gas holdup in th 0.21 m ID column.

14% for SASOL). At higher gas velocities (i.e. $u_g = 0.08$ and 0.12 m/s) the foam layer collapses and gas holdups with FT–300 wax and SASOL wax approach the same value. Gas holdup values obtained with SASOL wax were greater than those with FT–300 wax for experiments conducted in the continuous mode of operation in the presence of large iron oxide particles (Figure 2.32c). As described previously, iron oxide particles appear to be partially nonwettable in SASOL wax, and as a result, when the slip velocity between the gas and liquid phases is reduced, the gas holdup increases. However, at sufficiently high gas velocities, the turbulence created in the large diameter column is sufficient to reduce the adhesion of solid particles to the surface of the tiny gas bubbles, which results in slightly lower holdups. Thus, at higher gas velocities ($u_g \geq 0.08$ m/s), holdup values obtained from the experiments with SASOL reactor wax and FT–300 wax approach the same value.

Effect of Temperature

Experiments were conducted in the 0.05 m ID glass column to study the effect of temperature on average gas holdup (Bukur et al., 1987b; Bukur and Daly, 1987). Average gas holdup results for experiments conducted at temperatures in the range 160 to 280 °C with FT–300 wax are shown in Figure 2.33. In general, the gas holdup increased with increasing temperature. The highest gas holdups were obtained at a temperature of 280 °C; whereas, the lowest gas holdups were obtained with a temperature of 160 °C. For the experiment conducted at 265 °C, there was a transition from the foamy to nonfoamy regime. No foam was produced in the run conducted at 160 °C; therefore, gas holdup values were consistently lower for this run. In the absence of foam, the effect of temperature is less pronounced, with marginally lower holdups at lower temperatures. This behavior can be qualitatively explained in terms of the liquid viscosity (e.g. $\mu_\ell =$

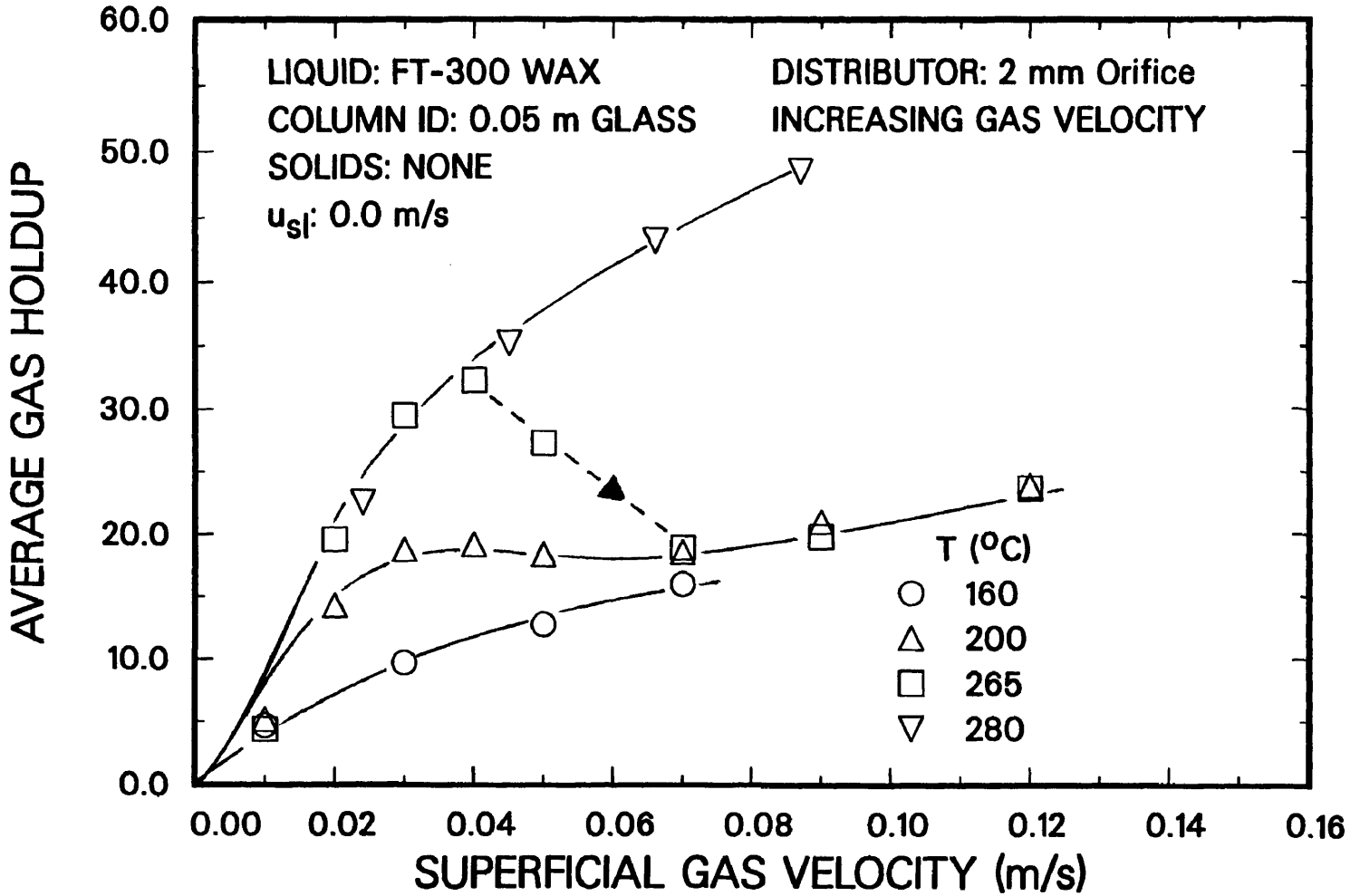

Figure 2.33. Effect of temperature on average gas holdup in the 0.05 m ID column.

0.0064 kg/m-s at 150 °C vs. 0.0028 kg/m-s at 260 °C, for FT–300 wax). Bubble coalescence increases with liquid viscosity (i.e. as temperature decreases) and fine bubbles, which are precursors of foam, do not accumulate at the top of the dispersion at low temperatures (Patel et al., 1990; Bukur et al., 1987c).

Experiments were also conducted with SASOL reactor wax at 200 and 265 °C. A marginal decrease in holdup was observed as the temperature was decreased from 265 to 200 °C. These results are in agreement with those of FT–300 in the absence of foam.

Several researchers have investigated the effect of temperature using paraffin waxes as the liquid medium. The majority of these studies were conducted in the presence of foam, and there are some discrepancies in results from these studies. Deckwer et al. (1980) found a significant decrease in gas holdup with increasing temperature for experiments conducted in a 0.04 m ID column, while no effect of temperature was found for runs conducted in a 0.10 m ID column. Experiments conducted by Quicker and Deckwer (1981), using FT–300 wax, showed consistently higher holdup values at 170 °C compared to values at 130 °C with both a 0.9 mm nozzle and a 19 x 1.1 mm perforated plate distributor. Researchers at Mobil (Kuo, 1985) used FT–200 wax as the liquid medium and found that holdup values at 138 °C were substantially lower than those at 260 °C. Despite some inconsistency in results, the overall trend is that gas holdup increases with increasing temperature when foam is present.

Effect of Distributor Type

A limited number of experiments were conducted with the bubble cap distributor in the large diameter column. Gas holdup values from experiments with the bubble cap distributor were consistently higher than those from experiments with the 19 x 2 mm perforated plate distributor. Figures 2.34a and 2.34b show results obtained with SASOL ($u_\ell = 0$ m/s) and FT–300 wax ($u_\ell = 0.005$ m/s), respectively. For both waxes,

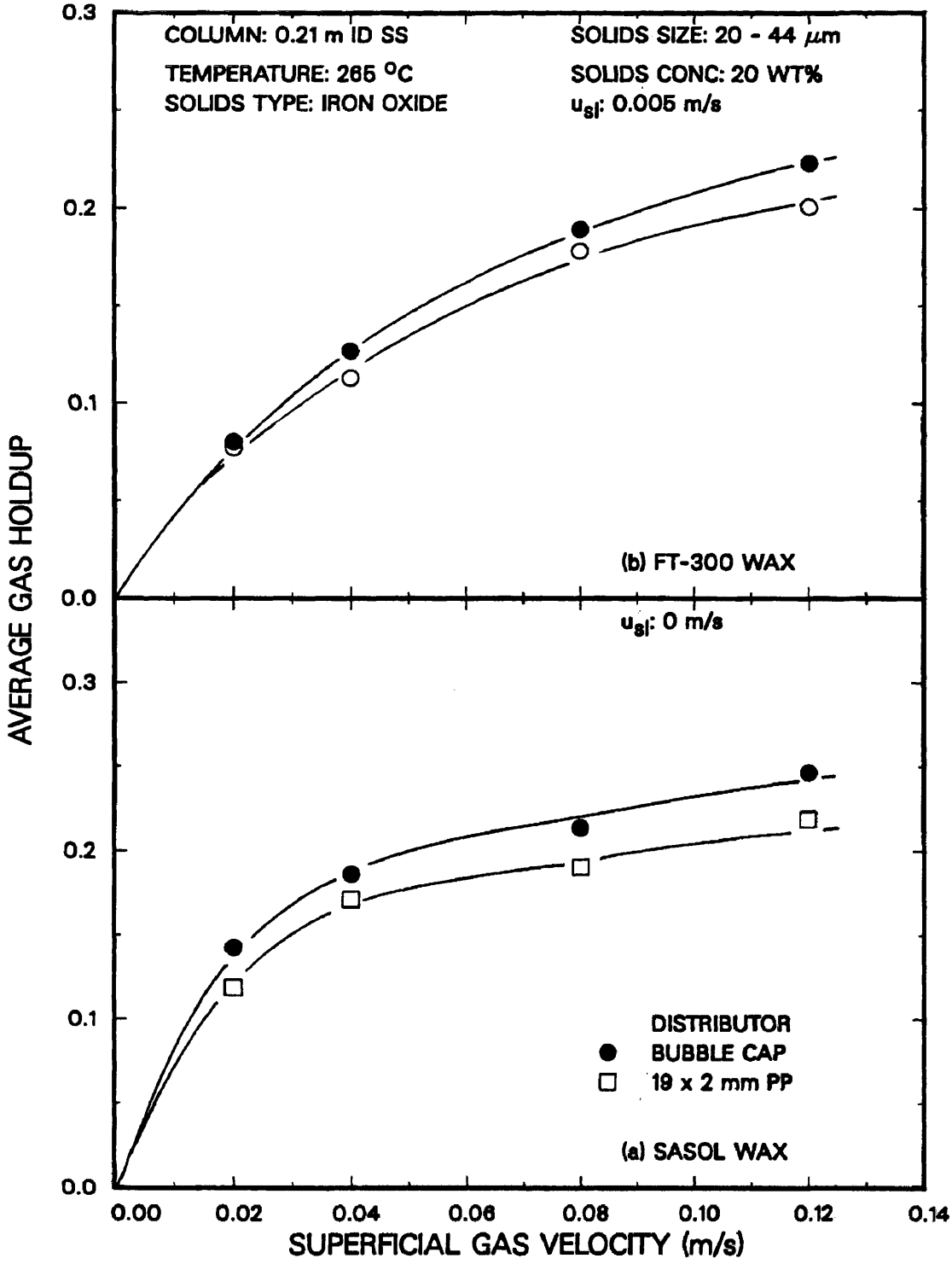

Figure 2.34. Effect of superficial gas velocity and distributor type on average gas holdup (20 - 44 μm iron oxide; (a) SASOL wax, u_{sl} = 0.0 m/s; (b) FT-300 wax, u_{sl} = 0.005 m/s).

holdups associated with the bubble cap distributor were slightly higher than those with the perforated plate distributor. The jet velocity through both distributors is essentially the same (e.g. at $u_g = 0.12$ m/s, the jet velocity through the perforated plate is 69 m/s while, with the bubble cap it is 63 m/s). Based solely on jet velocities, one would expect the gas holdups to be essentially the same for both distributors. However, we believe that the way in which the gas flows through the two different distributors is the primary cause of the increase in holdup observed with the bubble cap distributor. The bubble cap distributor is comprised of seven bubble caps, each with three 2 mm orifices. The flow of gas from each orifice is directed downward towards the distributor (see Figure 2.8). Thus, as the gas bubbles or gas jet exits the openings in the bubble caps, they are broken up by colliding with the distributor plate. On the other hand, as the gas exits the openings in the perforated plate distributor, it flows freely upward through the column; there are no obstacles in its path which may cause bubble breakup. Similar results were obtained for experiments conducted with small iron oxide particles in the batch and continuous modes of operation (see Figures 2.35a and 2.35b, respectively).

Effect of Column Diameter

Gas holdup values from experiments in the small diameter column with FT–300 wax were consistently higher than gas holdup values from experiments in the large diameter column (see Figure 2.36a). The main difference in gas holdups obtained in the two columns is that foam is produced more readily in the small diameter column and once produced, persists over a wider range of gas velocities. During one of the experiments in the small diameter column, the foam broke at a gas velocity of 0.09 m/s (see dashed line in Figure 2.36a) and the gas holdup value was similar to that obtained in the large diameter column. At a gas velocity of 0.02 m/s gas holdups in both columns are similar. This is expected, since at a velocity of 0.02 m/s, the homogeneous bubbling regime

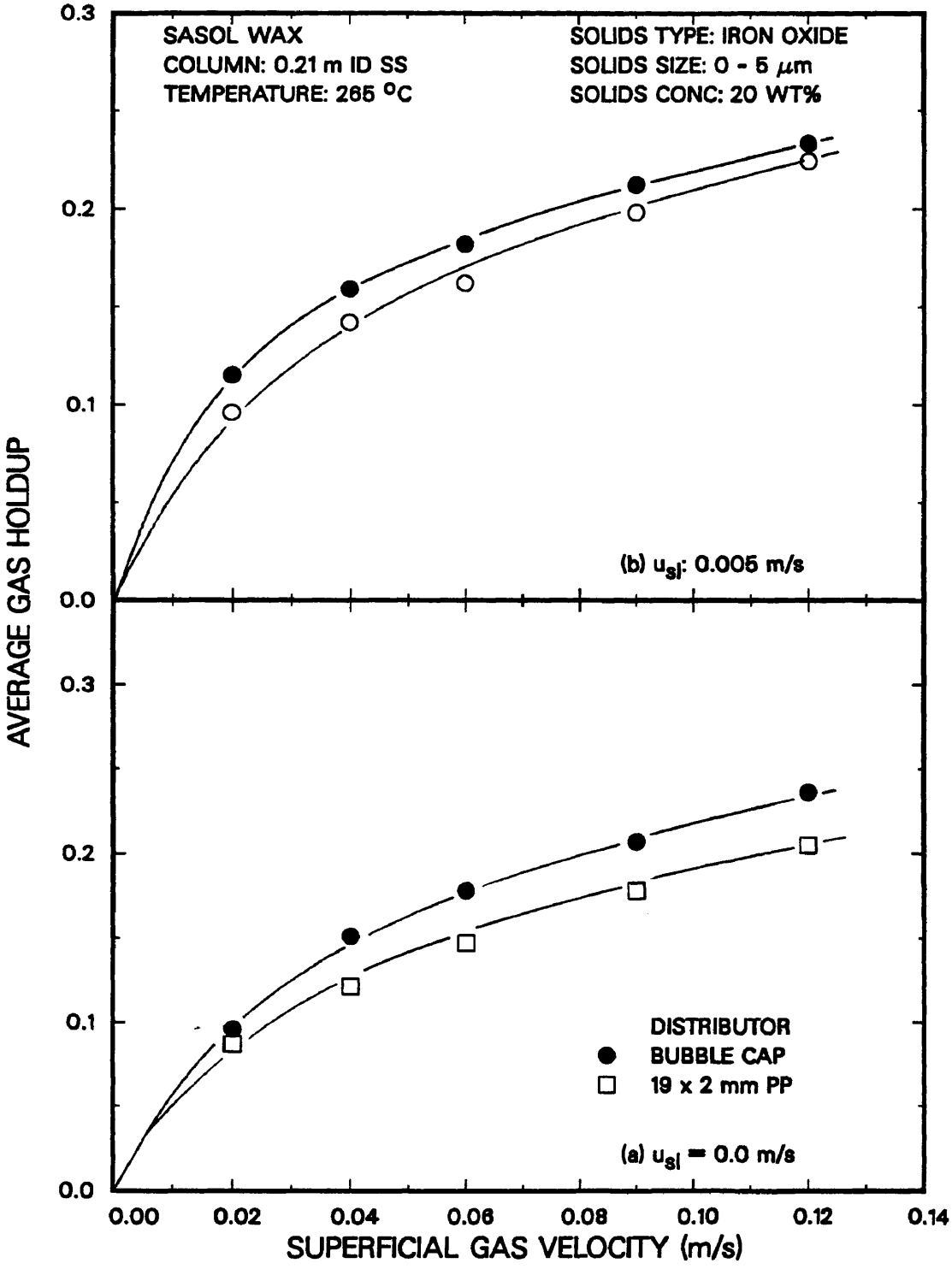

Figure 2.35. Effect of superficial gas velocity and distributor type on average gas holdup with SASOL wax (0 - 5 μm iron oxide; (a) u_{sl} = 0.0 m/s; (b) u_{sl} = 0.005 m/s).

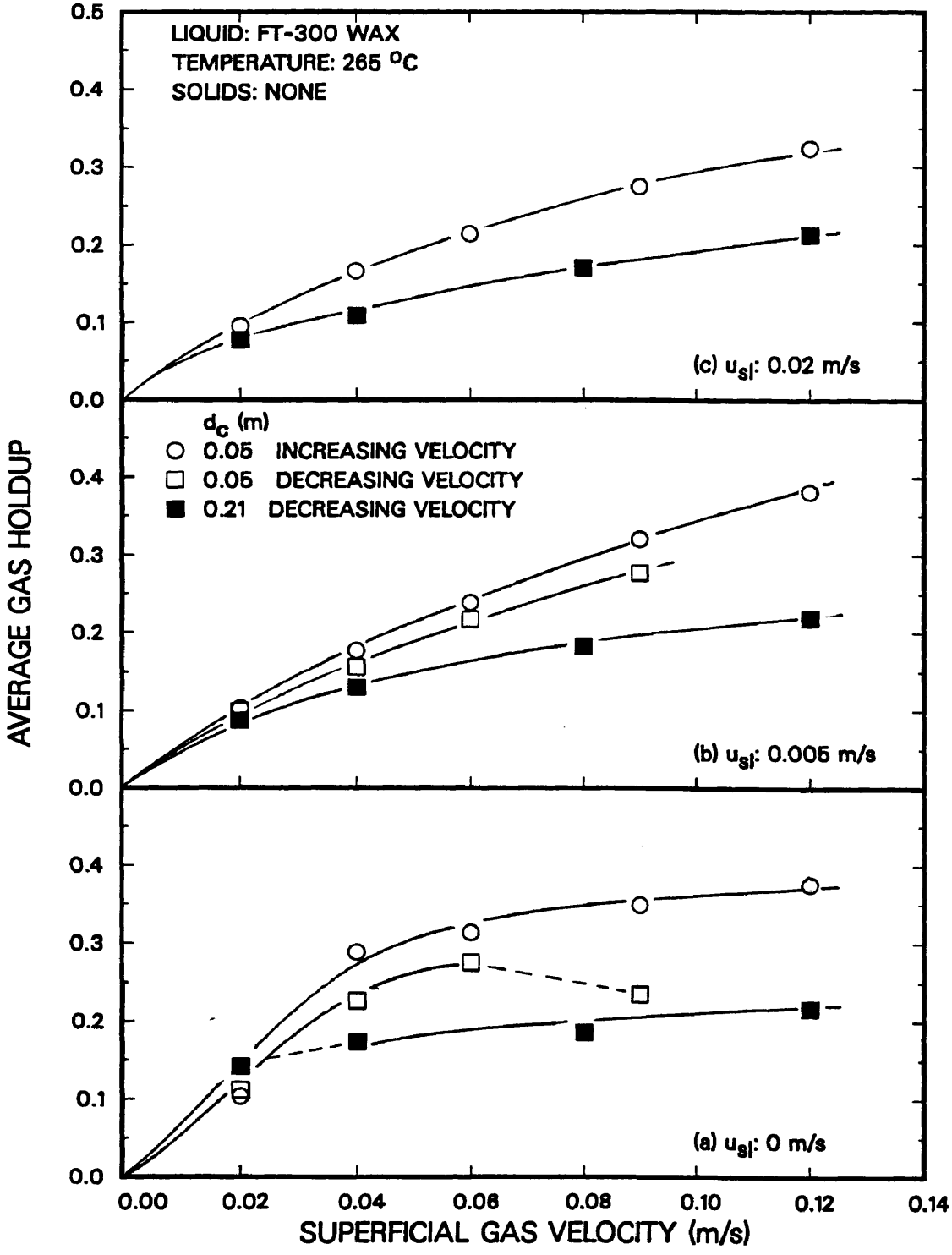

Figure 2.36. Effect of column diameter on average gas holdup with FT-300 wax.

exists in both columns. Gas holdups from experiments conducted in the continuous mode of operation in the small diameter column (see Figures 2.36b and 2.36c) were higher than those observed in the large diameter column. It should be pointed out that experiments in the small diameter column were conducted in an increasing order of gas velocities; whereas, experiments in the large diameter column were conducted in a decreasing order of gas velocities. Batch experiments were conducted in the small diameter column using a decreasing order of gas velocities with 20 wt%, 20 – 44 μm silica particles in FT–300 (see the Figure on page 99) In these experiments, gas holdups were substantially lower than those obtained from experiments conducted employing an increasing order of gas velocities. Thus, it appears that if a decreasing order of gas velocities were used, gas holdups in the two columns would be similar at high superficial gas velocities. Ample evidence of this was observed in our experiments in the glass columns (Bukur et al., 1987a; Bukur and Daly, 1987).

SASOL wax, on the other hand, does not produce foam. And, as a result, gas holdups obtained in the 0.05 and 0.21 m ID columns are similar regardless of operating procedures employed (see Figures 2.37a and 2.37b).

Very few experimental studies on the effect of column diameter have been conducted with molten waxes as the liquid medium. Only Mobil workers (Kuo, 1985) and Deckwer et al. (1980) have studied the effect of column diameter with molten waxes. Researchers at Mobil conducted experiments with FT–200 wax (MW = 640) in 0.03 and 0.05 m ID columns, each 2.2 m in height. Their results indicate that for similar jet velocities, column diameter did not have an effect on gas holdup. They also conducted similar studies in two tall columns (0.05 m ID and 0.10 m ID, 9.1 m tall) with FT–200 wax and reactor waxes produced in their bench scale bubble column slurry reactor. These studies showed no effect of column diameter of gas holdup for FT–200 wax; however, with experiments conducted with reactor waxes, slightly higher holdups were obtained

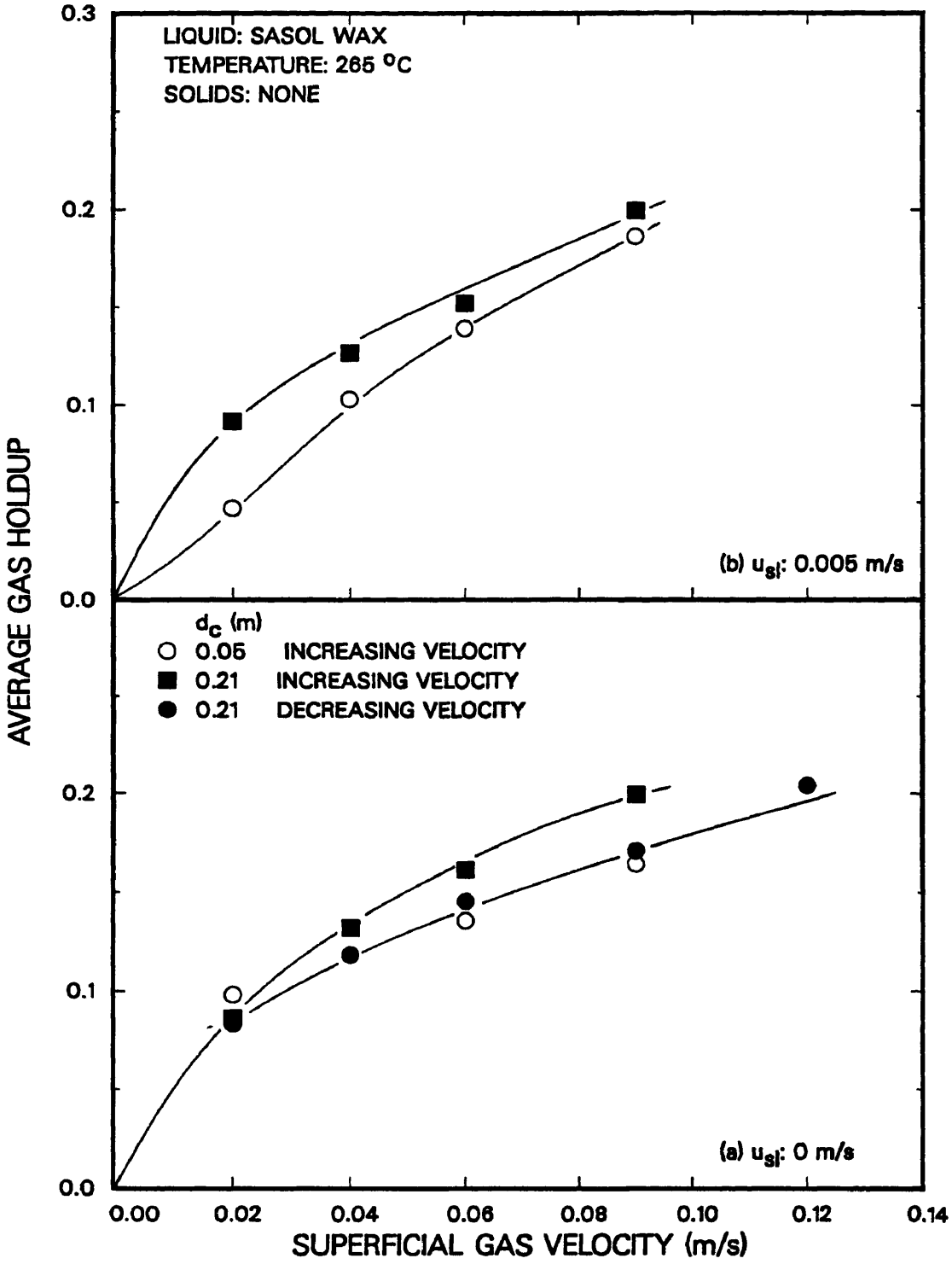

Figure 2.37. Effect of column diameter on average gas holdup with SASOL wax.

in the 0.10 m ID column. Deckwer et al. conducted experiments in two different diameter columns (0.04 m and 0.10 m ID). For temperatures below 250 °C holdups in the smaller diameter column were consistently higher than holdups in the large diameter column for the range of velocities studied (0.005 – 0.03 m/s). Foam was present under these conditions. However, for experiments conducted at temperatures greater than 250 °C, holdup values from the two columns were similar. Reilly et al., 1986 summarized the findings of various researchers for holdups in different diameter columns. They report that some discrepancy exists as to the effect of column diameter; however, they point out that for columns with diameters greater than 0.10 m, there is essentially no effect of column diameter. Shah et al. (1982) also summarized the findings of various researchers, from holdup measurements made in systems which did not produce foam (mostly air–water), which show that the effect of column diameter on the average gas holdup is minimal. In general, slightly lower holdups were observed in larger diameter columns compared to smaller diameter columns.

Reproducibility of Results and Effect of Operating Procedure

Reproducibility of average gas holdup measurements with FT–300 wax is significantly affected by the operating procedure, and to some extent by the age of the wax or the time on stream for a given batch of wax. Numerous experiments were conducted in the 0.05 m ID glass column to study the effect of operating procedure and age of wax on gas holdup (Bukur et al., 1987a,b; Bukur and Daly, 1987). Two different operating procedures (or startup procedures) were employed throughout our studies. Experiments conducted in an increasing order of gas velocities with FT–300 wax favored the formation of foam. During some of these experiments, a transition occurred between the foamy and nonfoamy (or slug flow) regime when the superficial gas velocity exceeded a certain critical value. Experiments conducted in a decreasing order of gas velocities

favored the slug flow regime; however, in some experiments, we observed a transition from the slug flow to the foamy regime when the gas velocity dropped below a certain critical value. The two critical velocities are different and a hysteresis loop is created. A typical hysteresis loop is shown in Figure 2.38. For the experiment conducted in an increasing order of gas velocities, the transition from the foamy to the slug flow regime occurred between superficial gas velocities of 0.05 and 0.07 m/s. However, for the experiment conducted in decreasing order of gas velocities, the transition from the slug flow to the foamy regime occurred between gas velocities of 0.05 and 0.03 m/s. The critical velocities at which these transitions occur were not reproducible. In some experiments, conducted in an increasing order of gas velocities, we never observed a transition from the foamy to the slug flow regime. And, for some experiments conducted in a decreasing order of gas velocities, the transition from the slug flow to the foamy regime never occurred. Gas holdups values varied in the foamy regime due to different amounts of foam; however, gas holdups in the absence of foam (i.e. slug flow regime) were reproducible.

Figure 2.39 shows average gas holdups obtained from experiments conducted in the glass column and the stainless steel column with FT–300 wax. The solid lines in Figure 2.39 represent the average values of gas holdups in the foamy and slug flow regime that were observed in the glass column from a total of 7 to 10 experiments. The shaded region represents the range of gas holdup values observed in the glass column in the foamy regime. There is no distinction made in the operating procedure. Two experiments were conducted in the stainless steel column using an increasing order of gas velocities. Results from these experiments are shown by the solid symbols. In one experiment (solid circles) we did not observe a transition from the foamy to the slug flow regime; whereas, in the other experiment (solid squares) a transition took place between gas velocities of 0.06 and 0.09 m/s. Gas holdups in the foamy regime observed

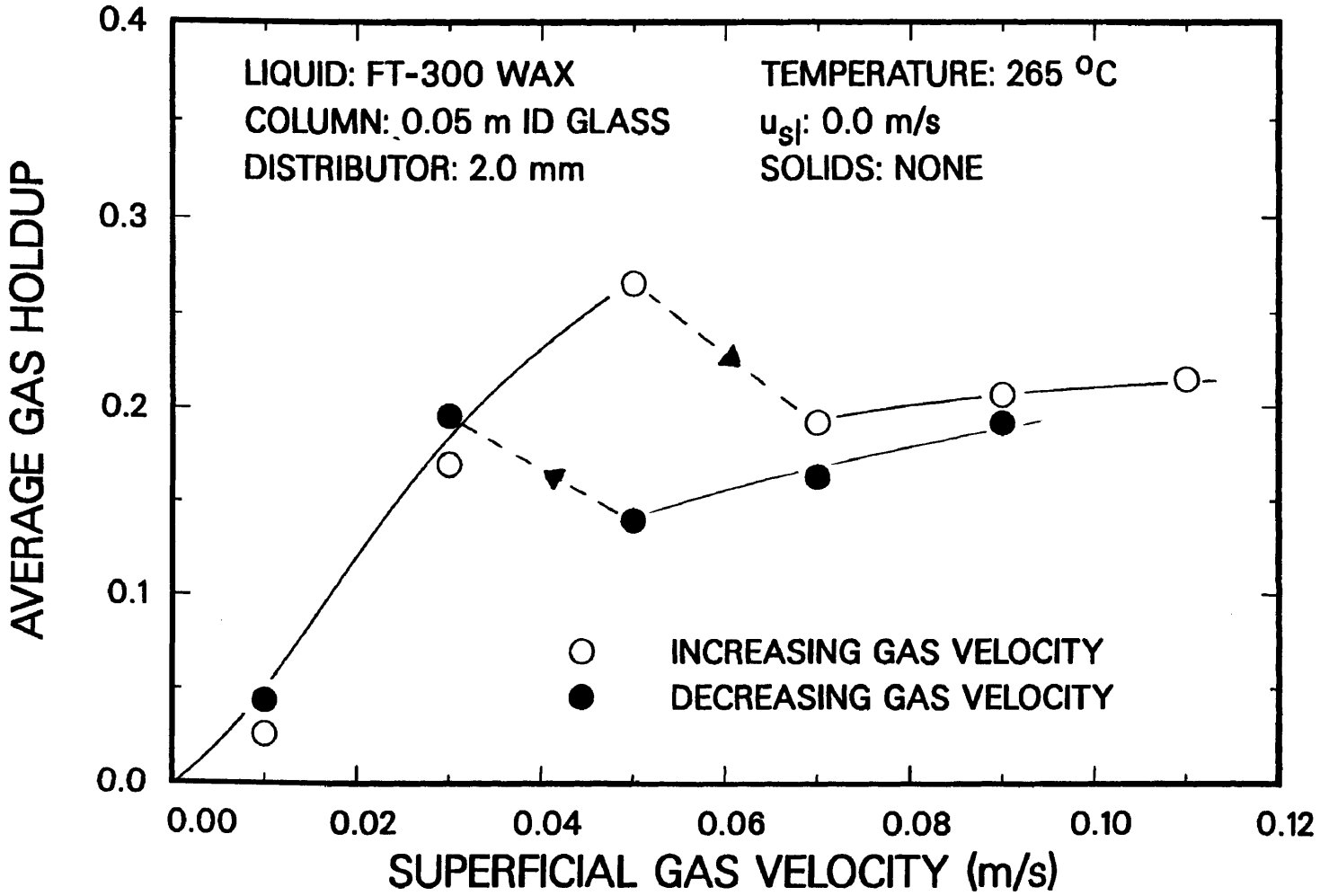

Figure 2.38. Typical hysteresis loop observed in 0.05 m ID glass column.

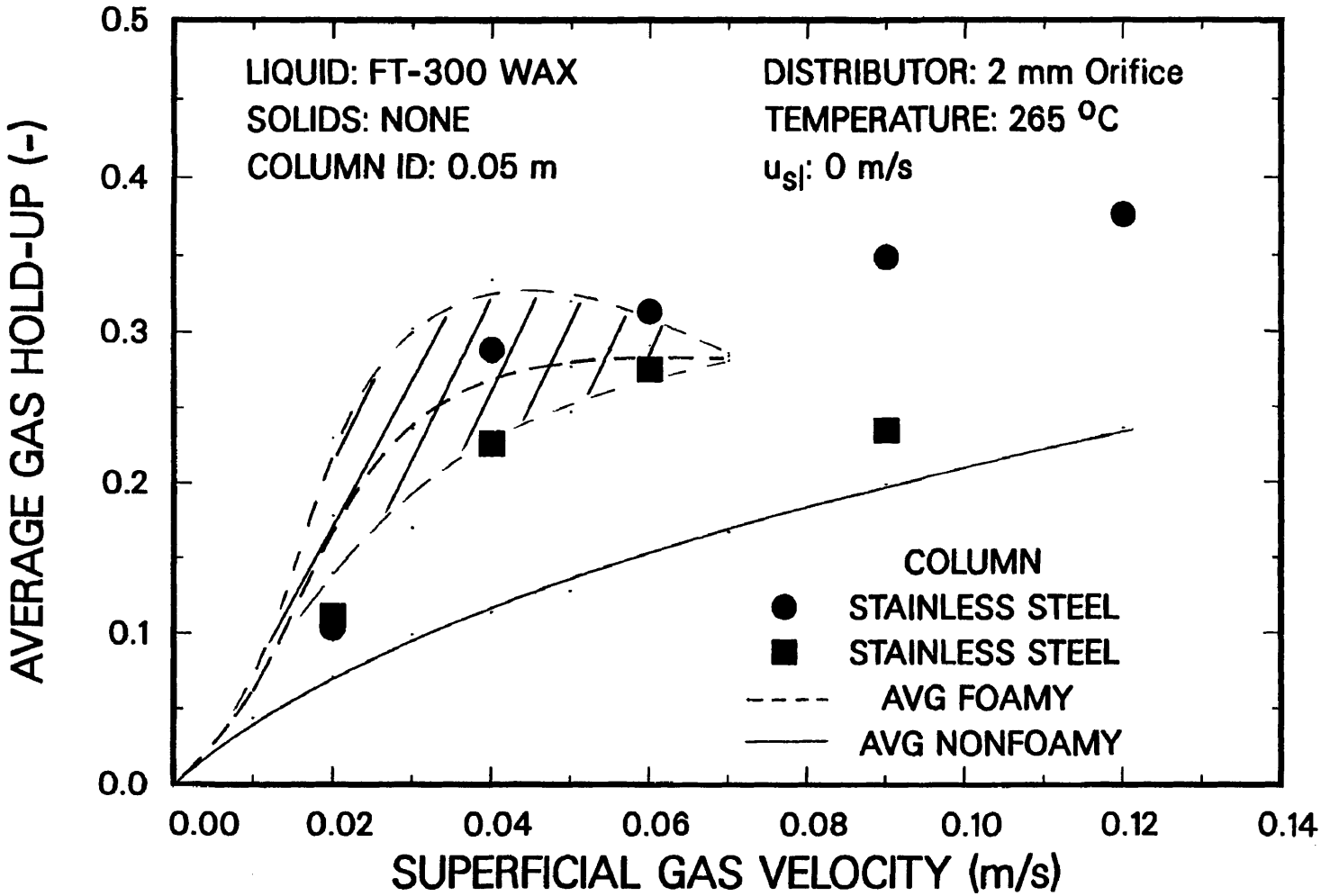

Figure 2.39. Reproducibility of results with FT-300 wax in the 0.05 m ID column.

in the stainless steel column compare favorably with those in the glass column up to a gas velocity of 0.07 m/s.

In order to check for reproducibility of results in the presence of solids, two experiments were conducted with large iron oxide particles and two experiments were conducted with large silica particles in the batch mode of operation (see Figures 2.40a and 2.40b, respectively). An increasing order of gas velocities was used in the experiments conducted with large iron oxide particles and a decreasing order of gas velocities was employed in the experiments with large silica particles. For the experiments conducted with large iron oxide particles, there was excellent agreement in gas holdup values. However, in one experiment conducted with silica, there was a transition from the slug flow to the foamy regime which occurred between gas velocities of 0.06 and 0.04 m/s; whereas, in the other experiment conducted with silica, no transition was observed.

Experiments were conducted with SASOL wax in both the small diameter stainless steel and glass columns. The experiment in the stainless steel column was performed in increasing order of gas velocities. Two experiments were conducted in the glass column, one in an increasing order of gas velocities and one in a decreasing order of gas velocities. Gas holdup values from these three experiments are shown in Figure 2.41. SASOL wax does not foam, and as a result, gas holdups are not affected by operating procedure. Results from all three experiments are in excellent agreement with each other.

Figure 2.42a shows results from experiments conducted with SASOL reactor wax in the large diameter column. As was the case for experiments conducted in the small diameter column (Figure 2.41), there was essentially no effect of operating procedure on gas holdup. Results from an experiment with FT–300 wax in the large diameter glass column, together with the results from the experiment with FT–300 wax in the

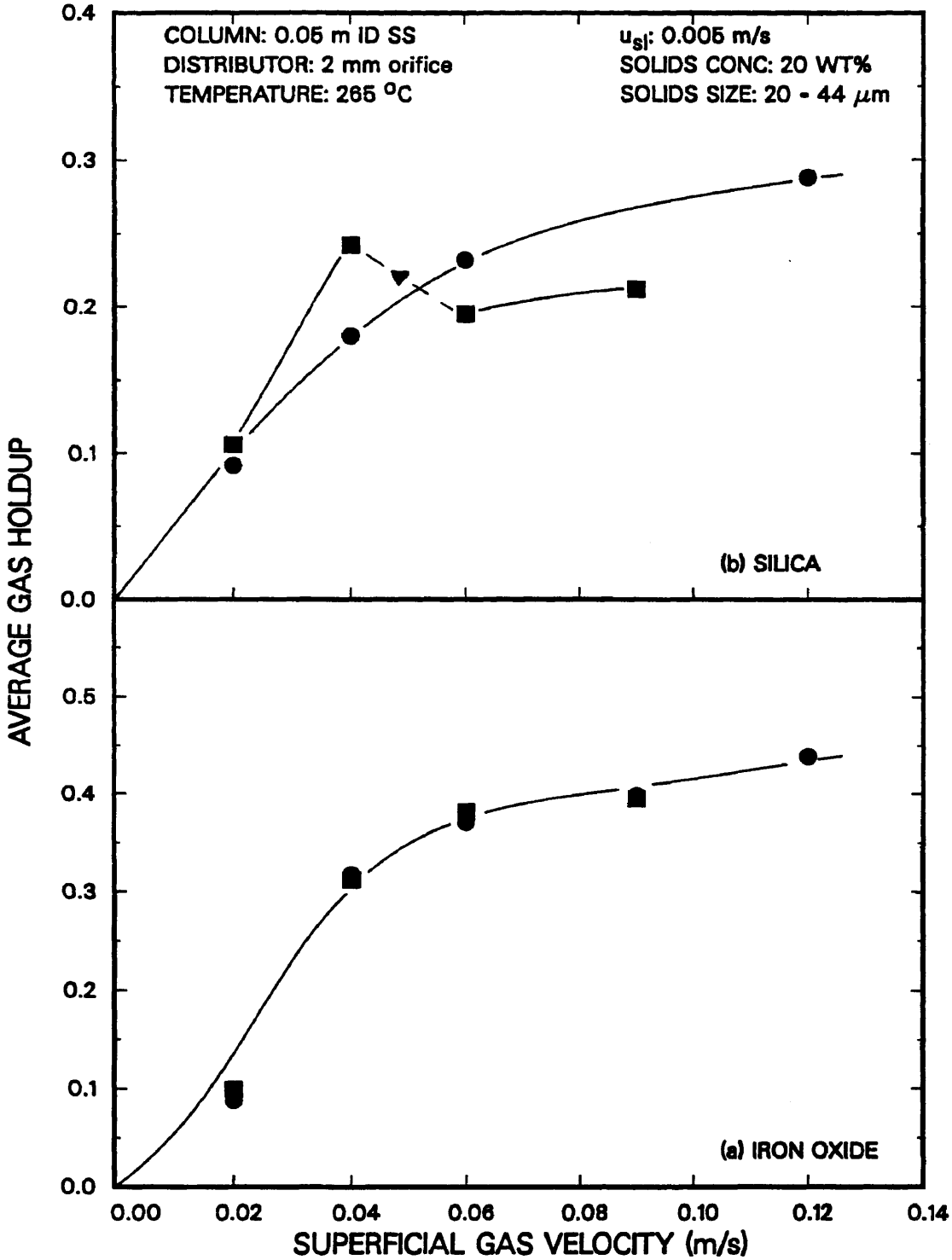

Figure 2.40. Reproducibility of results with FT-300 wax in the 0.05 m ID column (a) iron oxide; (b) silica.

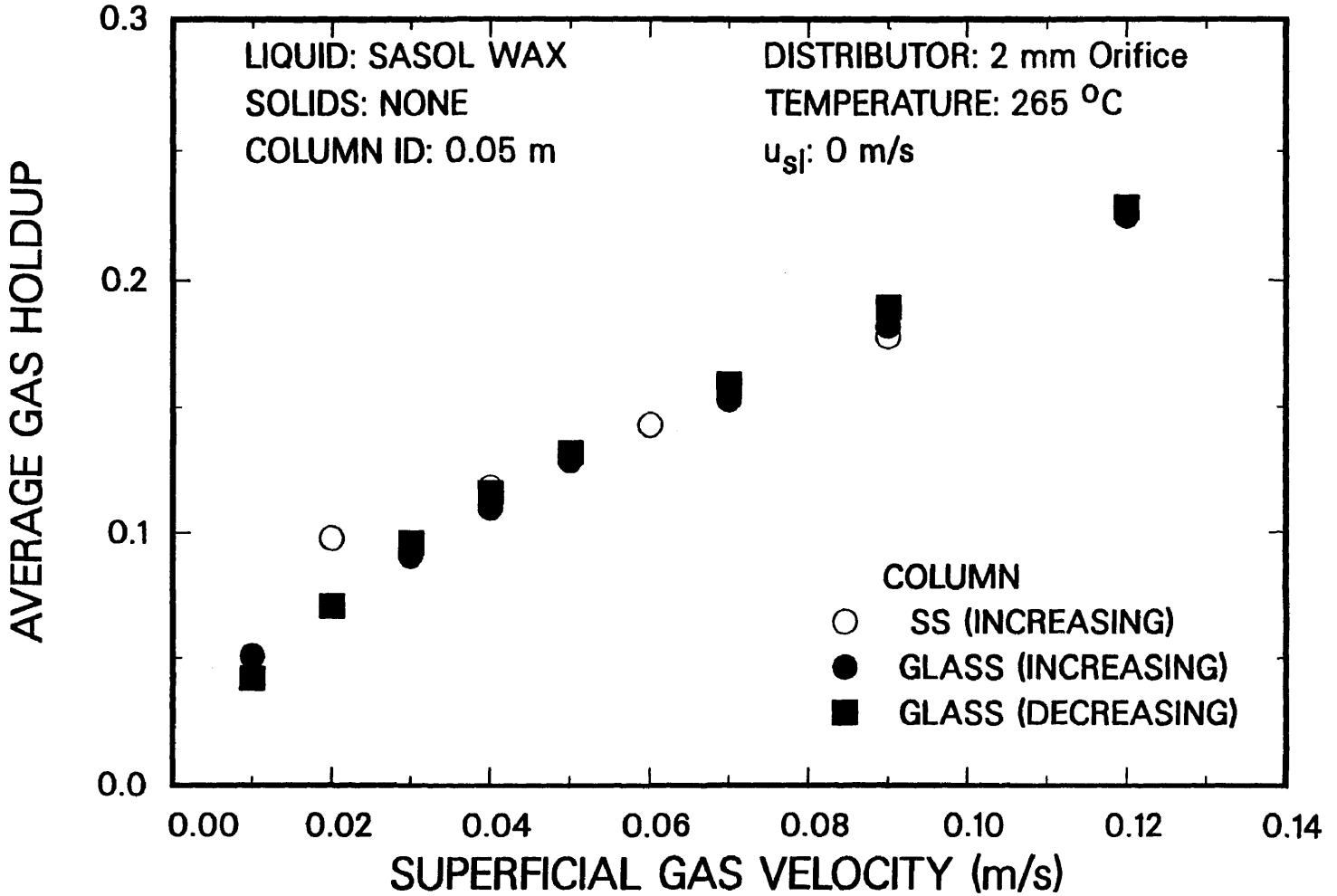

Figure 2.41. Reproducibility of results with SASOL wax in the 0.05 m ID columns.

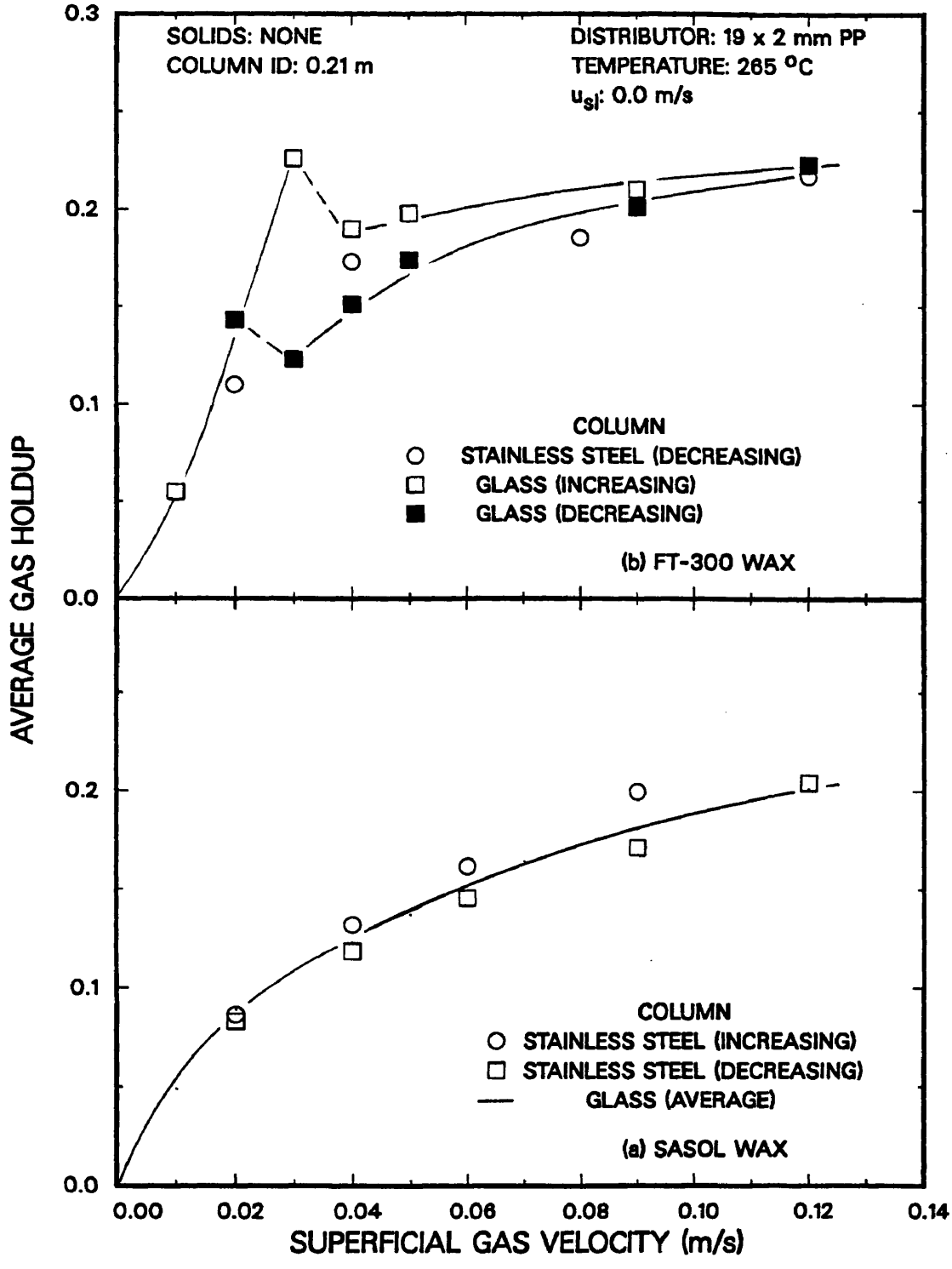

Figure 2.42. Reproducibility of gas holdup values and effect of operating procedure for batch experiments in the 0.21 m ID column ((a) SASOL wax; (b) FT-300 wax).

large diameter stainless steel column are shown in Figure 2.42b. For the experiment in the glass column, conducted in an increasing order of gas velocities, the gas holdup rises rapidly between 0.01 and 0.03 m/s due to the accumulation of foam at the top of the dispersion. The foam breakup, accompanied by a substantial decrease in gas holdup, occurred when the velocity was increased from 0.03 to 0.05 m/s. After that, the gas holdup increased gradually. In the same experiment, when the gas velocity was decreased from 0.15 to 0.03 m/s, slightly lower holdups were obtained than when the increasing order of gas velocities was employed. Differences in gas holdups were more pronounced in the range 0.03 – 0.05 m/s due to the virtual absence of foam during the experiment conducted in order of decreasing gas velocities. When the gas velocity was decreased from 0.03 to 0.02 m/s foaming took place which resulted in a higher gas holdup. Results from the experiment conducted in the stainless steel column (decreasing order of velocities) are in excellent agreement with those obtained in the glass column for the experiment conducted in a decreasing order of gas velocities except at a gas velocity of 0.02 m/s. During the experiment in the stainless steel column, no foam was observed at this gas velocity.

The effect of wax age was also investigated with small and large iron oxide particles using SASOL reactor wax. However, the results from these experiments were inconclusive. For the experiments with small iron oxide particles, the gas holdup decreased slightly with increasing time on stream (16 hours versus 56 hours, Figure 2.43a). Whereas, for the experiments conducted with large iron oxide particles, there was a slight increase in gas holdup with increasing time on stream (12 hours versus 36 hours, Figure 2.43b).

In summary, gas holdups with FT–300 wax exhibit hysteresis behavior which is affected by the order of gas velocities employed. Gas holdups values in the foamy regime

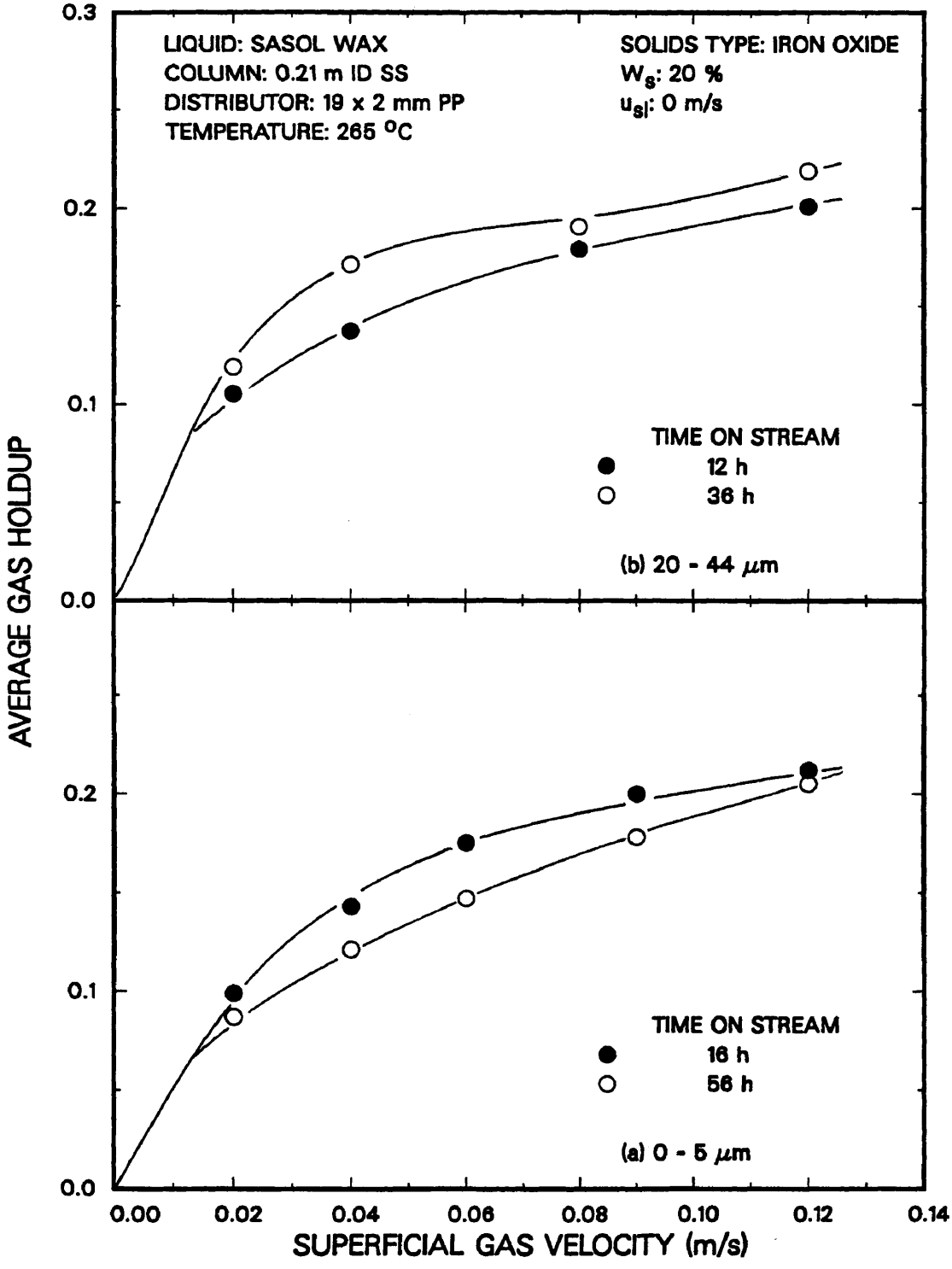

Figure 2.43. Effect of wax age on average gas holdup in the 0.21 m ID column with SASOL wax.

vary depending on the amount of foam present. However, in the slug flow and churn–turbulent flow regimes, the results from different experiments were very reproducible. The critical velocity at which the transition from the foamy to the slug flow or churn–turbulent flow regime (or vice versa) occurs is not reproducible. The variation in the critical velocity at which the transition occurs can result in different gas holdups at the same gas velocity for experiments conducted under similar operating conditions. Gas holdups with SASOL reactor wax (which does not foam) are very reproducible and do not appear to be affected by the operating procedure employed.

Physical Properties and Average Gas Holdup Correlations

Physical Property Measurements

The density and surface tension of FT–300 and SASOL wax were measured at different temperatures. The viscosity of both FT–300 wax and SASOL reactor wax was measured at 230 °C. The physical properties used in developing gas holdup correlations are presented in Table 2.6. The densities of iron oxide and silica particles are 2650 and 5100 kg/m^3, respectively.

Density Measurements

Densities of FT–300 and SASOL wax were measured using the pressure drop across known heights of liquid in the 0.05 m ID glass column. A differential pressure transducer was connected to the bottom of the glass column to measure the pressure drop across the column. The pressure transducer was calibrated with distilled water using the same procedure outlined earlier. The column was filled with the test liquid to a height of 2.5 m and brought to the desired temperature. Once at temperature, the pressure drop was recorded. A portion of the liquid was drained ($\approx$ 0.25 m) and the pressure drop was recorded again. This procedure was repeated until the liquid level in the column was approximately 1 m. The density of the wax at a given temperature was obtained from

Table 2.6. Physical Properties of FT–300 Wax and SASOL Wax

LIQUID	TEMPERATURE (°C)	DENSITY (kg/m^3)	VISCOSITY[a] FRESH WAX (kg/m-s)	VISCOSITY USED WAX (kg/m-s)	SURFACE TENSION FRESH WAX (N/m)	SURFACE TENSION[b] USED WAX (N/m)
	150	–	0.0064		0.024±0.0004	0.025
FT–300	200	722	0.0042		0.021±0.0006	0.02±0.001
	230	706	0.0036 (0.0023)[c]	0.0026–0.0041[d]	0.019±0.0005	0.019
	260	681	0.0028		0.017±0.001	0.017±0.0005
	150	–	0.0042		0.024	0.019±0.0005
SASOL	200	701	0.003		0.02±0.001	0.017±0.001
	230		0.0025		0.019	0.016±0.0009
	260	655	0.0022		0.016±0.0003	0.014±0.0008

[a] From Bukur et al., (1987c)

[b] Based on analysis of several samples – all contained solids

[c] Single measurement during this project

[d] Range of values (lowest for sample with no solids; highest for sample taken from slurry containing 30 wt% silica)

the slope of the pressure drop versus height plot, after appropriate corrections for the calibration factor.

Viscosity Measurements

Viscosity measurements were made in a Brookfield viscometer (LV series, 2.5X) using a cylindrical spindle (SC4-18) operating at 60 RPM. A Brookfield Thermosel system allowed measurements up to temperatures of 250 °C. The system was first calibrated using fluids of known viscosities. Three fluids were used; water (0.01 kg/m-s), and two viscosity standards (.051 and .081 kg/m-s – supplied by Brookfield). The standards were used before and after viscosity measurements with wax to monitor errors due to device drift. Each measurement required an 8 ml sample of the test fluid.

Results from these measurements together with those presented by Bukur et al. (1987c) are presented in Table 2.6. The viscosity of the fresh FT–300 sample at 230 °C obtained in the current study was significantly lower than that previously obtained (i.e. 0.0023 kg/m–s vs 0.0035 kg/m–s). The reason for this discrepancy is not known. Several samples of used wax were also analyzed, one without any solids (0.0026 kg/m–s) and several samples from experiments conducted with solids (both iron oxide and silica). The samples from the experiments conducted with solids were prepared as follows. The solidified slurry sample was melted and the solids were allowed to settle. The liquid was decanted and the viscosity of the decanted liquid was measured. The viscosity of wax from experiments with solids was higher than that from experiments without solids. More than likely, the observed increase in viscosity was due to the presence of some solids in the samples. The viscosity was highest (0.0041 kg/m–s) for the sample from the experiment conducted with 30 wt% 0 – 5 μm silica particles.

Surface Tension Measurements

Surface tension measurements were made using a Fischer Model 215 Autotensiomat. The surface tension apparatus was modified for high temperature measurements, as suggested by the manufacturer. The surface tension was measured three times for each sample at a given temperature using both fresh and used FT–300 and SASOL wax. The average surface tension values from these measurements are given in Table 2.6. Some of the surface tension values presented in Table 2.6 are average values based on analysis of more than one sample. For these values, the standard deviation is also given.

Jasper (1972) presents surface tension data for normal paraffins (C5 – C20, C26 and C60). The values reported by Jasper for C5 – C20 paraffins were obtained at temperatures between 10 and 120 °C and for C26 and C60 paraffins, surface tension values were obtained for temperatures up to 180 °C. According to Jasper, surface tension is a linear function of temperature for reduced temperatures ($T/T_{critical}$) of 0.4 to 0.7. Thus, for the data he presented, he also gave values of the slopes and intercepts obtained from a plot of surface tension versus temperature. Figure 2.44 shows the effect of temperature on surface tension for data obtained in this study. Surface tension values for fresh FT–300 wax, used FT–300 wax, and fresh SASOL wax are similar and they vary linearly with temperature. The surface tensions of used SASOL wax were consistently lower than those of fresh SASOL wax (Table 2.6 and Figure 2.44).

The surface tension values for fresh FT–300 and fresh SASOL wax were fitted to the following equation using linear regression

$$\sigma = \text{int} - \text{slope} * T \tag{2.29}$$

where σ is the surface tension in dynes/cm and T is the temperature in °C. The following slopes and intercepts were obtained

FRESH FT–300: SLOPE = 0.0606, INT = 33.1

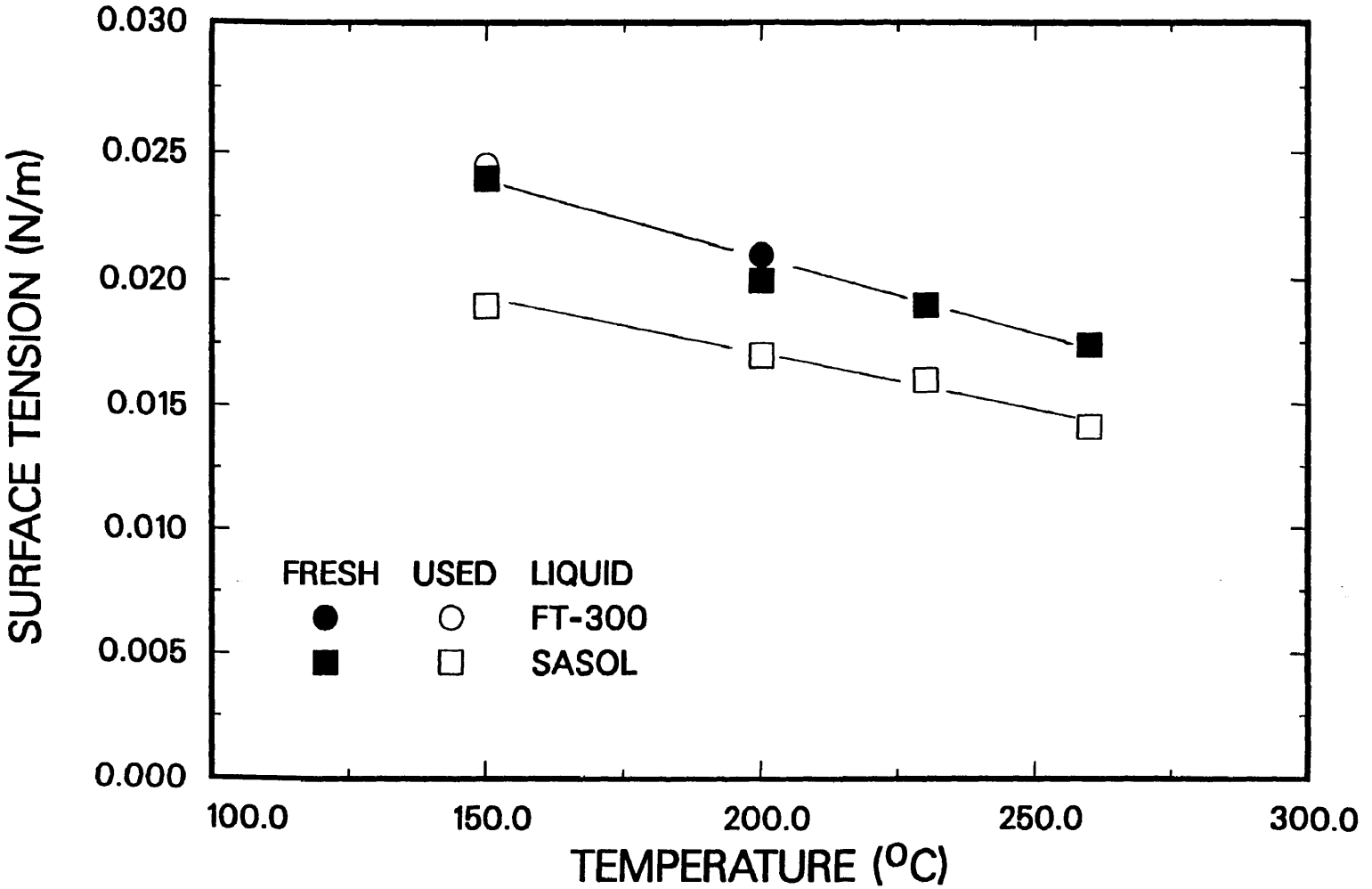

Figure 2.44. Effect of temperature on surface tension of fresh and used FT-300 and SASOL wax.

FRESH SASOL: SLOPE = 0.0659, INT = 33.7

FT–300 wax has a molecular weight of 730, which corresponds to a carbon number of 52. For a C26 paraffin, the slope and intercept values reported by Jasper were 0.07332 and 31.46, respectively and for a C60 paraffin the slope and intercept values were 0.05827 and 30.89, respectively. The results (i.e. slopes and intercepts) obtained in this study are in good agreement with the values reported by Jasper.

Gas Holdup Correlations

Numerous empirical correlations for predicting gas holdup in nonfoaming systems have been published (e.g. Hughmark, 1967; Akita and Yoshida, 1974; Bach and Pilhofer, 1978; Kara et al., 1982; Hatate et al., 1986, Badjugar et al., 1986, Zheng et al., 1988). The correlations evaluated in this study are presented in Table 2.7. Some researchers (e.g. Smith and Ruether, 1985; Fan, 1989) have found that in systems with low solids concentrations, correlations developed for two–phase systems can be applied to three–phase systems, if the physical properties (i.e density and viscosity) of the liquid are replaced by those of the slurry. The slurry density, $\rho_{s\ell}$ is obtained from:

$$\frac{1}{\rho_{s\ell}} = \frac{1}{\frac{\omega_s}{\rho_s} + \frac{1-\omega_s}{\rho_\ell}} \tag{2.30}$$

and the slurry viscosity may be estimated from

$$\mu_{s\ell} = \mu_\ell \frac{1 + 0.5\epsilon_s}{(1-\epsilon_s)^4} \tag{2.31}$$

Equation 2.31 is valid for $\epsilon_s < 0.4$ (Perry and Chilton, 1983), where ϵ_s is the volume fraction of solids in the liquid/solid slurry.

Average gas holdup results from our study can be divided into two groups: (1) results in which foam was observed and (2) results in which no foam was observed.

Table 2.7. Summary of Gas Holdup Correlations Presented in the Literature

CORRELATION	COLUMN ID	CONDITIONS	SYSTEM	REFERENCE
$\epsilon_g = aFr^b Ar^c Bo^d (1 + u_\ell / u_g)^e (1 - \epsilon_s)^f$	0.285 m	$0 < u_g < 0.16$	gas: air	Zheng et al., 1988
$Fr = \frac{u_g^2}{d_c g}$, $Ar = \frac{d_p^3 g(\rho_s - \rho_\ell)}{\rho_\ell \mu_\ell^2}$, $Bo = \frac{g d_p^2 \rho_\ell}{\sigma}$		$0 \leq u_\ell \leq 0.04$	liquid:water	
where a, b, c, d, and e, are adjustable parameters		$\rho_\ell = 1000$	solids:glass spheres	
which depend on flow regime		$d_p = 615$		
$\epsilon_g = 0.9(1 - \omega_s)^{0.7} u_g^{0.525}$	0.076 and 0.301 m	$0 < u_g \leq 0.14$	gas: air	Badgujar et al., 1986
		$0 \leq \omega_s \leq 0.20$	liquid: water, soltrol	
		$751 \leq \rho_\ell \leq 1000$	solids: glass spheres,	
		$0.001 \leq \mu_\ell \leq 0.0013$	ammonia synth. cat.,	
		$49 \leq d_p \leq 107$	Triple A cat., FCC	
$\epsilon_g = \frac{u_g/(u_g+u_\ell)}{1.20+0.35/\sqrt{Fr_t}}$	1.55 and 2.6 m	$0 \leq u_g < 5$	gas: air	Hatate et al., 1985
$Fr_t = \frac{(u_g+u_\ell)^2}{g d_c}$		$u_\ell = 0.15$ and 0.6	liquid: tap water	
		$0 \leq \omega_s \leq 0.60$	solids: glass spheres	
		$\rho_\ell = 1000$		
		$d_p = 30$, 63, and 100		

Table 2.7. (cont.)

CORRELATION	COLUMN ID	CONDITIONS	SYSTEM	REFERENCE
$\epsilon_g = \frac{Re_g}{A+BRe_g+CRe_{s\ell}+D\left(\frac{\epsilon_s}{\epsilon_s+\epsilon_\ell}\right)}$	0.152 m	$0 < u_g \leq 0.3$	gas: air	Kara et al., 1982
$Re_{s\ell} = \frac{d_c u_{s\ell} \rho_{s\ell}}{\mu_{s\ell}}$, $Re_g = \frac{d_c u_g \rho_g}{\mu_g}$		$0 \leq u_{s\ell} \leq 0.1$	liquid: water	
where A, B, C, D, and E are adjustable parameters		$0 \leq \frac{c_s}{\rho_{s\ell}} \leq 0.4$	solids: coal, dried mineral	
which depend on particle size		$d_p = 0, 10, 30, 70$		
$\epsilon_g = (2 + (0.35 / u_g)[(\rho_\ell / 1000)(\sigma_\ell / 0.072)]^{0.33})^{-1}$	< 0.1 m	$0.004 \leq u_g \leq 0.45$	gas: air	Hughmark, 1967
		$780 \leq \rho_\ell \leq 1700$	liquid: water, kerosene	
		$0.0009 \leq \mu_\ell \leq 0.152$	glycerol aqu. soln.,	
		$0.025 \leq \sigma \leq 0.076$	light oil, salt solns.	

u_i (m / s), ρ_i (kg / m^3), μ_i (kg / m − sec) where $i = g, s\ell, \ell$

d_p (μm), σ_ℓ(N / m)

Deckwer et al. (1980) used the following empirical correlation to correlate holdup values obtained using molten paraffin wax in the foamy regime

$$\epsilon_g = 8.4u_g^{1.1} \pm 0.015 \qquad u_g \leq 0.04\text{m/s} \tag{2.32}$$

Researchers at Mobil (Kuo, 1985) used a similar correlation to predict gas holdups with FT–200 wax (MW=630) under foaming conditions.

$$\epsilon_g = 10.3u_g^{1.1} \qquad u_g \leq 0.06\text{m/s} \tag{2.33}$$

The correlations presented above were obtained from experiments conducted in the batch mode of operation. While the two correlations are similar, the difference in the constant (8.4 and 10.3) is probably due to differences in the foaming characteristics of the systems studied. Two correlations were developed by Bukur et al. (1987a) for data obtained in the foamy regime. One correlation was developed from gas holdup data obtained using orifice plate distributors

$$\epsilon_g = 0.94u_g^{0.41} \qquad 0.01 \leq u_g \leq 0.07\text{m/s} \tag{2.34}$$

and the other correlation was developed from gas holdup data obtained using a 40 μm sintered metal plate distributor

$$\epsilon_g = 1.06u_g^{0.15} \qquad 0.01 \leq u_g \leq 0.12\text{m/s} \tag{2.35}$$

The correlations proposed by Deckwer et al. and Kuo (Eqs. 2.32 and 2.33, respectively) show that holdup increases almost proportionally with superficial gas velocity, while results from the study by Bukur et al. show that holdup values tend to level off at higher gas velocities. A possible explanation for the discrepancy is the range of gas velocities employed in the three studies. The studies by Deckwer et al. and Kuo were limited to low gas velocities, where the holdup increases linearly with gas velocity.

However, at higher gas velocities, holdup values level off. Thus, it is evident, that a single correlation cannot be developed for predicting holdup values in the foamy regime. Therefore, the correlations developed in the present study are based on data obtained in the slug flow and churn–turbulent flow regimes. In particular, gas holdup data obtained in the 0.05 m ID stainless steel column in the batch mode of operation with FT–300 wax have been omitted.

Measured gas holdups values were compared with values predicted using the correlations presented in Table 2.7. The correlations developed by Hughmark (1967) and Hatate et al. (1986) were based on data obtained from two–phase systems. For Hughmark's correlation, the slurry density was used as opposed to the density of the liquid. Since constants in Zheng et al.'s correlation depend on the flow regime, it was assumed that at a gas velocity of 0.02 m/s the homogeneous bubbling regime prevails, at a gas velocity of 0.04 m/s the transition regime exists, and for gas velocities greater than 0.04 m/s the column was assumed to operate in either the churn–turbulent (0.21 m ID) or slug flow (0.05 m ID) regime. The correlation presented by Kara et al. (1982) has variable parameters as well. The constants change depending on the size of particles used. Thus, in applying Kara et al.'s correlation to our system, we used constants for 10 μm particles to estimate gas holdups for slurries containing 0 – 5 μm particles, and constants for 30 μm particles to estimate gas holdups for slurries containing 20 – 44 μm particles. The number of data points associated with a given set of conditions, which were used in the correlations are presented in Table 2.8. A total of 222 points were used. Mean square errors (MSE), defined as

$$\mathrm{MSE} = \frac{\sum_i (\epsilon_{\mathrm{meas}_i} - \epsilon_{\mathrm{pred}_i})^2}{n-1} \qquad i = 1 \text{ to } n \tag{2.36}$$

were first estimated using the original values of constants in the literature correlations. The MSE values were between 0.0015 to 0.017 (Table 2.9). The magnitude of the

Table 2.8. Summary of Number of Points at a Given Set of Conditions

LIQUID	COLUMN ID (m)	SOLIDS TYPE	SOLIDS SIZE μm	$u_{s\ell}$ (m/s)	No. Pts.
FT–300	0.05	None	–	0.005	4
FT–300	0.05	Iron oxide	0 – 5	0.005	12
FT–300	0.05	Iron oxide	0 – 5	0.02	12
FT–300	0.05	Silica	0 – 5	0.005	12
FT–300	0.05	Silica	0 – 5	0.02	4
FT–300	0.05	Iron oxide	20 – 44	0.005	7
FT–300	0.05	Iron oxide	20 – 44	0.02	3
FT–300	0.05	Silica	20 – 44	0	4
FT–300	0.21	None	–	0	4
FT–300	0.21	None	–	0.005	4
FT–300	0.21	None	–	0.02	4
FT–300	0.21	Iron oxide	20 – 44	0	3
FT–300	0.21	Iron oxide	20 – 44	0.005	8
SASOL	0.05	None	–	0	8
SASOL	0.05	Iron oxide	0 – 5	0.005	4
SASOL	0.05	Iron oxide	20 – 44	0	4
SASOL	0.21	None	–	0	9
SASOL	0.21	None	–	0.005	12
SASOL	0.21	None	–	0.02	4
SASOL	0.21	Iron oxide	0 – 5	0	24
SASOL	0.21	Iron oxide	0 – 5	0.005	15
SASOL	0.21	Iron oxide	0 – 5	0.02	5
SASOL	0.21	Iron oxide	20 – 44	0	16
SASOL	0.21	Iron oxide	20 – 44	0.005	12
SASOL	0.21	Iron oxide	20 – 44	0.02	12
SASOL	0.21	Silica	20 – 44	0	4
SASOL	0.21	Silica	20 – 44	0.005	8
SASOL	0.21	Silica	20 – 44	0.02	4

MSE is a measure of the goodness of fit, and a smaller value implies better agreement between the measured and predicted values. We then calculated new values of constants in these correlations by minimizing the MSE via non-linear regression (NLIN procedure in SAS). The MSE values obtained using new values for the constants in the existing correlations were slightly smaller than those obtained when the original constants were employed as shown in Table 2.9.

Figure 2.45 compares parity plots obtained using the original correlations proposed by Badjugar et al. (1986) and Hughmark (1967) (Figures 2.45a and 2.45c, respectively) with those for the same two correlations after the constants were recalculated (Figures 2.45b and 2.45d, respectively). The correlation proposed by Badjugar et al. is a three–phase correlation, and the correlation proposed by Hughmark is a two–phase correlation. For Hughmark's correlation, the liquid density was replaced by the slurry density (see Eq. 2.30). In Figures 2.45a and 2.45b (Badjugar et al. correlation) 85% of the measured gas holdup values are within ±30% of the predicted values using the original constants (Figure 2.45a) and 94 % of the measured holdup values were with ±30% of the predicted values using the new constants(Figure 2.45b). Similar results (i.e. better agreement between predicted and measured holdup values) were obtained with Hughmark's correlation (see Figures 2.45c and 2.45d). It is also evident from Figure 2.45 that a two–phase correlation may be used to predict gas holdups in three–phase Fischer–Tropsch slurry bubble columns in the slug flow and churn–turbulent flow regimes.

The lowest MSE (0.0007) was obtained using Zheng et al.'s correlation with re-calculated constants (see Table 2.9). This was expected since this correlation has the largest number of adjustable parameters. However, the difference in mean square errors between Zheng et al.'s correlation and Badjugar et al's correlation with recalculated constants was not that significant (0.0007 vs. 0.0010) even though there are twice as

2.9. Mean Square Errors for Literature Correlations

CORRELATION[a]	MSE[b]	MSE[c]	REFERENCE
$\epsilon_g = 0.46 Fr^{0.26} Ar^{-0.009} Bo^{0.06} (1 + u_{s\ell} / u_g)^{0.04} (1 - \epsilon_s)^{0.19}$	0.0018	0.0007	Zheng et al., 1988[d]
$\epsilon_g = 0.7 (1 - \omega_s)^{-0.08} u_g^{0.5}$	0.0015	0.0010	Badgujar et al., 1986
$\epsilon_g = \frac{u_g/(u_g+u_\ell)}{2.75+0.12/\sqrt{Fr_t}}$	0.0017	0.0014	Hatate et al., 1986
$\epsilon_g = \frac{Re_g}{103.7+4.65Re_g+0.19Re_{s\ell}-573(\frac{\epsilon_s}{\epsilon_s+\epsilon_\ell})}$	0.0045	0.0032	Kara et al., 1982
$\epsilon_g = (2.74 + (0.29 / u_g)[(\rho_\ell / 1000)(\sigma_\ell / 0.072)]^{0.33})^{-1}$	0.0015	0.0012	Hughmark, 1967

[a] reevaluated constants

[b] based on original constants; 222 data points

[c] based on reevaluated constants; 222 data points

[d] Bond number is defined with respect to column diameter as opposed to particle diameter

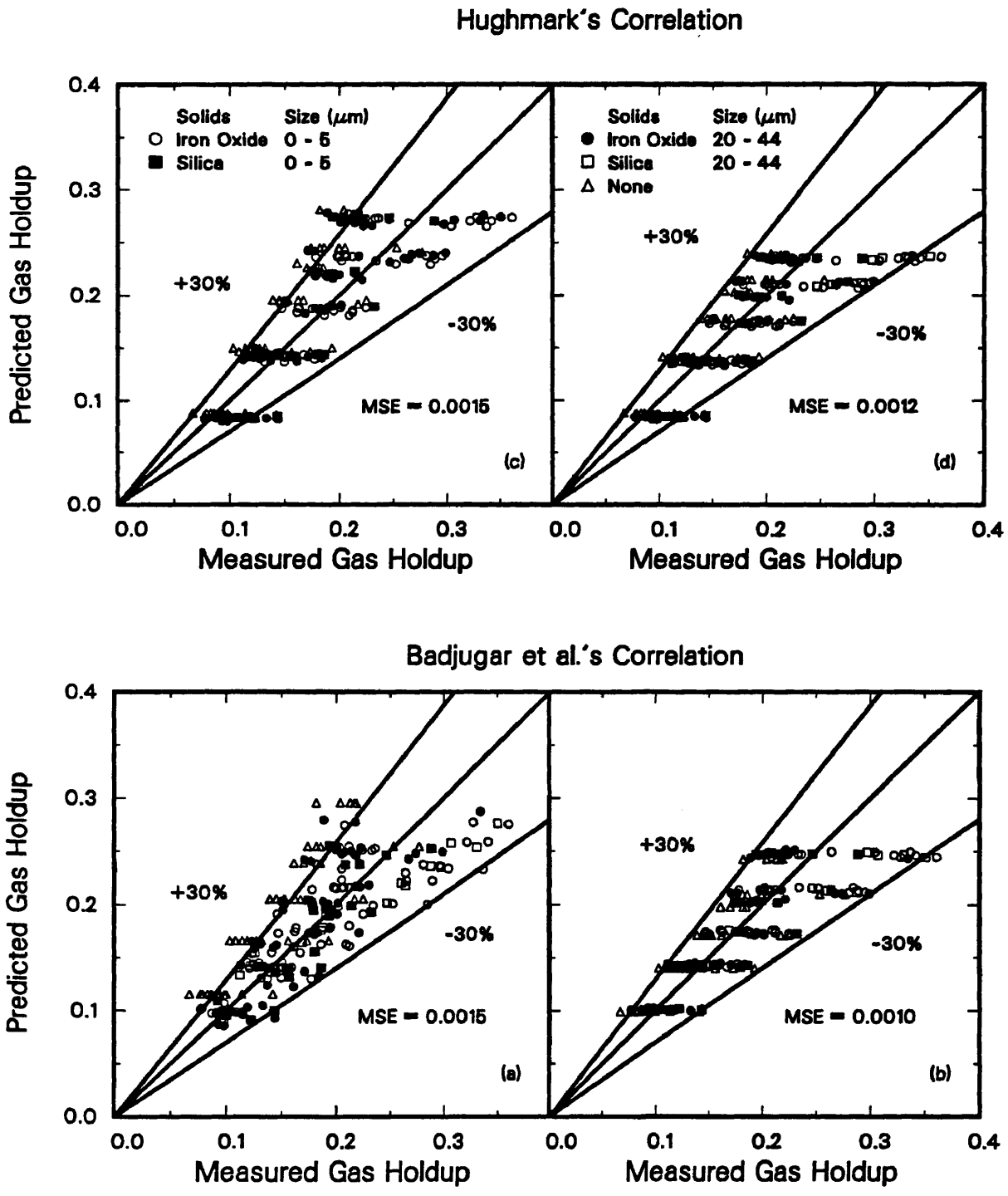

Figure 2.45. Parity plot of predicted versus measured gas holdup ((a and b) Badjugar et al., 1986; (c and d) Hughmark, 1967).

many adjustable parameters in the correlation proposed by Zheng et al. This is not surprising since we did not observe a significant effect of particle size, solids concentration, or slurry flow rate on gas holdup in the slug flow (0.05 m ID column) or churn–turbulent flow (0.21 m ID column) regimes. The following terms in the correlation proposed by Zheng et al., did not vary significantly over the range of conditions employed in this study

$$1.15 < Ar^{-0.009} < 1.21$$

$$1.0 < (1 - \epsilon_s)^{0.19} < 1.028$$

$$0.988 < (1 + u_{s\ell} / u_g) < 1.0$$

The correlation proposed by Badjugar et al. with recalculated constants also indicated that there was no significant effect of solids concentration on gas holdup, i.e.

$$1.0 < (1 - \omega_s)^{-0.08} < 1.03$$

Neglecting the terms presented above, the correlations proposed by Zheng et al., and Badjugar et al. are similar, with the exception of the fact that the former takes into account column diameter; whereas, the latter does not.

Since there was a negligible effect of solids size and concentration and slurry flow rate, the following dimensionless correlation was selected for further evaluation

$$\epsilon_g = aFr_g^b Bo^c \tag{2.37}$$

We observed an effect of column diameter for gas holdups with FT–300 wax (see Figure 2.36). Eq. 2.35 was evaluated using either all data points (222) or omitting those associated with FT–300 wax in the small stainless steel column (165 points). Table 2.10 summarizes the parameters and MSE's associated with this analysis. Figures 2.46a and 2.46b are parity plots of the measured gas holdup values versus the predicted gas holdup

Table 2.10. Goodness of Fit and Parameters for Empirical Holdup Correlation

CORRELATION:

$$\epsilon_g = a\,(Fr)^b\,(Bo)^c$$

where: $Fr = \dfrac{u_g^2}{g\,d_c}$; $Bo = \dfrac{d_c^2 \varrho_{sl}\, g}{\sigma_l}$

Number of Points	222	165
MSE	.0007	.0004
% Points within 30%	90	95
Parameters:		
a	0.51	0.24
b	0.26	0.22
c	0.05	0.11

Range of Variables:

$0 < u_g < 0.12$ m/s, u_l = 0, 0.005, 0.02 m/s , d_c = 0.05 and 0.21 m

σ_l = 0.016 – 0.017 N/m, $0 < \epsilon_{sl} < 0.1$, ϱ_s = 5100 and 2650 kg/m^3,

ϱ_l = 660 and 680 kg/m^3 , d_p = 0–5 and 20–44 μm, μ_{sl} = 0.028 and 0.022 kg/(m–s)

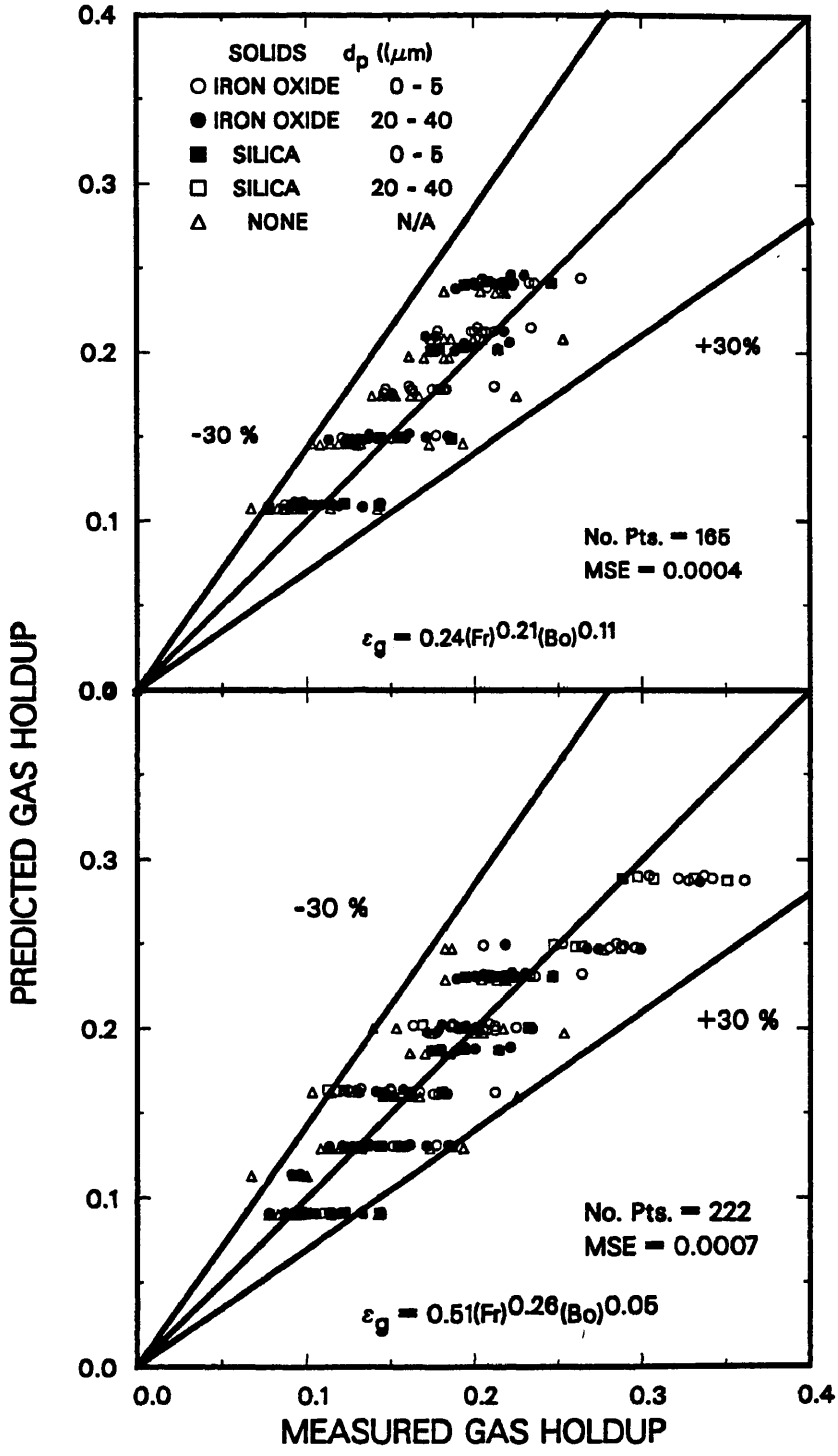

Figure 2.46. Parity plot of predicted versus measured gas holdups for the correlations developed in this study.

values when all data points (i.e. 222) were used and when data for FT–300 wax in the small diameter column were omitted (165 points), respectively. Approximately 90% of the predicted gas holdup values were within ± 30% of the measured values when all data points were used and 95% of the measured gas holdup values were within ±30% when data from the small diameter column for FT–300 wax were excluded.

Extensive two–phase studies were conducted by Bukur et al. (1987a,c) using FT–300 wax, FT–200 wax, Mobil reactor wax, and SASOL reactor wax in the glass columns. An empirical correlation was developed using 349 data points in the slug flow and churn–turbulent regimes. The correlation developed was similar to Eq. 2.37:

$$\epsilon_g = 0.247(Fr_g^{0.30} Bo^{0.15}) \tag{2.38}$$

Data from both our three–phase studies (excluding gas holdups in the small diameter column with FT–300 wax) and two–phase studies (Bukur et al.) were combined and the following general correlation was developed which may be used to predict gas holdups in Fischer–Tropsch slurry bubble column reactors operating in the slug flow or churn–turbulent regime:

$$\epsilon_g = 0.24(Fr_g^{0.28} Bo^{0.14}) \tag{2.39}$$

The MSE based on 514 data points was 0.0007. Figure 2.47 is a parity plot of the measured versus predicted gas holdups using Eq. 2.39. Approximately 94% of the experimental data were within ± 30% of the predicted values.

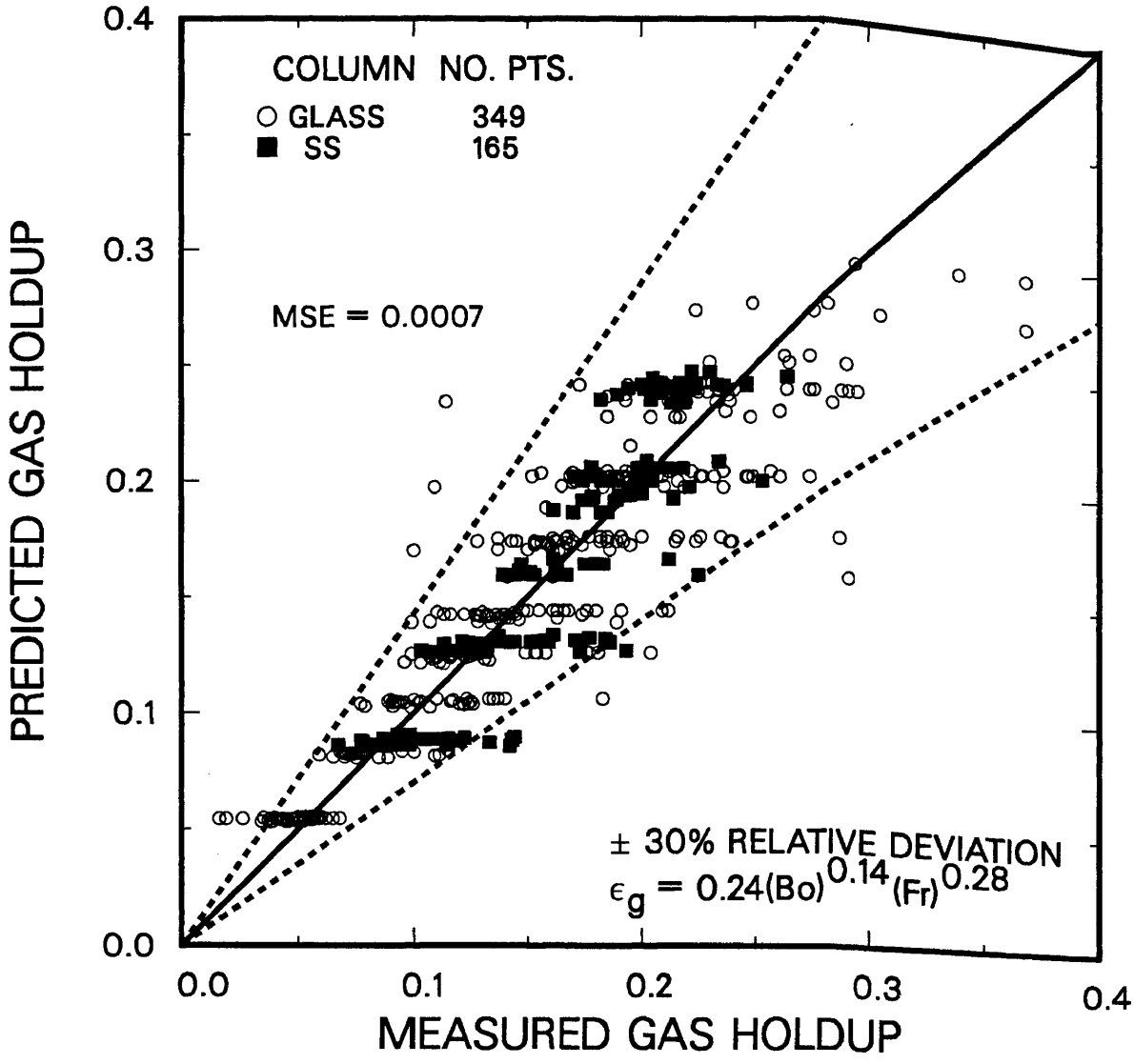

Figure 2.47. Parity plot of predicted versus measured gas holdup (wax type: SASOL, FT-300, Mobil; u_g=0.01 to 0.15 m/s; u_{sl}=0, 0.005, and 0.02 m/s; d_c= 0.05 and 0.21 m ID; solids: 0, 10, 20, and 30 wt% iron oxide and silica).

CHAPTER III

MEASUREMENT OF PHASE FRACTIONS BY GAMMA-RAY DENSITOMETRY

In many applications of industrial importance, systems operate at high temperatures and pressures. Under these conditions, experimental techniques commonly employed in hydrodynamic studies with systems that operate at low temperatures and pressures may not be applicable. Gamma–ray densitometry in a non–intrusive technique which may be used to measure various hydrodynamic parameters at high temperatures and pressures. The majority of previous investigations which have utilized this technique were limited to two–phase systems. Recently, several investigators (Seo and Gidaspow, 1987; Bernatowicz et al., 1987; and Abouelwafa and Kendall, 1980) have successfully used this technique to measure phase fractions in three–phase systems. However, the thickness of the absorbing media was less than 0.03 m. The objective of this work was to design and construct a dual energy gamma–ray densitometer which could be used to measure volume fractions (gas/liquid/solids) in a large diameter (0.21 m ID) bubble column.

Experiments were conducted using both two–phase and three–phase systems (see the Table on page 52). Volume fractions were measured with a dual energy gamma–ray densitometer during most of these experiments. The theory associated with gamma–ray absorption, the selection of sources, the experimental apparatus and calibration techniques used, the applicability of this technique to large diameter three–phase systems and results from experiments conducted in both two–phase and three–phase systems will be discussed.

Theoretical Discussion

Gamma–ray absorption is based on the fact that the intensity of radiation decreases as it passes through a material. The change in intensity, ΔI, is proportional to the

thickness of the material, Δx, and the incident intensity, I_o. Therefore,

$$\Delta I = -\mu I_o \Delta x \tag{3.1}$$

where μ is a proportionality constant called the mass attenuation coefficient. If the radiation is homogeneous, Eq. 3.1 may be written as:

$$dI = -\mu I_o dx \tag{3.2}$$

which upon integration yields:

$$I = I_o \exp(-\mu x) \tag{3.3}$$

The intensity of radiation is given by:

$$I = h\nu B \tag{3.4}$$

where $h\nu$ is the energy/photon, B_o is the incident number (i.e. no absorber) of photons crossing a unit area per unit time, and B is the number of uncollided photons crossing a unit area per unit time. Thus, Eq. 3.3 may be written in terms of the number of photons or counts per second,

$$B = B_o \exp(-\mu x) \tag{3.5}$$

As discussed by Attix (1968), attenuation of the energy of an incident photon may occur through both scattering and absorption of the photon. Attenuation by some purely elastic process in which a photon does not give up any of its initial energy to the medium, but is merely deflected, is called scattering (e.g. Raleigh scattering). Whereas, in absorption, the entire energy of the incident photon is absorbed. One type of absorption process is called the photoelectric effect. During this process, the entire energy of an incident photon is absorbed by an atom of the medium and an electron is emitted. Pair–production, is another process by which total absorption may occur. During pair–production, a photon may be totally absorbed in either the atomic nucleus

or the field of an atomic electron, and a positron–negatron pair is emitted. The Compton effect is the intermediate case, in which some of the energy of the incident photon is absorbed and appears as a Compton recoil electron, and the remaining incident energy is present as a Compton scattered electron. The attenuation process includes both scattering and absorption of the incident photon. Thus, the attenuation coefficient, μ is the sum of the absorption coefficients, μ_a and the scattering coefficients, μ_s.

For energies in the range 0.01 to 10 MeV, attenuation is due primarily to photoelectric interactions, Compton scattering and absorption, and pair–production. Figure 3.1 (from Evans, 1955), shows the energy ranges over which these competing effects dominate for various atomic numbers, Z. For relatively large values of Z, the photoelectric effect dominates at low energies and pair–production dominates at high energies.

Attix (1968) present interpolation formulas which may be used to estimate attenuation coefficients for compounds given attenuation coefficients for the elements comprising the compounds. They also give formulas for estimating absorption and scattering coefficients for elements for which experimental data are not available. The following formula may be used to estimate the attenuation coefficient, μ_{mix}, for a compound

$$\frac{\mu_{mix}}{\rho_{mix}} = \sum_i \frac{\mu_i}{\rho_i}\omega_i \qquad i = 1 \text{ to no. of components} \tag{3.6}$$

where μ_i is in cm^{-1} and ω_i is the weight fraction of component i. The following interpolation formula may be used to estimate either Compton absorption or Compton scattering coefficients, σ_i

$$\frac{\sigma_1}{\rho_1} = \left(\frac{\sigma_2}{\rho_2}\right)\left(\frac{A_2}{A_1}\right)\left(\frac{Z_1}{Z_2}\right) \tag{3.7}$$

where Z is the atomic number, A is the atomic mass, and the subsripts 1 and 2 represent any two elements. For the photoelectric effect, the interpolation formula for the absorption coefficient , τ_i, is

$$\frac{\tau_1}{\rho_1} = \left(\frac{\tau_2}{\rho_2}\right)\left(\frac{A_2}{A_1}\right)\left(\frac{Z_1}{Z_2}\right)^n \tag{3.8}$$

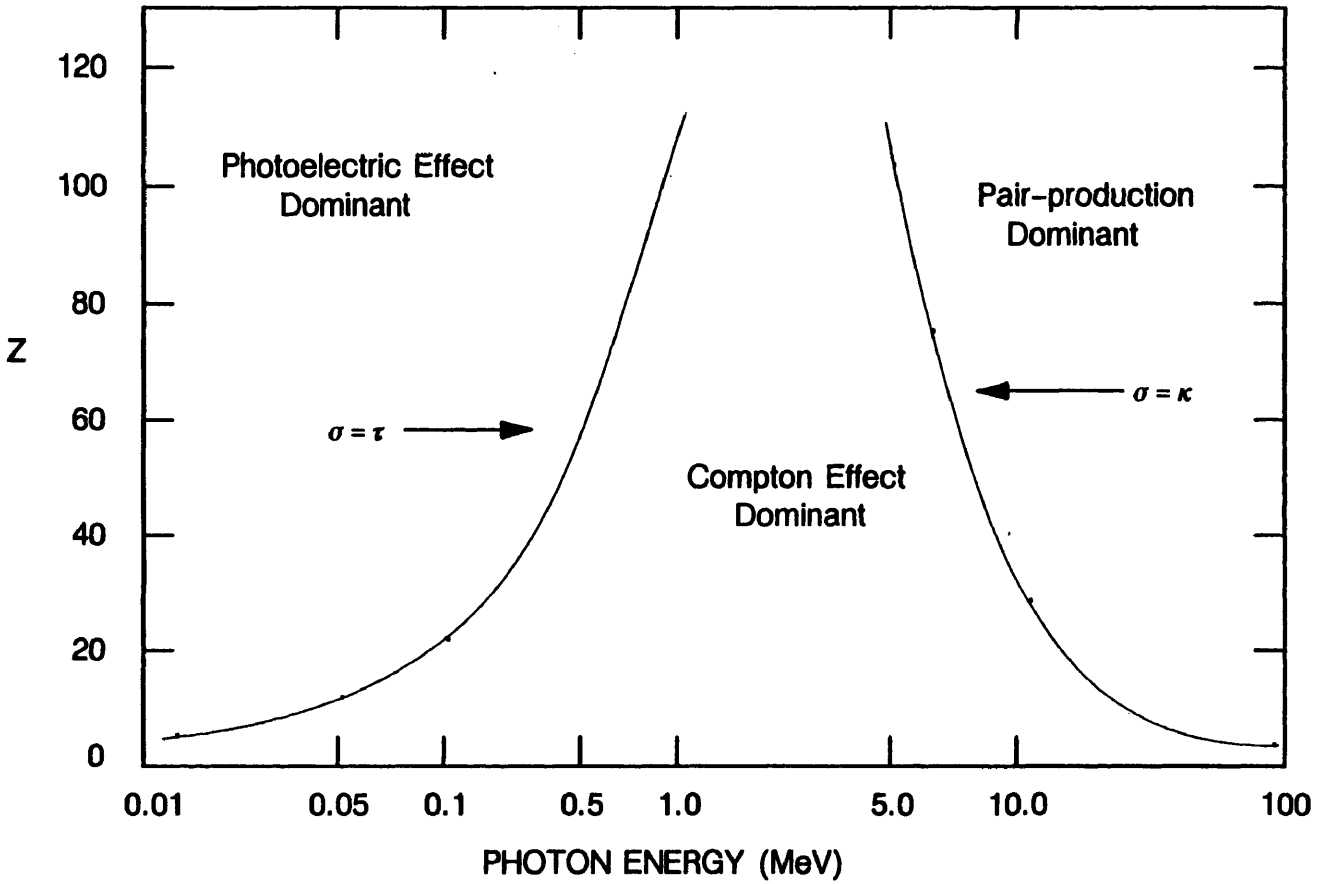

Figure 3.1. Relative importance of the three major types of gamma-ray attenuation.

where the exponent n is a function of the energy of the incident photon and ranges from 4 to 4.6. And, for pair–production,

$$\frac{\kappa_1}{\rho_1} = \left(\frac{\kappa_2}{\rho_2}\right)\left(\frac{A_2}{A_1}\right)\left(\frac{Z_1}{Z_2}\right)^2 \tag{3.9}$$

where κ_i is the absorption coefficient.

Models Used to Describe Three – Phase Systems

When the photons emitted from a radioactive source pass though a homogeneous material, a fraction of the energy associated with the photons is attenuated and Eq. 3.5 describes the absorption process. If multiple absorption mediums are aligned perpendicular to the incident beam of radiation (see Figure 3.2), the number of uncollided photons passing through the absorbing media per unit time is given by:

$$B = B_o \exp(-\sum_i \mu_i x_i) \qquad i = 1 \text{ to } n \tag{3.10}$$

where x_i is the thickness of absorber i; μ_i is the absorption coefficient for medium i; and n is the number of different absorbers.

In a three–phase bubble column, the gas, solid, and liquid phases are the absorbing media. The model used to describe the interaction between the beam of radiation and the three phases depends on the alignment of the three phases with respect to the beam of radiation. Two types of orientations were examined in this research. In one case, the three phases were assumed to be aligned perpendicular to the incident beam of radiation, and for the other case, all three phases were assumed to be aligned parallel to the beam of radiation. The two cases mentioned above represent the extremes of possible alignments.

Case I. Perpendicular Alignment

For the first case (i.e. perpendicular alignment), we assume that the beam of radiation may be represented by a cylinder, with the three phases occupying slices of

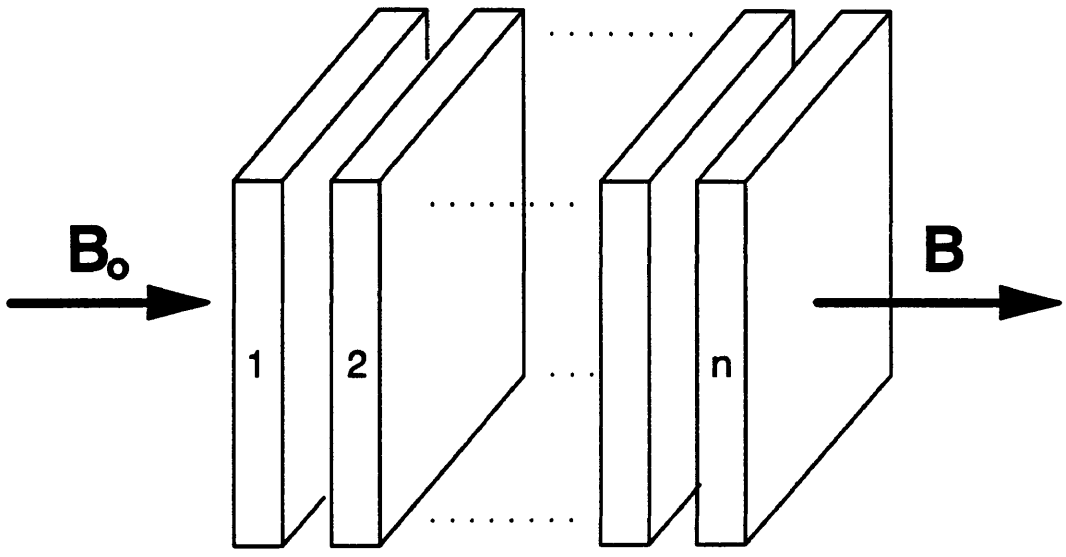

Figure 3.2. Schematic representation of multiple absorbers in series.

the cylinder (Figure 3.3). For this alignment, Eq. 3.10 may be used to describe the absorption process. The volume of phase i through which the beam of radiation passes is given by:

$$V_i = x_i A_x \qquad i = g, \ell, s \tag{3.11}$$

where A_x is the cross–sectional area of the absorbing media. The total volume of the absorbing media is

$$V_t = dA_x \tag{3.12}$$

The volume fraction of phase i, ϵ_i, is defined as the volume of phase i (Eq. 3.11) divided by the total volume (Eq. 3.12) and may be expressed as:

$$\epsilon_i = \frac{x_i A_x}{dA_x} \qquad i = g, \ell, s \tag{3.13}$$

or, the thickness of the absorbing media, x_i is

$$x_i = d\epsilon_i \qquad i = g, \ell, s \tag{3.14}$$

Substituting Eq. 3.14 into Eq. 3.10 for x_i yields the following expression for the amount of radiation transmitted through the column

$$B = B_o \exp[-d(\mu_g \epsilon_g + \mu_\ell \epsilon_\ell + \mu_s \epsilon_s)] \tag{3.15}$$

where the subscripts g, ℓ, and s refer to the gas, liquid, and solid phases, respectively. Equation 3.15 contains three unknowns, i.e. the volume fractions of the three phases. Thus, two additional equations are needed to characterize the system. Since attenuation coefficients are a function of radioactive source strength (i.e. energy), another equation arises from the use of an additional source. This equation is identical to Eq. 3.15 except that the values of the attenuation coefficients are different. These two equations along with a volume balance are used to obtain volume fractions of the individual phases.

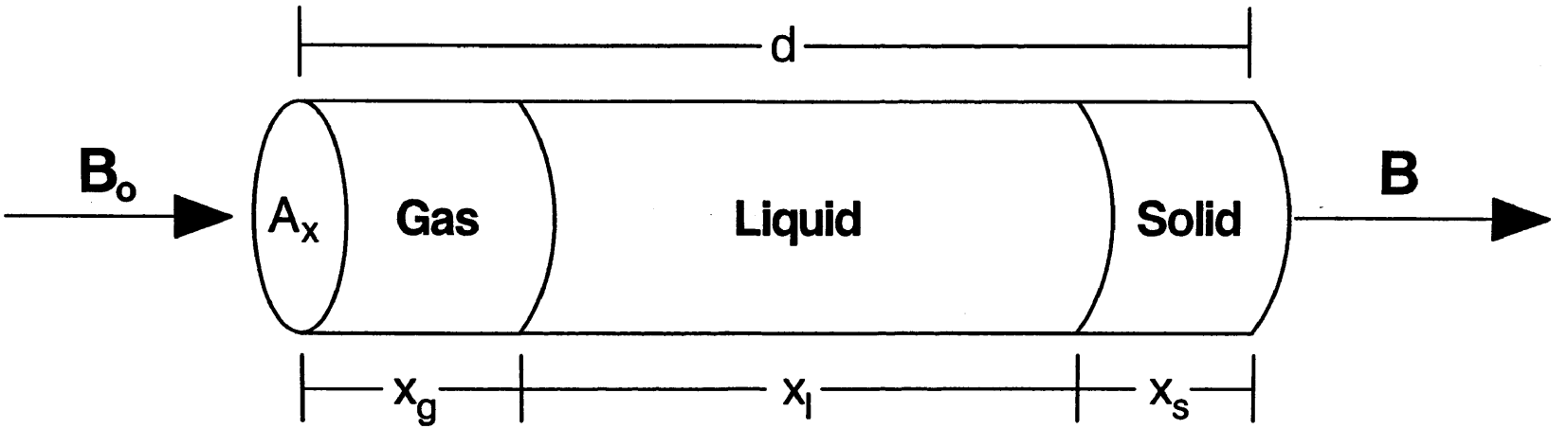

Figure 3.3. Schematic representation of Case I geometry (i.e. perpendicular alignment).

Thus, the set of equations used to determine volume fractions in a three–phase system is:

$$B_1 = B_{o1}\exp[-d(\mu_{g1}\epsilon_g + \mu_{\ell 1}\epsilon_\ell + \mu_{s1}\epsilon_s)] \tag{3.16}$$

$$B_2 = B_{o2}\exp[-d(\mu_{g2}\epsilon_g + \mu_{\ell 2}\epsilon_\ell + \mu_{s2}\epsilon_s)] \tag{3.17}$$

$$1 = \epsilon_g + \epsilon_\ell + \epsilon_s \tag{3.18}$$

where the subscripts 1 and 2 refer to the two different radioactive sources.

At atmospheric pressure, the attenuation of radiation due to the gas phase phase is negligible, and the quantity $\mu_{gi}\epsilon_{gi}$ may be omitted from equations 3.16 and 3.18. If the absorption by the gas phase is neglected, Eqs. 3.16 and 3.17 may be combined to yield a single expression for either the volume fraction of solids or the volume fraction of liquid. The volume fraction of the liquid phase is

$$\epsilon_\ell = \frac{\ln(B_1 / B_{o1})\mu_{s2} + \ln(B_2 / B_{o2})\mu_{s1}}{d(\mu_{\ell 2}\mu_{s1} - \mu_{\ell 1}\mu_{s2})} \tag{3.19}$$

Once the value of ϵ_ℓ is known, it is substituted into either Eq. 3.16 or Eq. 3.17 to obtain a value for ϵ_s. The gas holdup is then calculated from Eq. 3.18.

Case II. Parallel Alignment

Another possible geometric relationship between the incident beam of radiation and the absorbing media is when the three phases are aligned in parallel with respect to the beam of radiation (see Figure 3.4). A fraction of the incident beam of radiation passes through each phase separately. The fraction of the incident beam passing through a given phase is

$$f_{o_i} = \frac{A_i}{A_x} = \epsilon_i \qquad i = g, \ell, s \tag{3.20}$$

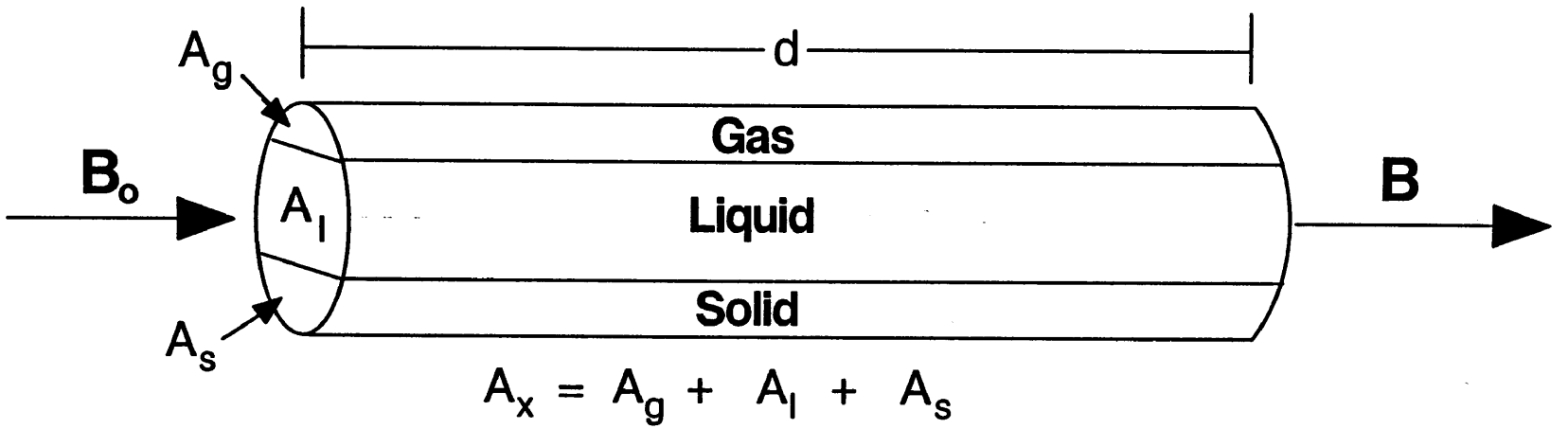

Figure 3.4. Schematic representation of Case II geometry (i.e. parallel alignment).

where A_i is the cross–sectional area of the cylinder occupied by the ith phase. Thus, the amount of radiation passing through a given phase is

$$B_i = B_o \epsilon_i \exp(-\mu_i d) \qquad i = g, \ell, s \tag{3.21}$$

The total amount of radiation which passes through the absorbing media is the sum of the amounts of radiation which passes through the three phases,

$$B = B_o[\epsilon_g \exp(-d\mu_g) + \epsilon_\ell \exp(-d\mu_\ell) + \epsilon_s \exp(-d\mu_s)] \tag{3.22}$$

Once again, two different radioactive sources are needed and we may assume that attenuation due to the gas phase is negligible. The final set of equations used to describe this type of configuration is:

$$B_1 = B_{o1}[\epsilon_g + \epsilon_\ell \exp(-d\mu_{\ell 1}) + \epsilon_s \exp(-d\mu_{s1})] \tag{3.23}$$

$$B_2 = B_{o2}[\epsilon_g + \epsilon_\ell \exp(-d\mu_{\ell 2}) + \epsilon_s \exp(-d\mu_{s2})] \tag{3.24}$$

$$1 = \epsilon_g + \epsilon_\ell + \epsilon_s \tag{3.25}$$

Equations 3.23 to 3.25 may be solved to obtain the following expression for ϵ_ℓ,

$$\epsilon_\ell = \frac{(B_1 / B_{o1}) - 1 - \frac{((B_2/B_{o2})-1)(\exp(-d\mu_{s1})-1)}{(\exp(-d\mu_{s2})-1)}}{(\exp(-d\mu_{\ell 1}) - 1) - \frac{(\exp(-d\mu_{\ell 2})-1)(\exp(-d\mu_{s1})-1)}{\exp(-d\mu_{s2})-1}} \tag{3.26}$$

Equation 3.25 may be substituted into either Eq. 3.23 or Eq. 3.24 to obtain an expression for ϵ_s in terms of ϵ_ℓ. If Eq. 3.24 is used, the expression for ϵ_s is

$$\epsilon_s = \frac{(B / B_{o2}) - 1 - \epsilon_\ell(\exp(-d\mu_{\ell 2}) - 1)}{\exp(-d\mu_{s2}) - 1} \tag{3.27}$$

Detailed derivations of Eqs. 3.26 and 3.27 are given in Appendix B. The value of ϵ_ℓ calculated from Eq. 3.26 is substituted into Eq. 3.27 to obtain a value for ϵ_s. Using these two values, the gas holdup, ϵ_g, is calculated directly from Eq. 3.25.

Comments on the Alignment of the Phases

Actual phase alignment with respect to the beam of radiation for two and three–phase flow will lie between the two cases described above. However, since there is a considerable amount of homogeneity in the flow patterns (except in the slug flow regime) in bubble columns, it may be assumed that the majority of the radiation will be attenuated according to Case I alignment.

Previous studies with three–phase systems (e.g. Bernatowicz et al., 1987; Seo and Gidaspow, 1987; Abouelwafa and Kendall, 1980) used Case I alignment (i.e. phases perpendicular to incident beam of radiation) to model the attenuation process. Petrick (1958) constructed several lucite models representative of different types of flow patterns in a two–phase system. There was excellent agreement between the predicted volume fractions and the actual volume fractions ($< 7\%$ relative error) assuming Case I alignment. In his experiments, he measured the volume fractions at various radial locations and used the average value. He also measured the volume fraction at a single location (i.e "one shot" method), and the error between the actual and predicted volume fractions was considerably higher ($< 36\%$ relative error) for models representative of non–homogeneous flow conditions. Under actual two–phase flow conditions in a vertical tube (air–water system), Petrick showed that when the width of the beam of radiation was equal to the width of the absorbing medium (i.e. the column diameter), there was no difference between volume fractions predicted using several measurements and averaging the results, and volume fractions obtained using the "one shot" method. However, when the column diameter was increased such that the width of the beam of radiation was less than the column diameter, he observed differences in the volume fraction calculated using the two techniques. He attributed the differences in results, to differences in the radial distribution of the volume fractions of air and water. Thus,

not only phase alignment, but also phase distributions (i.e. axial and radial variations in phase fractions) need to be taken into account when using the gamma–ray technique.

Figures 3.5a and 3.5b are schematic representations of two possible phase distributions (two–phases) in a square channel. Figure 3.5a represents annular flow, in which a gas fills the center of the duct, and Figure 3.5b, represents homogeneous flow (i.e. no radial variation in volume fractions). Based on the dimensionless distances given in Figure 3.5, the actual volume fraction of gas is 0.25 for both cases. For homogeneous flow conditions (Figure 3.5b), regardless of the radial location of the measurement, the volume fraction of gas (or liquid) may be accurately determined at any location assuming Case I alignment (i.e. using Eq. 3.10). However, for annular flow, if a single measurement is made in the center of the duct (see section A in Figure 3.5a), the measured volume fraction of gas obtained assuming Case I alignment would be 0.5 as opposed to the actual value of 0.25. Phase alignment becomes a problem, if measurements are made through section B in Figure 3.5a. In order to overcome these problems, measurements should be made at various locations across the duct and the volume fractions obtained from each measurement (via Eq. 3.10) should be averaged over the entire cross section of the duct to obtain an accurate estimate of the phase fractions.

Source Selection and Sensitivity Analysis

A gamma–ray densitometer system consists of three main parts: (1) radioactive sources, (2) detectors, and (3) associated electronic equipment. Of the three main components, the sources are the most important.

One must consider several factors, when selecting sources. These include transmission through the pipe walls and sensitivity to the slurry content. These two factors are competing. The lower the gamma–ray energy (i.e. higher attenuation) the more sensitive the system is to changes in the volume fractions of the slurry; however, with a

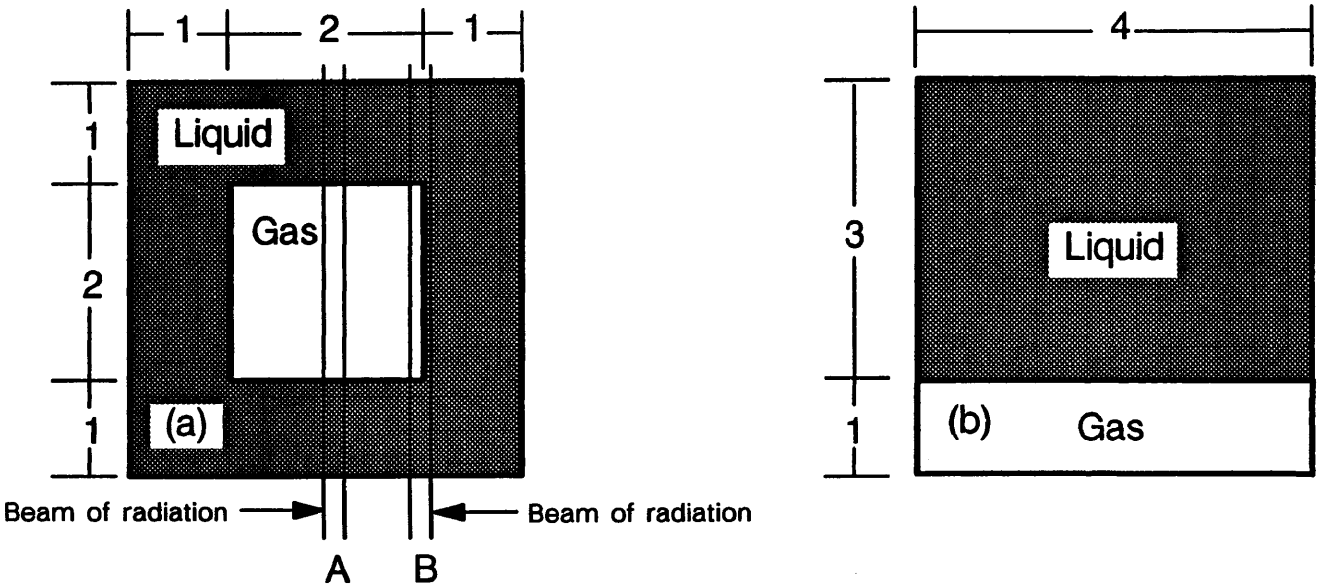

Figure 3.5. Schematic representations of (a) annular flow and (b) homogeneous flow in a square duct.

low energy source, more of the photons emitted from the source are attenuated by the vessel walls. This becomes a significant factor when the vessels (i.e. bubble column in this case) have thick metal walls. Other factors which need to be considered are the half–life of the source and the availability of the source. If a source with a very short half–life is used, then calibrations of the empty test section will have to be repeated frequently. This is to ensure that the initial count rate (or count rate through the empty pipe, B_o) is correct.

The factors described above need to be considered when selecting sources for both two–phase and three–phase applications. However, when two sources are required (i.e. three–phase measurements) one other criterion must be taken into account. Abouelwafa and Kendall (1980) contend that the gamma–ray technique may be applied to multiphase systems provided the attenuation coefficients for the various phases are "different" for the sources selected. However, they never quantify what is meant by "different". It is obvious from Eqs. 3.16 and 3.17 that the attenuation coefficients for each phase must be "different" for the equations to be independent. However, it should be pointed out that while this is true, the following restriction must also be applied

$$\left(\frac{\mu_{\ell_1}}{\mu_{s_1}}\right)\left(\frac{\mu_{s_2}}{\mu_{\ell_2}}\right) \neq 1 \tag{3.28}$$

If the above criterion is not satisfied, the denominator in Eq. 3.19 is zero and volume fractions cannot be calculated. This poses a serious problem when the gamma–ray technique is applied to large diameter systems. As discussed previously, attenuation is due primarily to the photoelectric effect, Compton scattering and absorption, and pair production. Furthermore the various types of attenuations (i.e. photoelectric, Compton, and pair production) dominate at certain energy levels as shown in Figure 3.1. If two different sources are selected, with different attenuation coefficients; however, if attenuation is dominated by the same process for both sources, the denominator in

Eq. 3.19 approaches 0.0 making the calculated value of ϵ_ℓ very sensitive to slight errors in the measured quantities (i.e. count rates). It follows from Eqs. 3.6 to 3.9 that the best results would be obtained if a low energy source (i.e. one in which attenuation was dominated by the photoelectric effect) and a relatively high energy source (i.e. one in which attenuation was dominated by Compton scattering and absorption) were used.

However, in a large diameter system, it may not be possible to use a low energy source since the majority of the radiation will be attenuated by the absorbing medium. Thus, it is necessary to use a higher energy source. If this is the case, then the second source would have to be extremely powerful (i.e. energy $>$ 10 MeV) to satisfy the criterion presented in Eq. 3.28. However, these sources pose serious safety problems and may not be readily available.

Nevertheless, for a given set of two sources, the appropriate source activity must be chosen. The activity required will depend on several factors, including the counting period, collimation diameter, length of the collimator, detector efficiency, and emission ratio of the desired gamma–rays (Chan and Banerjee, 1981).

It is well known that the counting process is a Poisson process, where the probability of n counts occurring in the time interval Δt is given by:

$$P_n = \frac{(B\Delta t)^n}{n!}\exp(B\Delta t) \tag{3.29}$$

The mean and variance of the Poisson process is B (i.e. the count rate). The standard deviation is $\sqrt{B}$. Thus, the actual count rate is the measured count rate $\pm\sqrt{B}$. Hence, the uncertainty in the count rate is $\frac{\sqrt{B}}{B}$. If B_o (i.e. empty column count rate) is measured over an extended period of time, the statistical error in B_o is assumed to be insignificantly small and the statistical error in void fractions may be calculated assuming only errors (or uncertainty) in the measured count rates (i.e. B).

Commercially available sources, with energies ranging from 0.0595 MeV (Americium – 241) to 1.17,1.33 MeV (Cobalt–60) were used to simulate the effect of uncertainty in the count rate on the predicted phase fractions. The two source combinations used to study the effect of errors in count rate on phase fractions were: (1) Americium – 241 – Cobalt–60 and (2) Cesium–137 (0.661 MeV) – Cobalt–60. For these simulations, the liquid phase was assumed to be a straight chain (C52) paraffin wax (MW = 730), and the solid phase was iron oxide. For the purpose of these calculations, Case 1 alignment was used, and the attenuation due to the gas phase was assumed negligible.

The attenuation coefficients for the solid and liquid phases for each source were estimated from data presented by Attix (1968). Attenuation coefficients are given by Attix for elements with atomic numbers up to 28 for energies ranging from 0.01 to 10 MeV. Equation 3.6 was used to estimate the attenuation coefficients for iron oxide and wax. Table 3.1 lists the attenuation coefficients used for sensitivity analysis. The criterion established in Eq. 3.28 is satisfied for both source combinations. For the Americium–Cobalt system, the quantity on the left hand side of Eq. 3.28 is 0.2, and for the Cesium–Cobalt system, the quantity on the left hand side of Eq. 3.28 is 0.98. Thus, one would expect that slight errors in measured quantities (i.e. count rates) would have less of an effect on the predicted volume fractions for the Americium–Cobalt system as compared to the Cesium–Cobalt system.

Tables 3.2a and 3.2b show results for the Americium–Cobalt system for errors in the count rate of Cobalt and errors in the count rate of Americium, respectively. An error of 1% in the Cobalt count rate corresponds to an error of approximately 10% in the predicted gas holdup. However, an error of 10 % in the Americium count rate would produce an error of only 4.5 % in the predicted gas holdup. Tables 3.3a and 3.3b show results for the Cesium–Cobalt system. For this system, an error of only 0.1 % in the count rates of Cesium or Cobalt produces an error of 19% and 26%, respectively, in the

Table 3.1. Attenuation Coefficients (cm^{-1}) Used for Error Analysis Calculations

ABSORBING MEDIUM	SOURCE		
	Am–241	Co–60	Cs–137
WAX ($C_{52}H_{106}$)	0.139	0.0423	0.0580
IRON OXIDE	4.575	0.2710	0.3820

Table 3.2a. Effect of Errors in the Count Rate of Co–60 on Volume Fractions Using the Am–241 and Co–60 System

% ERROR IN COUNT RATE	ϵ_g	% error	ϵ_s	% error
+0.1	0.152	1.3	0.0300	–
+0.5	0.157	4.7	0.0302	0.7
+1.0	0.165	10.0	0.0305	1.7
+5.0	0.223	48.7	0.0320	6.7
+10.0	0.294	96.0	0.0340	13.3

Table 3.2b. Effect of Errors in the Count Rate of Am–241 on Volume Fractions Using the Am–241 and Co–60 System

% ERROR IN COUNT RATE	ϵ_g	% error	ϵ_s	% error
+0.1	0.1500	–	0.0300	–
+0.5	0.1496	0.27	0.0299	0.3
+1.0	0.1492	0.5	0.0305	0.7
+5.0	0.1462	2.5	0.0320	2.3
+10.0	0.1426	4.9	0.0286	4.7

Base Conditions: $\epsilon_g = 0.15$, $\epsilon_\ell = 0.82$, and $\epsilon_s = 0.03$

Table 3.3a. Effect of Errors in the Count Rate of Co–60 on Volume Fractions Using the Cs–137 and Co–60 System

% ERROR IN COUNTRATE	ϵ_g	% error	ϵ_s	% error
+0.1	0.189	26	0.037	23
+0.5	0.344	129	0.065	117
+1.0	0.537	258	0.099	230
+5.0	2.050	1267	0.370	1133
+10.0	3.860	2473	0.694	2213

Table 3.3b. Effect of Errors in the Count Rate of Cs–137 on Volume Fractions Using the Cs–137 and Co–60 System

% ERROR IN COUNTRATE	ϵ_g	% error	ϵ_s	% error
+0.1	0.122	19	0.025	17
+0.5	0.013	91	0.0057	83
+1.0	-0.123	182	-0.021	170
+5.0	-1.170	893	-0.218	827
+10.0	-2.468	1745	-0.454	1613

Base Conditions: $\epsilon_g = 0.15$, $\epsilon_\ell = 0.82$, and $\epsilon_s = 0.03$

predicted gas holdup values. It is obvious from these results, that in order to accurately measure individual volume fractions in a three–phase system, one must use a relatively low energy source (e.g. Americium–241) and a high energy source (e.g. Cobalt–60).

If a suitable low energy gamma source is not available, then a three–phase system may be treated as a two–phase system (i.e. treat the solid phase and the liquid phase as a single phase), provided the weight fractions of the solid and liquid phases are known. These quantities are needed to calculate the attenuation coefficient for the slurry (see Eq. 3.6),

$$\frac{\mu_{s\ell}}{\rho_{s\ell}} = \sum_{i} \frac{\mu_i}{\rho_i}\omega_i \qquad i = 1 \text{ to no. of components} \tag{3.30}$$

The volume fraction of the slurry may be calculated using (see Eq. 3.10),

$$\epsilon_{s\ell} = \frac{-\ln(B\,/\,B_o)}{d\mu_{s\ell}} \tag{3.31}$$

where $\epsilon_{s\ell} = \epsilon_s + \epsilon_\ell$.

Experimental Apparatus and Operating Conditions

During some of the experiments in the 0.21 m ID column, the dual energy nuclear density gauge was used to determine gas holdups at various radial and axial locations. The density gauge system was composed of a movable assembly mechanism (MAM) which was used to transport the gauge both axially and radially along the column, two radioactive sources, two NaI detectors, and the associated electronics.

Movable Assembly Mechanism (MAM)

The MAM is used to transport the nuclear density gauges both axially and radially along the column. It is divided into two main parts, the axial movement mechanism (Figure 3.6) and the radial movement mechanism (Figure 3.7). Separate axial and radial movement mechanisms for the sources and detectors were constructed. Each axial movement mechanism consisted of a 6.35 cm diameter ball screw (Saginaw),

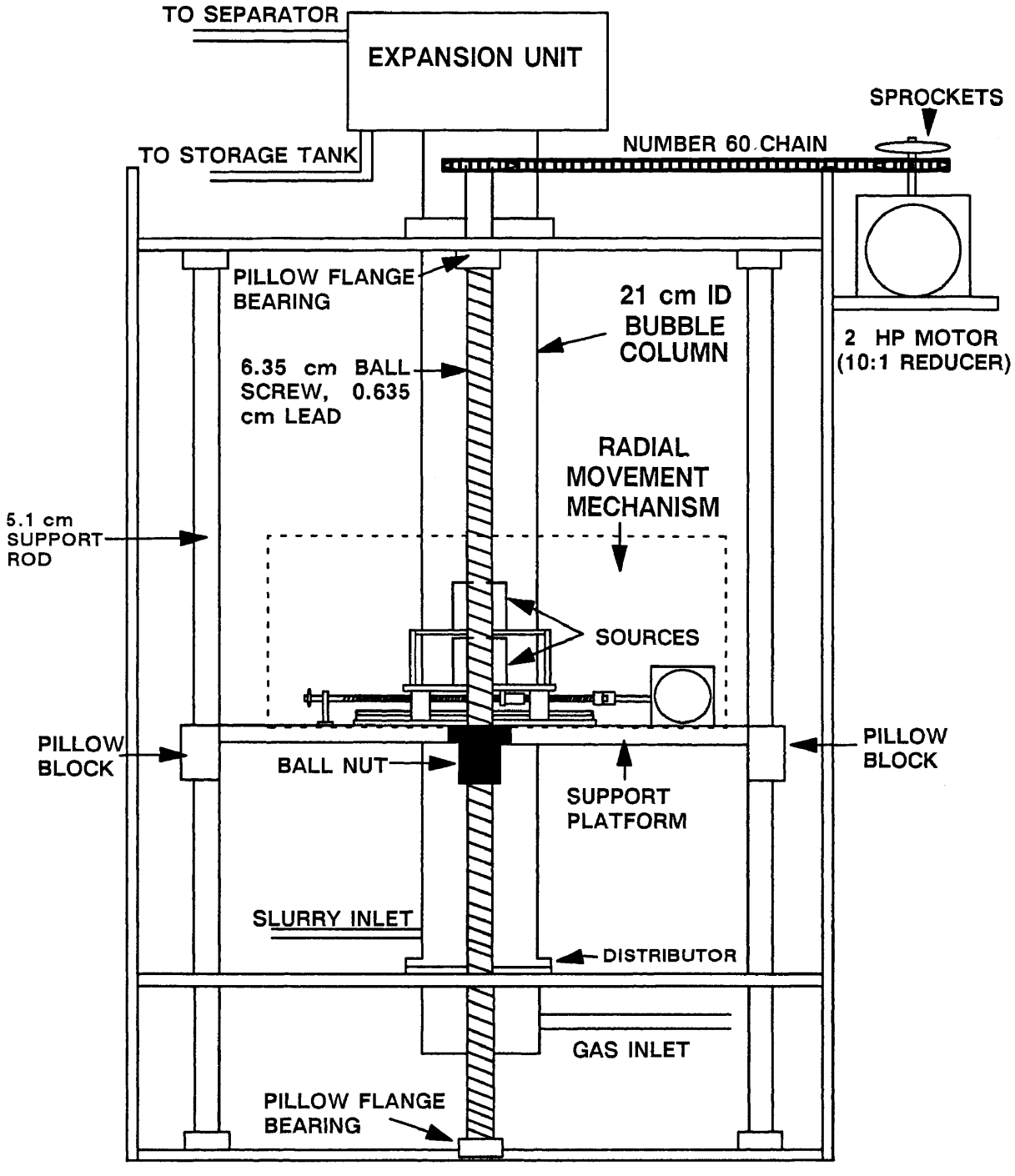

Figure 3.6. Schematic diagram of axial movement mechanism for the nuclear density gauge apparatus.

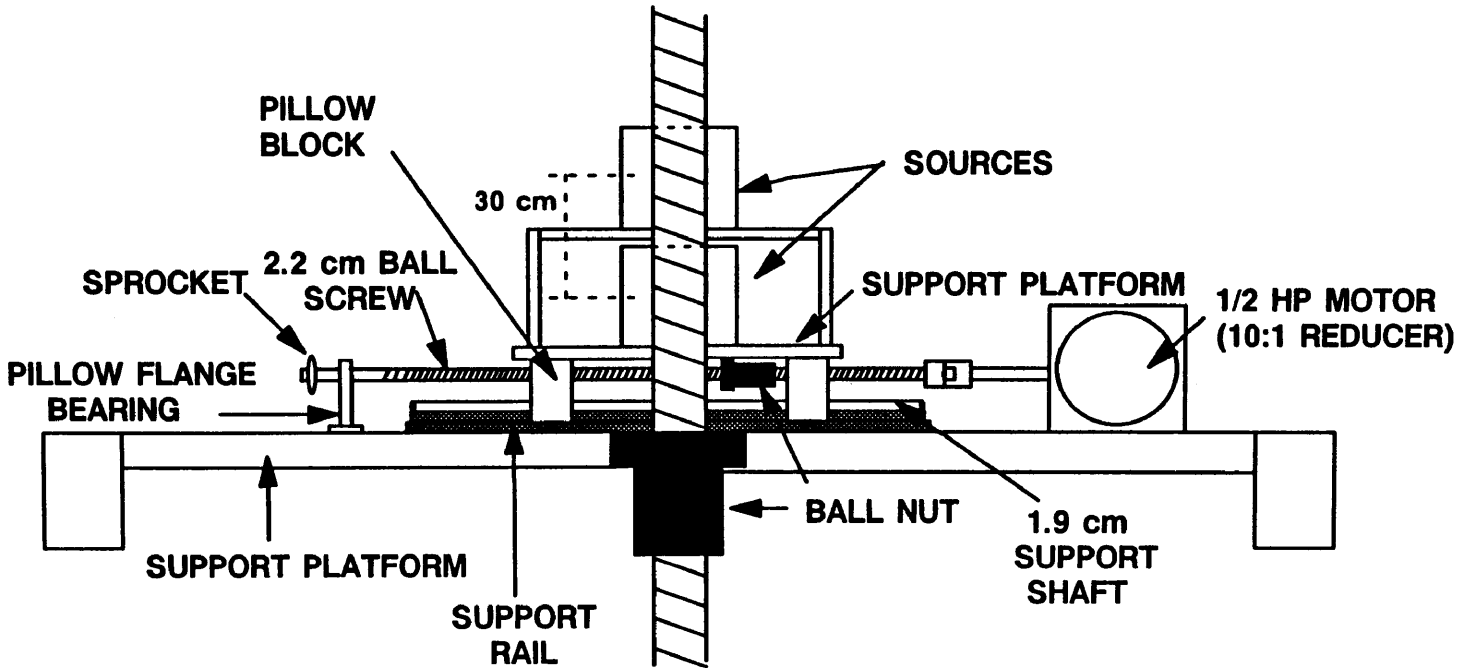

Figure 3.7. Schematic diagram of the radial movement mechanism for the nuclear density gauge apparatus.

3.3 m long, two support rods (5.1 cm diameter, 3.17 m long solids steel shafts), two 5.1 cm pillow blocks (Saginaw, SPB–32-ADJ), one non–preloaded ball nut (Saginaw, 5703263), two pillow flange bearings (Dodge, 059076), and one 1.27 cm thick aluminum plate on which the radial movement mechanism, was mounted. A 2 HP motor (Reliance, T16#3030) equipped with a 10:1 Tygear reducer (MR94667) and double single sprocket was mounted at the top of the apparatus and was used to transport the density gauge axially.

The radial movement mechanism was located on top of the aluminum plate described above (see Figure 3.7). Each radial movement mechanism consisted of two support shafts (1.9 cm diameter, 0.61 m long) which were mounted to two support rails (Saginaw, SR–12–PD), four pillow blocks (Saginaw, SPB–12–OPN), one ball screw 2.2 cm in diameter and 0.66 m long (Saginaw), one ball nut (Saginaw, 5708277), two pillow flange bearings (Dodge), and two 1.27 cm thick aluminum plates which supported the detectors or sources. A 1/4 HP motor (Reliance, T56H1019) equipped with a 10:1 Tygear reducer (MR94751) was mounted directly to the ball screw used to transport the sources radially. A chain and associated sprockets connected the radial movement mechanisms for the sources and detectors.

A series of magnetic switches were used to position the density gauge at predetermined locations (both axial and radial). The magnetic switches were connected to the motors and once activated, would turn–off the motor. Thus, measurements were made at the same location each time. This is extremely important for radial measurements, since the distance through the pipe varies with the radial position.

Sources and Detectors

A 35 mCi Cobalt–60 source, a 50 mCi Cesium–137 source, and a 300 mCi Americium – 241 source were used throughout our studies. The Cs–137 and Am–241 sources were donated by the Department of Energy and were previously used by Scientific

Applications Incorporated. The Cs–137 source was an encapsulated ceramic cylinder 3 mm in diameter and 3 mm long. The Co–60 source was an encapsulated metal cylinder of Cobalt–60, 1 mm by 1 mm. Am–241 was a disc source measuring approximately 12 mm in diameter. The Am–241 source was tested in our system by placing it in a source holder without any collimation and using a NaI (sodium iodide) detector (1.5" diameter crystal, 1 mm thick) with a beryllium window. The column was filled with water and air was bubbled through. The count rate measured at the detector was approximately 150 counts/sec. Once collimated, the count rate would be substantially lower. We consulted various manufacturers about low energy gamma sources; however, we were unable to locate a point source with sufficient activity for our application. The strongest low energy gamma source we were able to locate was a 5 Ci Am–241 disc source with an effective diameter of 40 mm. However, once collimated with a 2.54 cm long collimator, 0.63 cm in diameter, the estimated count rate would be approximately 30 counts/sec. One other alternative available was to have a low energy source manufactured which consisted of several disc or cylindrical sources aligned in series. Amersham makes a 25 Ci Am–241 source measuring 85 mm in length and 40 mm in diameter. If this source was used, we could expect a count rate of approximately 150 counts/sec, which is still extremely low. For dynamic systems, where the volume fraction of the individual phases at a given location fluctuate with time, higher count rates are required because the response time of the ratemeter is a function of the count rate. For a count rate of 150 counts/sec, it takes approximately 20 seconds (our system) for the count rate from the ratemeter to reach 99 % of its actual value. Thus, if count rates are measured over a short period of time, it is possible that they will not reflect the true (or average) count rate. Since, we were unable to obtain a low energy gamma source, we decided to use the Co–60 source and Cs–137 source as our two sources. We did not expect to obtain good results for three–phase measurements using this system (based on the discussion

presented in the section entitled Source Selection and Sensitivity Analysis); however, we felt we could always treat our three–phase system as a two–phase system using the measured weight fraction of solids (see Chapter II) to calculate a mean attenuation coefficient for the slurry.

The two source holders used to house the Co–60 and Cs–137 sources during measurements are shown in Figures 3.8 and 3.9, respectively. The Cobalt–60 source was collimated through a 76 mm long opening 5.1 mm in diameter and the Cesium source was collimated through a 50.8 mm long opening 6.35 mm in diameter. The source holders were designed such that the level of radiation detected at approximately 2 feet from the source (not including the open end) was less than 0.4 mrem/h.

NaI detectors (3.81 mm crystal diameter, 3.81 mm thick) manufactured by Bicron corporation were used with both the Co–60 source and Cs–137 source. The detectors were placed in an aluminum housings equipped with cooling coils (see Figure 3.10). A thermocouple was attached to the wall of the housing to monitor changes in the detector temperature. Collimators were also placed at the front of each detector and were approximately 38 mm long with a diameter of 6.35 mm.

Nuclear Electronics

A separate set of nuclear electronic components were used for each source–detector system so that data could be acquired simultaneously from both detectors. All nuclear electronics were manufactured by Tennelec and are listed in Table 3.4. Figure 3.11 is a schematic representation of the nuclear density gauge including the source, detector, electronics, and data acquisition system. The data acquisition system was the same as that used for acquiring data from the pressure transducers. The individual gamma pulses are amplified by the preamplifier, shaped and further amplified by an amplifier. Pulses from the amplifier pass through the single channel analyzer (SCA) which discriminates between different pulses so that only pulses corresponding to a given energy level are

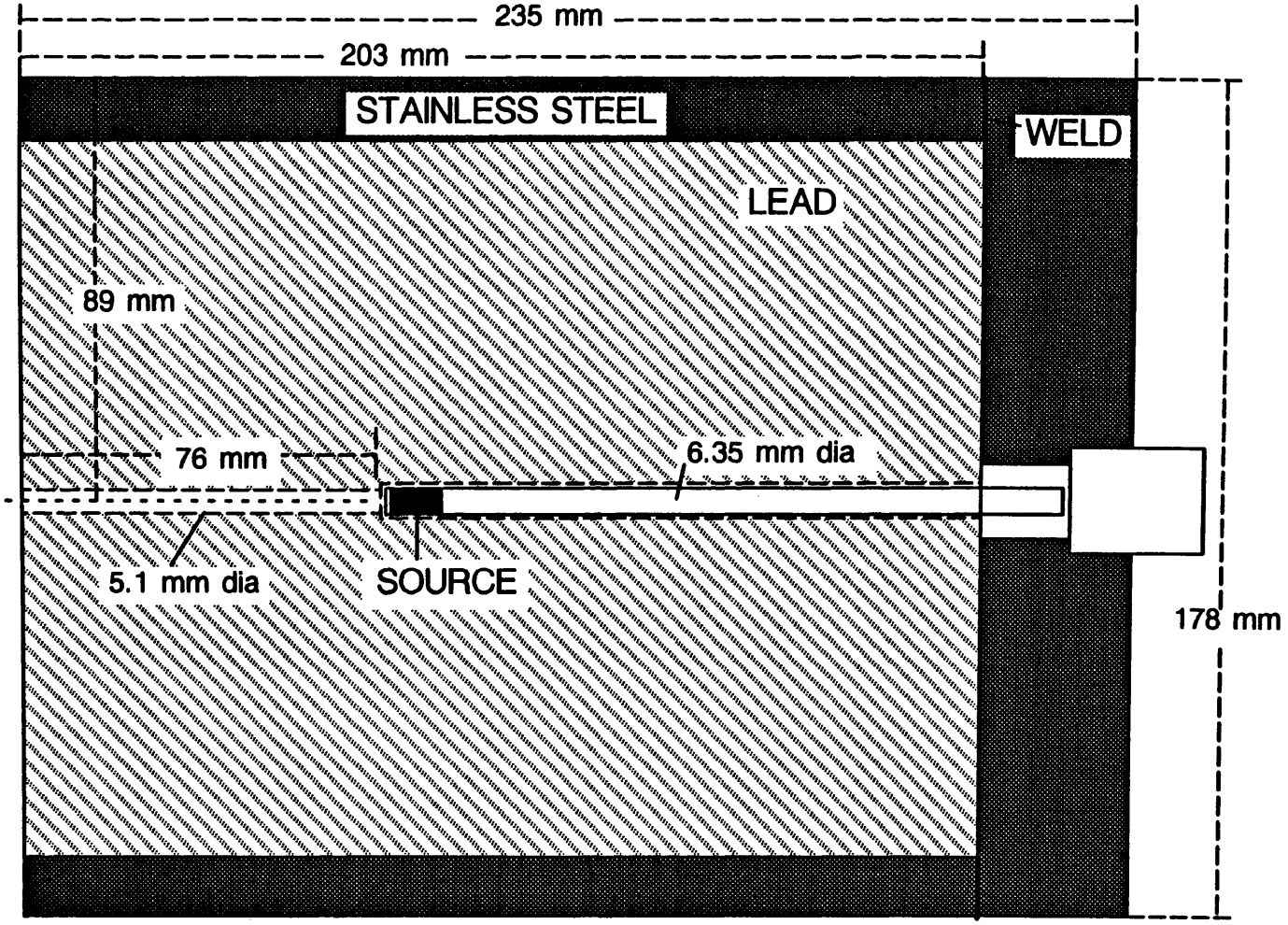

Figure 3.8. Schematic representation of the Cobalt-60 source holder.

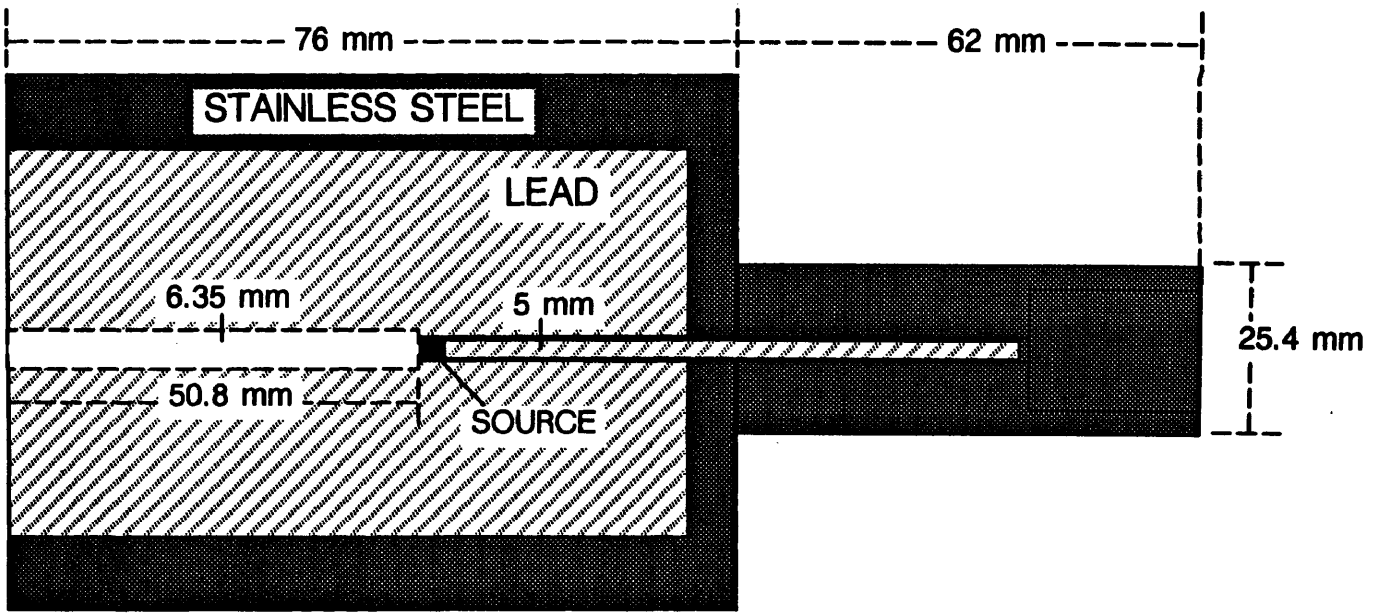

Figure 3.9. Schematic representation of the Cesium-137 source holder.

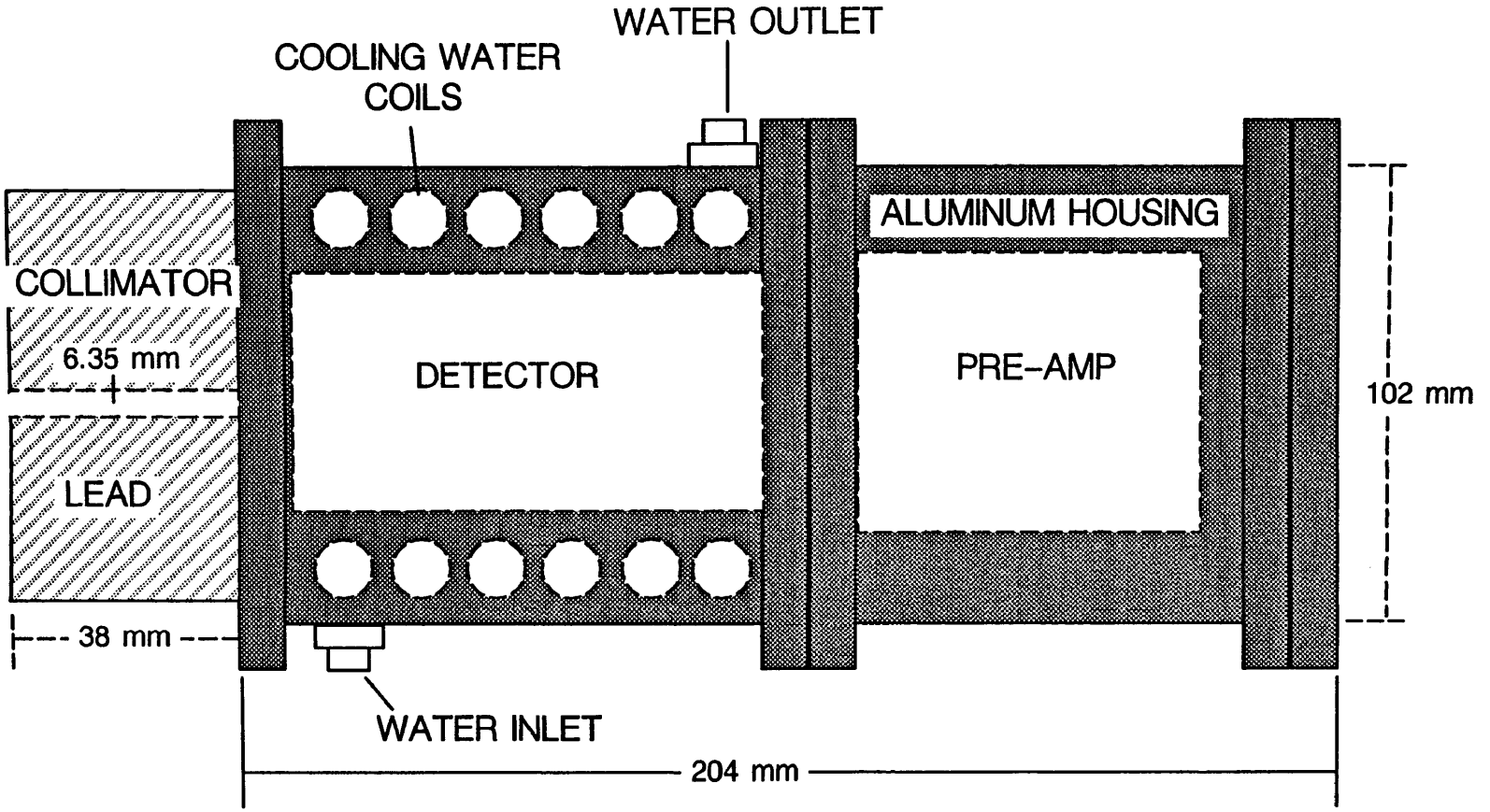

Figure 3.10. Schematic representation of the detector housing for the Cobalt-60 and Cesium-137 sources.

Table 3.4. Summary of Nuclear Density Gauge Electronics

EQUIPMENT	MANUFACTURER	MODEL #
DETECTOR	BICRON	1.5M1.5/1.5
HIGH VOLTAGE SUPPLY	TENNELEC	TC–948
PRE–AMPLIFIER	TENNELEC	TC–154A
AMPLIFIER	TENNELEC	TC–248
SCA[a]	TENNELEC	TC-450
RATEMETER	TENNELEC	TC-526

[a] SCA: Single channel analyzer

Table 3.5. Summary of Settings for the High Voltage Supply (HVS), Amplifier (AMP), and Single Channel Analyzer (SCA)

INSTRUMENT	DIAL	Co–60	Cs–137
HV	OUTPUT VOLTAGE	681	585
AMP	COARSE GAIN	100	50
	FINE GAIN	1.17	0.57
	TIMING AMP GAIN	50	50
SCA	UPPER LEVEL	9.5	5.0
	LOWER LEVEL	5.1	4.5

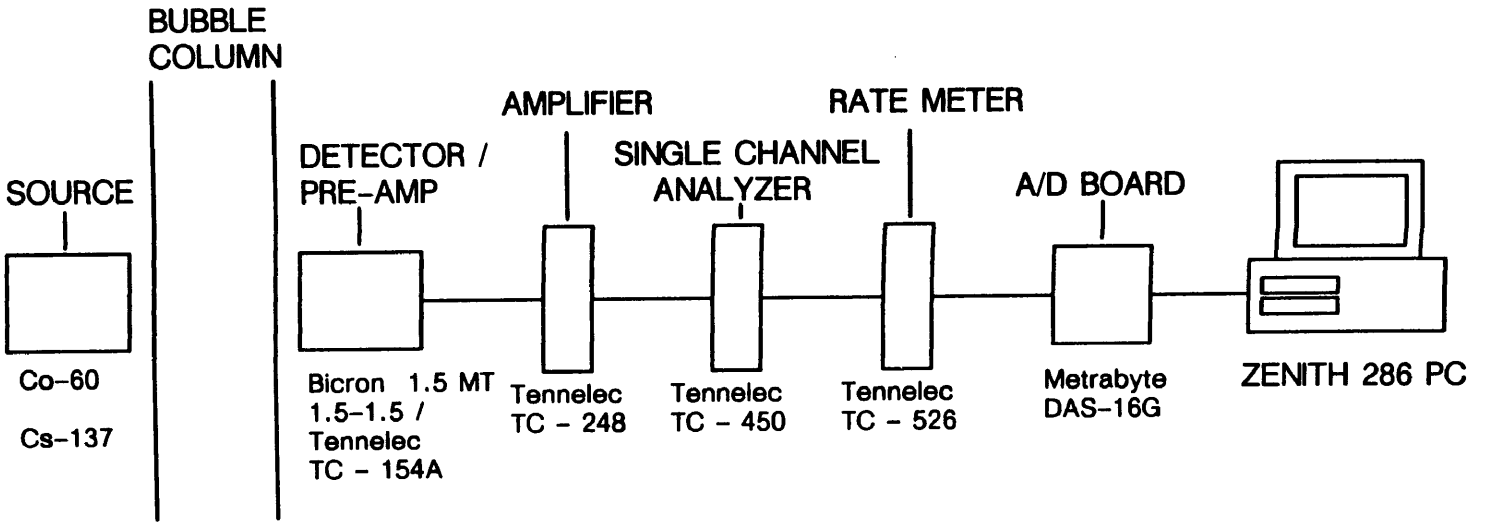

Figure 3.11. Schematic diagram of the nuclear density gauge electronic and data acquisition system.

counted. The output pulses from the SCA are then fed into the ratemeter and a voltage corresponding to the count rate is sent to the computer for data acquisition.

The single channel analyzers were operated in the normal mode of operation. Since we did not have access to a multichannel analyzer, the windows (i.e. lower level thresholds and upper level thresholds) were set experimentally using the procedure outlined in the SCA manual provided by Tennelec. The settings of the SCA as well as the other instrumentation is given in Table 3.5.

Calibration Procedures

Once the electronics were adjusted, calibration procedures were initiated to obtain attenuation coefficients for SASOL wax, FT–300 wax, iron oxide, and silica. A 0.1524 m wide x .1524 m deep x 0.61 m tall stainless steel chamber was constructed for conducting calibrations (see Figure 3.12). Attenuation coefficients were determined for wax at 265 ° C. In order to obtain the attenuation coefficient for pure wax (i.e. no solids), two measurements were made: (1) empty chamber, B_o and (2) full chamber, B. Knowing B, Bo and the thickness of the absorbing medium, d (i.e. 0.1524 m) the attenuation coefficient for the liquid phase was calculated using:

$$\mu_\ell = \frac{\ln(B / B_o)}{-d} \tag{3.32}$$

The attenuation coefficients for the solids (i.e. iron oxide and silica) could not be measured using the same procedure (i.e. filling the calibration chamber with pure solids) since voids exist between the individual solid particles. Due to the presence of the voids, the exact width of the absorbing medium is not known. To overcome this problem, a slurry composed of wax and solids was used to acquire the attenuation coefficients of the solids. First, an empty chamber count rate, B_o was obtained. Then, a known amount of wax was added to the calibration chamber and heated to 265 °C. Once at temperature, solids were added to form a 10 wt % slurry. A stirrer was used to

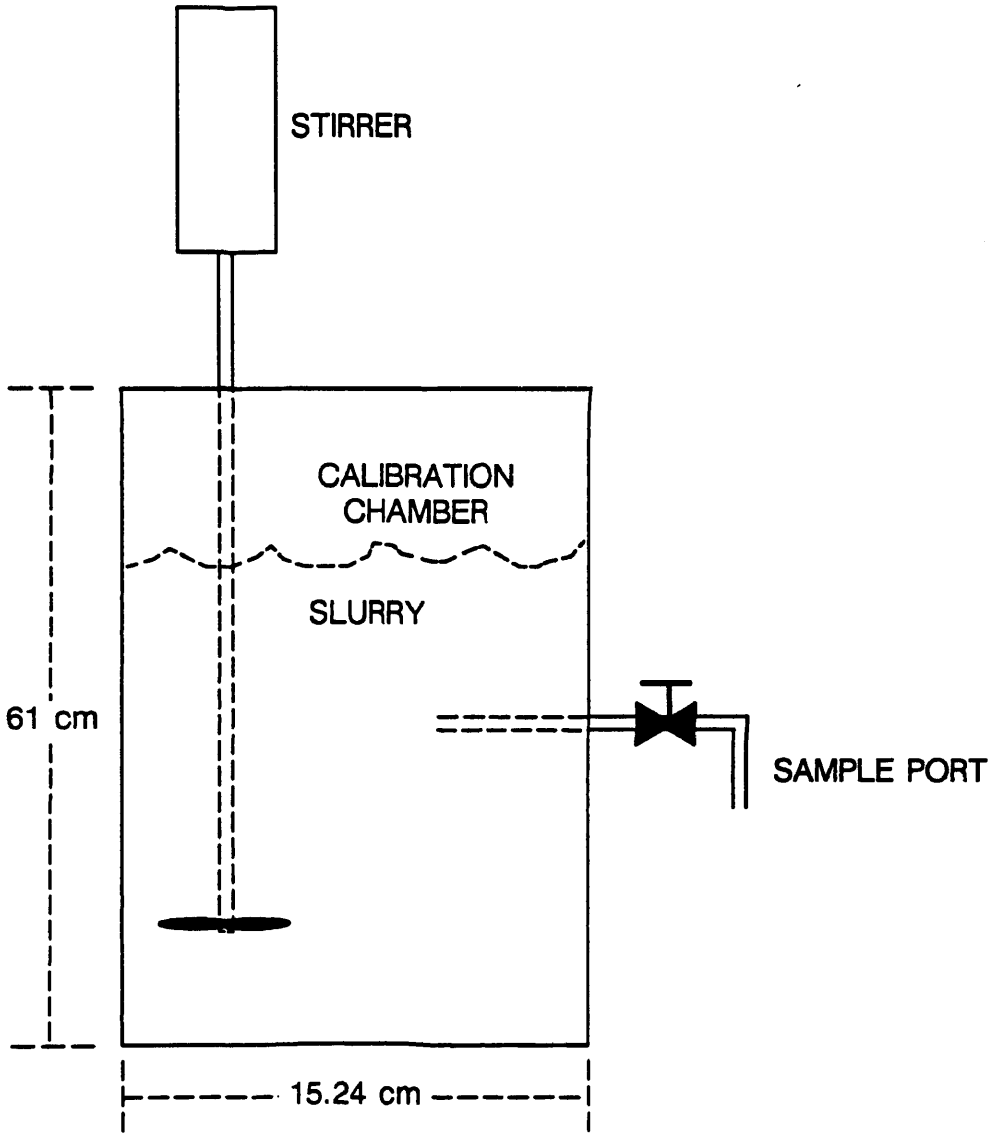

Figure 3.12. Schematic diagram of the calibration chamber.

suspend the solid particles. Once the system stabilized (approximately 30 minutes) a full chamber count rate, B was obtained, and a sample of the slurry was withdrawn at the same height at which the measurement was made and analyzed (using the procedure described in Chapter II) to determine the solids concentration in the slurry. The solids concentrations from the samples were within 3% (relative) of the solids concentrations calculated based on the amount of wax and solids added to the chamber. B, B_o, μ_ℓ, and the measured solids weight fraction were then used to calculate the attenuation coefficient for the solid phase (i.e. iron oxide or silica) using:

$$\mu_s = \frac{\frac{\ln(B/B_o)}{-d} - \frac{(1-\omega_s)\rho_{s\ell}\mu_\ell}{\rho_\ell}}{\frac{\omega_s \rho_{s\ell}}{\rho_s}} \tag{3.33}$$

This procedure was repeated with solids concentrations of 20 and 30 wt% for each solid type, and the average attenuation coefficient from the three measurements was used in subsequent calculations. Table 3.6 lists the measured attenuation coefficients for SASOL wax and FT–300 wax. Also shown in Table 3.6 is the measured attenuation coefficients for iron oxide and silica using 10, 20, and 30 wt% slurries, as well as the average values of the attenuation coefficient for each solid. There was very good agreement between attenuation coefficients obtained using different slurry concentrations.

Table 3.7 compares the measured attenuation coefficients to those calculated based on the data presented by Attix (1968) (see Table 3.1). Their is very good agreement between the measured and predicted attenuation coefficients.

Data Acquisition and Reduction Procedures

Nuclear density gauge measurements were made during the majority of experiments in the 0.21 m ID stainless steel column. As mentioned previously (see Chapter II), during experiments the system was allowed to remain at a given set of conditions (i.e. constant gas flow rate) for a period of one and a half hours. Measurements with the

Table 3.6. Measured Attenuation Coefficients (cm^{-1}) for FT–300 Wax, SASOL Wax, Iron Oxide, and Silica

ABSORBING MEDIUM	WT% SOLIDS	SOURCE	
		Co–60	Cs–137
FT–300 WAX	–	0.0421	0.0555
SASOL WAX	–	0.0415	0.0519
IRON OXIDE	10	0.2718	0.3910
	20	0.2690	0.3891
	30	0.2750	0.3920
SILICA	10	0.1411	0.2039
	20	0.1409	0.2072
	30	0.1380	0.2110
IRON OXIDE	AVERAGE	0.272	0.391
SILICA	AVERAGE	0.140	0.207

Table 3.7. Comparison of Measured and Theoretical Attenuation Coefficients (cm^{-1})

ABSORBING MEDIUM	Co–60		Cs–137	
	Measured	Theoretical	Measured	Theoretical
FT–300 WAX	0.0421	0.0423	0.0555	0.0580
IRON OXIDE	0.272	0.271	0.391	0.382
SILICA	0.140	0.148	0.207	0.205

nuclear density gauge were initiated after approximately one hour. The output voltage from the ratemeter is related to the count rate through a scaling factor, S_C. For all measurements, S_C was 500. The count rate at time i is calculated from the output voltage using the following expression

$$B_i = (\text{OutputVoltage})_i(S_C) \tag{3.34}$$

Count rates were determined from output voltage data recorded over a period of 2 to 3 minutes at a sampling frequency of 50 Hz using the data acquisition system described in Chapter II. The output voltages at each time, were converted to count rates via Eq. 3.34, and the average count rate, B, which was used in all calculations is

$$B = \frac{\sum_i^n B_i}{n} \tag{3.35}$$

where n is the total number of data points (e.g. if one samples at 50 Hz for 60 seconds, n would be 3000). The average count rate was used to determine the phase fractions in the system. Figure 3.13 is a schematic representation of the locations at which measurements were made. In some experiments, measurements were limited to heights of 0.91 and 1.52 m above the distributor. The distance through the column, which represents the thickness of the absorbing media, at each measurement location was measured experimentally by obtaining count rates for the empty column at each position and count rates with a full column of wax (i.e. no gas) at each position. These values, together with the attenuation coefficient for wax were used to calculate the distance through the column at each location using,

$$d_i = \frac{\ln(B_i \,/\, B_{o_i})}{-\mu_\ell} \tag{3.36}$$

where i represents the location of the density gauge (see Figure 3.13). Values of d_i were obtained at the beginning of each set (or batch) of experiments. These values

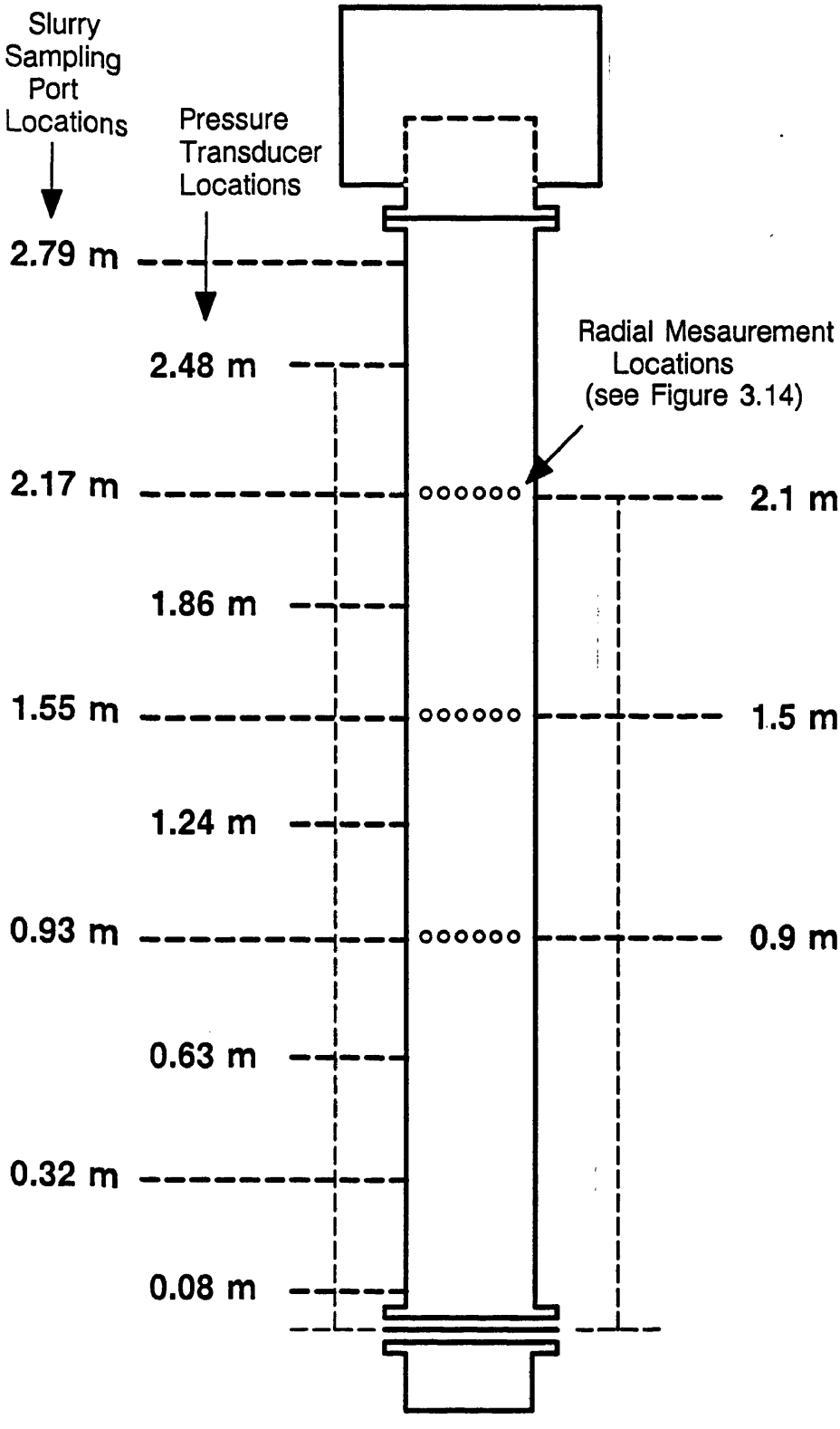

Figure 3.13. Schematic diagram of the nuclear density gauge measurement locations.

did not change by more than 1.5% throughout these studies, for either source. The distances through the column obtained prior to the experiments with FT–300 wax in the large column are given in Table 3.8. The distances are similar to the left and right of the center of the column for each source. The differences in the distance through the column for the two sources may be due to slightly different radial locations and/or axial locations.

Gas Holdups in Two – Phase Systems

Experiments were conducted using both two–phase (gas/liquid) and three–phase (gas/liquid/solid) systems. For two–phase experiments, gas holdups were obtained using each density gauge and the values compared. As described above, measurements were made at various radial and axial locations. The gas holdup at a given radial position, for both sources was calculated using:

$$\epsilon_{r_i} = 1 - \frac{\ln(B_i \,/\, B_{o_i})}{-d_i \mu_\ell} \tag{3.37}$$

Axial gas holdups were obtained from a volumetric weighted average of the radial gas holdups at a given axial location. Knowing the distance through the column at each radial position, d_i, and the column diameter, d_c, the radial position (measured from the center), r_{pos_i}, is

$$r_{pos_i} = \frac{\sqrt{d_c^2 - d_i^2}}{2} \tag{3.38}$$

Since the distances through the column did not vary significantly with axial position or column side (i.e. left or right of center), average values for r_{pos_i} and d_i were used to obtain the volumetric weights, w_i, needed to calculate the gas holdup at each axial location (see Eq. 3.40). The average values for r_{pos_i} and d_i that were used to calculate the weights are shown in Figure 3.14.

Table 3.8. Distance Through the Column for Both Sources at All Locations for the Experiments with FT–300 Wax

HEIGHT (m)	SOURCE	DISTANCE THROUGH THE COLUMN[a], d_i (m)					
		1	2	3	4	5	6
0.9	Co–60	16.10	18.62	20.23	20.11	18.42	16.30
	Cs–137	16.31	18.69	19.87	19.90	18.51	16.41
1.5	Co–60	15.81	18.77	20.07	20.06	18.76	16.49
	Cs–137	15.79	18.17	19.85	20.26	18.83	16.96
2.1	Co–60	16.33	18.97	20.31	20.45	18.87	16.63
	Cs–137	15.60	18.64	19.91	20.04	18.74	16.59

[a] Radial positions corresponding to numbers (1 to 6) are shown in Figures 3.13 and 3.14

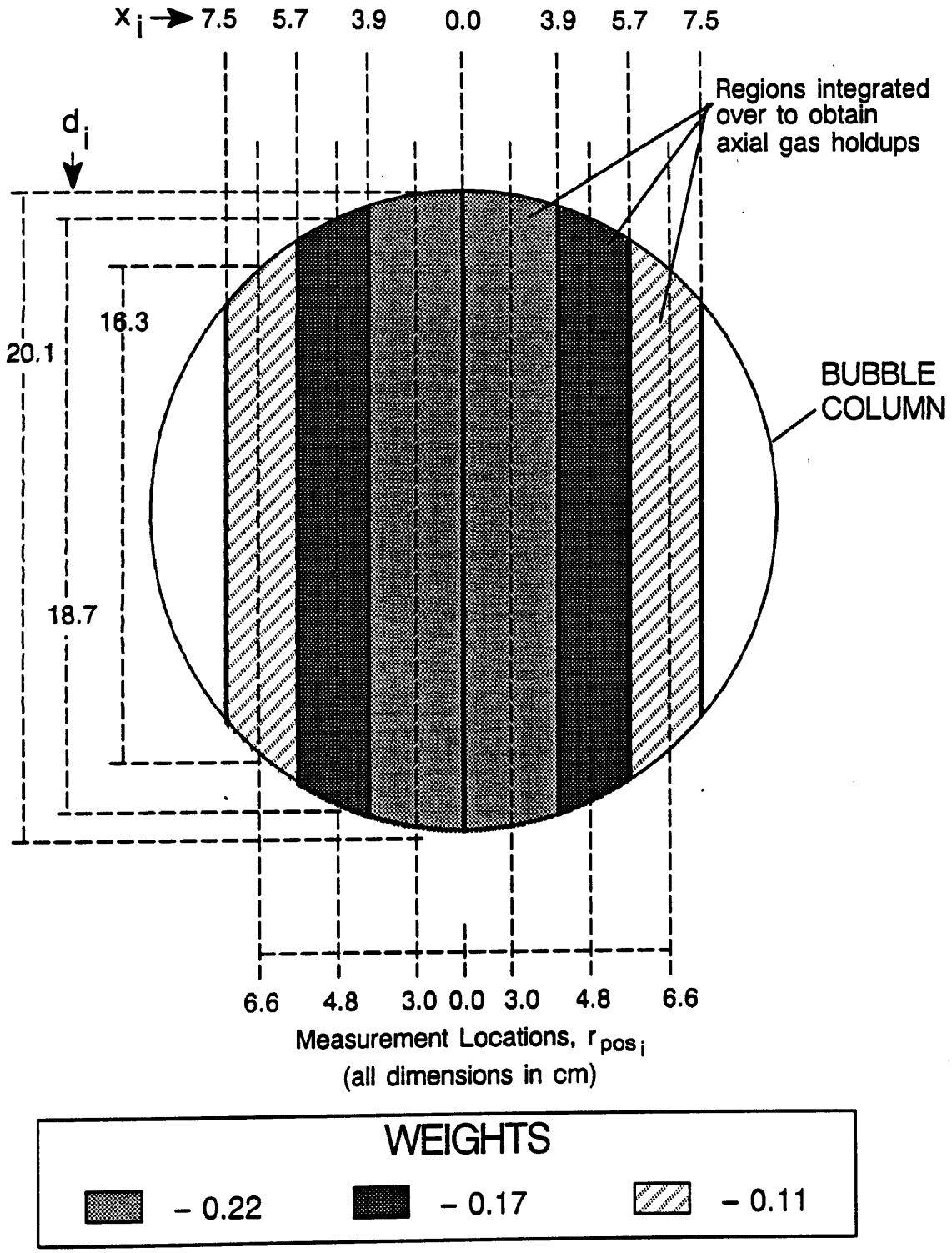

Figure 3.14. Schematic representation of the locations for radial measurements with the nuclear density gauge apparatus.

The column was divided into six sections (shaded regions in Figure 3.14) surrounding each measurement location. The cross–sectional area in a given shaded region, divided by the total area of the shaded regions was used as the weighting factor for measurements made in that region. The area of region i, A_{s_i} is given by:

$$A_{s_i} = [x_{i+1}\sqrt{r_c^2 - x_{i+1}^2} + r_c^2 \sin^{-1}(x_{i+1} / r_c)] - [x_i\sqrt{r_c^2 - x_i^2} + r_c^2 \sin^{-1}(x_i / r_c)] \quad (3.39)$$

where r_c is the radius of the column and x_i and x_{i+1} are the distances (measured from the center of the column) bounding the region to be evaluated. In particular, the values of x_i and x_{i+1} that were used are (0,3.9), (3.9,5.7), and (5.7,7.5). The area of each section was divided by the total area integrated over (i.e. sum of the area of each section) to obtain the appropriate weighting factor, w_i

$$w_i = \frac{A_{s_i}}{\sum_{i=1}^{6} A_{s_i}} \quad (3.40)$$

The weights obtained are given in Figure 3.14. The gas holdup at a given axial position was then calculated from:

$$\epsilon_{g_{ax}} = \sum_i \epsilon_{r_i} w_i \qquad i = 1 \text{ to } 6 \quad (3.41)$$

where $\epsilon_{g_{ax}}$ is the axial gas holdup and ϵ_{r_i} (see Eq. 3.37) is the radial gas holdup at location i.

Once axial gas holdups have been calculated, average gas holdups may be calculated. Recall that the average gas holdup is defined as

$$\epsilon_g = \frac{\text{volume of gas in the dispersion}}{\text{volume of the dispersion}} \quad (3.42)$$

Assuming the column can be divided into i sections, Eq. 3.42 may be rewritten as

$$\epsilon_g = \sum_i \frac{V_{g_i}}{V_{sect_i}} \frac{V_{sect_i}}{V_{exp}} = \sum_i \epsilon_{g_{ax_i}} \frac{h_i}{h_{exp}} \quad (3.43)$$

where V_{g_i} is the volume of gas in section i, V_{sect_i} is the total volume of section i, V_{exp} is the total volume of the dispersion, ϵ_{gax_i} is the gas holdup in section i, h_i is the length of section i, and h_{exp} is the expanded height of the slurry. Assuming h_i approaches 0, Eq. 3.43 may be rewritten in integral form as

$$\epsilon_g = \frac{1}{h_{exp}} \int_0^{h_{exp}} \epsilon_{gax} dh \tag{3.44}$$

Since measurements were made at three axial locations only, one may estimate the average gas holdup using various techniques. Three different approaches were examined in this study. First, the axial gas holdup data may be fitted to a curve. The equation for the curve may then be substituted into Eq. 3.44 for ϵ_{gax_i} to obtain an estimate for the average gas holdup. The second approach, uses the discretized form of Eq. 3.44 (i.e. Eq. 3.43) to obtain an estimate for the average gas holdup. Since measurements are made at three locations, the column may be divided into three sections. The sections used were (1) 0 to 1.2 m above the distributor, (2) 1.2 to 1.8 m above the distributor, and (3) 1.8 m above the distributor to the top of the dispersion (maximum of 3 m for continuous slurry flow). Thus, the values of h_i are 1.2 m, 0.6 m, and <1.2 m (see Figure 3.15). The third, and simplest approach would be to weight each axial gas holdup evenly. Using this approach, the average gas holdup is

$$\epsilon_g = \sum_i \frac{\epsilon_{gax_i}}{n} \qquad i = 1 \text{ to } 3 \tag{3.45}$$

Since axial gas holdups did not vary significantly, there were no significant differences in the values of gas holdup estimated using the three different approaches. Table 3.9 compares average gas holdups obtained using the three techniques described above for data obtained at gas velocities of 0.02 and 0.09 m/s, during experiment number 4 in Table 2.5. This experiment was conducted in the continuous mode of operation. As shown in Table 3.9a there is very little difference in gas holdups obtained using

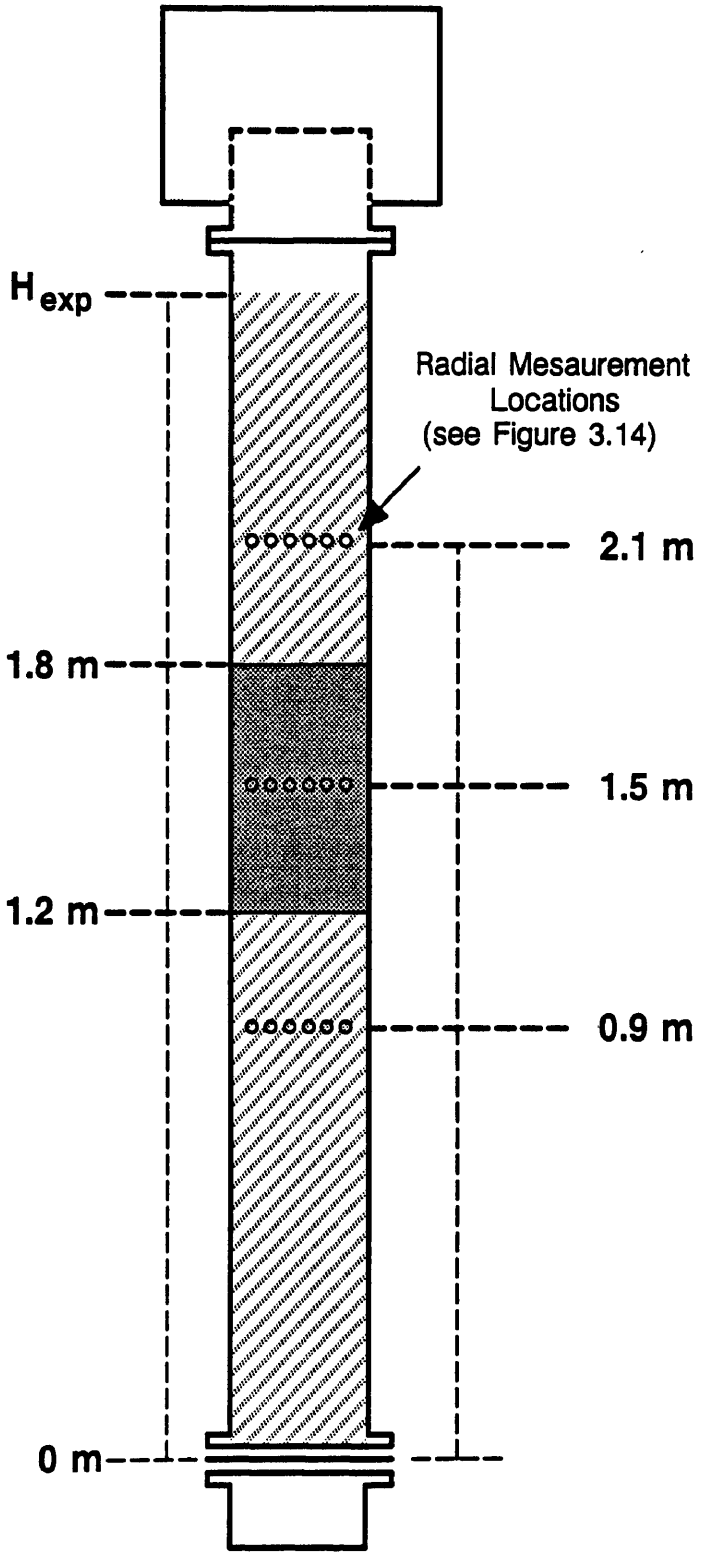

Figure 3.15. Schematic diagram of the regions used to obtain average gas holdups.

Table 3.9a. Effect of Technique Used to Obtain Average Gas Holdups from Axial Gas Holdups (Data from Experiment 4 in Table 2.5, $u_g = 0.02$ m/s)

EXP. HEIGHT (m)	HEIGHT (m)			ϵ_g^a	ϵ_g^b	ϵ_g^c
	0.9	1.5	2.1			
2.6[d]	0.0947	0.1083	0.1323	0.106	0.109	0.112
3.0[e]	0.0947	0.1083	0.1323	0.114	0.116	0.112

[a] Obtained from Eq. 3.44
[b] Obtained from Eq. 3.43
[c] Obtained from Eq. 3.45
[d] Representative of a batch mode experiment
[e] Representative of a continuous mode experiment, column height is 3.0 m

Table 3.9b. Effect of Technique Used to Obtain Average Gas Holdups from Axial Gas Holdups (Data from Experiment 4 in Table 2.5, $u_g = 0.09$ m/s)

EXP. HEIGHT (m)	HEIGHT (m)			ϵ_g^a	ϵ_g^b	ϵ_g^c
	0.9	1.5	2.1			
2.6[d]	0.2342	0.2446	0.2637	0.245	0.246	0.247
3.0[e]	0.2342	0.2446	0.2637	0.252	0.249	0.247

[a] Obtained from Eq. 3.44
[b] Obtained from Eq. 3.43
[c] Obtained from Eq. 3.45
[d] Representative of a batch mode experiment
[e] Representative of a continuous mode experiment, column height is 3.0 m

the various approaches. The data from this experiment were also analyzed assuming an expanded height of only 2.6 m (i.e. simulate a batch experiment). For this case (see Table 3.9b), the differences in the calculated gas holdups were slightly greater than those for the continuous case; however, they were still relatively small ($< 6\%$ difference). Thus, for simplicity, Eq. 3.45 was used to estimate the average gas holdup for all experiments.

Gas Holdups in Three – Phase Systems

Gas holdups for three–phase systems were calculated by treating all three phases independently, as well as, by treating the three–phase system as a two–phase system (i.e. grouping the liquid and solid phases together). When treating the three–phase system as a two–phase system, Eq. 3.37 is used to calculate radial gas holdups by replacing the liquid phase attenuation coefficient, μ_ℓ with the slurry phase attenuation coefficient, $\mu_{s\ell}$ (see Eq.3.30). If all three phases are treated separately, then Eqs. 3.16, 3.17, and 3.18 may be used to calculate radial gas holdups. Once radial gas holdups are obtained, axial and average gas holdups are calculated using Eqs. 3.41 and 3.45, respectively. Sample calculations for obtaining gas holdups using the two procedures described above (i.e. treating all three phases independently and grouping the liquid and solid phases together, i.e. pseudo two–phase) are presented in Appendix C.

Discussion of Results

Radial, axial and average gas holdups were measured with the nuclear density gauge during two–phase and three–phase experiments in the 0.21 m ID column. Data collected during all experiments were analyzed assuming Case I alignment. Furthermore, data from three–phase experiments were analyzed by two different methods: (1) treat all three phases independently and (2) group liquid and solids together to form a pseudo two–phase system.

Independent Treatment of all Three – Phases

Gas holdup values obtained from nuclear density gauge measurements, treating all three phases independently, were not good. However, this was not surprising, since sensitivity analysis revealed that very small errors in the count rate could produce substantial errors in volume fractions for the Co–60/Cs–137 system (see Table 3.3).

Data acquired from the density gauges during several experiments were analyzed to obtain radial gas holdups. Table 3.10a shows radial gas holdup values obtained from the batch experiment with 20 wt%, 20 – 44μm iron oxide particles in FT–300 wax. Radial gas holdups varied significantly for each gas velocity. In order to see what effect slight errors in the path length through the column, d, had on the gas holdups, it was varied. These results are shown in Table 3.10b for the experiment with FT–300 wax. We assumed that the volume fraction of solids did not vary with radial position and adjusted the value of d, until the volume fraction of solids, ϵ_s, was similar to that obtained from analysis of the slurry sample withdrawn at the same height of the density gauge measurement (see Figure 3.13). Once similar values of ϵ_s were obtained, axial gas holdups were calculated from the radial gas holdups using Eq. 3.41, and these values were compared to those values obtained at the same location (for this case, the axial gas holdups were compared to the measured gas holdups between pressure transducers 3 and 4; see Figure 3.13) using conventional techniques (see Chapter II). As shown in Table 3.10b, there was excellent agreement between axial gas holdups obtained using the different techniques. Also shown in Tables 3.10a and 3.10b is the distance through the column, d, for the high and low energy source, before and after altering its value, respectively. A range of values is presented in Table 3.10b, since different values of d were used at each gas velocity. For all experiments, the maximum percent difference between the measured value of d for each source and the altered value of d for each source at each radial location was less than 4%, and usually less than 2%. Thus

Table 3.10a. Gas holdups from Measurements with the Nuclear Density Gauge at a Height of 1.5 m Above the Distributor (FT-300 Wax, 20 wt% 20 – 44 μm Iron Oxide)

u_g	Radial Position[a]					
(m/s)	6.6	4.8	3.0	3.0	4.8	6.6
0.02	0.06	0.24	0.04	0.21	0.37	0.24
0.04	-0.09	0.27	0.03	0.23	0.07	0.16
0.08	-0.03	0.19	0.12	0.31	0.45	0.14
0.12	0.13	0.18	0.12	0.35	0.48	0.13
d_L^b	16.96	18.17	20.26	19.85	18.83	15.79
d_H^c	16.49	18.76	20.06	20.07	18.77	15.81

[a] – Measured from the center of the column (cm)
[b] – Distance through the column for the Cs–137 source (cm)
[c] – Distance through the column for the Co–60 source (cm)

Table 3.10b. Gas and Solids Holdups from Measurements with the Nuclear Density Gauge at a Height of 1.5 m Above the Distributor After Modifying the Thickness (d) of the Absorbing Media (FT-300 Wax, 20 wt% 20 – 44 μm Iron Oxide)

u_g	RADIAL POSITION[a]						ϵ_g^b	ϵ_g^c	ϵ_s^b	ϵ_s^c
(m/s)	6.6	4.8	3.0	3.0	4.8	6.6				
0.02	0.117	0.124	0.128	0.129	0.124	0.105	0.122	0.128	0.015	0.016
0.04	0.159	0.164	0.194	0.183	0.166	0.150	0.172	0.189	0.024	0.024
0.08	0.161	0.210	0.213	0.221	0.198	0.194	0.202	0.172	0.026	0.024
0.12	0.189	0.197	0.223	0.222	0.215	0.185	0.210	0.216	0.021	0.025
d_L^d	16.86-16.98	18.15-18.19	20.10-20.28	19.75-19.95	18.79-18.87	15.69-15.79				
d_H^e	16.6-16.8	18.9	20.25	19.9	18.8	15.6-15.9				

[a] – Measured from the center of the column (cm)
[b] – Axial holdups from nuclear density gauge measurements
[c] – Axial holdups from conventional measurements (Chapter II)
[d] – Range of values for the distance through the column for the Cs–137 source (cm)
[e] – Range of values for the distance through the column for the Co–60 source (cm)

indicating once again, that slight errors in the measured quantities (i.e. count rate, distance through the column, etc.) have a significant effect on the calculated holdups, when two "high" energy sources are employed. Data obtained from other experiments were also analyzed treating all three–phases independently. The results from these experiments are shown in Tables 3.11 to 3.14. Tables 3.11a and 3.11b show results obtained from the batch mode experiment with 20 wt% large silica particles in SASOL wax at a height of 1.5 m above the distributor. Results from this experiment were similar to those obtained during the experiment with large iron oxide particles suspended in FT–300 wax (Table 3.10). Namely, there was a significant variation in radial gas holdup profiles when the measured distances were used; however, upon slightly adjusting the distance through the column, more uniform radial holdup values were obtained. Axial holdups calculated from the modified radial profiles were comparable to those using conventional techniques (see Chapter II) were obtained. Similar results were also obtained at different heights and with small iron oxide particles. Radial gas holdup profiles for the experiment conducted with 20 – 44 μm iron oxide particles in FT–300 wax at a height of 2.1 m above the distributor are shown in Table 3.12. Results from the experiment with large silica particles in SASOL wax, at a height of 0.9 m above the distributor are shown in Table 3.13, and results from the experiment with small iron oxide particles at a slurry velocity of 0.005 m/s at a height of 1.5 m above the distributor are shown in Table 3.14.

Two – Phase and Pseudo Two – Phase Results

Figures 3.16 to 3.19 show radial gas holdup profiles at a height of 1.5 m above the distributor obtained from different experiments in two–phase (Figure 3.16) and three–phase systems (Figures 3.17, 3.18, and 3.19). The results shown for the three–phase system were obtained by treating it as a pseudo two–phase system (i.e. the liquid and solid phases were grouped together). Radial gas holdups for three–phase experiments

Table 3.11a. Gas Holdups from Measurements with the Nuclear Density at a Height of 1.5 m Above the Distributor (SASOL Wax, 20 wt% 20 – 44 μm Silica)

u_g	Radial Position[a]			
(m/s)	6.6	3.0	3.0	6.6
0.02	0.34	0.12	0.15	0.21
0.04	0.23	0.17	0.16	0.24
0.08	0.32	0.30	0.26	0.42
0.12	0.30	0.33	0.34	0.46
d_L^b	16.65	20.44	20.49	15.99
d_H^c	16.55	20.31	20.41	15.9

[a] – Measured from the center of the column (cm)
[b] – Distance through the column for the Cs–137 source (cm)
[c] – Distance through the column for the Co–60 source (cm)

Table 3.11b. Gas and Solids Holdups from Measurements with the Nuclear Density Gauge at a Height of 1.5 m Above the Distributor After Modifying the Thickness (d) of the Absorbing Media (SASOL Wax, 20 wt% 20 – 44 μm Silica)

u_g	RADIAL POSITION[a]				ϵ_g^b	ϵ_g^c	ϵ_s^b	ϵ_s^c
(m/s)	6.6	3.0	3.0	6.6				
0.02	0.104	0.116	0.120	0.115	0.117	0.115	0.067	0.066
0.04	0.146	0.168	0.162	0.143	0.157	0.150	0.066	0.066
0.08	0.206	0.224	0.230	0.207	0.218	0.191	0.070	0.065
0.12	0.205	0.262	0.266	0.225	0.244	0.253	0.067	0.066
d_L^d	16.5-16.95	20.45-20.49	20.49-20.59	16.3-16.4				
d_H^e	16.2	20.3	20.4	15.9				

[a] – Measured from the center of the column (cm)
[b] – Axial holdups from nuclear density gauge measurements
[c] – Axial holdups from conventional measurements (Chapter II)
[d] – Range of values for the distance through the column for the Cs–137 source (cm)
[e] – Range of values for the distance through the column for the Co–60 source (cm)

Table 3.12a. Gas Holdups from Measurements with the Nuclear Density Gauge at a Height of 2.1 m Above the Distributor (FT-300 Wax, 20 wt% 20 – 44 μm Iron Oxide)

u_g	Radial Position[a]					
(m/s)	6.6	4.8	3.0	3.0	4.8	6.6
0.02	0.03	0.02	0.07	0.13	0.08	-0.04
0.04	0.30	0.39	0.34	0.61	0.41	0.38
0.08	0.04	0.06	0.08	0.47	0.11	-0.01
0.12	0.02	-0.02	0.06	0.27	0.18	0.12
d_L^b	16.60	18.64	19.91	20.04	18.91	16.59
d_H^c	16.33	18.97	20.31	20.45	18.87	16.63

[a] – Measured from the center of the column (cm)
[b] – Distance through the column for the Cs–137 source (cm)
[c] – Distance through the column for the Co–60 source (cm)

Table 3.12b. Gas and Solids Holdups from Measurements with the Nuclear Density Gauge at a Height of 2.1 m Above the Distributor After Modifying the Thickness (d) of the Absorbing Media (FT-300 Wax, 20 wt% 20 – 44 μm Iron Oxide)

u_g	RADIAL POSITION[a]						ϵ_g^b	ϵ_g^c	ϵ_s^b	ϵ_s^c
(m/s)	6.6	4.8	3.0	3.0	4.8	6.6				
0.02	0.131	0.152	0.171	0.169	0.149	0.140	0.151	0.137	0.014	0.014
0.04	0.220	0.279	0.282	0.301	0.280	0.259	0.271	0.274	0.023	0.021
0.08	0.161	0.230	0.233	0.260	0.211	0.187	0.221	0.232	0.023	0.023
0.12	0.170	0.247	0.261	0.272	0.251	0.219	0.224	0.240	0.023	0.024
d_L^d	16.4-16.5	18.1-18.4	19.5-20.0	20.0-20.5	18.6-19.0	16.1-16.4				
d_H^e	16.33	18.97	20.31	20.45	18.87	16.63				

[a] – Measured from the center of the column (cm)
[b] – Axial holdups from nuclear density gauge measurements
[c] – Axial holdups from conventional measurements (Chapter II)
[d] – Range of values for the distance through the column for the Cs–137 source (cm)
[e] – Range of values for the distance through the column for the Co–60 source (cm)

Table 3.13a. Gas Holdups from Measurements with the Nuclear Density Gauge at a Height of 0.9 m Above the Distributor (SASOL Wax, 20 wt% 20 – 44 μm Silica)

u_g	Radial Position[a]			
(m/s)	6.6	3.0	3.0	6.6
0.02	0.11	0.10	0.18	0.01
0.04	0.19	0.11	0.14	0.11
0.08	0.36	0.29	0.25	0.29
0.12	0.22	0.25	0.21	0.32
d_L^b	16.32	19.84	19.92	16.39
d_H^c	16.41	20.19	20.09	16.52

[a] – Measured from the center of the column (cm)
[b] – Distance through the column for the Cs–137 source (cm)
[c] – Distance through the column for the Co–60 source (cm)

Table 3.13b. Gas and Solids Holdups from Measurements with the Nuclear Density Gauge at a Height of 0.9 m Above the Distributor After Modifying the Thickness (d) of the Absorbing Media (SASOL Wax, 20 wt% 20 – 44 μm Silica)

u_g	RADIAL POSITION[a]				ϵ_g^b	ϵ_g^c	ϵ_s^b	ϵ_s^c
(m/s)	6.6	3.0	3.0	6.6				
0.02	0.08	0.11	0.12	0.08	0.10	0.10	0.08	0.07
0.04	0.10	0.13	0.13	0.09	0.12	0.14	0.07	0.07
0.08	0.17	0.20	0.20	0.16	0.18	0.14	0.07	0.07
0.12	0.18	0.22	0.21	0.18	0.20	0.20	0.07	0.06
d_L^d	16.4-16.9	19.8-20.2	19.95-20.1	16.2-16.6				
d_H^e	16.4	20.2	20.1	16.5				

[a] – Measured from the center of the column (cm)
[b] – Axial holdups from nuclear density gauge measurements
[c] – Axial holdups from conventional measurements (Chapter II)
[d] – Range of values for the distance through the column for the Cs–137 source (cm)
[e] – Range of values for the distance through the column for the Co–60 source (cm)

Table 3.14a. Gas Holdups from Measurements with the Nuclear Density Gauge at a Height of 1.5 m Above the Distributor (SASOL Wax, 20 wt% 0 – 5 μm Iron Oxide)

u_g	Radial Position[a]					
(m/s)	6.6	4.8	3.0	3.0	4.8	6.6
0.02	-0.016	0.055	0.005	0.037	0.035	0.047
0.04	0.337	0.382	0.289	0.314	0.172	0.071
0.06	0.238	0.300	0.297	0.226	0.210	0.081
0.09	0.203		0.313	0.189		-0.001
0.12	0.351	0.389	0.277	0.282	0.091	0.025
d_L^b	16.57	19.20	20.70	20.59	18.99	16.76
d_H^c	16.48	19.17	20.42	20.47	18.97	16.86

[a] – Measured from the center of the column (cm)
[b] – Distance through the column for the Cs–137 source (cm)
[c] – Distance through the column for the Co–60 source (cm)

Table 3.14b. Gas and Solids Holdups from Measurements with the Nuclear Density Gauge at a Height of 1.5 m Above the Distributor After Modifying the Thickness (d) of the Absorbing Media (SASOL Wax, 20 wt% 0 – 5 μm Iron Oxide)

u_g	RADIAL POSITION[a]						ϵ_g^b	ϵ_g^c	ϵ_s^b	ϵ_s^c
(m/s)	6.6	4.8	3.0	3.0	4.8	6.6				
0.02	0.105	0.134	0.125	0.123	0.129	0.108	0.121	0.107	0.029	0.029
0.04	0.152	0.175	0.180	0.189	0.165	0.147	0.169	0.157	0.029	0.028
0.06	0.140	0.170	0.188	0.193	0.169	0.145	0.171	0.175	0.027	0.027
0.09	0.159		0.226	0.223		0.164	0.200	0.211	0.026	0.026
0.12	0.186	0.219	0.238	0.245	0.216	0.188	0.219	0.208	0.025	0.025
d_L^d	15.9-16.2	18.6-19.0	20.0-20.3	20.3-20.7	18.5-19.0	16.5-16.8				
d_H^e	16.48	19.17	20.42	20.47	18.97	16.86				

[a] – Measured from the center of the column (cm)
[b] – Axial holdups from nuclear density gauge measurements
[c] – Axial holdups from conventional measurements (Chapter II)
[d] – Range of values for the distance through the column for the Cs–137 source (cm)
[e] – Range of values for the distance through the column for the Co–60 source (cm)

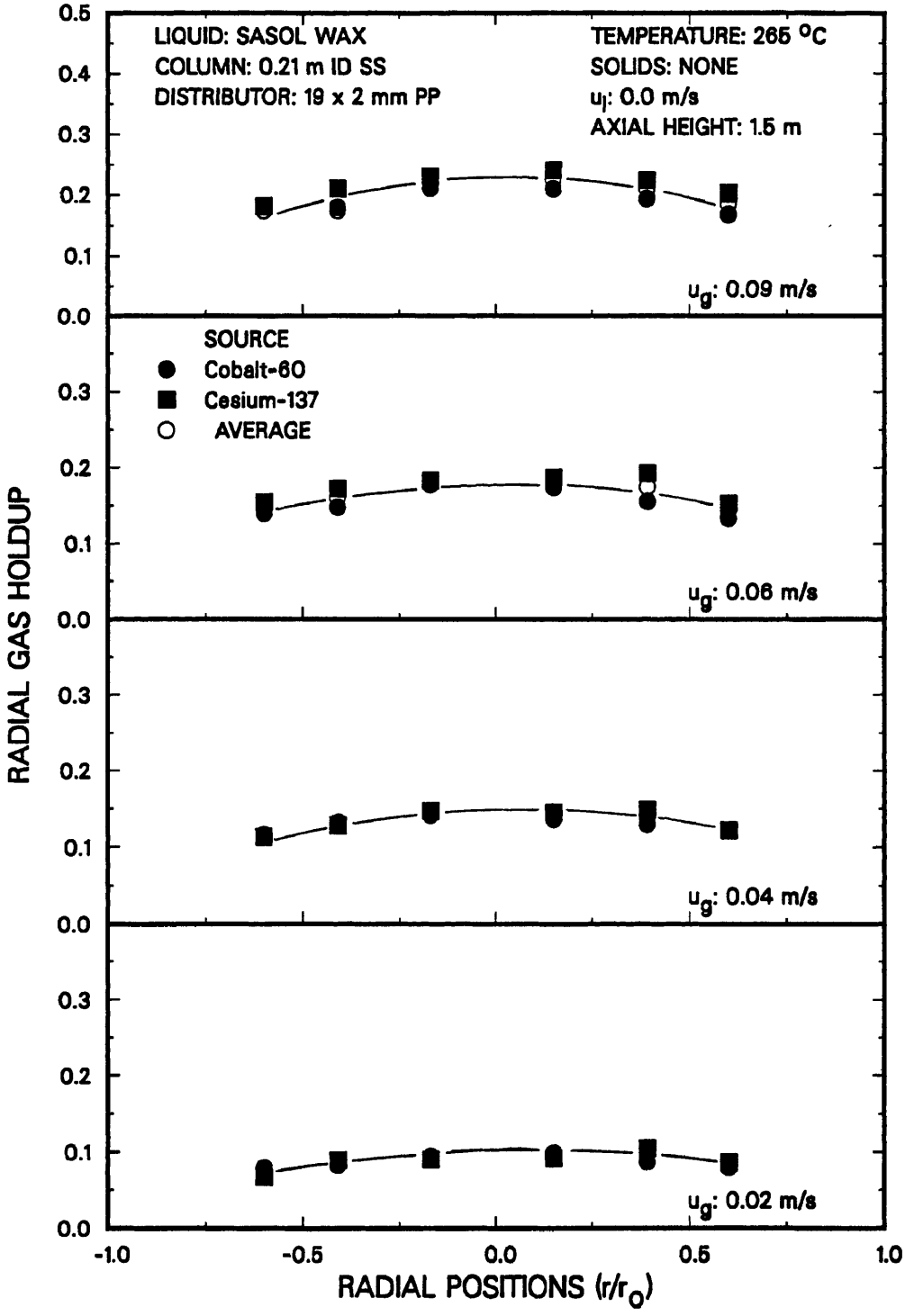

Figure 3.16. Effect of superficial gas velocity on radial gas holdup (SASOL wax, no solids, u_l = 0.0 m/s).

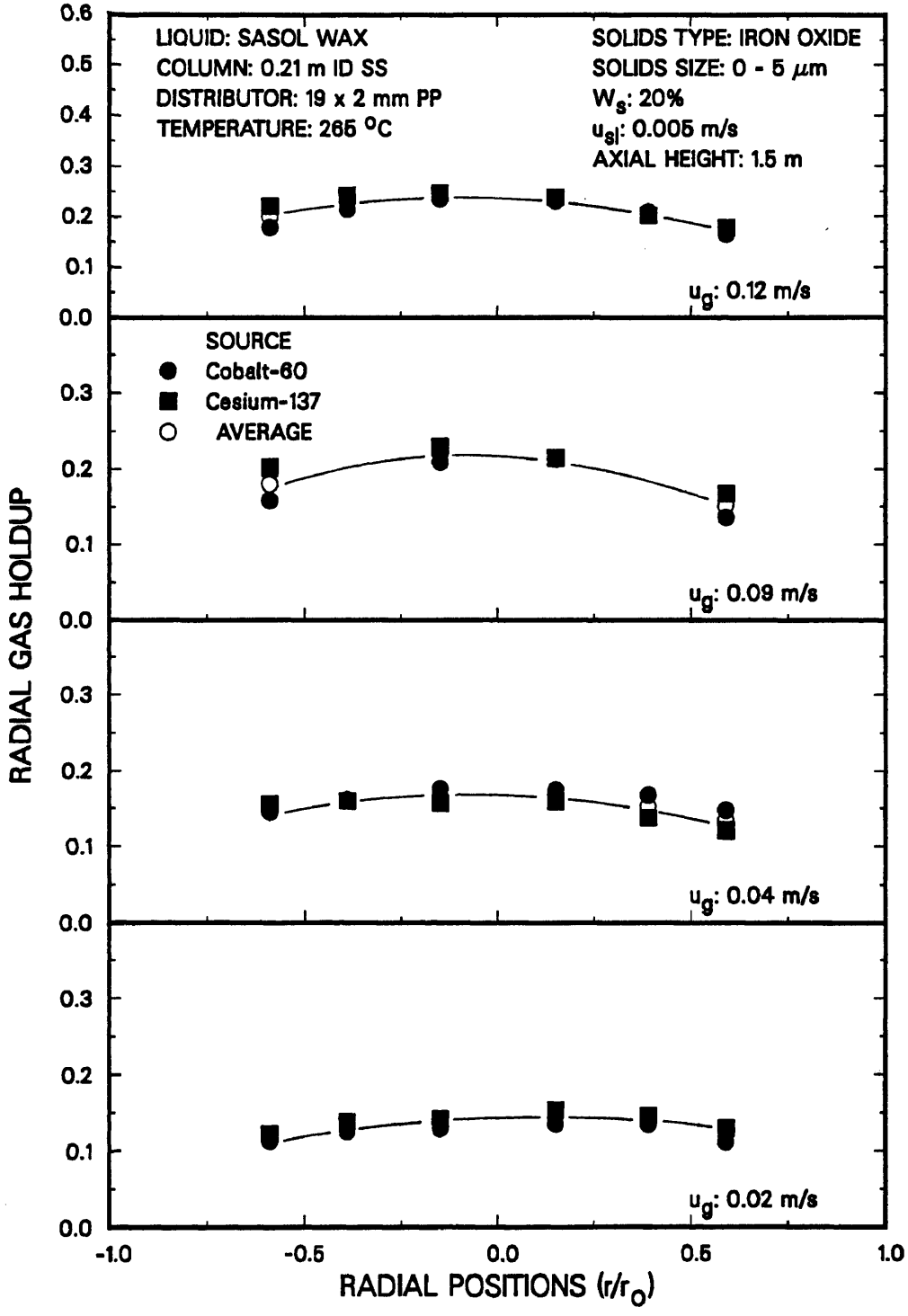

Figure 3.17. Effect of superficial gas velocity on radial gas holdup (SASOL wax, 20 wt% 0 - 5 μm iron oxide, u_{sl} = 0.005 m/s).

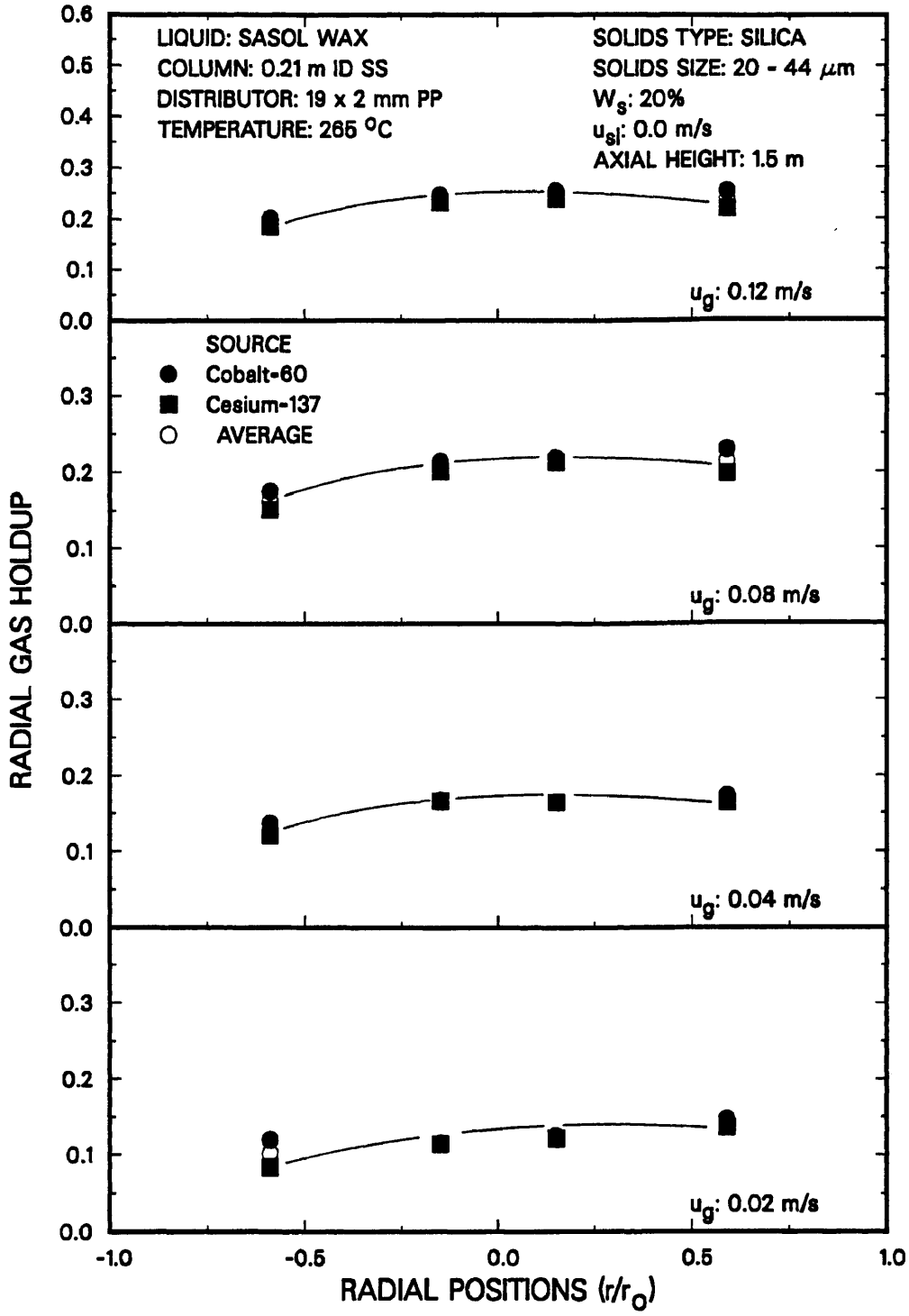

Figure 3.18. Effect of superficial gas velocity on radial gas holdup (SASOL wax, 20 wt% 20 - 44 μm silica, u_{sl} = 0.0 m/s).

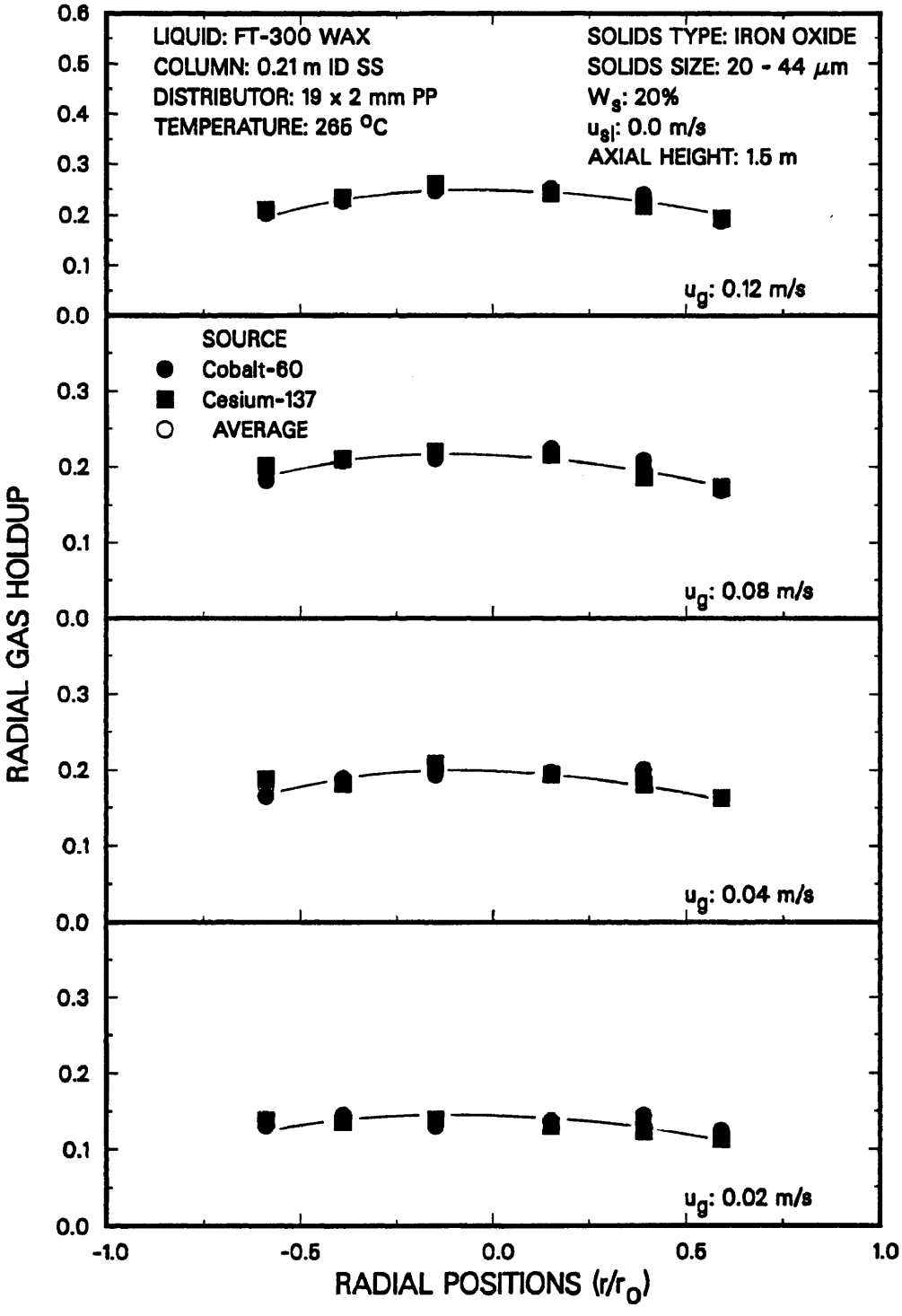

Figure 3.19. Effect of superficial gas velocity on radial gas holdup (FT-300 wax, 20 wt% 20 - 44 μm iron oxide, u_{sl} = 0.0 m/s).

were obtained using Eq. 3.37, and replacing the attenuation coefficient of the liquid, μ_ℓ, by the attenuation coefficient of the liquid/solid mixture – see Eq. 3.6). Since a pseudo two–phase system was assumed (three–phase systems), independent results could be obtained from each density gauge. For each case, independent results from the two density gauges are presented along with with average values of the radial gas holdup. The average values are simply an arithmetic average of the holdup values obtained from the two sources. In general, radial gas holdup profiles were fairly uniform at a gas velocity of 0.02 m/s, which was expected since flow is in the homogeneous bubbling regime at this velocity. However, as the gas velocity increases, the flow becomes slightly non–uniform with higher holdups in the center of the column. At higher gas velocities, larger gas bubbles are produced which tend to move upward through the center of the column and this in turn results in higher gas holdups in the center of the column. The trends observed at the other two heights (0.9 and 2.1 m) were similar to those shown at a height of 1.5 m above the distributor.

The radial holdups shown in Figures 3.16 to 3.19 are also presented in tabular form (see Tables 3.15 to 3.18, respectively). Also shown in these tables are the values of the attenuation coefficients and the initial (or empty column) count rates that were used. Empty column count rates at a given radial position did not vary by more than 2% between experiments. The empty column count rate decreases with increasing distance from the center of the column. This decrease in the count rate with increasing distance from the center of the column is because the thickness of the column changes due to its curvature (see Figure 3.20).

For all of the results shown in Figures 3.17 to 3.19 (three–phase systems), the attenuation coefficient was assumed to be constant at all gas velocities, since the solids concentration did not vary significantly with gas velocity in the large column (see Chapter IV), with the exception of the experiments conducted with large iron oxide particles.

Table 3.15a. Radial Gas Holdups Obtained Using the Co–60 Source
(SASOL Wax, No Solids, $u_\ell = 0$ m/s)

u_g	$\mu_{s\ell}$	Radial Position[a]					
(m/s)	(cm^{-1})	6.6	4.8	3.0	3.0	4.8	6.6
0.02	0.0415	0.102	0.113	0.145	0.115	0.111	0.101
0.04	0.0415	0.132	0.143	0.154	0.146	0.135	0.136
0.06	0.0415	0.151	0.178	0.178	0.183	0.180	0.156
0.09	0.0415	0.171	0.209	0.219	0.223	0.212	0.181
B_o^b		3582	3805	3926	3957	3852	3742
d^c		16.10	17.70	19.18	19.43	18.16	16.40

[a] – Measured from the center of the column (cm)
[b] – Empty column count rate (counts/sec)
[c] – Distance through the column (cm)

Table 3.15b. Radial Gas Holdups Obtained Using the Cs–137 Source
(SASOL Wax, No Solids, $u_\ell = 0$ m/s)

u_g	$\mu_{s\ell}$	Radial Position[a]					
(m/s)	(cm^{-1})	6.6	4.8	3.0	3.0	4.8	6.6
0.02	0.0519	0.106	0.109	0.117	0.118	0.095	0.099
0.04	0.0519	0.141	0.155	0.167	0.158	0.137	0.136
0.06	0.0519	0.171	0.190	0.199	0.204	0.170	0.175
0.09	0.0519	0.205	0.229	0.245	0.246	0.212	0.202
B_o^b		1958	2082	2149	2164	2120	2011
d^c		16.20	18.78	20.60	20.70	19.23	17.38

[a] – Measured from the center of the column (cm)
[b] – Empty column count rate (counts/sec)
[c] – Distance through the column (cm)

Table 3.16a. Radial Gas Holdups Obtained Using the Co–60 Source
(SASOL Wax, 20 wt% 0 – 5 μm Iron Oxide, $u_{s\ell}$ = 0.005 m/s)

u_g	$\mu_{s\ell}$	Radial Position[a]					
(m/s)	(cm^{-1})	6.6	4.8	3.0	3.0	4.8	6.6
0.02	0.0494	0.111	0.134	0.135	0.128	0.126	0.113
0.04	0.0494	0.147	0.149	0.174	0.176	0.161	0.145
0.06	0.0494	0.149	0.177	0.192	0.191	0.173	0.157
0.09	0.0494	0.171		0.214	0.209		0.177
0.12	0.0494	0.199	0.209	0.231	0.235	0.215	0.197
B_o^b		3618	3828	3903	3901	3815	3677
d^c		16.48	19.17	20.42	20.47	18.97	16.86

[a] – Measured from the center of the column (cm)
[b] – Empty column count rate (counts/sec)
[c] – Distance through the column (cm)

Table 3.16b. Radial Gas Holdups Obtained Using the Cs–137 Source
(SASOL Wax, 20 wt% 0 – 5 μm Iron Oxide, $u_{s\ell}$ = 0.005 m/s)

u_g	$\mu_{s\ell}$	Radial Position[a]					
(m/s)	(cm^{-1})	6.6	4.8	3.0	3.0	4.8	6.6
0.02	0.0635	0.129	0.146	0.154	0.142	0.138	0.122
0.04	0.0635	0.121	0.137	0.181	0.157	0.160	0.145
0.06	0.0635	0.157	0.159	0.176	0.187	0.168	0.158
0.09	0.0635	0.167		0.215	0.230		0.192
0.12	0.0635	0.210	0.203	0.239	0.246	0.242	0.211
B_o^b		2007	2116	2174	2185	2108	1997
d^c		16.57	19.20	20.70	20.59	18.99	16.76

[a] – Measured from the center of the column (cm)
[b] – Empty column count rate (counts/sec)
[c] – Distance through the column (cm)

Table 3.17a. Radial Gas Holdups Obtained Using the Co–60 Source
(SASOL Wax, 20 wt% 20 – 44 μm Silica, $u_{s\ell} = 0$ m/s)

u_g	$\mu_{s\ell}$	Radial Position[a]			
(m/s)	(cm^{-1})	6.6	3.0	3.0	6.6
0.02	0.0478	0.131	0.125	0.115	0.111
0.04	0.0478	0.157	0.164	0.167	0.128
0.08	0.0478	0.214	0.219	0.214	0.167
0.12	0.0478	0.235	0.254	0.246	0.196
B_o^b		3619	3953	3970	3675
d^c		16.55	20.31	20.41	15.9

[a] – Measured from the center of the column (cm)
[b] – Empty column count rate (counts/sec)
[c] – Distance through the column (cm)

Table 3.17b. Radial Gas Holdups Obtained Using the Cs–137 Source
(SASOL Wax, 20 wt% 20 – 44 μm Silica, $u_{s\ell} = 0$ m/s)

u_g	$\mu_{s\ell}$	Radial Position[a]			
(m/s)	(cm^{-1})	6.6	3.0	3.0	6.6
0.02	0.0642	0.137	0.121	0.114	0.084
0.04	0.0642	0.163	0.164	0.166	0.121
0.06	0.0642	0.198	0.213	0.201	0.151
0.12	0.0642	0.219	0.239	0.232	0.186
B_o^b		2049	2226	2230	2050
d^c		16.65	20.44	20.49	16.0

[a] – Measured from the center of the column (cm)
[b] – Empty column count rate (counts/sec)
[c] – Distance through the column (cm)

Table 3.18a. Radial Gas Holdups Obtained Using the Co–60 Source
(FT–300 Wax, 20 wt% 20 – 44 μm Iron Oxide, $u_{s\ell} = 0$ m/s)

u_g	$\mu_{s\ell}$	Radial Position[a]					
(m/s)	(cm^{-1})	6.6	4.8	3.0	3.0	4.8	6.6
0.02	0.0466	0.123	0.144	0.137	0.131	0.144	0.131
0.04	0.0495	0.163	0.199	0.197	0.193	0.188	0.165
0.08	0.0495	0.170	0.208	0.223	0.211	0.208	0.183
0.12	0.0495	0.188	0.238	0.250	0.248	0.228	0.204
B_o^b		3603	3821	3941	3981	3837	3691
d^c		16.49	18.76	20.06	20.07	18.77	15.81

[a] – Measured from the center of the column (cm)
[b] – Empty column count rate (counts/sec)
[c] – Distance through the column (cm)

Table 3.18b. Radial Gas Holdups Obtained Using the Cs–137 Source
(FT–300 Wax, 20 wt% 20 – 44 μm Iron Oxide, $u_{s\ell} = 0$ m/s)

u_g	$\mu_{s\ell}$	Radial Position[a]					
(m/s)	(cm^{-1})	6.6	4.8	3.0	3.0	4.8	6.6
0.02	0.0619	0.112	0.122	0.130	0.139	0.136	0.138
0.04	0.0662	0.163	0.181	0.194	0.208	0.181	0.187
0.08	0.0662	0.173	0.189	0.216	0.219	0.210	0.200
0.12	0.0662	0.194	0.228	0.242	0.259	0.236	0.210
B_o^b		2065	2197	2252	2273	2216	2102
d^c		16.96	18.17	20.26	19.85	18.83	15.79

[a] – Measured from the center of the column (cm)
[b] – Empty column count rate (counts/sec)
[c] – Distance through the column (cm)

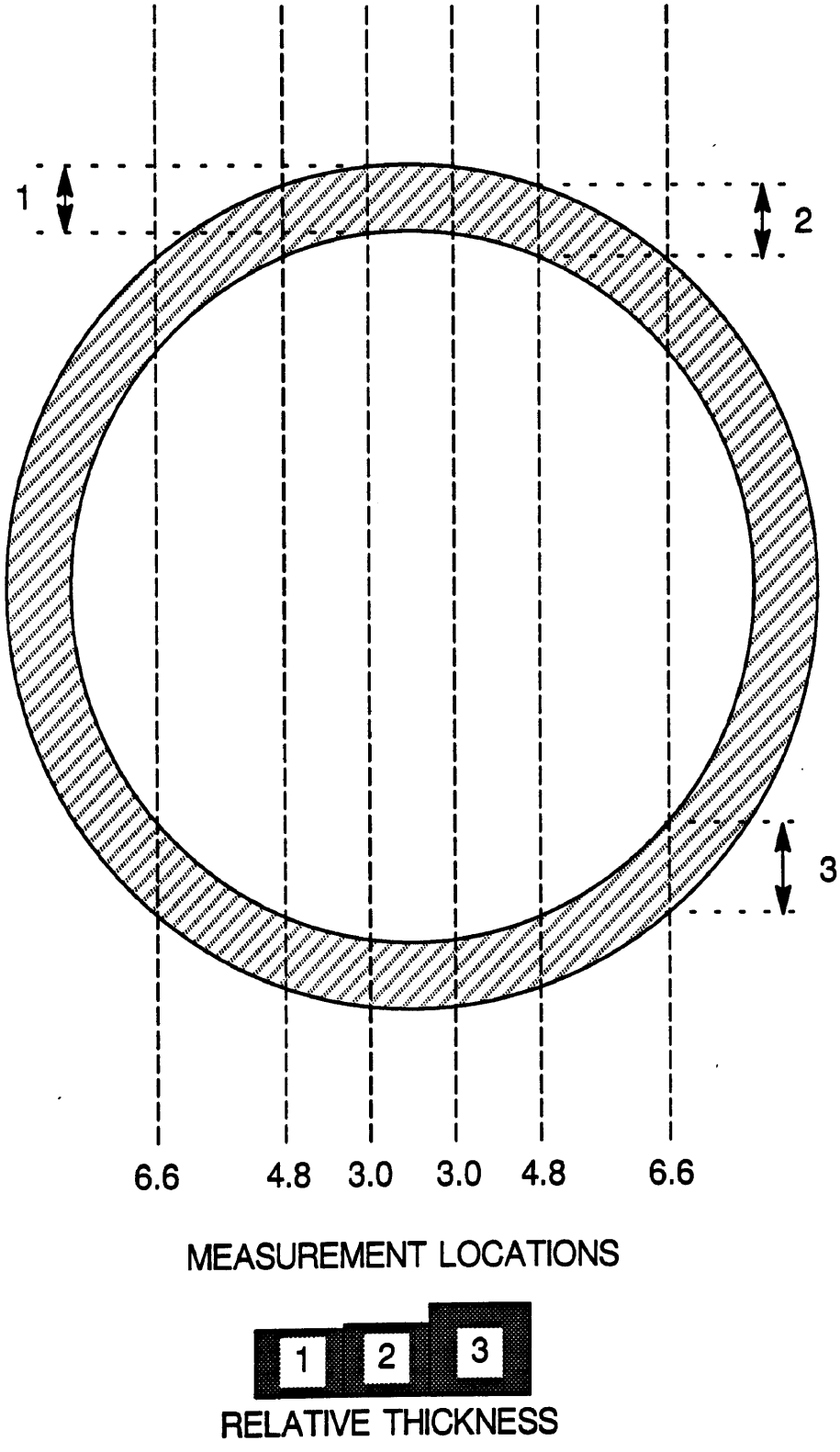

Figure 3.20. Schematic representation of bubble column wall.

During these experiments, the solids concentration in the column was lower at a gas velocity of 0.02 m/s than at higher gas velocities and thus, the attenuation coefficient of the slurry at this gas velocity was different than those at other velocities (see Table 3.18).

Figures 3.21a and 3.21b compare average gas holdup values obtained using pressure measurements to those obtained with the nuclear density gauges for experiments with SASOL wax (no solids) at liquid velocities of 0 m/s and 0.005 m/s, respectively. There is very good agreement between different sets of values for both runs. For the batch experiment (Figure 3.20a), gas holdup values obtained using pressure measurements were somewhat lower than those from the density gauge using the Cs–137 source and comparable to those obtained with the density gauge using the Co–60 source.

Figures 3.22a, 3.22b, and 3.22c compare average gas holdups from pressure measurements with those obtained using the nuclear density gauges for experiments with SASOL wax (20 wt% 0 – 5 μm iron oxide particles) at slurry velocities of 0 m/s, 0.005 m/s, and 0.02 m/s, respectively. There is excellent agreement in results obtained in the continuous mode of operation (Figures 3.22a and 3.22b) using the different methods. However, for the batch experiment, gas holdup values obtained using pressure measurements were consistently lower than those obtained using either of the density gauges. As mentioned previously, average gas holdups for the NDG technique were calculated by simply using an arithmetic average of the axial gas holdups (see Eq. 3.45). In order to determine if this method for calculating the average gas holdups caused the differences, average holdups were also calculated by fitting the data to a curve and integrating across the expanded height (see Eq. 3.44). While average holdups were slightly lower using this technique (between 0.4% and 2.0% - relative), they were still higher than the values obtained using the pressure transducers. Axial gas holdups measured using the density gauges for this experiment at gas velocities of 0.04 and 0.09 m/s are compared

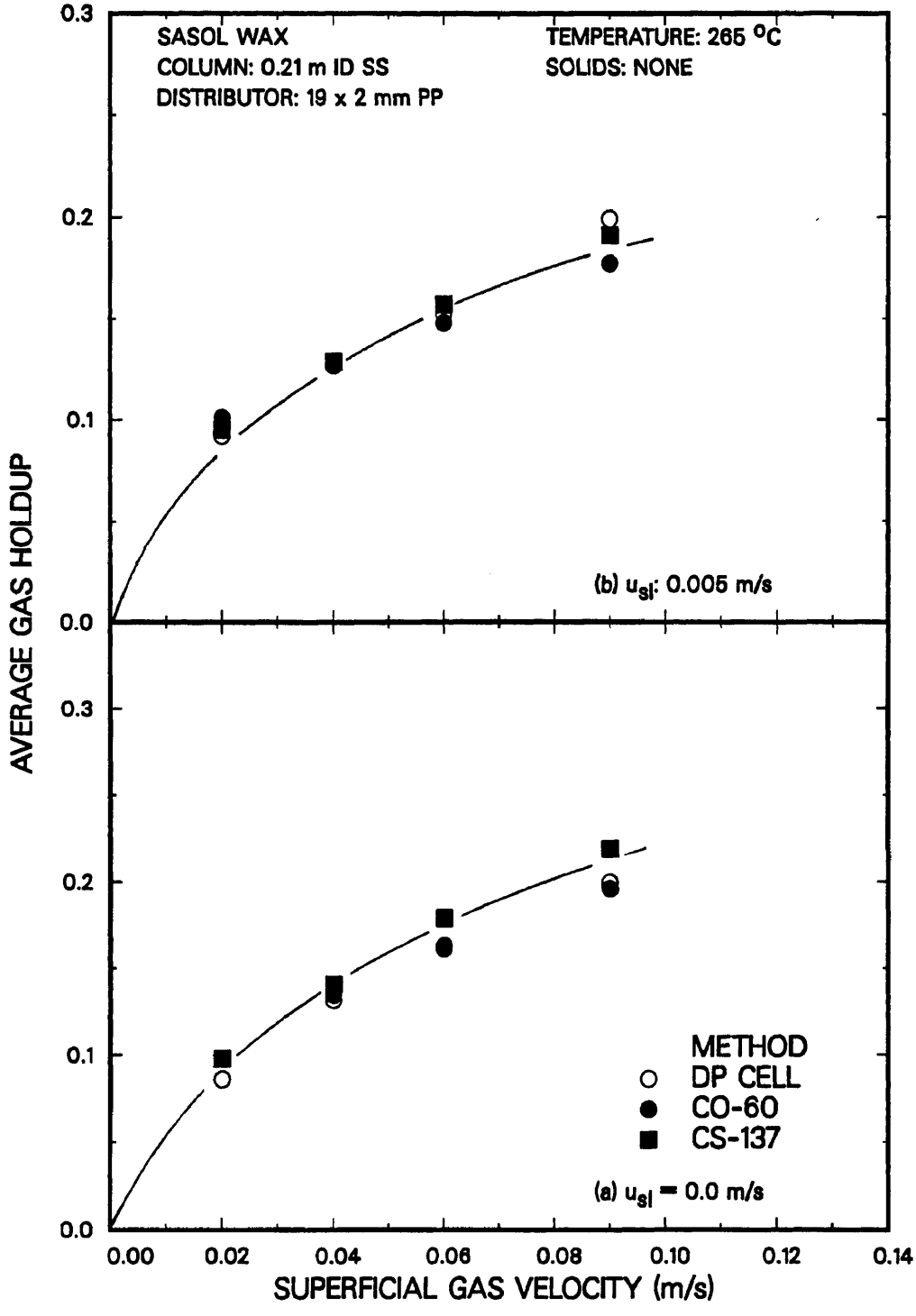

Figure 3.21. Comparison of average gas holdups from the DP cells and nuclear density gauges (SASOL wax, no solids; (a) u_l = 0.0 m/s; (b) u_l = 0.005 m/s).

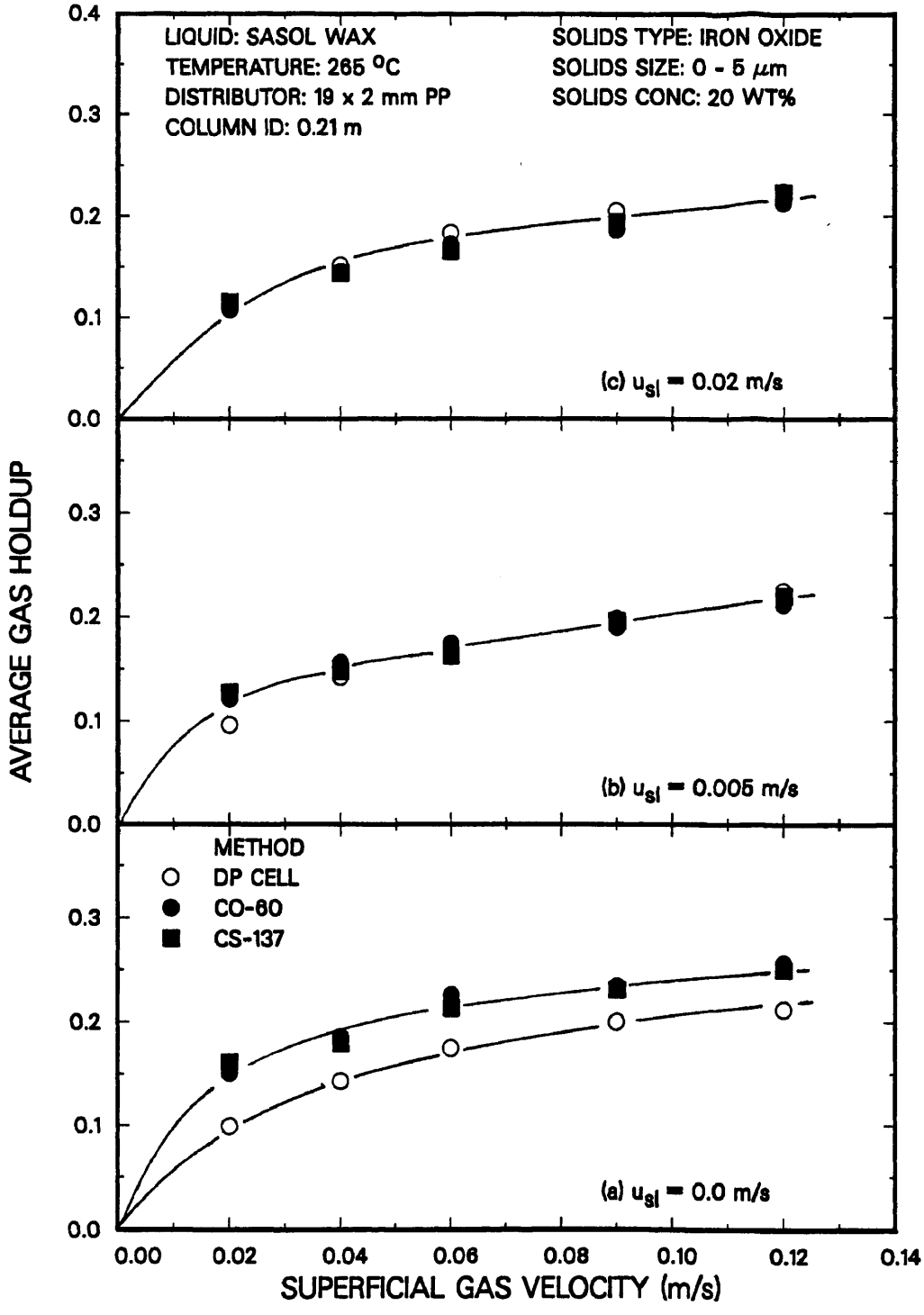

Figure 3.22. Comparison of average gas holdups from the DP cells and nuclear density gauges (SASOL wax, 20 wt% 0 - 5 μm iron oxide; (a) u_{sl} = 0.0 m/s, (b) u_{sl} = 0.005 m/s, (c) u_{sl} = 0.02 m/s).

to axial gas holdups obtained using pressure measurements in Figure 3.23a and 3.23b, respectively. At a gas velocity of 0.04 m/s, the axial gas holdups obtained from pressure measurements were somewhat lower than those obtained using the density gauge. At the present time, we do not know what caused this difference (i.e. if it was due to errors in pressure readings, solids concentrations, or density gauge measurements). At a gas velocity of 0.09 m/s, axial gas holdups obtained from pressure measurements and density gauge measurements were comparable. However, in the bottom most section of the column (0.31 m), the axial gas holdup (pressure measurements) is considerably lower. As a result, the average gas holdup obtained from the density gauges is higher than that obtained from the pressure measurements. This implies, that if axial gas holdups vary considerably over the height of the dispersion, more measurements with the density gauge are needed to obtain an accurate estimate for the average gas holdup. As shown in Figure 2.15, axial gas holdups from continuous experiments varied almost linearly with height. Thus, it is not surprising that average gas holdups obtained with the density gauge were comparable to those obtained with the pressure transducers.

Average gas holdup results from batch experiments with 20 wt% large iron oxide and silica particles are shown in Figures 3.24a and 3.24b, respectively. Once again, gas holdups from the two density gauges were comparable. However, gas holdup values obtained by conventional techniques (pressure measurements) were lower, especially for the experiment with large iron oxide particles. During this experiment, axial gas holdups in the bottom section of the column (i.e. 0.31 m above the distributor) were substantially lower than those at heights of 0.9, 1.5 and 2.1 m as shown in Figure 3.25a and 3.25b. Axial gas holdups from pressure measurements and density gauge measurements were comparable at heights of 0.9, 1.5, and 2.1 m above the distributor, once again indicating that a better estimate for the average gas holdup would be obtained if measurements were made at additional axial positions. During the experiment with large

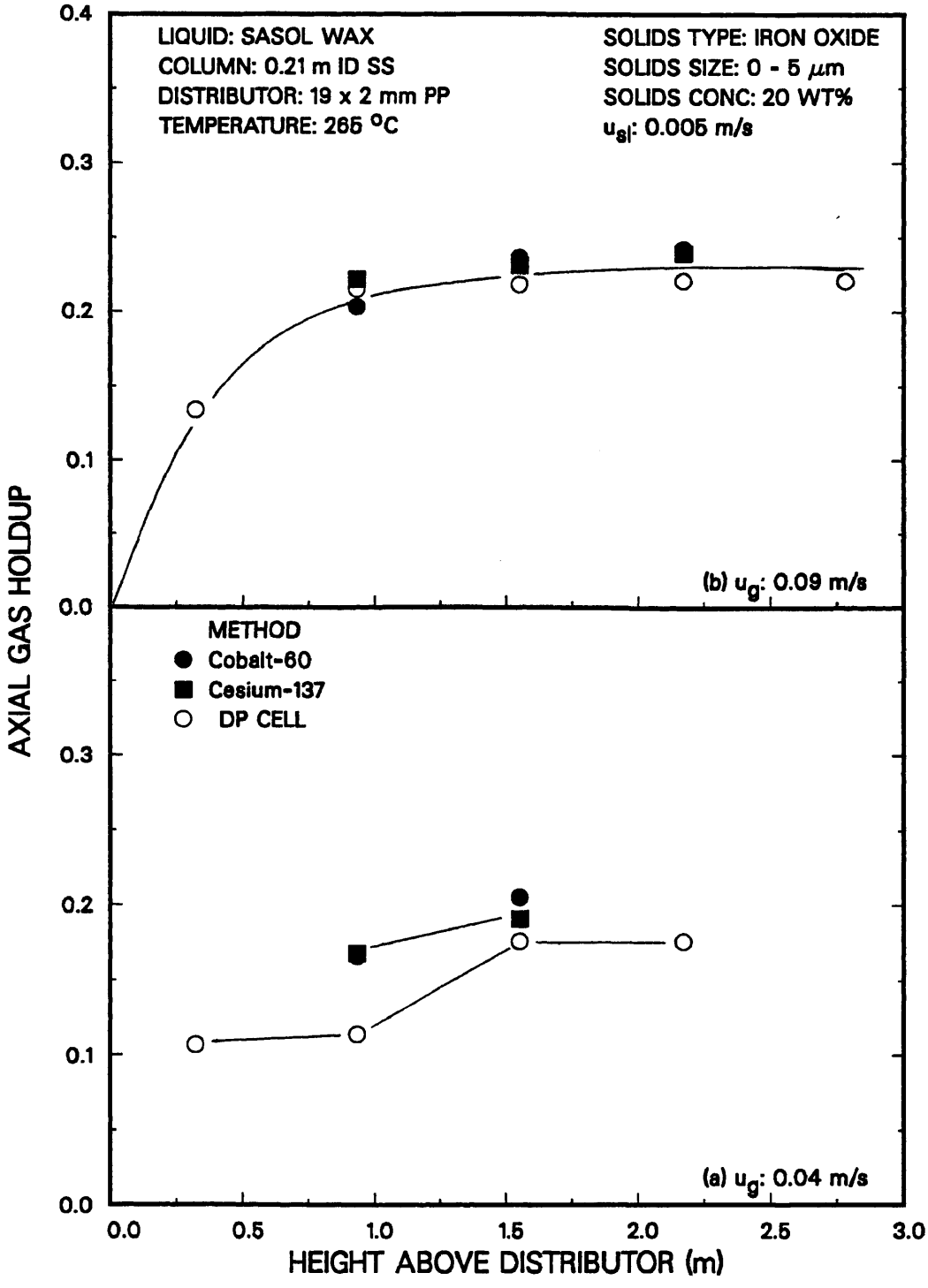

Figure 3.23. Comparison of axial gas holdups from the DP cells and nuclear density gauges (SASOL wax, no solids; (a) u_g = 0.04 m/s; (b) u_g = 0.09 m/s).

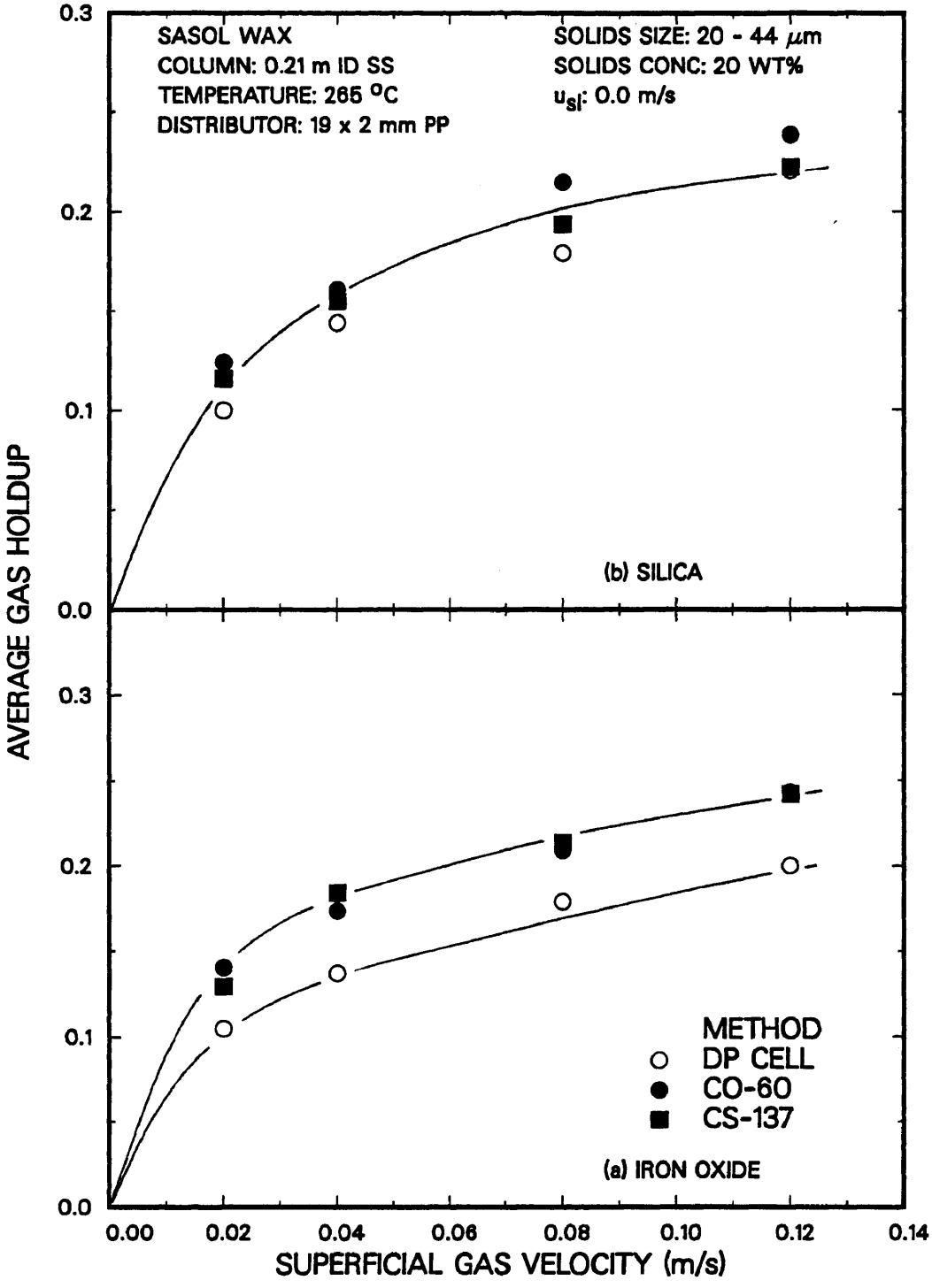

Figure 3.24. Comparison of average gas holdups from the DP cells and nuclear density gauges (SASOL wax; u_{sl} = 0.0 m/s; (a) 20 wt% 20 - 44 μm iron oxide; (b) 20 wt% 20 - 44 μm silica).

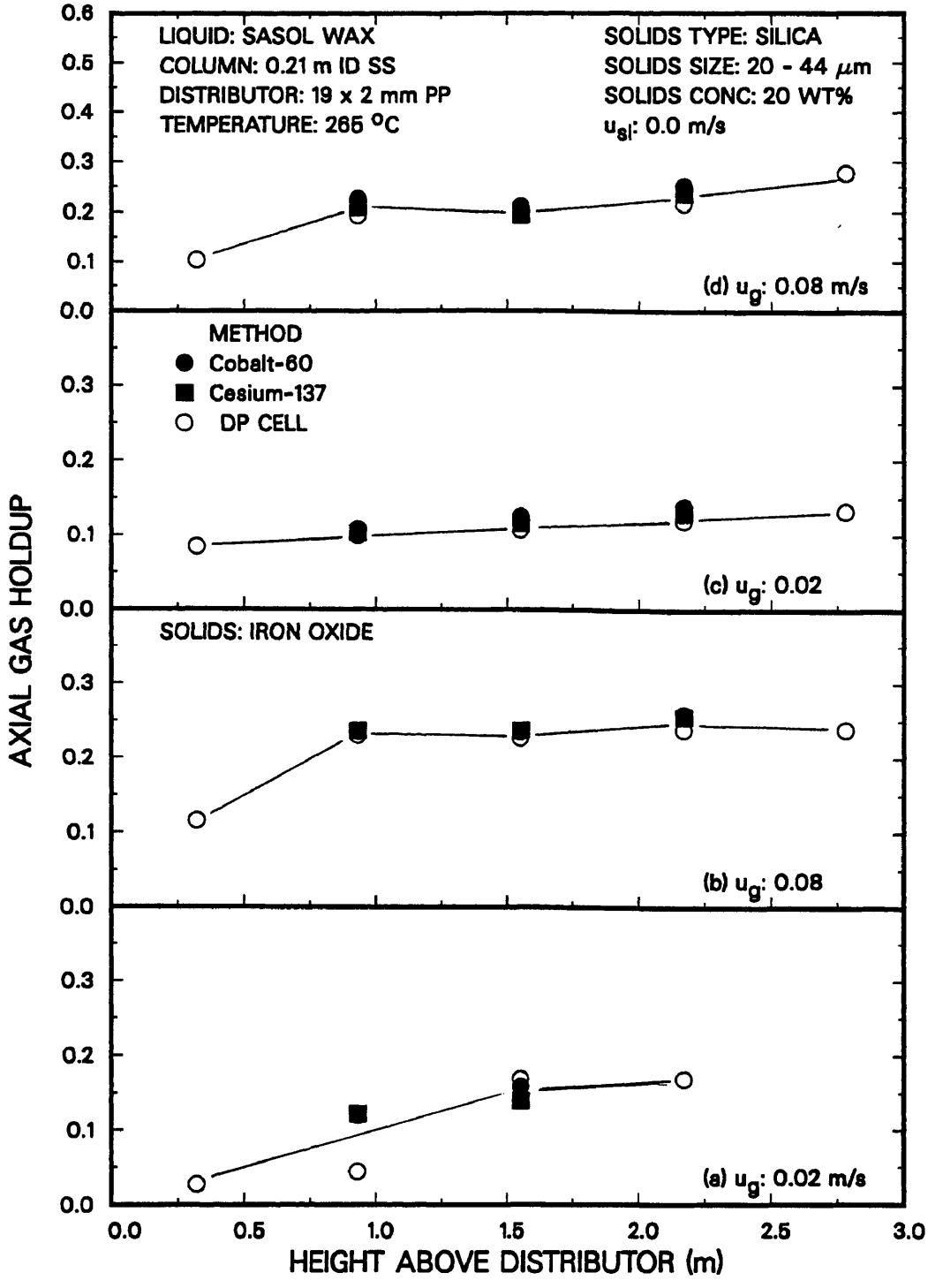

Figure 3.25. Comparison of axial gas holdups from the DP cells and nuclear density gauges (SASOL wax, 20 wt% 20 - 44 μm iron oxide - (a) u_g = 0.02 m/s; (b) u_g = 0.08 m/s; SASOL wax, 20 wt% 20 - 44 μm silica - (c) u_g = 0.02 m/s; (d) u_g = 0.08 m/s).

silica particles, we did not observe as significant difference in axial gas holdups between heights of 0.3 and 0.9 m above the distributor (see Figure 3.25c and 3.25d), consequently, the average gas holdup values obtained using the density gauges compared favorably with those obtained using the pressure transducers.

Figure 3.26 compares average gas holdup values from pressure measurements with those obtained from density gauge measurements for experiments with FT–300 wax. In particular, Figures 3.26a and 3.26b show results from two–phase experiments at slurry velocities of 0.0 and 0.005 m/s, respectively. There is excellent agreement in gas holdups obtained using both pressure measurements and density gauge measurements. For the batch mode experiment with large iron oxide particles, average gas holdups from pressure measurements and density gauge measurements were comparable at all gas velocities except at a velocity of 0.04 m/s (see Figure 3.26c). At this gas velocity, the average gas holdup obtained from pressure measurements was substantially larger than that obtained from density gauge measurements. Once again, this difference is due to the fact that measurements with the density gauges were made at only three positions (i.e. 0.9, 1.5, and 2.1 m); whereas, measurements with the pressure transducers were made at five positions. For this experiment, foam the uppermost region of the column (i.e. above 2.1 m), and the axial gas holdup in this region was 0.68. Since density gauge measurements were limited to heights below this, the average gas holdup estimated from analysis of density gauge data (for both sources) was less than the actual gas holdup.

Axial gas holdups at velocities of 0.04 and 0.12 m/s for the two experiments with no solids are presented in Figure 3.27. The axial gas holdup profile obtained from pressure measurements did not vary significantly with axial position during either of these experiments. Axial gas holdups obtained from density gauge measurements were similar to those obtained from pressure measurements. Axial gas holdups did not vary significantly over the length of the column, and since axial gas holdups from conventional

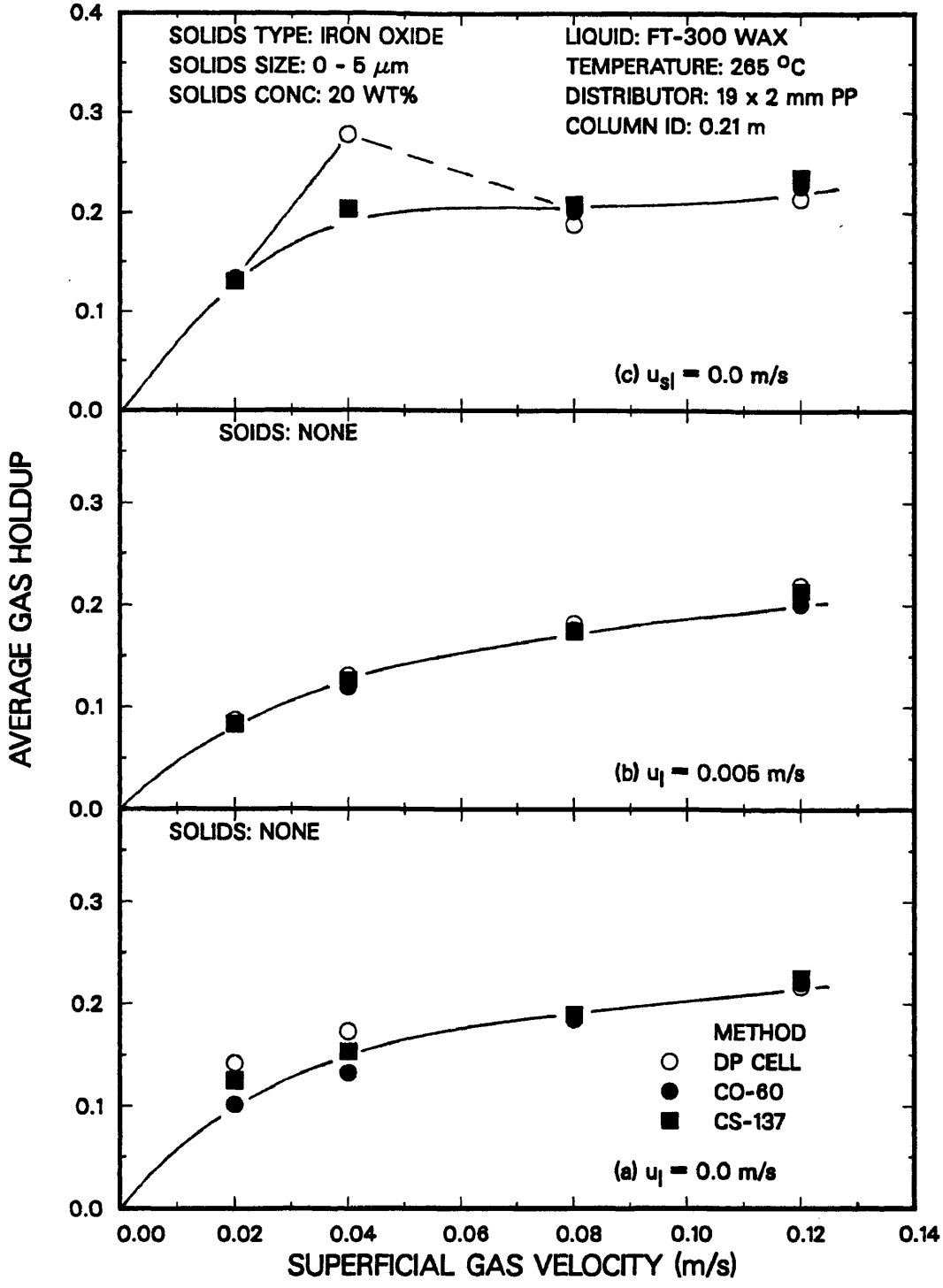

Figure 3.26. Comparison of average gas holdups from the DP cells and nuclear density gauges (FT-300 wax; (a) u_l = 0.0 m/s, no solids; (b) u_l = 0.005 m/s, no solids; (c) u_{sl} = 0.0 m/s, 20 wt% 20 - 44 μm iron oxide).

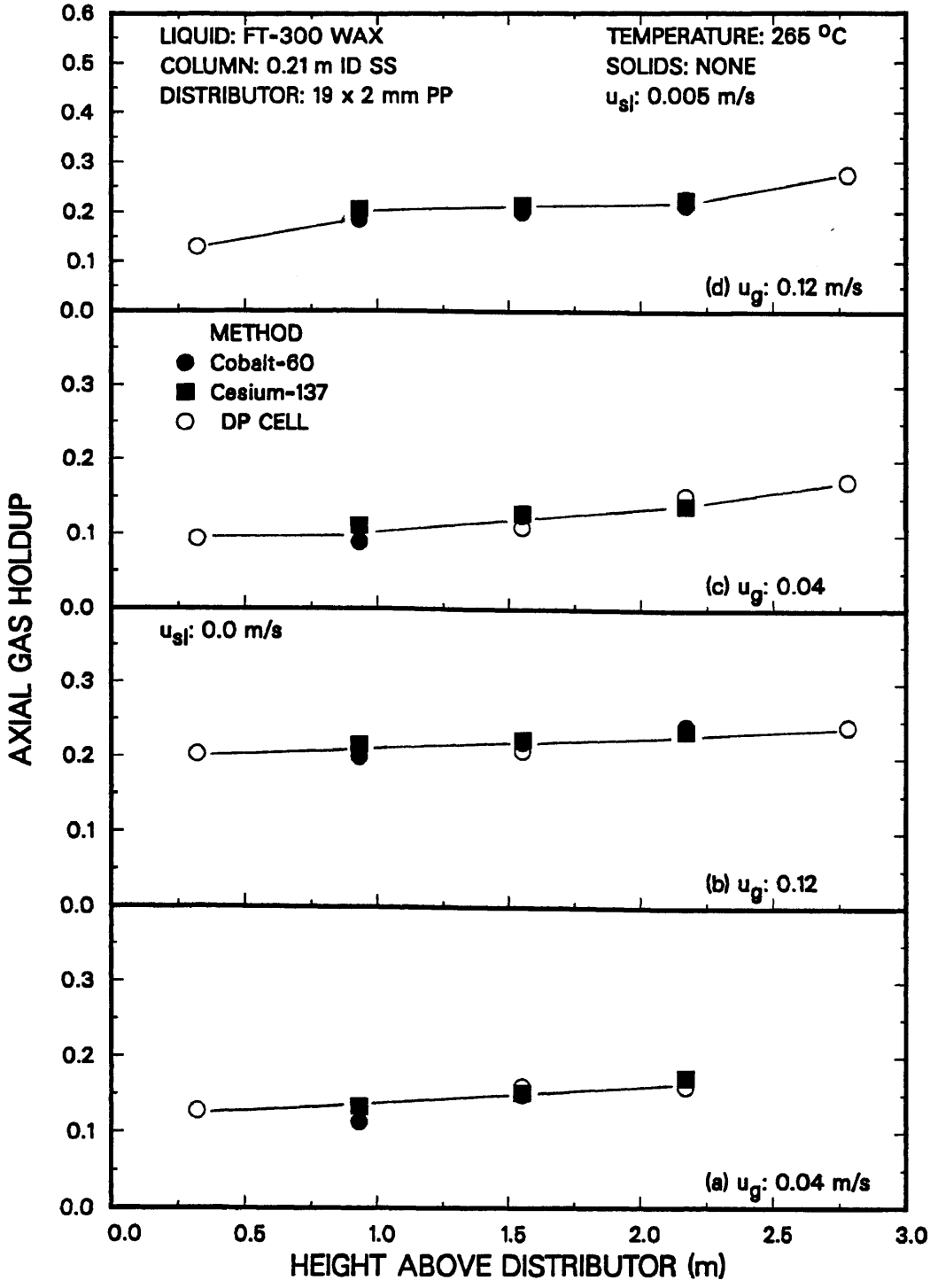

Figure 3.27. Comparison of axial gas holdups from the DP cells and nuclear density gauges with FT-300 wax and no solids (u_l = 0.0 m/s - (a) u_g = 0.04 m/s; (b) u_g = 0.12 m/s; u_l = 0.005 m/s - (c) u_g = 0.04 m/s; (d) u_g = 0.12 m/s).

measurements and density gauge measurements were comparable at heights of 0.9, 1.5 and 2.1 m above the distributor, it is not surprising that there was excellent agreement in average gas holdups obtained from the different techniques. Figure 3.28 shows axial gas holdups obtained from the batch experiment with large iron oxide particles (see Figure 3.26c) at gas velocities of 0.02, 0.04, and 0.08 m/s. During this experiment axial gas holdups almost varied linearly with height above the distributor, with the exception of the axial gas holdup in the uppermost section of the column at a gas velocity of 0.04 m/s. Thus, average gas holdups obtained from the pressure measurements are higher than those obtained from the density gauge measurements at this gas velocity.

Overall, axial gas holdups obtained from the nuclear density gauges compared favorably with those obtained using pressure measurements. For experiments in which either there was not a significant gradient in axial gas holdups, or where axial gas holdup increased linearly with height the average gas holdup values from the different methods were similar. Based on our results from pressure measurements, it appears that axial gas holdups are essentially uniform (or vary only slightly) in the central portion of the column; however, in the uppermost region of the column, or at the bottom of the column, axial gas holdups can be substantially different. Thus, a better estimate of the average gas holdup could be obtained if density gauge measurements were made in the top and bottom regions of the column.

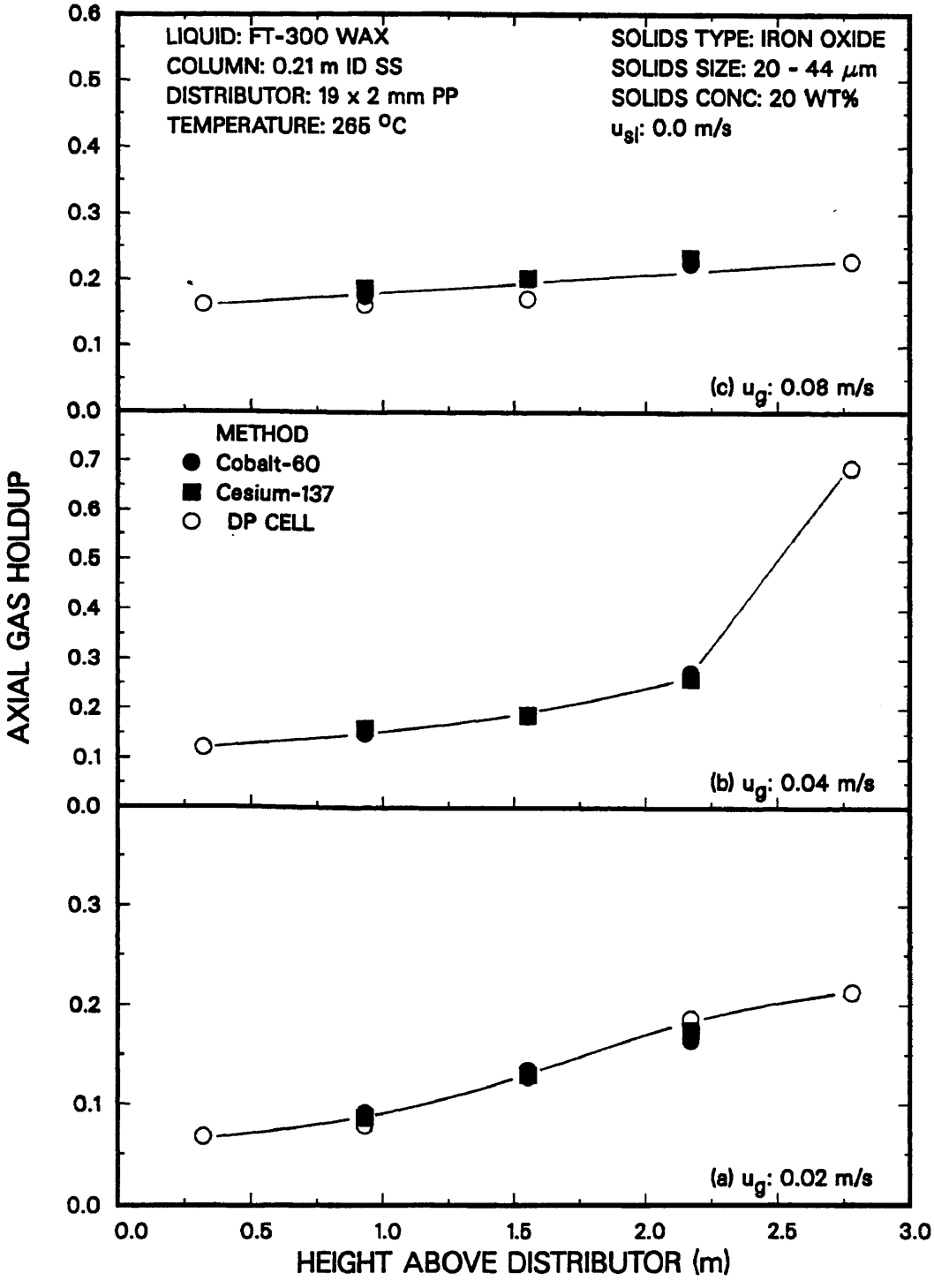

Figure 3.28. Comparison of axial gas holdups from the DP cells and nuclear density gauges (FT-300 wax, 20 wt% 20 - 44 μm iron oxide - (a) u_g = 0.02 m/s; (b) u_g = 0.04 m/s; (c) u_g = 0.08 m/s).